# Photopatterned polyacrylamide gels enable efficient microfluidic protein assays

*Chenlu Hou*

Electrical Engineering and Computer Sciences
University of California at Berkeley

May 13, 2011

Photopatterned Polyacrylamide Gels Enable Efficient Microfluidic
Protein Assays

by

Chenlu Hou


A dissertation submitted in partial satisfaction of the

requirements for the degree of

Doctor of Philosophy

in

Engineering – Electrical Engineering and Computer Sciences

in the

Graduate Division

of the

University of California, Berkeley


Committee in charge:

Professor Amy E. Herr, Co-chair
Professor Ming C. Wu, Co-chair
Professor Bernhard E. Boser
Professor Danica Chen


Spring 2011

Abstract

Photopatterned Polyacrylamide Gels Enable Efficient Microfluidic Protein Assays

by

Chenlu Hou

Doctor of Philosophy in Electrical Engineering

University of California, Berkeley

Professor Amy E. Herr, Co-chair

Professor Ming C. Wu, Co-chair

Electrophoretic separation is a powerful technique in life sciences to identify and characterize biological species. Microfluidic implementation of electrophoretic separations reduces sample and reagent consumption and offers seamless integration of multiple functionalities. This dissertation reports the application and optimization of photopatterned polyacrylamide gels to improve the effectiveness of electrophoretic separations in microfluidic devices. Specifically, we demonstrate microfluidic implementation of two assays for protein analysis: a homogeneous immunoassay to quantify protein biomarker concentrations and a western blotting assay to report protein sizes and antibody-binding characteristics.

To realize efficient homogeneous electrophoretic immunoassays, we optimize photopatterned polyacrylamide gels that enable quantitative assay completion in separation lengths as short as 350 μm in < 10 s. The demonstrated separation length is an order of magnitude shorter than the separation length previously reported for on-chip gel electrophoresis and two orders of magnitude shorter than that achieved using capillary electrophoresis. The required separation lengths translate to less than 3.5 V for assay operation as compared to hundreds and thousands of volts currently in use for homogeneous immunoassays. A discontinuous gel sieving matrix architecture introduced in our work forms a key step towards realizing battery-operated electrophoresis systems for quantitation of protein biomarkers in near-patient environments.

In our implementation of microfluidic western blotting assay, we developed a novel strategy for on-chip protein renaturation which utilizes electrophoretic separations to isolate denaturing detergents from proteins. Furthermore, photopatterning of polyacrylamide gels within a 2D chamber enables seamless integration of protein renaturation with upstream sizing and downstream immunoaffinity recognition. The entire assay is completed within 3 minutes in a single device as compared to conventional western blotting assays which require hours to a day, multiple pieces of instruments, and frequent human intervention. Given the appreciable assay speed, this assay may comprise part of a tool set necessary to accelerate biomarker discoveries for personalized medicine.

# Acknowledgements

The past six years has been a long and fulfilling journey. I am extremely thankful for having met and worked with many talented people who continue to inspire me.

First and foremost, I would like to thank my thesis advisor, Dr. Amy Herr, for her guidance and support. When I first met Amy four years ago to discuss the possibility of joining her lab, I had no prior experience in microfluidics or bioMEMS; in fact, I had never worked with proteins and had never touched a pipette. All I had was an interest to spend my PhD working in an area that really excited me, which was and still is microfluidics. I am forever grateful to Amy for giving me the opportunity and for being a great advisor. Her technical insights, her advices, and her encouragements really made this work possible. Her dedication to creating new technologies to advance healthcare is truly inspirational. She has helped me in conceiving the major ideas presented in this work. She has also provided many helpful suggestions that led to successful demonstrations of both assay platforms. When my devices were not working, Amy never ran out of ideas on why they didn't work and how we can fix them. I remembered times of being totally clueless regarding which direction(s) to proceed; at those times, she was always able to provide clear guidance and advices. Amy is a great mentor who would do anything to make sure that her students will succeed in their studies as well as professional careers. Through all the practice talks we have had, she has taught me how to effectively communicate my research. Through all the edits we have gone through on my manuscripts, she has taught me how to present my ideas and data with clarity. I would like to thank Amy for not only guiding us to produce great work individually, but also for creating a great group dynamic where everyone collaborates to generate more ideas. She is also very supportive of my future career choice and made sure I can make a smooth transition from graduate school to my next endeavor.

Next, I would like to thank Professor Ming Wu for serving as my EECS co-advisor and for all the help and support he has provided me. I would like to thank Professor Bernhard Boser and Professor Danica Chen for serving on my thesis committee and all the helpful feedback they have provided.

I would like to thank my colleagues at the Herr Lab for their help and support. I have learned so much from the discussions we had at group meetings and also in lab. Thanks to everyone for sitting through many practice talks and providing helpful suggestions on my qualify exam presentation and conference presentations. Especially, I would like to thank Dr. Mei He, Kwasi Apori, Kelly Karns, Sam Tia, Dr. Dohyun Kim, Alex Hughes, Dr. Xiaofang Chen, Augusto Tentori, Monica Kapil, Zohora Iqbal, Sasha Denisin, Todd Duncombe, and Edward Jung. I apologize in advance if I have missed anyone (it was not intentional). Dr. Mei He has led the development of microfluidic western blotting in which my work built upon. She has offered many helpful technical insights and provided guidance on experimental implementation. *Mei*: thank you for not only being an amazing colleague but also a great friend; thanks for sharing your expertise and always showing us better ways to do things; and thanks for encouraging me when I was frustrated with research or personal life. *Kwasi:* thank you for teaching me gel fabrication and assay characterization when I first joined the lab; thank you for making sure the lab is safe and clean so we can work more productively. *Kelly:* thank you for putting together the two-color detection system which I used for the spectrally multiplexed immunoassays; thank you

*To My Parents*

献给我亲爱的爸爸妈妈

# Table of Contents

# Chapter 1 Introduction

## 1.1 Benefits of miniaturized analysis

Advances in microfabrication technology enable laboratory analysis to be performed within microfluidic devices[1]. Biological and chemical analysis benefit from miniaturization due to: reduced sample and reagent consumption, seamless integration of sample preparatory and analytical functions, and improved portability.

Reduced sample consumption and lossless analysis significantly improve the amount of diagnostic and prognostic information that can be extracted from low abundance proximal fluids (e.g., tears, gingival crevicular fluid, and archived samples). As a result of proximal fluid analysis, biomarkers with better specificity to physiological conditions may emerge to replace more generic serum and urine markers[2].

Microfabrication enables integration and automated operation of multiple assay steps on a single device[3]. Single-chip integration improves assay throughput and reproducibility by reducing human intervention and analysis time. For example, serial processing of a single sample (i.e., sample preparation followed by analysis) has been demonstrated for quantitation of protein biomarkers in complex sample matrices such as saliva[4], dissected muscle tissues[5], and whole blood[6]. On the other hand, multiplexed analysis (i.e., analysis of multiple samples and/or analysis of multiple analytes) have been demonstrated for high throughput DNA sequencing[7].

Furthermore, microfluidic devices can take advantage of fluid mechanisms that become dominant at microscale. For example, capillary flow is the driving force behind self-powered diagnostic tests using glass/PDMS[8] or paper[9]. Digital microfluidics utilize surface tension properties of liquid for manipulation of nanoliter droplets to accomplish a diverse set of functionalities[10].

All together, the benefits of miniaturization have been fueling the growing interests in applying microfluidic devices for laboratory analysis[11], clinical diagnostics[12, 13], and improving global health[14, 15]. Recently, mobile phone based microscopes, which combine imaging, detection, and communication capability, have been integrated with microfluidic devices for near-patient settings[16]. Nevertheless, more applications could benefit from microfluidics. Beyond reducing sample consumption and enabling automation, microfluidic devices need to offer significantly improved performance and/or provide new functionality to be widely adopted in life science laboratories and clinical settings.

## 1.2 Photopatterning of in-situ sieving matrices improves performance of existing microfluidic analytical tools

As an example, we demonstrate why, despite their faster analysis time and compact size, microchip-based electrophoresis has not replaced slab gels. Yet, at the same time, photopolymerization, which is a central theme of this work, can overcome the limitations of microchip-based electrophoresis and bring microfluidics to life science laboratories by improving analysis speed and reducing sample and reagent consumption.

### 1.2.1 Electrophoretic separation is ubiquitous for life science research

Slab gels were developed more than 40 years ago and their basic designs were still widely used today in all life science laboratories. Ubiquitous adoption of slab gels has been chronicled by one of its inventors[17]. Electrophoresis separates proteins based on charge to size ratio which reflects protein size and conformation. Electrophoresis describes the motion of charged particles (i.e., proteins) relative to a stationary fluid medium under an electric field. Electrophoretic mobility of a charged particle is solved by balancing the electrical force and the Stokes' drag force the particle experiences in opposite directions: $\sum F = F_{el} + F_{drag} = zE - 6\pi\eta aU = 0$ where $z$ is the particle charge, $a$ is the particle size, $U$ is the migration velocity, and $\eta$ is the viscosity of the separation medium. Electrophoretic velocity is: $U = \frac{z}{6\pi\eta a}E = \mu E$ with electrophoretic mobility ($\mu$) directly proportional to charge and inversely proportional to size ($a$).

Besides using slab gels, electrophoresis has also been conducted in paper[18], capillaries[19], and microchips[20]. Applications of slab gels span from protein detection and quantification[21], purification[22], proteomic analysis[23], and biomarker discoveries[24]. Typical PAGE of proteins requires more than 1 hour to complete and consumes sample volume in tens of μLs. Microchip-based electrophoresis is an implementation of capillary electrophoresis on glass chips by microfabrication. Etched glass chips with micrometer scale channels are fabricated through photolithography, etching, and bonding. Microchip electrophoresis has been applied toward clinical analysis[25], chiral separations[26], and high throughput DNA sequencing[27]. Compared to the capillary counterpart, microfluidic implementation significantly reduces device footprint and improves analysis throughput when multiple channel networks are integrated on a single device. The Agilent Bioanalyzer 2100[28] is a commercially available microchip electrophoresis platform for sizing, quantification, and quality control of DNA, RNA, proteins, and cells.

### 1.2.2 Separation resolution is the key performance metric for separations

The key performance metric for separations is separation resolution which signifies the capability to resolve two neighboring peaks. For a microfluidic-based separation technology to replace slab gels, it would need to offer superior separation resolution. Mathematically, separation resolution is defined as peak-to-peak distance between the neighboring analytes ($\Delta L$) divided by average analyte peak width ($2\sigma_1 + 2\sigma_2$) as illustrated in Figure 1-1. The top image represents a fluorescence micrograph of two intersection microfluidic channels. The bottom image illustrates the average axial intensity profile obtained by image analysis.
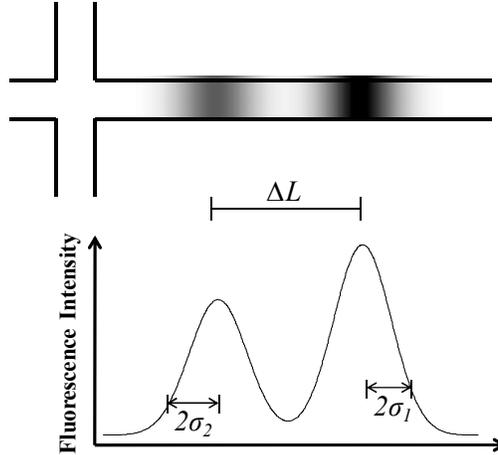
Figure 1-1. Separation resolution is a key performance metric in electrophoretic separation.

Besides measuring separation resolution experimentally, separation resolution can also be derived theoretically from mass transport equations. Expression of separation resolution as a function of device dimension and operating parameters provides insights on how separation resolution scales with miniaturization. At injection, the analyte peak axial intensity profile can be modeled by a Gaussian distribution with $C(x,0) = \frac{m_0}{\sigma_0\sqrt{2\pi}} e^{-\frac{x^2}{2\sigma_0^2}}$ where $m_0$ reflects the total mass contained in the injected plug and $\sigma_0$ is the initial standard deviation of the injected peak. $\frac{m_0}{\sigma_0\sqrt{2\pi}}$ represents the peak analyte concentration which can be quantified by measuring fluorescence intensity for labeled proteins. The following mass transport equation, which assumes constant electrophoretic velocity ($U$) and diffusivity ($D$), relates analyte migration as a function of time and space:

$$\frac{\partial c}{\partial t} = -U\frac{\partial c}{\partial x} + D\frac{\partial^2 c}{\partial x^2}$$

The transport equation above assumes no chemical reactions occurring during separation. In other words, the total mass within the injected plug is conserved over time. Solving the transport equation gives analyte peak intensity profile as a function of migration time: $C(x,t) = \frac{m_0}{\sigma\sqrt{2\pi}} e^{-\frac{(x-Ut)^2}{2\sigma^2}}$ where $\sigma^2 = \sigma_0^2 + 2Dt$. Therefore, separation resolution between two neighboring analyte peaks can be written as

$$SR = \frac{\Delta L}{2\sqrt{\sigma_0^2 + 2D_1 t} + 2\sqrt{\sigma_0^2 + 2D_2 t}}$$

Assuming the separation is conducted in a homogeneous media where analytes exhibit constant diffusivity and mobility over the course of separation, peak-to-peak distance can be substituted as $\Delta L = \Delta\mu E t$. Separation resolution is then expressed as a function of elapsed separation time ($t$):

$$SR = \frac{\Delta\mu E t}{2\sqrt{\sigma_0^2 + 2D_1 t} + 2\sqrt{\sigma_0^2 + 2D_2 t}}$$

3

Device scaling mainly affects electric field ($E$) and injection plug width ($4\sigma_0$). The sieving matrix that separation is conducted in determines mobility difference ($\Delta\mu$) and diffusivity ($D$). Next, we use the expression of separation resolution to analyze, predict, and compare separation performance obtained on slab gels, microchip capillary electrophoresis, and microchip gel electrophoresis.

### 1.2.3 Why microchip capillary electrophoresis has not replaced slab gels

At first glance, conducting separations in glass capillaries or microchannels improves separation resolution by allowing the application of a higher electric field. At a given electric field, heat generation from Joule heating scales with $a^2$ whereas heat dissipation scales with $a$; $a$ symbolizes the cross sectional device dimension. Reducing $a$ improves heat dissipation with respect to heat generation and allows application of a higher electric field. However, separations conducted in free solution cannot generate sufficient mobility differences ($\Delta\mu$) among different proteins to resolve the species (i.e., SR > 1). In free solution, proteins often exhibit similar charge to mass ratios. Hence, free solution electrophoresis of proteins usually requires separation distances of several centimeters [29, 30].

### 1.2.4 On-chip gel electrophoresis offers superior separation resolution than microchip CE and slab gels

Using cross-linked gels photopolymerized within microfluidic channels, sizing of four proteins with molecular weights ranging from 14 kDa to 39 kDa was completed within 5 mm and within 6.5 s[31]. Photopolymerization enables integration of a traditional and validated separation media into microfluidic channels to fully utilize the benefits of miniaturization. Using the expression of separation resolution, we prove why on-chip gel electrophoresis can achieve significant reduction in separation length and separation time compared to its macroscale analog (i.e., slab gels) and microscale counterpart (i.e., on-chip capillary electrophoresis).

On-chip gel electrophoresis completes separations in a shorter distance than on-chip capillary electrophoresis by enhancing mobility differences among analytes. We first express SR as a function of leading analyte migration distance ($L$) by substituting $t = \frac{L}{\mu_1 E}$:

$$SR = \frac{\Delta\mu E \dfrac{L}{\mu_1 E}}{2\sqrt{\sigma_0^2 + 2D_1 \dfrac{L}{\mu_1 E}} + 2\sqrt{\sigma_0^2 + 2D_2 \dfrac{L}{\mu_1 E}}}$$

For the same initial injection plug width ($4\sigma_0$) and applied electric field (E), gel electrophoresis achieves better separation resolution at a given migration distance by enhancing $\Delta\mu/\mu$. Free solution electrophoresis separates proteins based on differences in their charge to mass ratios which can be negligible as larger proteins with additional amino acids often possess more charges. On the other hand, gel electrophoresis introduces another sieving factor based on size according to the Ferguson relationship[32]: $\mu = \mu_0 10^{-KT}$ where $\mu_0$ is the free solution electrophoretic mobility, $K$ is the retardation coefficient, and $T$ is the total acrylamide concentration in the polyacrylamide gel precursor solution. $T$ is inversely proportional to gel pore sizes. Larger proteins have larger retardation coefficients compared to smaller proteins. Therefore, larger proteins exhibit more dramatic decrease in mobility with decreasing pore size.

4

As a result, gel electrophoresis can complete separation in much shorter channel lengths compared to free solution electrophoresis.

On-chip gel electrophoresis completes separation in shorter distance and time compared to slab gels due to a reduced initial plug width ($4\sigma_0$) and an increased electric field ($E$). On-chip electrophoresis can define a tight sample plug by channel geometry. Loading in a double T cross channel illustrated in Figure 1-1 with 100 μm channel width achieves a sample plug with $\sigma_0 = 25$ μm. In comparison, the sample plug in slab gels has a $\sigma_0$ of at least 100 μm. In addition, significantly higher electric field (300 V/cm) can be applied in on-chip gel electrophoresis as compared to the ~20V/cm applied in slab gels. The improvement in electric field application is a result of reduced Joule heating (as explained in 1.2.3) and reduced separation channel length. Depending on whether the analyte peak width ($\sigma = \sqrt{\sigma_0^2 + 2D\frac{L}{\mu E}}$) is dominated by the initial injection plug width ($\sigma_0$) or diffusion ($2Dt$), separation resolution scales somewhere in between $L/\sigma$ and $\sqrt{LE}$. Conversely, the migration distance ($L$) required to achieve a given separation resolution scales somewhere in between $\sigma$ and $1/E$. Therefore, the combined effect of 4 times reduction in $\sigma_0$ and 15 times improvement in $E$ contributes to separation completion in 5 mm for microchip gel electrophoresis whereas the same separation requires > 5 cm in slab gels. As total assay time is directly proportional to required migration distance and inversely proportional to applied electric field, a significant reduction of necessary migration distance to achieve a desired separation resolution and a 15 times increase in $E$ explain why on-chip gel electrophoresis completes within 10 sec while slab gels can take hours.

## 1.3 Organizational overview

This dissertation reports the application and optimization of photopatterned polyacrylamide gels to improve the effectiveness of electrophoretic separations in microfluidic devices. As discussed in the previous section, polyacrylamide gels improve separation efficiency by enhancing analyte mobility differences. Photopatterning of polyacrylamide gels enables seamless integration of multiple functional units and offers fine control over gel pore sizes for optimal separation resolution. As summarized in Figure 1-2, photopatterning of polyacrylamide gels is applied to improve the performance of existing macroscale and microscale protein assays as well as to integrate new functionality.

The first part of my thesis work (Chapter 2-6) focuses on realization of efficient homogeneous electrophoretic immunoassays. Homogeneous immunoassays utilize electrophoresis to separate immune complexes from unbound affinity probes. Compared to heterogeneous immunoassays or surface-based biosensors, homogeneous immunoassays provide continuous monitoring capabilities for point-of-care testing. However, the portability and field adaptability of homogeneous immunoassays are limited in part by the need for high voltage power supplies. Thus, a reduction in the required separation length would, in turn, reduce applied electrical potential (voltage) constraints, while allowing high electric field strength operation. We optimize photopatterned polyacrylamide gels to enhance the separation resolution between the bound immune complexes and the unbound affinity probes. As a result, we are able to complete protein biomarker measurement in separation lengths as short as 350 μm in < 10 s.

The second part of my thesis work (Chapter 7 – 10) focuses on the development of microfluidic western blotting assay with on-chip protein renaturation. Western blotting assays, which combine electrophoretic separation with affinity interactions, are widely used in life sciences to assay proteins in complex samples and applied as confirmatory diagnostic tests. We developed a novel strategy for on-chip protein renaturation which utilizes electrophoretic separations to isolate denaturing detergents from proteins. Furthermore, photopatterning of polyacrylamide gels in a 2D chamber enables seamless integration of protein renaturation with upstream sizing and downstream immunoaffinity recognition. The entire assay is completed within 3 minutes.

Photopatterning of polyacrylamide gels:
- Fine control over gel pore sizes
- Integration of multiple functional units

Optimization of separation resolution during electrophoretic transport

Resolve immune complexes from antibodies

Isolate denaturing SDS detergent from proteins

Ultra-short separation length homogeneous immunoassay

Microfluidic western blotting assay with on-chip protein renaturation
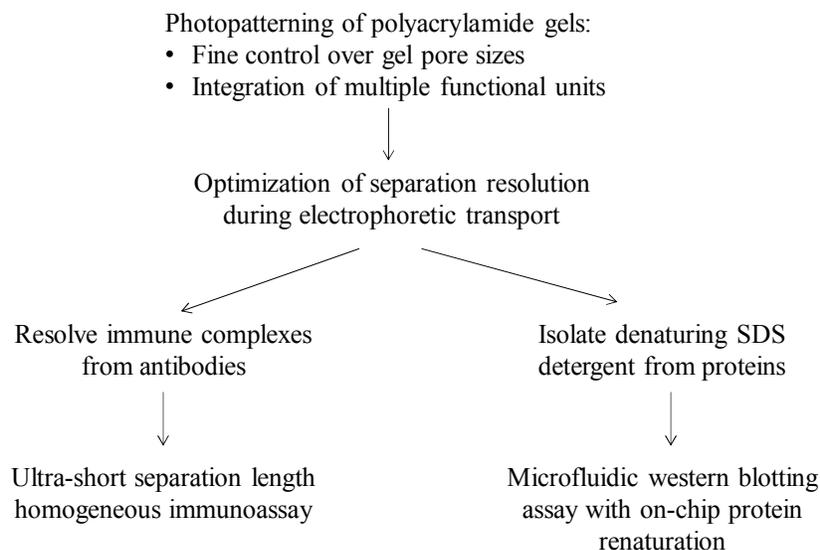
Figure 1-2. Photopatterning of polyacrylamide gels enables optimization of separation efficiency.

## 1.4 References

(1)     Whitesides, G. M. *Nature* **2006**, *442*, 368-373.
(2)     Teng, P. N.; Bateman, N. W.; Hood, B. L.; Conrads, T. P. *Journal of Proteome Research* **2010**, *9*, 6091-6100.
(3)     Haeberle, S.; Zengerle, R. *Lab on a chip* **2007**, *7*, 1094-1110.
(4)     Herr, A. E.; Hatch, A. V.; Throckmorton, D. J.; Tran, H. M.; Brennan, J. S.; Giannobile, W. V.; Singh, A. K. *Proceedings of the National Academy of Sciences of the United States of America* **2007**, *104*, 5268-5273.
(5)     Phillips, T. M.; Wellner, E. F. *Electrophoresis* **2007**, *28*, 3041-3048.
(6)     Fan, R.; Vermesh, O.; Srivastava, A.; Yen, B. K. H.; Qin, L. D.; Ahmad, H.; Kwong, G. A.; Liu, C. C.; Gould, J.; Hood, L.; Heath, J. R. *Nature Biotechnology* **2008**, *26*, 1373-1378.
(7)     Emrich, C. A.; Tian, H. J.; Medintz, I. L.; Mathies, R. A. *Analytical Chemistry* **2002**, *74*, 5076-5083.
(8)     Gervais, L.; Delamarche, E. *Lab on a Chip* **2009**, *9*, 3330-3337.
(9)     Martinez, A. W.; Phillips, S. T.; Whitesides, G. M.; Carrilho, E. *Analytical Chemistry* **2010**, *82*, 3-10.
(10)    Teh, S. Y.; Lin, R.; Hung, L. H.; Lee, A. P. *Lab on a chip* **2008**, *8*, 198-220.

(11)     Verpoorte, E. *Electrophoresis* **2002**, *23*, 677-712.

(12)     von Lode, P. *Clinical Biochemistry* **2005**, *38*, 591-606.

(13)     Crevillen, A. G.; Hervas, M.; Lopez, M. A.; Gonzalez, M. C.; Escarpa, A. *Talanta* **2007**, *74*, 342-357.

(14)     Yager, P.; Edwards, T.; Fu, E.; Helton, K.; Nelson, K.; Tam, M. R.; Weigl, B. H. *Nature* **2006**, *442*, 412-418.

(15)     Chin, C. D.; Linder, V.; Sia, S. K. *Lab on a chip* **2007**, *7*, 41-57.

(16)     Breslauer, D. N.; Maamari, R. N.; Switz, N. A.; Lam, W. A.; Fletcher, D. A. *Plos One* **2009**, *4*, 7.

(17)     Studier, F. W. *Trends in Biochemical Sciences* **2000**, *25*, 588-590.

(18)     Martin, N. H.; Franglen, G. T. *Journal of Clinical Pathology* **1954**, *7*, 87-105.

(19)     Frost, N. W.; Jing, M.; Bowser, M. T. *Analytical Chemistry* **2010**, *82*, 4682-4698.

(20)     Dolnik, V.; Liu, S. R. *Journal of Separation Science* **2005**, *28*, 1994-2009.

(21)     Syrovy, I.; Hodny, Z. *Journal of Chromatography-Biomedical Applications* **1991**, *569*, 175-196.

(22)     Spiker, S.; Isenberg, I. *Methods in Enzymology* **1983**, *91*, 214-226.

(23)     Zhou, M.; Yu, L. R. In *Proteome Characterization and Proteomics*; Academic Press Inc: San Diego, 2003; Vol. 65, pp 57-84.

(24)     Issaq, H. J.; Veenstra, T. D. *Electrophoresis* **2007**, *28*, 1980-1988.

(25)     Li, S. F. Y.; Kricka, L. J. *Clinical Chemistry* **2006**, *52*, 37-45.

(26)     Belder, D.; Ludwig, M. *Electrophoresis* **2003**, *24*, 2422-2430.

(27)     Chen, L.; Ren, J. C. *Combinatorial Chemistry & High Throughput Screening* **2004**, *7*, 29-43.

(28)http://www.genomics.agilent.com/CollectionOverview.aspx?PageType=Application&SubPageType=ApplicationOverview&PageID=275.

(29)     Colyer, C. L.; Mangru, S. D.; Harrison, D. J. *Journal of Chromatography A* **1997**, *781*, 271-276.

(30)     Yao, S.; Anex, D. S.; Caldwell, W. B.; Arnold, D. W.; Smith, K. B.; Schultz, P. G. *Proceedings of the National Academy of Sciences of the United States of America* **1999**, *96*, 5372-5377.

(31)     Herr, A. E.; Singh, A. K. *Analytical Chemistry* **2004**, *76*, 4727-4733.

(32)     Ferguson, K. A. *Metabolism-Clinical and Experimental* **1964**, *13*, 985-1002.

# Chapter 2 Motivation for On-chip Homogeneous Immunoassay Development

Point of care diagnostics are biochemical tests that can screen for potentially fatal conditions at an early stage. Instead of waiting days or weeks to hear back from centralized laboratories, with the right instrumentation, such tests can be done within minutes at the point of care (i.e., emergency room, ambulance, doctor's office, community health center, and resource-poor community settings). The diagnosis relies on quantitation of one or several protein biomarkers specific to a clinical condition. Measurement of biomarker concentration can be used to identify diseased state at an early stage (Figure 2-1A), to monitor treatment efficacy following diagnosis (Figure 2-1B), or to classify patients into different groups to determine best treatment options (Figure 2-1C)[1]. Therefore, POC diagnostics based on biomarker measurement can enable early detection and improve treatment efficacy[2]. Despite the tremendous impact POC would make, we are seeing very limited use. One reason is the lack of POC diagnostic instrumentation that can perform rapid and sensitive biomarker quantitation with minimum sample consumption in a low power, automated, portable fashion.
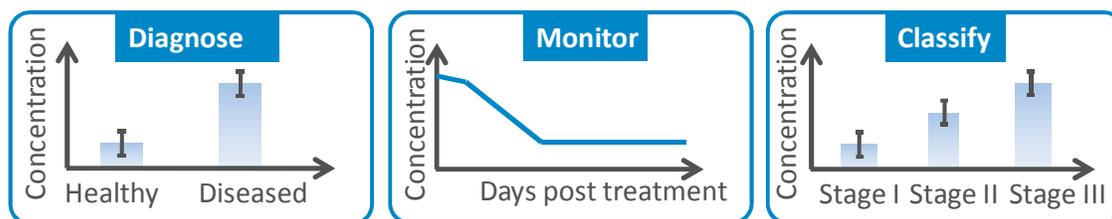


Figure 2-1. Measurement of biomarker concentration can reveal critical information regarding diseased condition.

This chapter first motivates how homogeneous immunoassay, which utilizes on-chip electrophoresis, can overcome limitations of existing immunoassay formats for POC diagnostics. Then we evaluate opportunities presented by previous efforts in developing efficient homogeneous immunoassays. Finally, we summarize my thesis contribution in developing ultra-short separation length homogeneous immunoassays.

## 2.1 Existing immunoassay formats for POC diagnostics

### 2.1.1 Lateral flow assay gives simple yes/no readouts

An assay platform currently in use for near-patient settings is the lateral flow or dip stick test. The home pregnancy test is an example of a lateral flow assay which detects human chorionic gonadotropiun (hCG). Lateral flow assays are simple and easy to use and can yield results in minutes. The operating principle of a lateral flow assay is depicted in Figure 2-2. The lateral flow assay is often packaged with detector reagent in the conjugate pad. The test line and control line contain capture antibodies (Figure 2-2, top). When the sample flows into the conjugate pad, the detection antibodies labeled with reporters (i.e., gold particles, colored particles, or dyes) are re-dissolved, bind to the target analyte in the sample, and form immune complexes (Figure 2-2, middle). The immune complexes and unbound detection antibodies then move toward the test line and the control line via capillary flow through the nitrocellulose membrane. The antibody-antigen complexes would bind to capture antibodies on the test line and form a visible line which indicates a positive test result. The unbound antibodies would bind to the control line which

indicates a valid result. Thus, a simple "yes/no" answer is obtained by reading the color of the test and control lines (Figure 2-2, bottom).

Although commercially available lateral flow tests such as the home pregnancy tests only give simple "yes/no" answers, lateral flow tests are capable of producing quantitative readouts with some design modifications. Monoclonal antibodies recognize a single epitope on the analyte of interest. The amount immune complexes formed between monoclonal antibodies and target analytes is directly proportional to target analyte concentration. Furthermore, a commercially available fluorescence reader such as the Cholestech LDX system[3] can be used to quantify fluorescence signal of the test line.
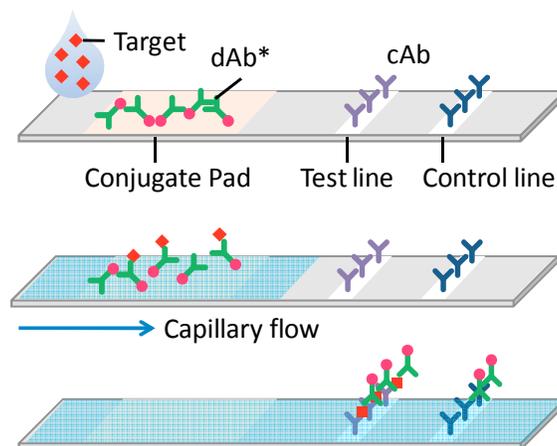


Figure 2-2. Operating principle of a lateral flow test.

### 2.1.2 Microfuidic implementation improves lateral flow assay performance

The main disadvantage of the lateral flow test is its insufficient precision due to material variability[4]. The pore-size and wettability of different materials used in the test influence flow rate and flow volume which, in turn, determines the amount of analytes that can bound to the test line. To have precise control over flow rate and flow volume, the lateral flow test has been implemented using microfluidic technology. A microfluidic capillary system was fabricated in silicon wafer via standard photolithography, deep reactive ion etching, and bonding with PDMS[5]. As in the conventional lateral flow test, detection and capture antibodies were pre-patterned on the chip by nonspecific adsorption onto the PDMS substrate. An on-chip capillary system, which included capillary pumps, vents, and flow resistors fabricated in silicon, precisely controlled flow rate and flow volume. Compared to lateral flow assays made of conventional materials (such as nitrocellulose), microfluidic implementation improves assay sensitivity and reduces sample consumption as shown in Table 2-1. The improvement in sensitivity was due to continuous flow of available sample volume over a 100 μm wide detection areas for 14 minutes which led to an analyte concentration effect.

Table 2-1. Microfluidic implementation improves assay performance

|  | Cholestech LDX Analyzer[3] | Microfluidic POC Assay[5] |
|---|---|---|
| **Sample volume** | 40 μL | 5 μL |
| **Assay time** | 4 – 7 minutes | 14 minutes |
| **Assay range** | 0.3 – 8.0 μg/mL | 0.001 – 1 μg/mL |

### 2.1.3   Main limitation of existing assay formats: lack of continuous monitoring capability

While lateral flow tests are low-cost and easy to use, they have limited applications at point of care settings where continuous monitoring is required for patients in critical conditions. After a single use, target analytes can saturate capture antibody binding sites and capillary flow is stopped once the channel/nitrocellulose material is filled with fluid. Heterogeneous immunoassays, which include lateral flow test, require surface immobilization of a capture probe or multiple washing steps for high-specificity[5-8]. Most heterogeneous immunoassays demonstrated to date are single use only as capture probes cannot be easily regenerated without losing biological activities. Therefore, heterogeneous assays are not suitable for continuous monitoring at point-of-care settings.

## 2.2    Introduction to homogeneous immunoassay

Homogeneous immunoassay formats utilize electrophoresis to separate immune complexes and unbound affinity probes. Elimination of surface immobilization and washing steps simplifies assay implementation, reduces reagent consumption, and allows sequential measurements. Two assay strategies are commonly used, namely direct and competitive immunoassays. Both direct and competitive homogeneous immunoassays employ the formation of immune complexes to indicate the concentration of target protein in a sample[9]. Figure 2-3 illustrates the operating principle of a direct homogeneous immunoassay. Sample containing a target analyte is incubated with a fluorescently labeled monoclonal antibody (Ab*) that is in excess concentration compared to the antigen (Figure 2-3A). The amount of immune complex formed between Ab* and target analyte is directly proportional to original analyte concentration over specific regions of the dose-response curve. To isolate the immune complexes for quantitation, the sample is introduced to a glass capillary or a microfluidic channel (Figure 2-3B). Under an electric field, the complex is resolved from unbound antibodies due to their different electrophoretic mobilities. Native conditions facilitate formation of immune complexes, but present a challenge to electrophoresis as the resulting immune complexes and unbound antibodies possess similar charge-to-mass ratios[10].
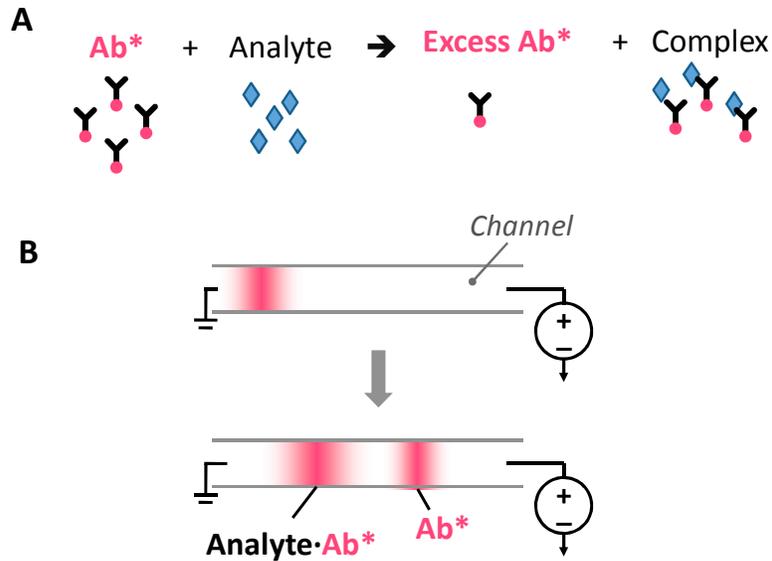
Figure 2-3. Homogeneous immunoassay utilizes electrophoresis to resolve immune complexes.

Alternatively, antigen detection can be accomplished via a competitive assay where the antibody (Ab) is limited in quantity and a fluorescently labeled antigen (Ag*) acts as the affinity reagent. During incubation, target analyte in the sample competes with the labeled antigen for limited binding sites. The governing reaction is: $Ag + Ag* + Ab$ (limited) $\leftrightarrow$ $Ab\text{-}Ag + Ab\text{-}Ag* + Ag + Ag*$. Electrophoretic separation resolves Ag* from Ab-Ag* peaks with increased targeting analyte concentration leading to a decrease in Ab-Ag* peak. Protein detection is usually accomplished via the competitive assay as it is easier to resolve the much smaller Ag* (1 – 100 kDa) from the immune complex than to resolve the larger Ab* (150 kDa) from the immune complex.

## 2.3    Microfluidic implementation of homogeneous immunoassays

### 2.3.1    Microfluidic implementation improves assay throughput
On-chip immunoassays typically employ the competitive format as it is easier to electrophoretically resolve labeled antigens (instead of larger antibodies) from immune complexes. For example, on-chip competitive immunoassays relying on separation of labeled antigens from immune complexes are applied toward detecting small hormones[11-13], drug molecules[14], and proteins[15-17]. Despite the challenge presented by separation, direct immunoassays are desirable due to straightforward implementation and often superior sensitivity[18].

When implemented with technologies including microfluidics, homogeneous assays become amenable for use in point-of-care settings[19-21]. In conjunction with a lab-on-a-chip format, automated operation of the immunoassays is conducive to single device integration of upstream sample preparation (i.e., mixing, incubation of probe with sample matrix, analyte enrichment)[22, 23]. Further, microfluidic homogeneous electrophoretic immunoassays support concurrent multi-analyte and/or multi-sample analysis[17, 24-26].

11

### 2.3.2 POC application is limited by high voltage requirement due to long separation length

Nevertheless, while microfluidic technology affords sophisticated, multi-stage analyses with quick reporting of results, the portability and field adaptability of electrophoretic immunoassays are limited in part by the need for high voltage power supplies. Thus, a reduction in the required separation length would, in turn, reduce applied electrical potential (voltage) constraints, while allowing high electric field strength operation. The first part of my thesis work contributes to improving portability of on-chip homogeneous immunoassays by completing separations within an ultra-short separation distance through design optimization.

### 2.3.3 Previous approaches to reduce assay separation length

While a recent review summarizes on-chip electrophoretic immunoassay developments[21], highlighted here are the previously reported state-of-the-art approaches to shorten direct immunoassay separation lengths, which translates to reduce voltage application. Approaches to improve separation resolution within a limited separation length include: (1) modification of affinity reagent mobility to enhance mobility differences between resolving species, (2) creation of counter flow to reduce assay separation distance, and (3) use of in-situ sieving matrices to maximize separation resolution.

As derived in chapter 1, separation resolution is directly proportional to relative mobility differences between target analytes. To sharpen peaks and enhance mobility differences between resolving species, a recent approach uses the high charge-to-mass ratio of DNA to mask antibody Fab fragment charge heterogeneity by conjugating DNA to Fab fragments[22, 26, 27]. Using the approach, anti-prostate specific antigen (PSA) Fab coupled with 245-bp DNA was resolved from PSA-Fab-DNA complex in ~ 1 cm using the Agilent 2100 Bioanalyzer[26]. In comparison, coupling 626-bp DNA to anti-alpha-fetoprotein (AFP) Fab was less successful and required formation of a sandwich immune complex with an additional antibody to fully resolve the immune complex.

Electrophoretic immunoassays completed in millimeters-long separation lengths have also been reported using bulk flow, including electroosmosis and pressure driven flow, to counteract electrophoresis[28, 29]. A gradient elution moving boundary electrophoresis (GEMBE) assay enabled electrophoretic immunoassays for protein kinase A in 3 mm separation lengths [28]. During separation, a pressure and electroosmotic-driven buffer counter flow was gradually decreased, thus allowing elution of target analytes one-by-one into a capillary in order of decreasing electrophoretic mobility. Detection was accomplished by monitoring either a step increase in fluorescence passing by a single-point detector [30] or a change in channel current [28] (which indicated entry of new target analyte into the channel) thus obviating the need to spatially resolve analytes into individual bands, as is required in conventional electrophoresis. Lastly, techniques such as spectral multiplexing and concurrent two-color detection[31] as well as affinity reagent mobility adjustment[26, 32] enabled development of simultaneous immunoassays in a single channel without increasing separation length or chip footprint.

Microfluidic formats incorporating *in-situ* sieving matrices have also improved electrophoretic immunoassay performance and have been implemented in a wide range of formats (i.e., cross-linked gels[23, 33, 34], non-cross-linked gels[22, 27, 35], nanofabricated structures[29]). Sieving matrices

enhance mobility differences among analytes and can be optimized by tuning the pore-size, while eliminating bulk flow and minimizing non-specific adsorption. Using 1% methylcellulose as a sieving matrix, a competitive immunoassay toward human serum albumin resolved species in a separation length of 1 cm at 300 V/cm[35]. In a different approach to sieving matrices, two-dimensional nano-sieving arrays with anisotropically etched trenches resolved large immune complexes from smaller antibodies in a 400 μm x 1 mm sub-region of a 5 mm x 5 mm chamber[29]. In yet a different approach, photopatterned cross-linked gels yield nanoporous sieving structures without dedicated nanofabrication facilities. Photopolymerization enables spatial control of characteristics such as gel pore-size and pore-size gradients, thus allowing optimization of separation performance and integration of preparatory functionality.

Use of uniform pore-size polyacrylamide (PA) gels was demonstrated by our group and collaborators for protein sizing and homogeneous immunoassays[33, 34, 36]. Direct assays for tetanus antibody and competitive assays for tetanus toxin were completed in an effective separation length of 6 mm at 300 V/cm[33]. Also using uniform pore-size PA gels, ricin toxin was quantified with an effective separation length of 5 mm[34]; however, an overlap of toxin-antibody complex peak and antibody peak at the detection point suggests separation performance for ricin detection could be further improved through, for example, spatially tuning the pore-size of the sieving matrix. While homogeneous electrophoretic immunoassays in gradient gels have not been reported, protein sizing using gradient pore-size gels and pore limit gel electrophoresis have shown promise [37, 38]. A microscale gradient gel with a large-to-small pore-size distribution in the separation channel resolved SDS-treated proteins with molecular weights ranging from 20 to 205 kDa in a separation length of 4 mm at 298 V/cm.[37] Just as in the slab-gel macroscale counterpart, decreasing pore-size gradients impart additional resolution and sensitivity, as species migrating along the separation axis continuously sharpen. While microchip discontinuous (stacking) gels have been previously described for microfluidic DNA[39] and protein sizing[40, 41], no known efforts exist to harness the format for ultra-short separation length electrophoretic immunoassays.

## 2.4 Thesis contribution: development of homogeneous immunoassay with ultra-short separation length

In the first part of my thesis work (chapters 2 – 6), I present the development, optimization, and demonstration of electrophoretic immunoassays with an ultra-short separation length. A systematic approach to assay development allows us to optimize the homogeneous electrophoretic immunoassay performance.

Key design and implementation considerations for homogeneous immunoassays are first discussed in Chapter 3. In particular, we optimized assay operation for (1) reliable complex formation during the incubation stage and (2) effective resolution of immune complexes during the separation stage. Photopolymerization allows spatial control of gel composition: a large pore size loading gel facilitates introduction of large immune complexes and a decreasing pore-size gradient separation gel resolves immune complexes. Using gradient gels, immunoassays for inflammation biomarkers were completed within separation lengths of 1 mm and in < 1 min.

Multiplexed biomarker measurements using spectral multiplexing are presented in Chapter 4. Simultaneous quantitation of the proteins C reactive protein (CRP) and tumor necrosis factor-

alpha (TNF-α) is performed on gradient pore-size separation gels using spectral multiplexing. Both proteins are important components of inflammation and host response[42-44]. Spectral multiplexing increases the number of markers analyzed without increasing separation channel length or separation time and without increasing the number of channel networks and electrical connections

Analysis of separation resolution revealed assay implementation in discontinuous pore-size gels can further improve separation efficiency. While gradient gel may be more appropriate for fractionation of proteins spanning a large range of molecular weights, discontinuous gels are optimal for separation of antibodies and immune complexes by enhancing the relative mobility difference ($\Delta\mu/\mu$) between the pair of interests. During optimization, we introduce a new fabrication technique to eliminate protein exclusion and "destacking" dispersion associated with previously reported on-chip discontinuous gels[33, 41]. The optimized fabrication technique introduced in Chapter 5 is widely applicable to fabrication of various functional polymer units (e.g., membranes, filters, and blotting gels) in microfluidic channels.

Chapter 6 presents the optimization of discontinuous gel architecture for homogeneous immunoassays. At baseline resolution for the CRP assay, the discontinuous gel architecture yields 3 to 5 times reduction in separation length and time as compared to our previous gradient gels. Furthermore, the pore-size discontinuity acts to "stack" the proteins, thus improving the signal-to-noise ratio by up to 8 times. By accomplishing separations in unprecedented separation lengths (< 350 μm) through design optimization, our development contributes to improving portability of on-chip homogeneous immunoassays. Besides the capability to quantify multiple biomarkers in a rapid and low power fashion, the discontinuous gel architecture is also suitable for continuous monitoring through sequential loading and injections. Lastly, we present future design ideas to adapt discontinuous gel architecture for point-of-care testing.

## 2.5    References

(1)    Zolg, J. W.; Langen, H. *Molecular & Cellular Proteomics* **2004**, *3*, 345-354.
(2)    Etzioni, R.; Urban, N.; Ramsey, S.; McIntosh, M.; Schwartz, S.; Reid, B.; Radich, J.; Anderson, G.; Hartwell, L. *Nature Reviews Cancer* **2003**, *3*, 243-252.
(3)    Cholestech. http://www.cholestech.com/products/ldx_overview.htm
(4)    Millipore,2008.
       http://www.millipore.com/publications.nsf/a73664f9f981af8c852569b9005b4eee/348ee7
       096d93729b85256bf40066a40d/$FILE/tb500en00.pdf
(5)    Gervais, L.; Delamarche, E. *Lab on a Chip* **2009**, *9*, 3330-3337.
(6)    Hosokawa, K.; Omata, M.; Sato, K.; Maeda, M. *Lab on a Chip* **2006**, *6*, 236-241.
(7)    Fan, R.; Vermesh, O.; Srivastava, A.; Yen, B. K. H.; Qin, L. D.; Ahmad, H.; Kwong, G. A.; Liu, C. C.; Gould, J.; Hood, L.; Heath, J. R. *Nature Biotechnology* **2008**, *26*, 1373-1378.
(8)    Bernard, A.; Michel, B.; Delamarche, E. *Analytical Chemistry* **2001**, *73*, 8-12.
(9)    Yeung, W. S. B.; Luo, G. A.; Wang, Q. G.; Ou, J. P. *J Chromatogr B* **2003**, *797*, 217-228.
(10)   Ou, J. P.; Wang, Q. G.; Cheung, T. M.; Chan, S. T. H.; Yeung, W. S. B. *Journal of Chromatography B* **1999**, *727*, 63-71.

(11) Koutny, L. B.; Schmalzing, D.; Taylor, T. A.; Fuchs, M. *Analytical Chemistry* **1996**, *68*, 18-22.

(12) Schmalzing, D.; Koutny, L. B.; Taylor, T. A.; Nashabeh, W.; Fuchs, M. *Journal of Chromatography B* **1997**, *697*, 175-180.

(13) Taylor, J.; Picelli, G.; Harrison, D. J. *Electrophoresis* **2001**, *22*, 3699-3708.

(14) Chiem, N.; Harrison, D. J. *Analytical Chemistry* **1997**, *69*, 373-378.

(15) Roper, M. G.; Shackman, J. G.; Dahlgren, G. M.; Kennedy, R. T. *Analytical Chemistry* **2003**, *75*, 4711-4717.

(16) Dishinger, J. F.; Kennedy, R. T. *Analytical Chemistry* **2007**, *79*, 947-954.

(17) Dishinger, J. F.; Reid, K. R.; Kennedy, R. T. *Analytical Chemistry* **2009**, *81*, 3119-3127.

(18) Heegaard, N. H. H.; Kennedy, R. T. *Journal of Chromatography B-Analytical Technologies in the Biomedical and Life Sciences* **2002**, *768*, 93-103.

(19) Verpoorte, E. *Electrophoresis* **2002**, *23*, 677-712.

(20) Amundsen, L. K.; Siren, H. *Electrophoresis* **2007**, *28*, 99-113.

(21) Hou, C.; Herr, A. E. *Electrophoresis* **2008**, *29*, 3306-3319.

(22) Kawabata, T.; Wada, H. G.; Watanabe, M.; Satomura, S. *Electrophoresis* **2008**, *29*, 1399-1406.

(23) Herr, A. E.; Hatch, A. V.; Throckmorton, D. J.; Tran, H. M.; Brennan, J. S.; Giannobile, W. V.; Singh, A. K. *Proceedings of the National Academy of Sciences of the United States of America* **2007**, *104*, 5268-5273.

(24) Cheng, S. B.; Skinner, C. D.; Taylor, J.; Attiya, S.; Lee, W. E.; Picelli, G.; Harrison, D. J. *Analytical Chemistry* **2001**, *73*, 1472-1479.

(25) Bromberg, A.; Mathies, R. A. *Electrophoresis* **2004**, *25*, 1895-1900.

(26) Kawabata, T.; Watanabe, M.; Nakamura, K.; Satomura, S. *Analytical Chemistry* **2005**, *77*, 5579-5582.

(27) Park, C. C.; Kazakova, I.; Kawabata, T.; Spaid, M.; Chien, R. L.; Wada, H. G.; Satomura, S. *Analytical Chemistry* **2008**, *80*, 808-814.

(28) Ross, D.; Kralj, J. G. *Analytical Chemistry* **2008**, *80*, 9467-9474.

(29) Yamada, M.; Mao, P.; Fu, J. P.; Han, J. Y. *Analytical Chemistry* **2009**, *81*, 7067-7074.

(30) Shackman, J. G.; Munson, M. S.; Ross, D. *Analytical Chemistry* **2007**, *79*, 565-571.

(31) Guillo, C.; Roper, M. G. *Electrophoresis* **2008**, *29*, 410-416.

(32) Yang, P. L.; Whelan, R. J.; Mao, Y. W.; Lee, A. W. M.; Carter-Su, C.; Kennedy, R. T. *Analytical Chemistry* **2007**, *79*, 1690-1695.

(33) Herr, A. E.; Throckmorton, D. J.; Davenport, A. A.; Singh, A. K. *Analytical Chemistry* **2005**, *77*, 585-590.

(34) Meagher, R. J.; Hatch, A. V.; Renzi, R. F.; Singh, A. K. *Lab on a Chip* **2008**, *8*, 2046-2053.

(35) Mohamadi, M. R.; Kaji, N.; Tokeshi, M.; Baba, Y. *Analytical Chemistry* **2007**, *79*, 3667-3672.

(36) Herr, A. E.; Singh, A. K. *Analytical Chemistry* **2004**, *76*, 4727-4733.

(37) Lo, C. T.; Throckmorton, D. J.; Singh, A. K.; Herr, A. E. *Lab on a Chip* **2008**, *8*, 1273-1279.

(38) Sommer, G. J.; Singh, A. K.; Hatch, A. V. *Lab on a Chip* **2009**, *9*, 2729-2737.

(39) Brahmasandra, S. N.; Ugaz, V. M.; Burke, D. T.; Mastrangelo, C. H.; Burns, M. A. *Electrophoresis* **2001**, *22*, 300-311.

(40) Das, C.; Zhang, J.; Denslow, N. D.; Fan, Z. H. *Lab on a Chip* **2007**, *7*, 1806-1812.

(41)    Yang, S.; Liu, J. K.; Lee, C. S.; Devoe, D. L. *Lab on a Chip* **2009**, *9*, 592-599.

(42)    Ridker, P. M.; Hennekens, C. H.; Buring, J. E.; Rifai, N. *New England Journal of Medicine* **2000**, *342*, 836-843.

(43)    Ulloa, L.; Tracey, K. J. *Trends in Molecular Medicine* **2005**, *11*, 56-63.

(44)    Kishore, U.; Gaboriaud, C.; Waters, P.; Shrive, A. K.; Greenhough, T. J.; Reid, K. B. M.; Sim, R. B.; Arlaud, G. J. *Trends in Immunology* **2004**, *25*, 551-561.

# Chapter 3 On-chip Homogeneous Immunoassay Design and Development

This chapter discusses implementation of on-chip homogeneous immunoassays from a design perspective. Homogeneous immunoassays rely on formation and detection of immune complexes to measure target analyte concentration. Therefore, we optimized assay operation for (1) reliable complex formation during the incubation stage and (2) effective resolution of immune complexes from excess affinity probes during the separation stage. The studies documented in this chapter form the basis for our published work on ultra-short separation length homogeneous immunoassays using microchip polyacrylamide gradient and discontinuous gels[1, 2].

This chapter first describes a typical workflow of using microchip gel electrophoresis for protein analysis (3.2) with details provided on how to achieve void-free separation matrices (3.3) and how to optimize voltage programming for efficient separations (3.4). Next, we present the challenges that we have encountered in resolving immune complexes which led to the application of microchip gradient gels for immunoassays (3.5). Lastly, we will present three approaches to improve assay sensitivity (3.6).

## 3.1    Inflammation biomarker of interests

We are interested in developing on-chip immunoassays for rapid quantitation of C reactive protein (CRP) and tumor necrosis factor-alpha (TNF-α). CRP is an indicator of cardiovascular risk[3] and TNF-α is a marker of inflammation with putative potential for sepsis diagnosis and treatment[4]. Both analytes play important roles in the basic mechanisms of inflammatory response[5]. CRP exists as a pentamer with monomeric molecular mass of 23 kDa. TNF-α has a monomeric molecular mass of 17 kDa and forms trimers in biological systems. Measurement of CRP is clinically applied toward assessment of cardiovascular risk[6]: CRP concentration less than 1 mg/L indicates a low risk and a concentration higher than 3 mg/L indicates a high risk; moreover, repeated measurements of CRP concentration above 10 mg/L indicate presence of infections, inflammatory diseases, and/or trauma. Rapid measurement of TNF-α, which enables more timely delivery of TNF antibody, can increase treatment effectiveness for severe sepsis.

## 3.2    Overview of assay workflow

Figure 3-1 depicts a typical work flow for implementing an on-chip homogeneous immunoassay. Homogeneous immunoassays eliminate surface immobilization and uses electrophoresis to resolve bound immune complexes. The sample, which contains analytes of interest, is incubated in an eppendorf tube with fluorescently labeled antibodies with specificity toward the target analytes. When the antibody concentration is in excess of the analyte concentration, the amount of immune complexes formed is directly proportional to target analyte concentration. Following incubation, 5 μL of incubate mixture is transferred into chip reservoirs for on-chip analysis. Sample injection and separation are initiated by applying voltages through platinum electrodes inserted in individual reservoirs. By applying an electric field across the top and bottom wells, sample is first loaded vertically. A tight injection plug is formed by voltage pinching from the horizontal channels. The electric field is subsequently switched across the horizontal channels and the separation step is initiated. With optimized separation conditions, the larger immune

complexes are resolved from the smaller antibodies. In our work, imaging uses an inverted epi-fluorescence microscope (Olympus IX70) equipped with a cooled CCD camera (CoolSnap HQ2, Princeton Instruments). Besides using a CCD camera to image a region of interest, fluorescence intensity at a detector point within the channel can also be plotted versus time as an electropherogram. In summary, electrophoretic immunoassays accomplish analyte detection in 2 steps (i.e., loading and separation) as compared to the 5-6 steps required by even the simplest surface based biosensors.
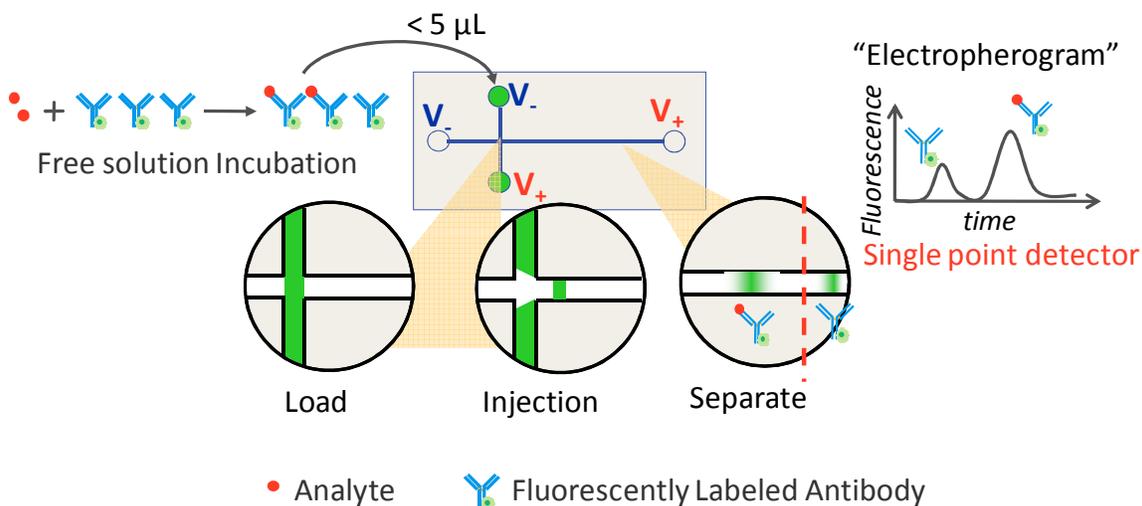


Figure 3-1. On-chip homogeneous immunoassays accomplish analyte detection by electrophoretic separation.

A key step in homogeneous immunoassays is to resolve immune complexes from antibodies within the allowed separation length. Proper choice of sieving matrices leads to successful assay completion. Therefore, significant efforts have been devoted to optimizing gel fabrication and characterizing separation performance. Figure 3-2 outlines a typical workflow of assay characterization with equipment listed for each step. Details on gel fabrication, imaging, and assay characterization are provided in section 3.3 and 3.4.
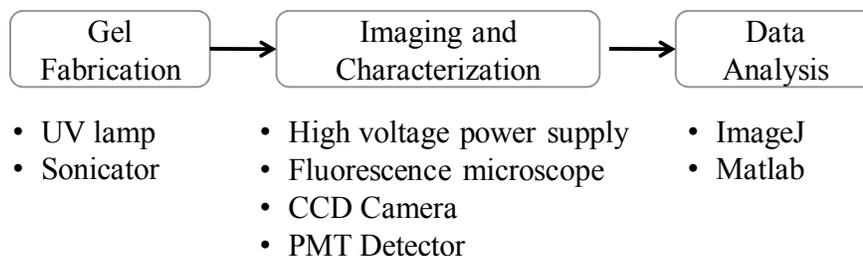


Figure 3-2. A typical workflow to characterize on-chip homogeneous immunoassays.

## 3.3    Fabrication of in-situ sieving matrices

Polyacrylamide (PA) gel is fabricated within microfluidic channels via photopolymerization to increase relative mobility differences between the immune complexes and antibodies. As the

18

larger immune complexes would be retarded more significantly compared to unbound affinity reagents (i.e., smaller antibodies), performing separations in PA gel lead to assay completion in shorter times as well as shorter separation lengths as compared to electrophoretic separations in free solution. Figure 3-3 outlines a protocol of fabricating polyacrylamide gel within microfluidic channels. The purpose, reagents required, and equipment used are summarized for each step. Also included are brief notes on achieving void-free and high quality PA gel for conducting homogeneous immunoassays. After each fabrication step, chips are inspected on a microscope under bright field view. As we shall see in later sections, there are two advantages of using photopolymerized PA gels: (1) the pore-size of the PA gel can be tuned by adjusting precursor concentration and (2) photopatterning allows spatial control over gel pore-sizes within the microfluidic channels. The following sections (3.3.1-3.3.4) provide a more comprehensive protocol of PA gel fabrication within microfluidic channels.

| | NaOH Wash | → | Silane Coating | → | Prepare and Load PA Precursor | → | Gel Polymerization |
|---|---|---|---|---|---|---|---|
| **Purpose** | Clean channels and deprotonate silanol groups | | Enable covalent attachement of PA to glass walls | | Control gel composition | | Create sieving matrix |
| **Chemicals needed** | • NaOH<br>• DI Water | | • Silane<br>• Acetic acid<br>• Methanol<br>• Water | | • Photoinitiator<br>• Acrylamide/bisacryl amide solution<br>• Buffer<br>• Water | | |
| **Equipments used** | Vacuum | | • Vacuum<br>• Sonicator | | • Vacuum<br>• Sonicator | | • UV lamp<br>• UV meter |
| **Notes to achieve high quality PA gels** | Clean chip wells using vacuum prior to introducing new fluid | | Make sure no bubbles were loaded into the channel. Remove all silane after incubation. | | Perform thorough degassing of precursor solution. Load precursor solution into channels immediately after use. | | Align lamp to the center of the chip. |

Figure 3-3. Overview of gel fabrication within a microfluidic channel. Depicted here is a general protocol of fabricating uniform pore size gels with 1 photopatterning step.

### 3.3.1 Surface treatment

To enable covalent attachment of the PA gel to channel walls, microchannels were coated with a self-assembled silane monolayer[7] (Figure 3-4). Bare channels were first incubated with 1 M NaOH for 10 minutes, flushed with DI water, and then purged by vacuum. NaOH removes debris in the microfluidic channels and deprotonates silanol groups on the glass walls. A degassed 2:3:5 (v/v/v) mixture of 3-(trimethoxysilyl)-propyl methacrylate, glacial acetic acid, and DI water was then introduced into the channels via capillary flow for silane monolayer formation. Following a 30 min incubation, the channels were rinsed for 10 min with methanol, DI water and purged with vacuum.
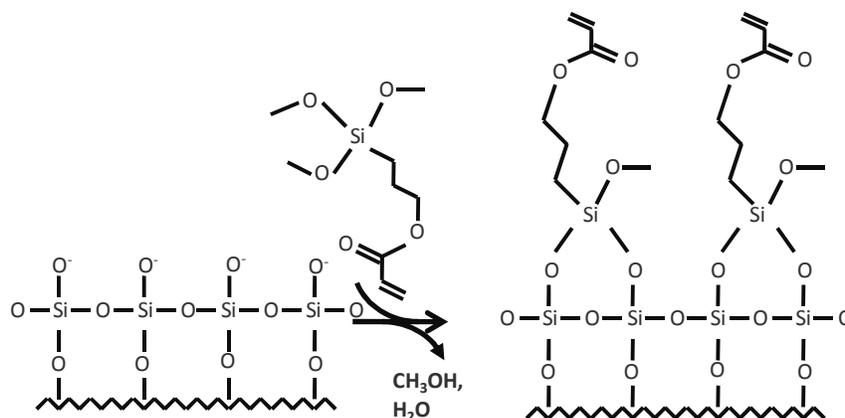
Figure 3-4. Silane coating of glass channels enables covalent linkage to polyacrylamide gels.

Tips for surface treatment: To prevent introduction of new debris into the channels, the chip wells were vacuum prior to introduction of any fluids. All silane within the channel must be removed after the 30 min silanization period else silane residue may lead to bubble formation during gel polymerization process. Provided here is a procedure with high efficacy in removing silane residues. Following a 30 min incubation period, silane solution from the channels was first purged by vacuum, methanol was then wicked into the channels and purged by vacuum, and water was subsequently wicked into all channels and removed by vacuum. Two to three iterations of methanol and water rinse are often required to remove all silane residue.

### 3.3.2    Precursor solution preparation

PA gel precursor solutions of the appropriate acrylamide concentration (T) were prepared by diluting 30% (w/v) acrylamide/bis-acrylamide solution with Tris/glycine native electrophoresis buffer to a total volume containing 0.2% (w/v) VA-086 photoinitiator (PI). A general formula to calculate 30% (w/v) stock solution, 10x Tris/glycine buffer, and water needed to prepare precursor solution with a target acrylamide concentration of T is provided below:

$$\text{30\% Acrylamide Stock Solution Needed (\textmu L)}=\frac{\text{target acrylamide concentration (w/v)}}{\text{30\% (w/v)}}$$

$$\cdot\frac{\text{weight of PI (mg)}}{\text{1 mg}}\cdot 500\ \text{\textmu L}$$

$$\text{10x Tris/Glycine Buffer Needed (\textmu L)}=\frac{\text{weight of PI (mg)}}{\text{1 mg}}\cdot 50\ \text{\textmu L}$$

$$\text{DI water (\textmu L)}=\frac{\text{weight of PI (mg)}}{\text{1 mg}}\cdot 500\ \text{\textmu L}$$
$$-\ \text{10x Tris/Glycine Buffer Used (\textmu L)} - \text{30\% Acrylamide stock solution used (\textmu L)}$$

The above formulation works well for fabricating gels with %Ts ranging from 3% to 8%. Reducing PI concentration to 0.18% (w/v) is more suitable for fabricating 2.5%T gels. Reducing photoinitiator concentration promotes the growth of long linear polymer strands and improves gel rigidity at low acrylamide concentration[8].

Precursor solutions were vigorously sonicated and degassed prior to use, as is critical to ensure a void-free PA gel. Immediately after preparation, precursor solutions were wicked into microfluidic channels by capillary flow.

Tips for effective sonication: effective degassing is achieved with ~500 μL liquid in eppendorf tubes and water level in sonicator at ~5mm below the liquid level in eppendorf tubes. Agitation at different frequencies helps to remove air bubbles. For sonication lasting longer than 5 min, monitor water temperature in the sonicator and replenish water if necessary to prevent heating.

Tips for precursor solution introduction: precursor solution is first introduced into the well that was connected to the channel with the lowest hydrodynamic resistance. After the solution has wicked through all channels, fill all other wells with precursor solutions. Inspect under a microscope to make sure there are no air bubbles within the channels. If bubbles are found, remove precursor solution by vacuum, rinse with water, and reintroduce precursor solution. To prevent evaporation during flood exposure of the entire chip, pipette tips were fitted into the chip wells and 7- 10 μL precursor solution was introduced into each reservoir.

### 3.3.3 UV Polymerization

PA gel was created via UV initiated polymerization. UV radiation initiates formation of free radicals that lead to polymerization. As shown in Figure 3-5, linear acrylamide polymer strands are crosslinked by bisacrylamide bridges.
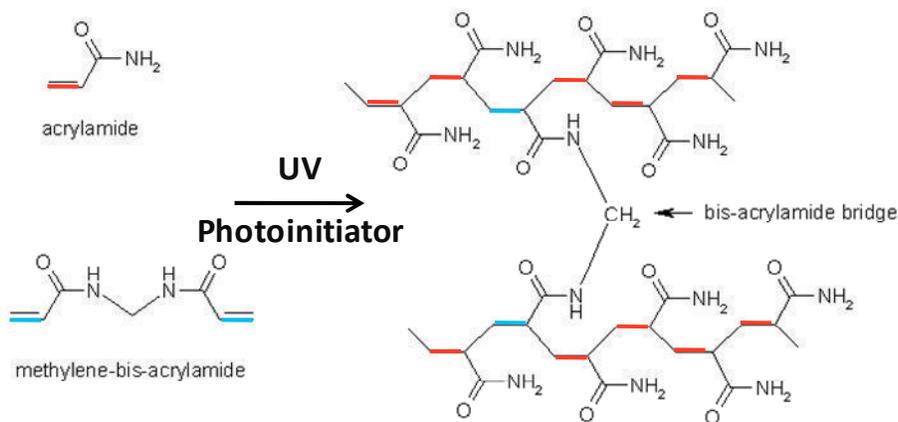


Figure 3-5. UV irradiation initiates polyacrylamide gel formation.

For uniform gel polymerization, the chip, which contained precursor solution with desired acrylamide concentration (T), was first aligned to a UV light source located 18 cm away (at a power intensity of 10 mW/cm$^2$ measured at the plane of the chip). The chip was then exposed for 8 min via flood exposure to a fan-cooled, spectrally filtered mercury lamp (300 – 380 nm, 100W, UVP, B100-AP, Upland, CA). After polymerization, the chips were inspected under a microscope to ensure there were no bubbles in the loading and separation gels. Chips were stored in 1x Tris/glycine buffer at 4C prior to use.

Tips for polymerization using UV lamp: the UV lamp requires a warm up time of ~5 min for stabilized power intensity. Guided by UV intensity measurement, align the chip to the center of the illumination source and adjust the chip to lamp distance for consistent illumination power.

Turn on cooling system to prevent heating which leads to bubble formation during polymerization process.

### 3.3.4 Gradient gel fabrication

Decreasing pore-size gradient gels have been reported by our group and collaborators previously for protein sizing[9] with the capability of sizing 20-116 kDa proteins within 3 mm of separation distance. As uniform pore gels are not optimal for on-chip separations of immune complexes from antibodies (3.5.4), we applied gradient gels for immunoassay development.

Described here is an optimized protocol for fabricating a 2.5%T-to-8%T gradient gel. Surface treatment and precursor preparation follow the protocol for uniform gel fabrication. The pore-size gradient is created through two photopatterning steps with different precursor concentrations and a diffusion step was performed in between. High percentage acrylamide gel precursor solution (8%T) was introduced into all channels (Figure 3-6-1), a 6 min exposure to UV (fan-cooled 100 W mercury lamp 16 cm away, 12 mW/cm$^2$ at chip plane) with photomasking yielded a gel plug at the end of the separation channel (Figure 3-6-2), unpolymerized high percentage acrylamide gel precursor solution in the loading channel was flushed out and replaced with low percentage gel acrylamide precursor solution (2.5%T) (Figure 3-6-3), a gradient-generating diffusion period of 5 min ensued, and lastly an 8 min flood UV exposure of the entire chip at 10 mW/cm$^2$ was completed (Figure 3-6-4). Consequently, the loading channel housed a large pore-size (2.5%T) PA gel and the separation channel housed a large-to-small pore-size PA gel gradient (i.e., 2.5%T-to-8%T).
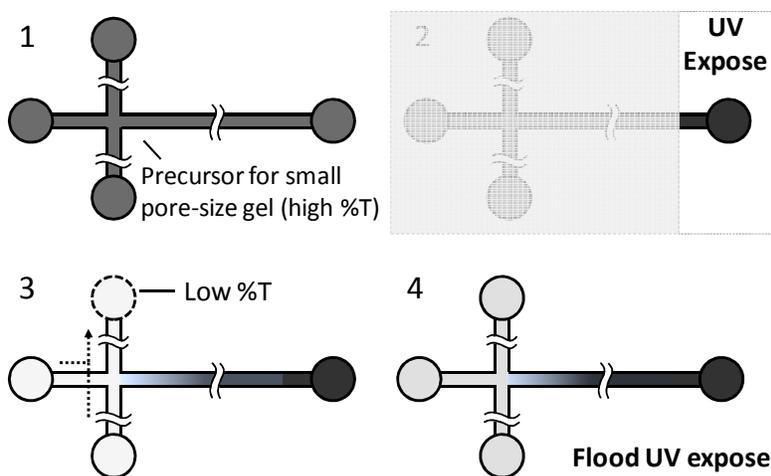


Figure 3-6. Gradient gel fabrication within microfluidic glass channels: a 2-step photopatterning process enables spatial control of nanoporous structures.

## 3.4 Imaging and characterization of on-chip gel electrophoresis

### 3.4.1 Optimized voltage programming for efficient injection and separation

As depicted in Figure 3-1, voltage programming initiates sample loading and separation. For efficient interfacing of microfluidic channels to external control, an in-house machined manifold clamped the chip between a Delrin top housing and an aluminum frame; O-rings in the top housing sealed around the chip reservoirs. The four reservoirs in use are designated as Sample

(S), Sample Waste (SW), Buffer (B), and Buffer Waste (BW). The SW, B, BW reservoirs were filled with 50 µL of 1x native Tris-glycine buffer and a 5 µL protein sample filled the S reservoir. Voltage was applied using a programmable high voltage power supply (LabSmith, Livermore, CA) and platinum electrodes inserted into the top manifold reservoirs.

Figure 3-7 shows two types of channel networks for on-chip immunoassay development. For the NS12 chip, the distances from chip intersection to S, SW, B, and BW reservoirs are 0.39, 1.51, 0.74, and 4.56 cm, respectively. For the NS7 chip, the distances from chip intersection to S1/S2, SW, B, and BW reservoirs are 1.072, 1.042, 1.042, and 2.295 cm, respectively. Unless specified, the first mm of the separation channel is imaged during separation.

**NS12 Chip**                    **NS7 Chip**
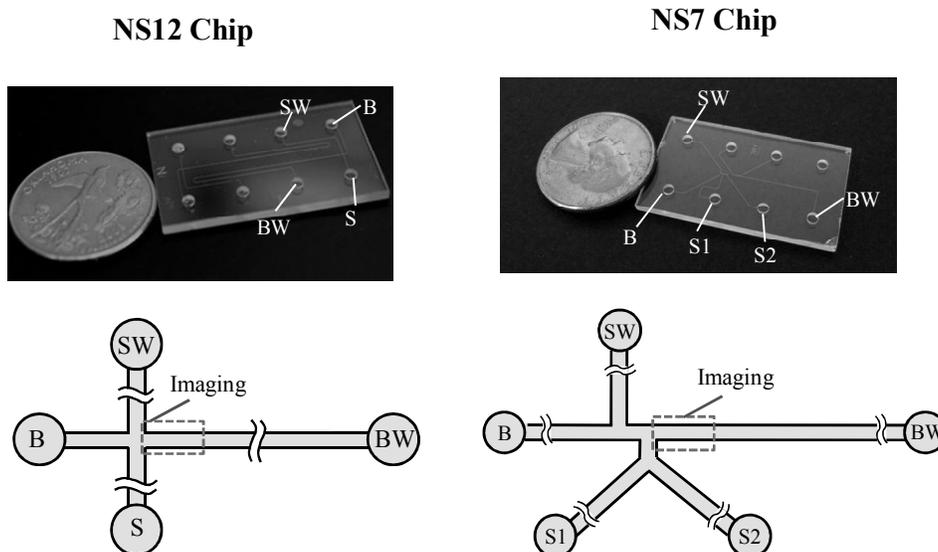


Figure 3-7. Photographs and schematics of microfluidic chips for on-chip immunoassay (Schematics are not drawn to scale).

The electric field within each channel segment was calculated by employing Kirchoff's current law at the injection junction:

$$\frac{V_S - V_O}{R_{SO}} + \frac{V_B - V_O}{R_{BO}} + \frac{V_{SW} - V_O}{R_{SWO}} + \frac{V_{BW} - V_O}{R_{BWO}} = 0$$

$V_S$, $V_{SW}$, $V_B$, and $V_{BW}$ are voltages applied in the sample, sample waste, buffer, and buffer waste wells, respectively. $V_o$ is the voltage at the injection intersection. $R_{SO}$, $R_{BO}$, $R_{SWO}$, and $R_{BWO}$ are resistances of the channel network from injection intersection to S, B, SW, and BW wells, respectively. Assuming uniform channel cross section as well as uniform gel resistivity throughout the chip, channel resistance is proportional to channel length. Voltages at different nodes can be expressed as a function of channel lengths:

$$\frac{V_S - V_O}{L_{SO}} + \frac{V_B - V_O}{L_{BO}} + \frac{V_{SW} - V_O}{L_{SWO}} + \frac{V_{BW} - V_O}{L_{BWO}} = 0$$

The voltage at the injection junction ($V_o$) can be solved by substituting applied voltages at each well and lengths of each channel segments into the above equation. Electric field within each channel segment is calculated through dividing the voltage drop between each well and $V_0$ by the length of the corresponding channel segment.

Optimization of voltage application results in tightly confined sample plug during loading and symmetric sample plug during separation. Described here is a voltage program optimized for conducting separations on the NS12 chip. Samples were electrophoretically loaded for 2 min by applying 450 V to SW while the S, B, and BW reservoirs were grounded ($E = 160$ V/cm in loading channel). Prior to separation, -100 V was applied to the BW reservoir for 10 s to form a symmetrically pinched injection plug. Separation was initiated by applying 800 V to BW, grounding B, 400 V to S, and 600 V to SW to inject a well-defined "pinched" sample plug. The resulting electric field strength in the separation channel was $E = 102$ V/cm.

Table 3-1 summarizes the electric field calculated for each channel segment during on-chip testing. A positive electric field indicates that negatively charged proteins and buffer ions are flowing into the corresponding wells whereas a negative electric field indicates that negatively charged species are flowing out of the corresponding wells. During separation, applying "pull-back" voltages at S and SW wells and balancing the electric field in the SO and SWO branches result in a symmetric injected plug with minimal leakage. As illustrated in chapter 1, minimizing injection plug standard deviation ($\sigma_0$) improves separation resolution (SR). However, pull-back voltages applied in wells S and SW cannot be increased indefinitely as further increasing pull voltages would reduce electric field in the separation channel ($E_{BWO}$) and increase electric field in the channel segment between O and B ($E_{BO}$). Reducing $E_{BWO}$ leads to decreased separation speed and separation resolution; increasing $E_{BO}$ leads to gel breakdown due to Joule heating.

Table 3-1. Equivalent electric fields within each channel segment during loading, pinched injection, and separation.

| Programming Steps | $E_{SO}$ | $E_{SWO}$ | $E_{BO}$ | $E_{BWO}$ |
|---|---|---|---|---|
| Loading | -160 V/cm | 257 V/cm | -84 V/cm | -13.6 V/cm |
| Pinched Injection | -147 V/cm | 260 V/cm | -78 V/cm | -35 V/cm |
| Separation | 171 V/cm | 176 V/cm | -450 V/cm | 102 V/cm |

### 3.4.2 Full field images and electropherograms to quantify immune complex formation

During chip testing, images were collected using an inverted epi-fluorescence microscope (Olympus IX70) equipped with a 100W mercury arc lamp, a 10x objective, and a Peltier-cooled CCD camera (CoolSNAP HQ2, Roper Scientific, Trenton, NJ). A 0.63x demagnifier (Diagnostic Instruments Inc., Sterling Heights, MI) was used to increase the field of view projected onto the CCD. Unless otherwise stated, the CCD exposure time was 150 ms and images were collected with a $4 \times 4$ pixel binning. Separation results were saved as a stack of images that were later analyzed using image processing software (ImageJ) to generate separation montages and to plot axial intensity profile within the separation channel. Data obtained from ImageJ can be further processed by Matlab to obtain separation resolution for each given time frame.

In this chapter, separation results are presented in two forms: one is a full-field image of the separation channel at a given time and the second is an electropherogram which plots fluorescence intensity at a detector point versus elapsed separation time. Using ImageJ, electropherograms are generated by calculating the average fluorescence intensity within a binned 6 μm × 25 μm region across all separation frames.

## 3.5    Resolving immune complexes

### 3.5.1    Overview of problems and solutions

Homogeneous immunoassays utilize electrophoresis to separate immune complexes from unbound affinity probes. Therefore, the assay is completed when two peaks (antibody and complex) are resolved in the separation channel. In our initial development of homogeneous immunoassays, often only one peak was visible in the separation channel which cannot be used to quantify biomarker concentration. Figure 3-8 summarizes 3 major scenarios that we have encountered in assay troubleshooting, characteristics that can distinguish one cause from another, and solutions that led to successful assay completion.

| Causes of Assay Failures | Characterization | Solutions | |
|---|---|---|---|
| Lack of complex formation | Alternate assay formats (i.e. dot blot assay) confirm little complex formation | Use antibody with high binding affinity | |
| Exclusion of complex | Antibody peak decreases with increasing analyte concentration | Use large pore size loading gel | Use large-to-small gradient pore size gel |
| Poor separation resolution | Alternate assay formats confirm complex formation and slight peak mobility shift observed with increasing analyte concentration | Use small pore size separation gel | |

Figure 3-8. A summary of causes, characteristics, and solutions to assay failures.

The rest of this section details experiments conducted to elucidate the cause toward each assay failure that resulted in application of gradient pore-size gels for on-chip immunoassay.

### 3.5.2    Use high affinity antibody

Poor antibody-antigen binding results in a lack of immune complex formation during incubation. Therefore, only a single peak was observed during analysis. My very first immunoassay for CRP used an antibody (clone CRP-8, Sigma Adlrich) that was developed for western blotting applications. The antibody recognizes an epitope located on CRP that was previously denatured and reduced but has low affinity toward native CRP which was the target analyte in my assay. As a result, only the antibody peak was visible during separation. As commercial vendors do not provide antibody binding affinity, a dot blot assay can confirm antibody-antigen binding affinity by probing proteins printed on a glass slide with fluorescently labeled antibodies[10]. For subsequent CRP immunoassays, using a monoclonal antibody with specificity to full length native protein (clone C5, AbCam, catalog number ab8279) resulted in adequate complex formation even at low nM target analyte concentrations.

Overlabeling of antibodies with fluorescence dyes could adversely affect binding affinity. Appendix A provides an optimized fluorescence labeling protocol. Incubation of antibodies with Alexa Fluor (Invitrogen) dyes at a 1:55 molar ratio attaches 4-8 moles of dyes to 1 mole of

antibody. As shown in later sections, the fluorescently labeled antibodies, which still have sufficient binding affinity, can bind to analytes at low nM concentration.

### 3.5.3 Reduce exclusion of immune complexes

Smaller than desired loading gel pore-sizes exclude immune complexes from entering the separation channel and result in a single peak that belongs to the antibodies in separation. In 3.5.2, a lack of immune complex formation due to insufficient binding affinity is accompanied by little change in the antibody peak shape regardless of target analyte concentration. Here, a decrease in antibody peak height with increasing target analyte concentration indicates formation of immune complexes that are excluded from entering the loading gel. Figure 3-9 shows a set of electropherograms that are generated for CRP immunoassay in a 3.5%T-to-8%T gradient pore-size gel. As shown in Figure 3-9, the decreased Ab* peak height with increased [CRP] indicates that complexes are formed but not introduced into the separation channel.
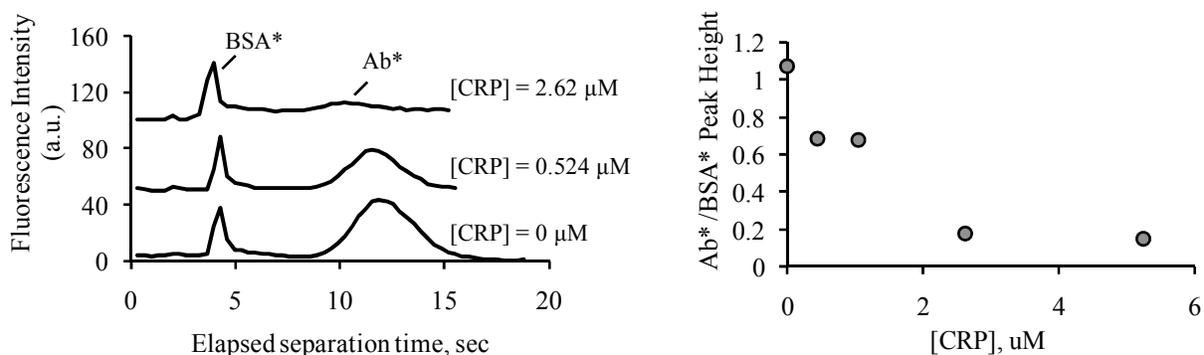


Figure 3-9. Increasing analyte concentration decreases antibody peak height with respect to the internal standard using bovine serum albumin (BSA*). Fluorescence intensity was monitored at 0.8 mm after the injection junction as a function of elapsed separation time. Antibody peak height was normalized to BSA* peak height at different CRP concentrations.

Increasing loading time introduces more complexes for on-chip separation. In a 3.5%T-to-8%T gradient pore-size gel, a loading time of 15 minutes was required to fully introduce the complexes through the injection junction for on-chip separation. Figure 3-10 shows CCD images of the first mm of the 3.5%T-to-8%T gradient pore-size gel after an elapsed separation time of 6 sec. With increased CRP concentration, an increased amount of CRP immune complexes and a decreased amount of Ab* were observed in the separation channel.
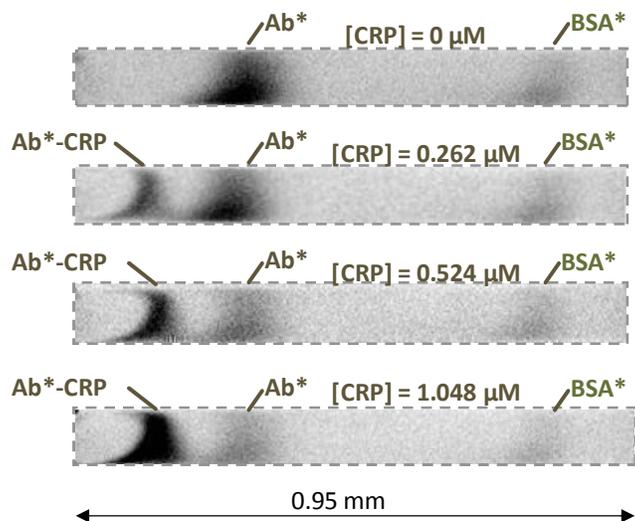
Figure 3-10. The immune complex was resolved from Ab* within the first mm of separation channel on a 3.5%T-to-8%T gradient gel. The initial concentration of anti-CRP Ab* was held constant at 0.45 μM while the concentration of native CRP protein was varied (as indicated on top of each separation image).  BSA* at 0.15 μM was used as an internal standard.

Using larger pore-size loading gels is a more preferred method to introduce immune complexes for on-chip separation. Loading through a 2.5%T requires less than 2 minutes for CRP and TNF complexes in the NS12 chip geometry. However, large pore-size separation gel cannot efficiently resolve immune complexes from antibodies as revealed by only one peak in the separation channel.

### 3.5.4   Apply gradient gels for on-chip immunoassay

Observation of a single peak in separation could be due to the presence of immune complexes that are not resolved from unbound affinity reagents (Ab*). As shown in Figure 3-11, uniform large pore size gels cannot resolve immune complexes from antibodies.  The long loading time required by 3.5%T-to-8%T gradient gels and the poor resolution of 2.5%T uniform gels led to the application of 2.5%T-to-8%T gradient gels for on-chip homogeneous immunoassays.
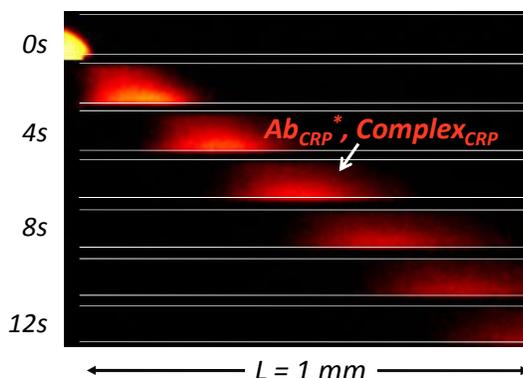


Figure 3-11. Large pore size separation gels (2.5%T) cannot resolve immune complexes from antibodies. Separation was conducted on a NS7 chip. Anti-CRP Ab was labeled with Alexa Fluor 568 dye and imaged using a dsRed2 filter cube.

Using the gradient gel, larger immune complexes can be easily loaded within 2 minutes to the injection junction and are rapidly resolved from antibodies during separation. Using a 2.5%T-to-8%T gradient gel, a direct assay was successfully developed for TNF-α (Figure 3-12). Electrophoregrams (Figure 3-12A), which were generated by monitoring fluorescence intensity at 0.9 mm downstream from the injection junction, revealed all three peaks (BSA*, Ab*, and TNF immune complexes). Immune complex formation (Figure 3-12C) and antibody consumption (Figure 3-12B) were quantified from electropherograms. Increasing TNF-α concentration increases complex formation and decreases the amount of free Ab*. The TNF-α assay developed exhibited a lower limit of detection of 55 nM and was linear up to 550 nM. The decrease in complex formation at TNF-α concentration above 1μM is referred as the "hook" effect[11] possibly due to multivalent interactions between antibodies and trimeric TNF-α proteins. As the "hook" effect can lead to false negative readings, the demonstrated assay is appropriate for measuring target analyte concentration under 550 nM.
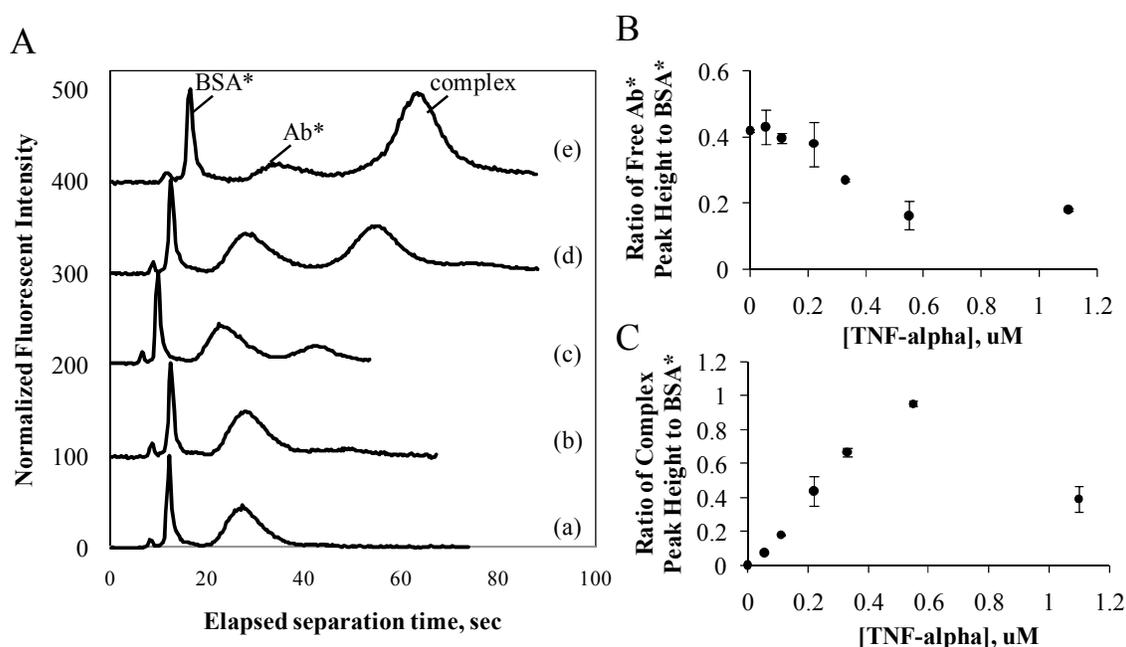


Figure 3-12. Quantitation of TNF-α on a microchip gradient gel. (A) Single point detection of TNF-alpha assay on a NS7A chip with a 2.5%T-to-8%T gradient gel. Anti-TNF-α Ab* concentration is held constant at 0.23 μM and BSA* is held constant at 0.15 μM with increasing [TNF-alpha] at (a) 0 μM, (b) 0.055 μM, (c) 0.11 μM, (d) 0.22 μM, and (e) 0.55 μM. Peak 1 corresponds to free dyes, peak 2 corresponds to BSA*, peak 3 corresponds to free Ab*, and peak 4 corresponds to the immune complex. (B) Ab* peak height is plotted versus [TNF-α]. (C) Complex peak height is plotted versus [TNF-α]. Each data point is averaged from 3 – 5 runs.

## 3.6    Improving assay sensitivity

With the initial assay demonstration in the 2.5%T-to-8%T separation gel, we then improved assay sensitivity from the current 50 nM range to a low nM range. Three strategies were evoked in parallel: (1) decreasing Ab* concentration to resolve low abundance immune complexes

during separation, (2) surface treatment of eppendorf tubes to prevent protein loss during incubation, and (3) selecting antibody with high affinity to promote complex formation during incubation and to reduce complex dissociation during separation.

### 3.6.1 Reducing affinity reagent concentration improves complex visibility

As shown in Figure 3-13, the most equivalent Ab* to complex concentration ratio resolves immune complexes most readily. Although all of the three cases that are displayed exhibit a mathematical separation resolution of 1, reducing relative peak height differences improves the ability to visually resolve neighboring peaks. Therefore, Ab* concentration should be held within a corresponding range of expected target analyte concentration during incubation.
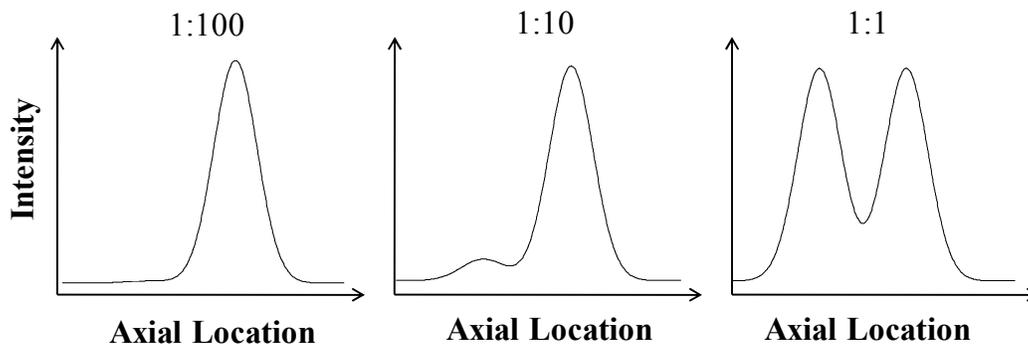


Figure 3-13. Despite the same separation resolution mathematically, visual detection improves when two peaks have similar peak heights. All three separations have a mathematical separation resolution of 1.

### 3.6.2 Surface treatment prevents analyte loss

Nonspecific adsorption of proteins onto eppendorf tubes results in significant protein loss during dilution, mixing, and incubation. Analyte loss due to nonspecific adsorption is especially detrimental when the target analyte is present in low concentration. Coating eppendorf tubes with 5% (w/v) BSA solution prior to protein addition was effective in preventing protein loss. As shown in Figure 3-14B, mixing, diluting, and incubating proteins in 5% (w/v) BSA coated tubes result in detection of immune complexes whereas dilution, mixing, and incubation performed in regular and commercially available nonstick tubes result in significant protein loss (Figure 3-14A).
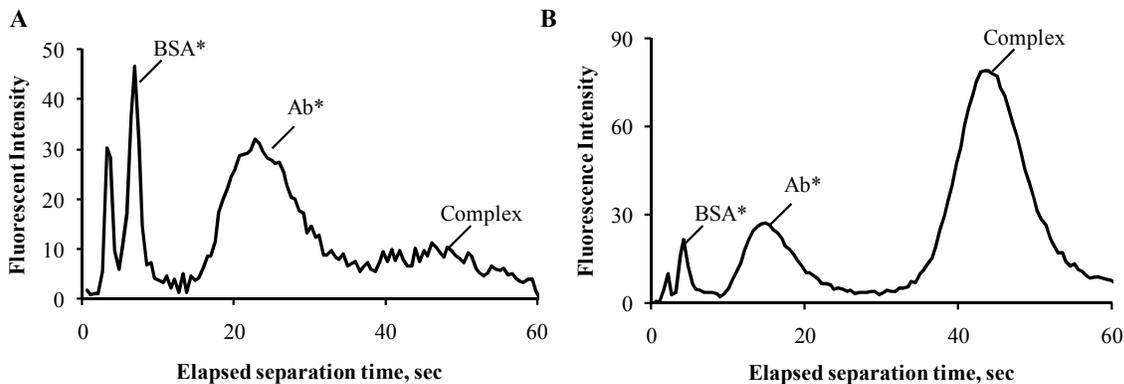


Figure 3-14. Diluting, mixing, and incubating Ab* and target analyte in 5% (w/v) BSA coated tubes recover complex formation. [BSA*] = 30 nM, [Ab*] = 46 nM, and [TNF-α] = 55 nM were

29

diluted, mixed, and incubated in commercially available nonstick and regular eppendorf tubes in (A) whereas they are diluted, mixed, and incubated in tubes previously coated with 5% (w/v) BSA in (B). Both assays were conducted on 2.5%T-to-8%T gradient gels under the same separation conditions.

By optimizing antibody concentration and preventing protein loss during mixing, dilution, and incubation, we are able to complete TNF-α immunoassay on a 2.5%T-to-8%T gradient gel within 1 minute of separation time and 1 mm of separation length. Assay performance was characterized through both full-field imaging within the first mm of separation length (Figure 3-15A) and electropherograms generated at a detector point located 0.85 mm downstream from the injection junction (Figure 3-15B). As shown in both full-field images and electropherograms, complex peak intensity increases with increased presence of Ag in incubation where Ab* peak decreases.
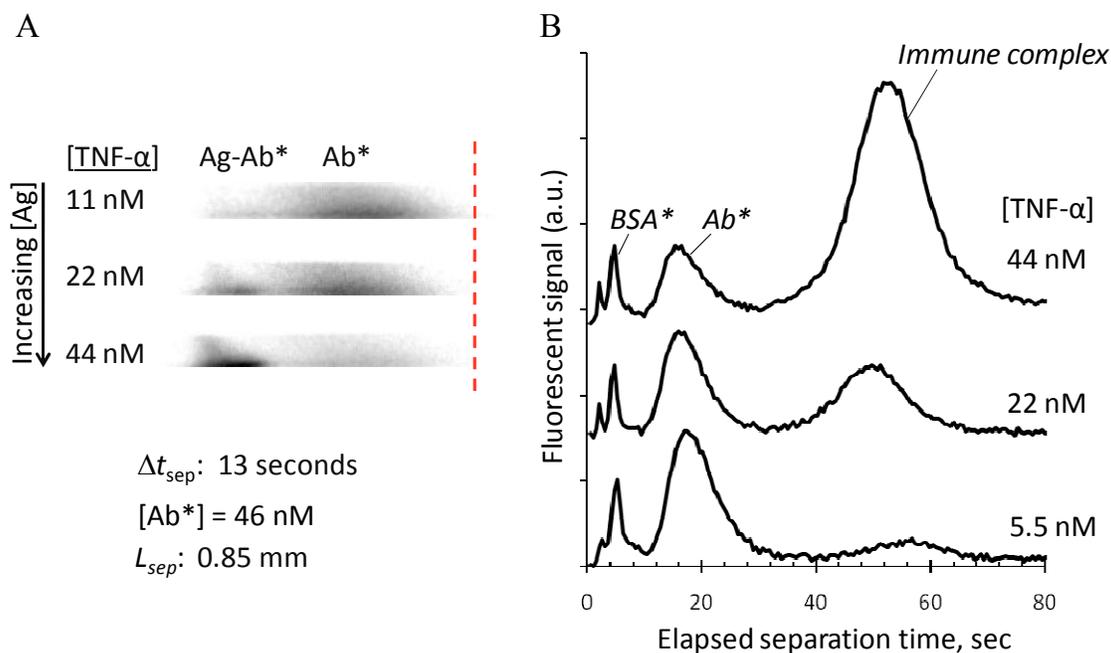


Figure 3-15. TNF-α assay was successfully conducted on a 2.5%T-to-8%T gradient gel in a NS7 chip with improved sensitivity than that was displayed in Figure 3-12. (A) Images of the separation channel at an elapsed separation time of 13 seconds are displayed for three separations with different antigen concentrations. (B) Electropherograms are generated by plotting fluorescence intensity at 0.85 mm downstream from injection junction. Fluorescence intensity signal was normalized to BSA*.

### 3.6.3 Using high affinity antibody increases complex formation
Using antibodies with high affinity toward target analyte enables detection of low concentration immune complexes. Assuming a 1:1 interaction between the antibody and target analyte ($Ab^* + Ag \leftrightarrow Ab^* \cdot Ag$), the amount of immune complex formed is a product of unbound antigen and antibodies divided by the dissociation constant ($K_d$):

$$[Ab^* \cdot Ag] = \frac{1}{K_d}[Ab^*]_{free} \cdot [Ag]_{free}$$

30

Assuming all antibodies ($[Ab^*]_{total}$) in the system are either bound ($[Ab^*{\cdot}Ag]$) or unbound ($[Ab^*]_{free}$), $[Ab^*]_{total} = [Ab^*]_{free} + [Ab^* \cdot Ag]$. We now have: $[Ab^* \cdot Ag] = [Ab^*]_{total} \cdot \frac{[Ag]_{free}}{[Ag]_{free}+K_d}$. Similarly, all antigens in the system are either bound or unbound: $[Ag]_{total} = [Ab^* \cdot Ag] + [Ag]_{free}$. Figure 3-16 plots complex formation ($[Ab^*{\cdot}Ab]$) as a function of total target analyte concentration ($[Ag]_{total}$) for antibodies with different dissociation constants ($K_d$). An antibody with lower dissociation constant has higher affinity toward the antigen and forms more complex at low antigen concentrations. While a low $K_d$ ensures formation of complexes during incubation, a low complex dissociation rate constant ($k_{off}$) ensures integrity of immune complexes during separation. Previous mathematical modeling of nonequilibrium capillary electrophoresis of equilibrium mixtures shows that significant smearing or disappearance of immune complex peak occurs when dissociation rate is larger than the reciprocal separation time[12]. Therefore, antibodies with low dissociation constant and dissociation rate are necessary for complex formation and detection especially at low concentrations.
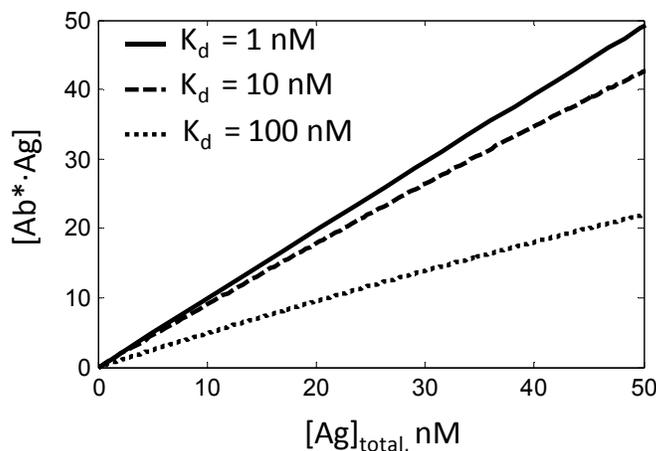


Figure 3-16. Low dissociation constant value, which reflects strong antibody-antigen interactions, improves complex formation at low analyte concentration. $[Ab^*]_{total} = 100$ nM.

Figure 3-17 compares electropherograms generated on 2.5%T-to-8%T gradient gels when CRP was incubated with 2 different monoclonal antibodies (clones C5 and C6, AbCam). When C6 Ab was used, multiple complex peaks, which require additional time to reach the single point detector, were observed in the separation channel. The multiple complex peaks either arise from multivalent interaction between the CRP pentamer and the Ab or from dissociation of complexes due to a high dissociation rate. On the other hand, the C5 Ab, which has higher affinity toward CRP, allows for detection of CRP in the low nM range. Hence, we selected the C5 Ab for future CRP assay development.
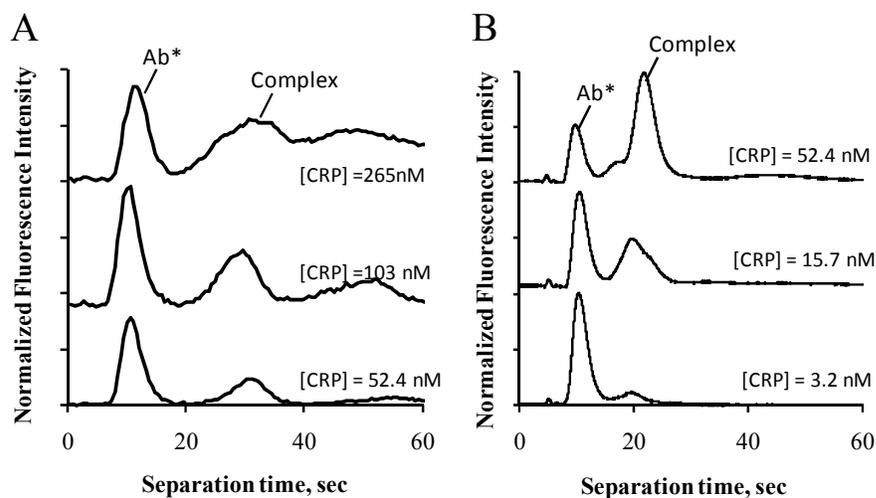
Figure 3-17. Choice of antibodies affects complex formation and detection. Both electropherograms are generated on 2.5%T-to-8%T gradient gels with an injection to detector distance of 0.8 mm. (A) C6 anti-CRP Ab* was labeled with Alexa Fluor 568 and incubated with CRP. (B) C5 anti-CRP Ab* was labeled with Alexa Fluor 568 dyes and incubated with CRP. Antibody concentration was held constant while CRP concentration was increased for different separations.

## 3.7    Summary

In summary, by optimizing sieving matrix composition, immunoassays for inflammation biomarkers (TNF-α and CRP) are developed on microchip gradient gels. Photopolymerization allows spatial control of gel composition: a large pore size loading gel facilitates introduction of large immune complexes and a decreasing pore-size gradient separation gel resolves immune complexes. Separation on gradient gels completes assay within 1 mm of separation length. Three efforts improved assay sensitivity: (1) matching affinity reagent concentration to target analyte concentration, (2) preventing protein loss using surface coatings during incubation, and (3) selecting high affinity antibodies to increase complex formation during incubation and to prevent complex dissociation during separation.  The next 3 chapters build on efforts described here to develop spectrally multiplexed biomarker measurement (chapter 4) and to further reduce separation length which results in lower power electrophoretic assays conducive to battery operation (chapter 5 and 6).

## 3.8    References

(1)    Hou, C.; Herr, A. E. In *Solid-State Sensors, Actuators and Microsystems Conference, 2009.* : Denver, Co, 2009, pp 1574-1577.
(2)    Hou, C.; Herr, A. E. *Analytical Chemistry* **2010**, *82*, 3343-3351.
(3)    Ridker, P. M.; Hennekens, C. H.; Buring, J. E.; Rifai, N. *New England Journal of Medicine* **2000**, *342*, 836-843.
(4)    Ulloa, L.; Tracey, K. J. *Trends in Molecular Medicine* **2005**, *11*, 56-63.

(5)     Kishore, U.; Gaboriaud, C.; Waters, P.; Shrive, A. K.; Greenhough, T. J.; Reid, K. B. M.; Sim, R. B.; Arlaud, G. J. *Trends in Immunology* **2004**, *25*, 551-561.

(6)     Pepys, M. B.; Hirschfield, G. M. *Journal of Clinical Investigation* **2003**, *111*, 1805-1812.

(7)     Herr, A. E.; Singh, A. K. *Analytical Chemistry* **2004**, *76*, 4727-4733.

(8)     BioRad Laboratories.

(9)     Lo, C. T.; Throckmorton, D. J.; Singh, A. K.; Herr, A. E. *Lab on a Chip* **2008**, *8*, 1273-1279.

(10)    Rucker, V. C.; Havenstrite, K. L.; Herr, A. E. *Analytical Biochemistry* **2005**, *339*, 262-270.

(11)    Fernando, S. A.; Sportsman, J. R.; Wilson, G. S. *Journal of Immunological Methods* **1992**, *151*, 27-46.

(12)    Okhonin, V.; Krylova, S. M.; Krylov, S. N. *Analytical Chemistry* **2004**, *76*, 1507-1512.

# Chapter 4 Multiplexed Analysis of Inflammation Biomarkers using Spectrally Encoded On-chip Electrophoresis

## 4.1 Motivation for multiplexed biomarker measurement

Diseases exhibit substantial heterogeneity between individuals; the same disease can be initiated by numerous factors and cause a range of molecular changes and physical manifestations. Consequently, many state-of-the-art single marker diagnostics suffer from a lack of clinical sensitivity and specificity[1]. In contrast, diagnostics that measure or 'profile' multiple protein biomarkers may perform more effectively. We see the development of multiplexed (multi-analyte) clinical and point-of-care diagnostic tools benefitting from microfluidic integration and rapid analyses.

In this chapter, we will describe our contributions in developing technologies that provide multiplexed inflammation biomarker measurements. Inflammation cytokines (i.e., TNF-α, CRP, and interleukins) are produced by the innate immune system as a defense mechanism toward injury, trauma, and infection[2]. However, excess production of these cytokines can be more dangerous than the original stimuli. In the case of severe sepsis, they cause lethal organ failure which leads to death. Severe sepsis is the leading cause of death in intensive care unit and accounts for 9.3% overall death in U.S. Unfortunately, therapeutic treatments by neutralizing cytokines with antibodies have had limited successes. Part of the reason is due to a lack of technologies to quantify inflammation biomarkers (such as TNF-α) with high temporal resolution so neutralizing antibodies can be delivered in the most effective time window[3]. Multiplexed biomarker measurements will provide better understanding of cytokine secretion during severe sepsis and offer new insights for designing future clinical trials. In addition, rapid biomarker measurements afforded by our approach will also allow delivery of treatments in a timely manner.

## 4.2 Existing approaches to multiplexed biomarker detection in electrophoretic immunoassays

Being homogeneous in nature, eletrophoretic immunoassays form the basis for a reusable platform for a multitude of biomarkers. It is rapid and can be automated with programmable power supplies. We can multiplex electrophoretic immunoassays using affinity reagents with specificity toward different biomarkers. Figure 4-1 depicts three different strategies for multiplexed biomarker detection in electrophoretic immunoassays. As different immune complexes exhibit similar mobility, spatial overlap of immune complexes is observed for concurrent assay separations performed in a single channel[4] (Figure 4-1A). Alternatively, separations can be performed in multiple channels in parallel by dedicating each channel to one biomarker (Figure 4-1B). This is currently implemented to improve analysis throughput by microfabricating several networks on a single device[5]. However, usage of multiple channel networks increases the number of electrical connections and requires scanning optical detectors[6].
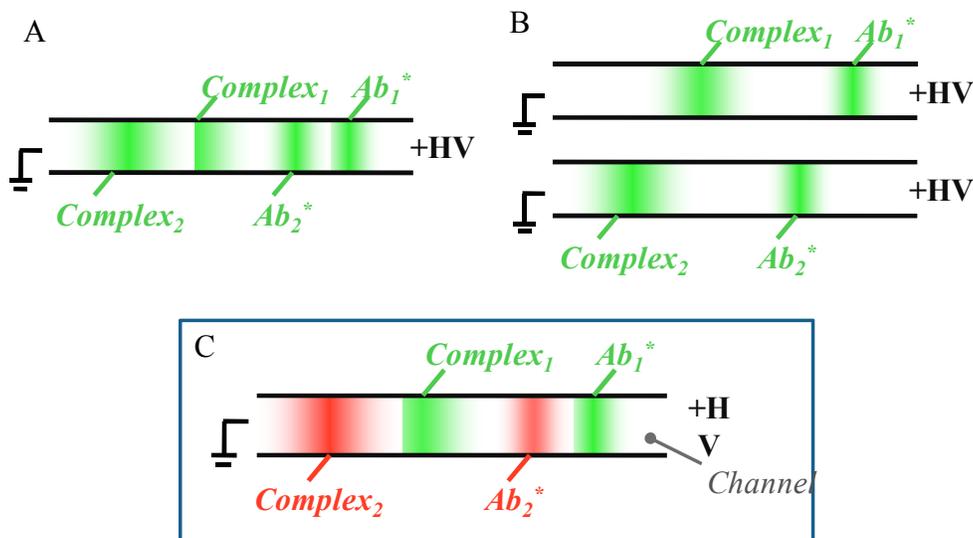
Figure 4-1. Multiplexed biomarker detection can be accomplished in a single channel (A), parallel channels (B), or spectrally multiplexed in a single channel (C).

## 4.3    Our approach: spectral multiplexing

For our multiplexed inflammation biomarker measurement, we employ spectral multiplexing using affinity reagents labeled with spectrally distinct fluorophores (Figure 4-1C). During electropherotic separation, immune complexes with similar mobility are still resolved from each other due to spectral encoding.  Therefore, spectral multiplexing increases the number of markers analyzed without increasing separation channel length or separation time and without increasing the number of channel networks and electrical connections.  Simultaneous measurement of glucagon and insulin was recently demonstrated in a commercial capillary system[7]. Separation was performed in a 30 cm long capillary; custom designed dual fluorescence measurement enabled single point quantitation of insulin and glucagon immune complexes.  In our work, we perform multiplexed detection of TNF-α and CRP in a microfluidic chip for its low sample consumption and compactness.  In addition, application of pore-size gradient gels allows rapid biomarker quantitation within a separation length of 1 mm and a separation time of 1 minute.

## 4.4    Dual color imaging to characterize separation performance

Dual color CCD imaging relied on the use of two filter cubes and independent realizations of separations in each color signal.  To produce two-color CCD images, image sequences collected on one spectral channel (AF 488 with Omega Optical GFP filter cube) were summed with image sequences taken on the second spectral channel (AF568 with Omega Optical dsRed2 filter cube) from back-to-back injections of the same multi-component samples.  Image sequences for each spectral channel were processed using ImageJ to produce two-color separation montages.

For our assay, we use antibodies labeled with green and red fluorophores that are specific toward TNF-α and CRP, two inflammation biomarkers. Additionally, CRP measurement is used clinically to evaluate cardiovascular disease risk. Following incubation, sample is electrokinetically loaded and injected into the separation channel as described in section 3.4.1.

As illustrated in Figure 4-1, we expect to resolve 4 peaks during separation: the faster being the affinity reagents and the slower being the immune complexes.

Figure 4-2 compares assay separation performed on a uniform large pore-size (2.5%T) gel with separation performed on a decreasing pore-size gradient (2.5%T-to-8%T) gel. Both sieving matrices were fabricated in situ within NS7 channel networks. The 2.5%T-to-8%T pore-size gradient gel was fabricated by following the protocol described in section 3.3.4. The large pore-size loading gel enables unbiased loading of both antibodies and immune complexes into the injection junction while the decreasing pore-size gradient in separation channel aids in efficient separation of larger immune complexes from the antibodies. Using gradient gels in combination with spectral encoding, we are able to resolve both complexes in 15 seconds and within a separation length of 1 mm. As complexes migrate through the decreasing pore-size gradient, they are stacked into thinner bands as a result of decreasing migration velocity. The stacking effect improves detection sensitivity.
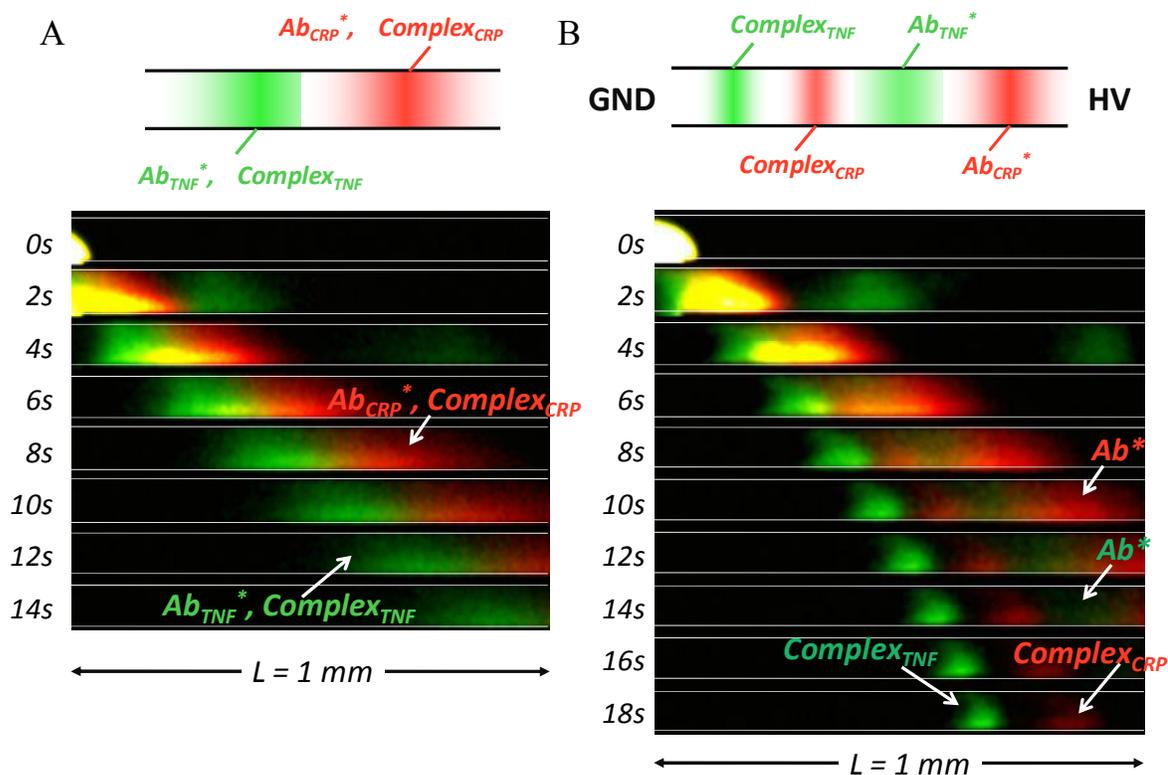


Figure 4-2. Separation in decreasing pore-size gradient gel (B) resolved immune complexes within a separation length of 1 mm while the immune complexes were not resolved in a large pore-size uniform gel (A). Separations were performed on NS7 chips under E = 100 V/cm. anti-TNF Ab* was labeled with AF 488 dyes while anti-CRP Ab* was labeled with AF568 dyes. [anti-TNF Ab*] = 68 nM; [anti-CRP Ab*] = 66 nM; [TNF-$\alpha$] = 22 nM; [CRP] = 15.7 nM. A cartoon depicting the composition of each peak is displayed on top of corresponding separation montage.

## 4.5 Simultaneous biomarker measurement using single-point two-color PMT detection

36

Simultaneous immunoassays were completed in a single separation channel using single-point two-color detection. As shown in Figure 4-3A, quantitation of TNF-α and CRP utilized a custom filter cube on an IX70 microscope and a two-channel photomultiplier tube (PMT) detection system (Photon Technology International) mounted to the IX70. Mercury arc lamp excitation was spectrally filtered with a 490 and 577 nm dual band excitation filter (XF1051, Omega Optical) and reflected off a dichroic mirror (490 and 575 nm notch filter, XF2044 by Omega Optical). A 40x objective (N.A. = 0.60) focused on the separation channel defined the detection point. Fluorescence was spatially filtered (iris) prior to PMT detection. A dichroic mirror (560 nm long pass, XF2017 by Omega Optical) split emissions from the fluorophores into red and green channels. Each channel was further filtered by individual emission filters (XF3081 and XF3301, Omega Optical) to minimize crosstalk. Figure 4-3B illustrates transmission inside the 2-color PMT detection unit. The optical components are selected to effectively isolate AF 488 (green) from AF 568 (red) fluorescence. As a result, there is no bleed-through of red fluorescence into the green channel and a 7.5% bleed-through of green fluorescence into the red channel. The theoretical bleed-through value of 7.5% is calculated by dividing the transmission of AF 488 fluorescence into the red channel by transmission of AF 488 fluorescence into the green channel.
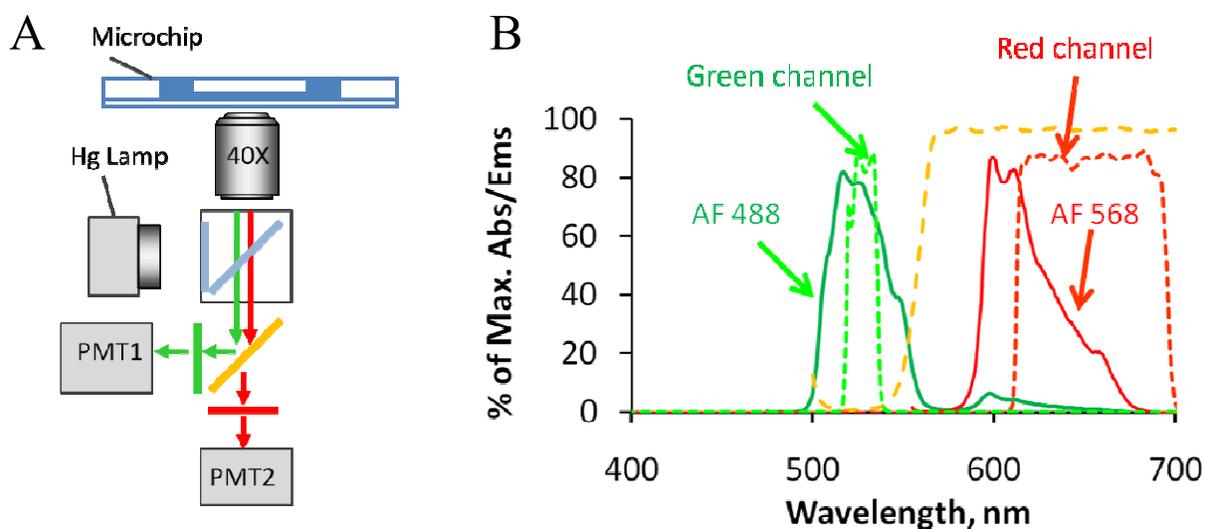


Figure 4-3. Emission spectrum of AF 488 and AF 568 fluorophores entering the 2-color detection unit (green and red solid lines in B) was split by a dichroic mirror (orange mirror in A and orange dash line in B) and further filtered by band pass filters (red and green mirror in A and green and red dash line in B).

### 4.5.1  Setup

Fluorescence intensity at the single point detector was normalized by the fluorescence intensity in the loading channel. The PMT high voltage control was set at 600 – 700 V to produce consistent output signal amplitude. In addition, the time constant of the filters in the built-in analog circuitry was set at 50 ms for optimal noise filtering without compromising fast migrating peaks. Signals from the PMTs were collected via a data acquisition board and electropherograms were generated using an in-house LabView program.

### 4.5.2 Crosstalk measurement

To experimentally evaluate optical crosstalk, samples containing a single fluorophore (either AF 488 or AF 568) were analyzed on a 2.5%T-to-8%T gradient gel with both red and green fluorescence recorded using the 2-color PMT detection system. As shown in Figure 4-4A and Figure 4-4B, there is less than 2% optical crosstalk between the red and green channels. Figure 4-4C shows simultaneous detection of TNF-α and CRP. Compared to single biomarker analysis (Figure 4-4A, Figure 4-4B), simultaneous incubation and multiplexed detection have no negative impacts on separation resolution, migration, and assay reproducibility. Furthermore, as shown in Figure 4-4D, spectral encoding is needed to resolve the CRP complex which partially overlaps with the TNF-α Ab*.
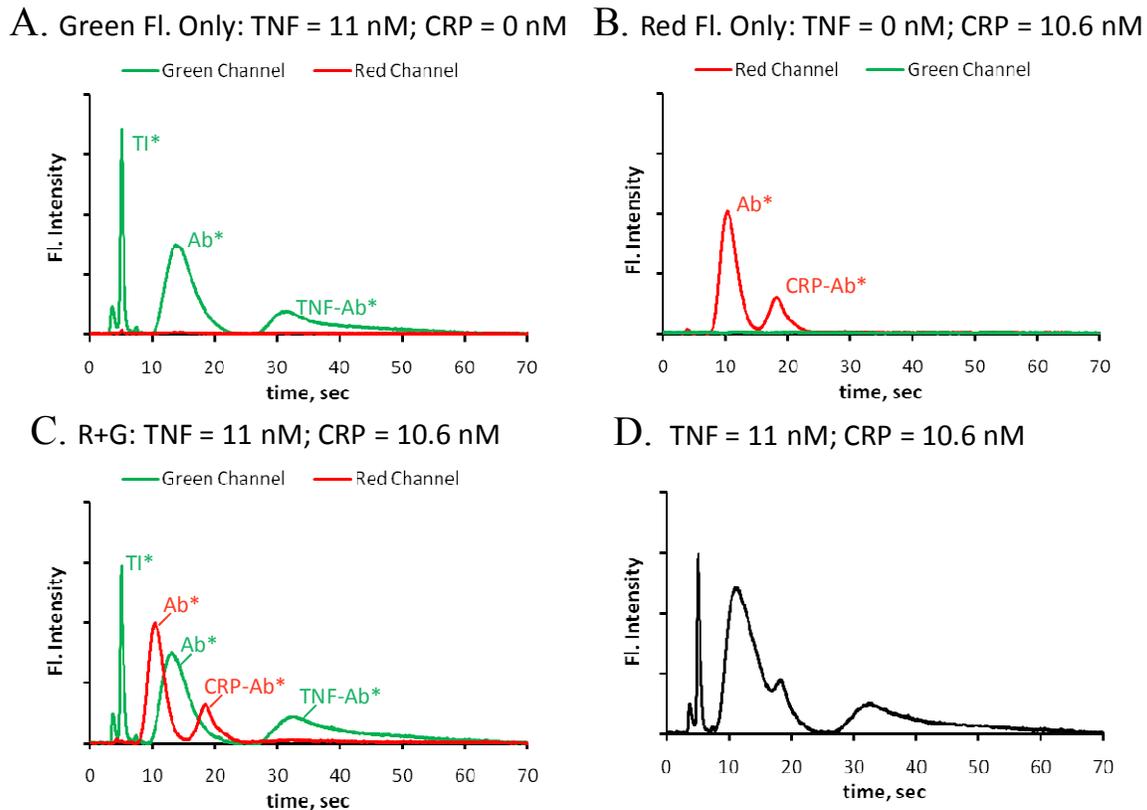


Figure 4-4. Spectral multiplexing improves assay throughput without compromising separation efficiency. (A) TNF-α only: AF488 labeled anti-TNF-α Ab*(46 nM) was incubated with 11 nM TNF-α protein. (B) CRP only: AF568 labeled anti-CRP Ab* (66 nM) was incubated with 10.5 nM CRP. (C) Two color: both proteins and Ab* were present in the injected sample. All samples contained 50 nM Trypsin inhibitor (TI*) which was used as an internal standard to normalize fluorescence intensity across different separations.

### 4.5.3 Quantitative biomarker measurement

Our 2-color biomarker measurement is also quantitative. Figure 4-5 shows the separation of 3 different samples on a 2.5%T-to-8%T gradient gel. Fluorescence intensity was monitored using the 2-color PMT detection system. The detector is placed 0.9 mm downstream from the injection junction. As TNF-alpha and CRP concentration were increased from left to right, peak heights

for both complexes, which are indicated by the red and green asterisks, also increased. Using this set of electropherograms, dose response curves were generated by plotting complex peak heights versus biomarker concentration (Figure 4-6). Using the gradient gels, we are able to detect TNF-alpha down to 2 nM and CRP down to 1 nM. The CRP dose response is linear over a 2-log concentration range. Furthermore, we noted no cross reactivity between anti-TNF-α Ab* and CRP as well as no cross reactivity between anti-CRP Ab* and TNF-α.
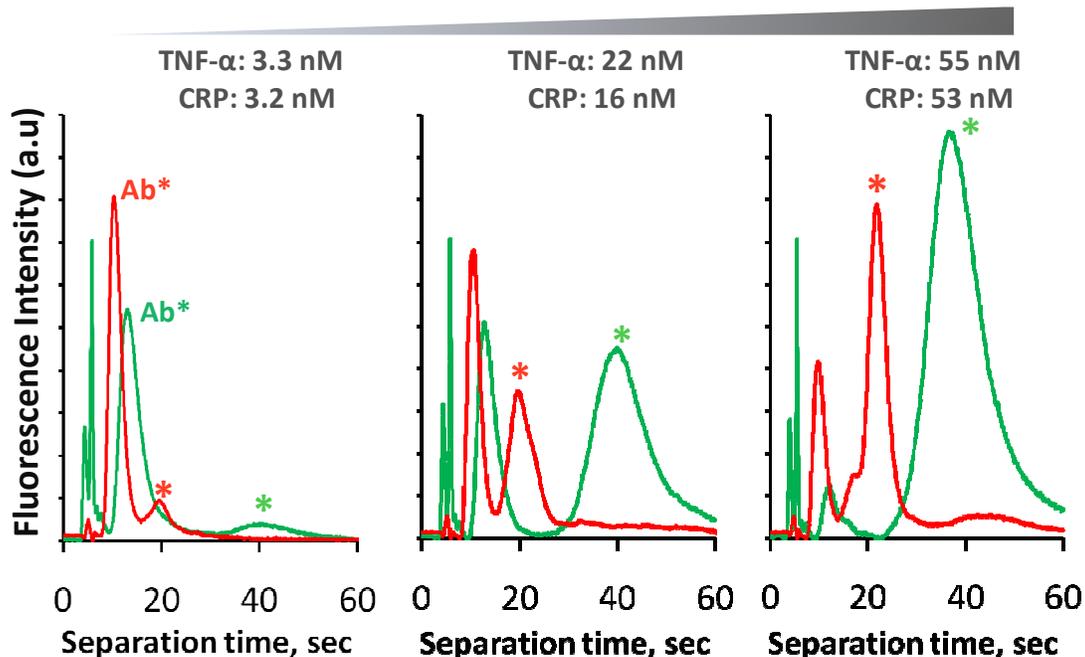


Figure 4-5. Spectral multiplexing enables simultaneous quantitation of TNF-α and CRP within a single separation channel. TNF-α and CRP with concentration shown above each electropherogram were incubated with [anti-TNF Ab*] = 46 nM and [anti-CRP Ab*] = 66 nM.
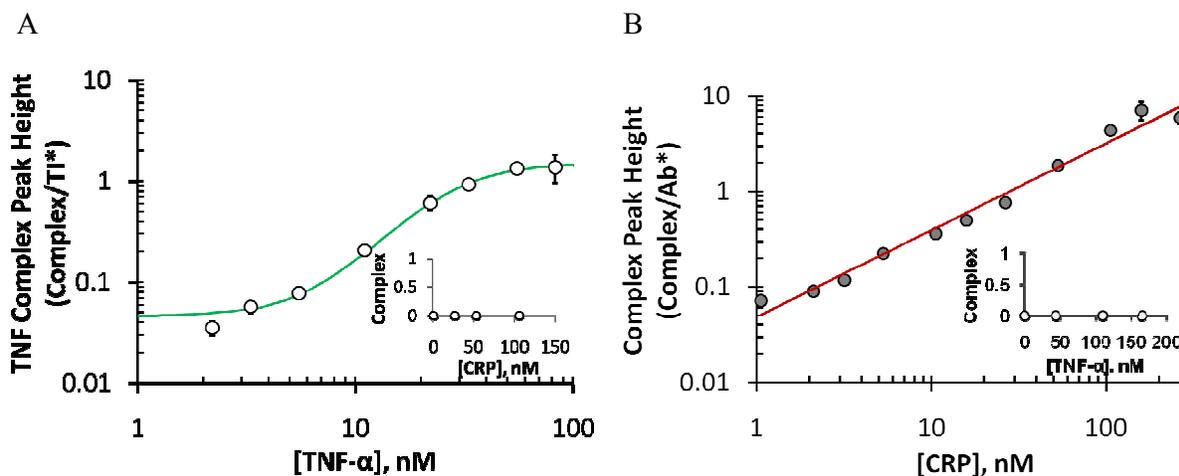


Figure 4-6. Dose response curves for TNF-α (A) and CRP (B) obtained by on-chip PAGE immunoassays using decreasing pore-size gradient gels. (A) Open symbols correspond to TNF-α complex peak heights from incubation of TNF-α at various concentrations with constant anti-TNF-α Ab* concentration at 46 nM. Anti-TNF-α was labeled with AF 488.  Insert shows that

anti-TNF-α antibody does not react with CRP. (B) Solid symbols correspond to CRP complex peak height from incubation of CRP at various concentrations with constant anti-CRP Ab* concentration at 66 nM. Anti-TNF-α was labeled with AF 568. Insert shows that anti-CRP antibody does not react with TNF-α. Error bars indicate run-to-run variations (n>3).

To calculate analyte concentration based on immune complex formation, the TNF-α dose response curve was fit using a four-parameter logistic model:

$$B = \beta_2 + \frac{(\beta_1 - \beta_2)}{1 + ([Ag]/\beta_3)^{\beta_4}}$$

where $B$ is the complex peak height (normalized to internal standards) and $[Ag]$ is the target analyte concentration ([TNF-α]). $\beta_1$ is the expected response as $[Ag] \rightarrow 0$, $\beta_2$ is the expected response as $[Ag] \rightarrow \infty$, $\beta_3$ is the $[Ag]$ at the response midpoint, and $\beta_4$ corresponds to the steepness of the dose response curve. Using a built-in least square curve fit function in Matlab, we obtained the following equation:

$$TNF\ Complex = 1.50 + \frac{-1.1}{1 + ([TNF-\alpha]/26.7\text{nM})^{2.45}}$$

Using the 4-parameter logistic fit model, we can back-calculate biomarker concentration in the original sample from measured complex peak height.

### 4.5.4  Analysis of multiple samples in a single channel network

As there is no surface immobilization involved and no non-specific adsorption, more than one sample can be analyzed in a single separation channel. Two samples each containing inflammatory biomarkers at different concentrations was placed in sample wells S1 and S2 in the NS7 chip (Chapter 3, Figure 3-7). The composition of both samples is displayed in Table 4-1: affinity reagent concentration was held constant while target analyte concentration was varied. The samples were analyzed sequentially via electrokinetic injection followed by separation and 2-color imaging (Figure 4-7). Sample 1 contains a higher CRP concentration and a lower TNF-α concentration compared to sample 2; therefore, sample 1 exhibits a larger CRP complex peak and a smaller TNF complex peak in the electrophoregram.  Here we use sequential analysis to quantify biomarkers in two different samples. Sequential analyses can also be utilized to increase the number of biomarkers measured in a given biological sample by using different affinity reagents (Ab*) for incubates placed in each well, therefore, detecting different target analytes in each separation.

Table 4-1. Composition of incubates placed in sample wells S1 and S2 for sequential 2-color analys.

|    | Anti-CRP Ab* (nM) | CRP (nM) | Anti-TNF Ab* (nM) | TNF-α (nM) |
|----|----|----|----|----|
| S1 | 66 | 26.5 | 46 | 5.5 |
| S2 | 66 | 5.3 | 46 | 22 |
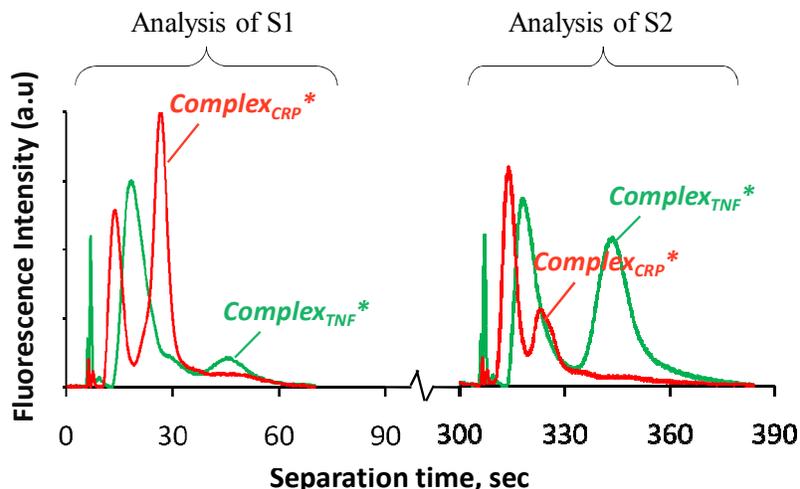
Figure 4-7. Additional multiplexing arises from combining spectral encoding with sequential analyses within a single channel. Sample placed in S1 (with composition listed in Table 4-1) was first analyzed. Sample placed in S2 (with composition listed in Table 4-1) was sequentially injected and separated. The elapsed separation time in between two sets of electrophoregrams corresponds to the time in between two injections.

## 4.6   Summary

We present for the first time a spectrally multiplexed homogeneous electrophoretic immunoassay for inflammatory biomarkers. Biomarkers of inflammation are resolved quickly (< 15 s), in ultra-short separation lengths (< 1 mm), and at clinically relevant concentrations (nM). The reported assay format is applicable to a wide variety of analytes. Incorporation of additional affinity reagents labeled with spectrally distinct fluorophores would further improve assay throughput.

## 4.7   References

(1)     Anderson, N. L.; Anderson, N. G. *Mol Cell Proteomics* **2002**, *1*, 845-867.
(2)     Goldsby, R. A.; Kindt, T. J.; Osborne, B. A.; Kuby, J. *Immunology*, 5th ed.; W.H. Freeman and Company: New York, 2003.
(3)     Ulloa, L.; Tracey, K. J. *Trends in Molecular Medicine* **2005**, *11*, 56-63.
(4)     German, I.; Kennedy, R. T. *Journal of Chromatography B-Analytical Technologies in the Biomedical and Life Sciences* **2000**, *742*, 353-362.
(5)     Dishinger, J. F.; Reid, K. R.; Kennedy, R. T. *Analytical Chemistry* **2009**, *81*, 3119-3127.
(6)     Cheng, S. B.; Skinner, C. D.; Taylor, J.; Attiya, S.; Lee, W. E.; Picelli, G.; Harrison, D. J. *Analytical Chemistry* **2001**, *73*, 1472-1479.
(7)     Christelle, G.; Michael, G. R. *Electrophoresis* **2008**, *29*, 410-416.

# Chapter 5 Optimized Photopatterning of Discontinuous Gels within Microfluidic Channels

In my thesis work, photopatterned polyacrylamide gels enabled the development of two efficient microfluidic-based electrophoretic assays: homogeneous immunoassay with an ultra-short separation length (chapter 2 – chapter 6) and western blotting assay with on-chip protein renaturation (chapter 7 – chapter 10). Optimization of sieving matrix properties such as gel pore-sizes results in significant performance improvements compared to previous demonstrations. While sequential patterning of different sieving matrices using partial illumination is straightforward in concept, we observed non-idealities in gel pore-size distribution when the illumination settings were not optimized. Hence, this chapter focuses on optimizing photopatterning of discontinuous gels for on-chip immunoassays. The optimized photopatterning technique is later applied in fabricating discrete functional units within a 2D chamber for western blotting assays.

Previously, separations performed on microchip gradient gels allow assay completion within a separation length of 1 mm. In this chapter, we show that, through theoretical analysis of SR, separation resolution of electrophoretic immunoassays can be further improved by using on-chip discontinuous gels (section 5.1). Next, we discuss non-idealities encountered when fabricating the discontinuous gel architecture using a mask-based partial illumination approach (section 5.3). Addressing the non-ideal pore-size distribution (section 5.5) led to demonstration of ultra-short separation length homogeneous immunoassays (chapter 6).

## 5.1    SR on gradient gels can be further improved

The portability and field adaptability of electrophoretic immunoassays are limited in part by the need for high voltage power supplies. At an applied electric field of 100's V/cm, centimeters of separation length required to resolve the immune complex translate to hundreds and thousands of volts applied across the channel. Therefore, our design goal is to minimize the separation length necessary to achieve SR = 1, in another word, complete immunoassay in as short separation length as possible.

In chapter 1, we have derived separation resolution between two neighboring analyte peaks as a function of leading analyte migration distance ($L$):

$$SR = \frac{\Delta\mu E \frac{L}{\mu_1 E}}{2\sqrt{\sigma_0^2 + 2D_1 \frac{L}{\mu_1 E}} + 2\sqrt{\sigma_0^2 + 2D_2 \frac{L}{\mu_1 E}}}$$

This derivation assumes that the separation is conducted in a homogeneous media where analyte mobility ($\mu$) and diffusivity ($D$) are constant over the entire separation length. At a given analyte migration distance, gel electrophoresis achieves better separation resolution than free solution electrophoresis by enhancing $\Delta\mu/\mu$.

As illustrated in Chapter 4, performing separations on decreasing pore-size gradient gels resolve immune complexes within 1 mm of separation length. Figure 5-1 traces antibody and immune complex migration on a large pore uniform gel (in A) and a decreasing pore-size gradient gel (in

42

B), both sieving structures were fabricated within NS7 chips. The separation resolution was estimated to be 0.33 for the large pore-size uniform gel whereas the decreasing pore-size gradient gel achieved SR = 1 at an antibody migration distance of 0.7 mm. Decreasing pore-size gels retard larger immune complexes more than significantly than antibodies. As a result, a larger peak-to-peak separation ($\Delta L$) length and larger separation resolution are obtained.

A

Large pore (2.5%T)

B

Large pore (2.5%T)        Small pore (8%T)
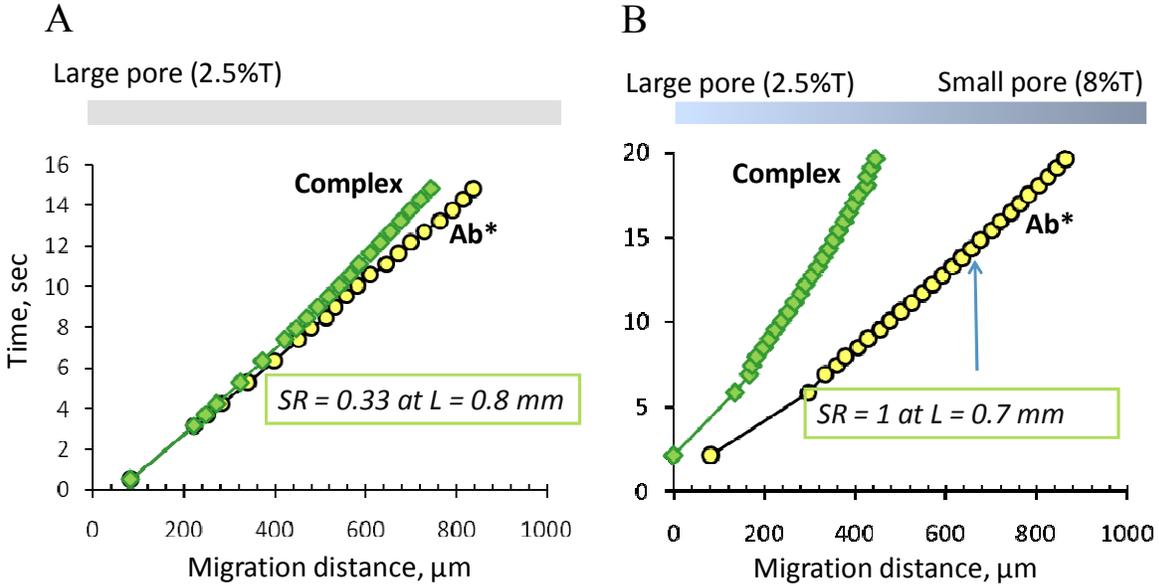


Figure 5-1. Antibody and complex migration were traced on a large pore-size uniform gel and a decreasing pore-size gradient gel with improved peak-to-peak separation on the gradient gel.

Analysis of relative mobility differences ($\Delta\mu/\mu$) suggests separation performance on gradient gels can be further improved. At an antibody migration distance of 0.7 mm (as pointed by the arrow in Figure 5-1B), $\Delta\mu/\mu$ for the uniform gel is $\frac{\mu_{Ab-2.5\%}-\mu_{complex-2.5\%}}{\mu_{Ab-2.5\%}}$ where $\mu_{Ab-2.5\%}$ is antibody mobility in the 2.5%T gel and $\mu_{complex-2.5\%}$ is complex mobility in the 2.5%T gel. Similarly, $\Delta\mu/\mu$ for the gradient gel is $\frac{\mu_{Ab-6\%}-\mu_{complex-4\%}}{\mu_{Ab-6\%}}$ as the antibody is in approximately 6%T and the complex is in approximately 4%T for the corresponding time frame.

Performing separations in 6%T gel can further improve $\Delta\mu/\mu$ to $\frac{\mu_{Ab-6\%}-\mu_{complex-6\%}}{\mu_{Ab-6\%}}$ as complex exhibits slower mobility in 6%T compared to 4%T gel. However, as shown in Chapter 3, small gel pore sizes (i.e., acrylamide concentration higher than 3.5%T) exclude larger immune complexes and result in absence of immune complexes in separation. A discontinuous gel architecture with large pore-size loading gel and small pore-size separation gel is developed to increase separation resolution within a limited separation length.

## 5.2    Overview of discontinuous gel fabrication

Similar to the gradient gel fabrication protocol introduced in chapter 3, discontinuous gels are created with a two-step photopatterning process with the caveat that the first exposure now polymerizes the entire separation length. Chip cleaning using NaOH and surface treatment by

silanization follow the general gel fabrication protocol outlined in chapter 3. As shown in Figure 5-2, the chip was aligned to a transparency mask (designed in house and fabricated by Fineline Imaging, Colorado Springs, CO) and the separation channel was exposed to UV illumination. After alignment, the separation gel precursor solution (T = 2.5, 3.5, 4, 5, 6, or 8%) was wicked into all channels and excess precursor solution was removed from channel reservoirs, drops of high viscosity 5% (w/v) 2-hydroxyethyl cellulose (HEC) were applied to each reservoir and equilibrated for 10 min to yield quiescent flow conditions, the precursor filled microchannels were then exposed to UV excitation for a set duration, unpolymerized separation gel precursor solution in the loading channel was then flushed out and replaced with loading gel precursor solution (2.5%T) via pressure driven flow, and finally the unmasked chip was flood exposed for 8 min on a 100 W UV lamp (10 mW/cm$^2$). The choice of light source, exposure intensity, and illumination intensity during the first exposure step can significantly affect pore-size distribution after the discontinuous interface.
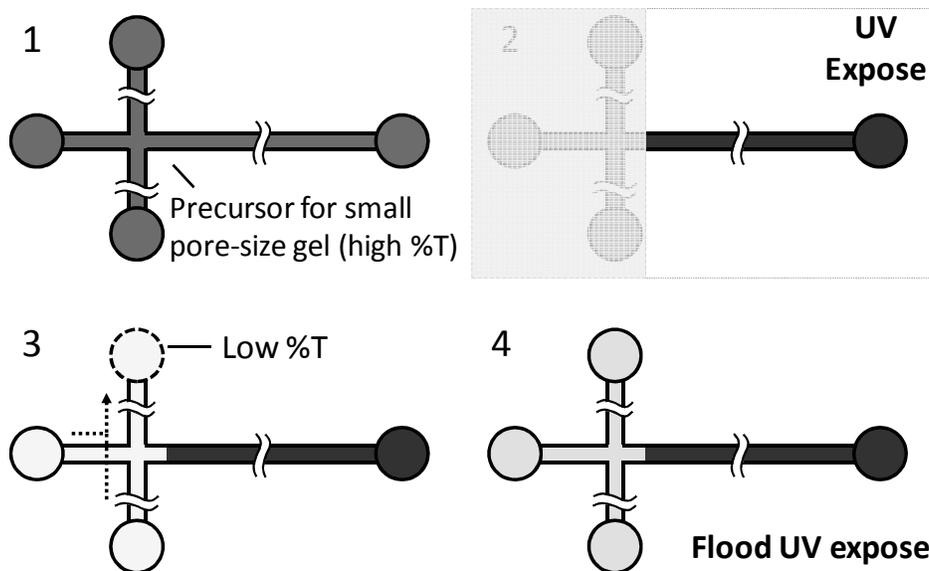


Figure 5-2. Discontinuous pore-size gel fabrication within microfluidic glass channels: mask-based photolithography creates functional units with different pore sizes.

## 5.3    Initial demonstration motivates further fabrication optimization

The separation gel was first exposed with a 100 W UV lamp (300 – 380 nm UVP, B100-AP, Upland, CA) that was also used for later flood exposure of the entire chip. As shown in Figure 5-3, the immune complexes were resolved from the antibody within 200 μm of the discontinuous interface. Figure 5-4 traces antibody and immune complex migration on a decreasing pore-size gradient gel (in A) and a discontinuous pore-size gel (in B). As indicated by the three colored arrows, for the TNF-α assay, separation on discontinuous gels achieved a separation resolution of 1 at an antibody migration distance of 75 μm after the discontinuous interface. Separation on the discontinuous gel achieved SR > 1.5 at an antibody migration distance of 100 μm after the discontinuous interface.
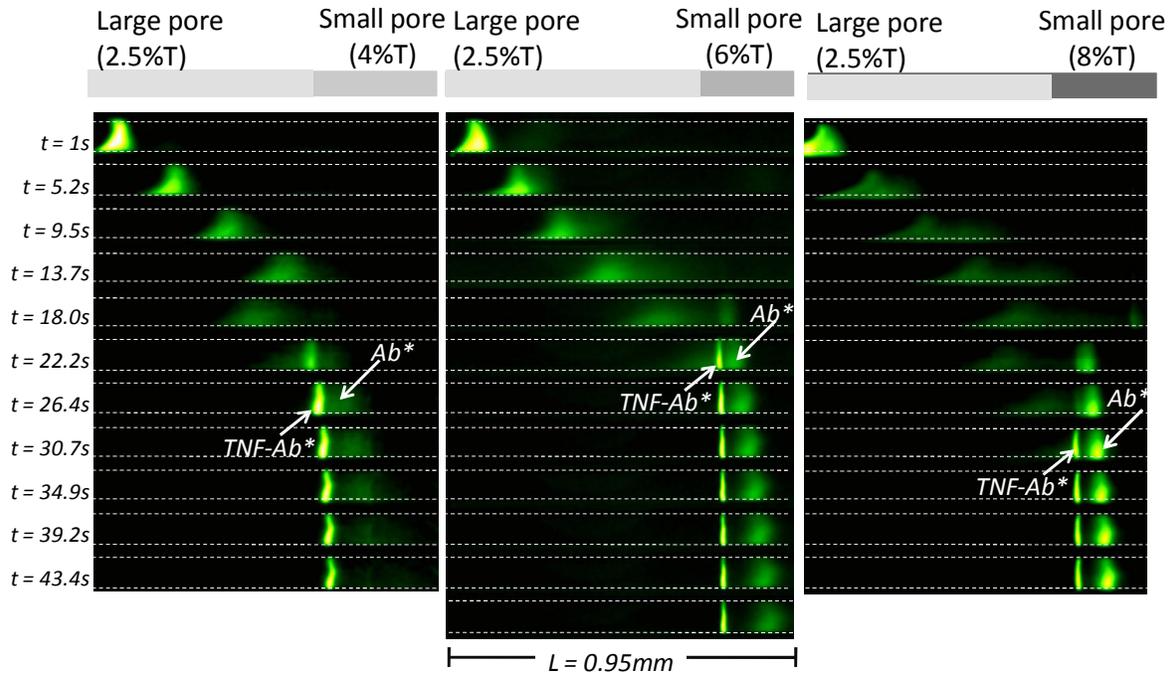
Figure 5-3. Comparison of TNF-α assay separation among three discontinuous gel formats with increased separation gel %T. All devices were exposed under the same illumination conditions with the mask aligned to the same reference location. The precursor solution composition that was used for fabrication of small pore-size gels was displayed above the corresponding separation montage. In the 2.5/4%T and 2.5/8%T gel, the field of view was shifted at $t = 18 \, s$ to image discontinuous interfaces that were located more than 1 mm downstream of the injection junction.
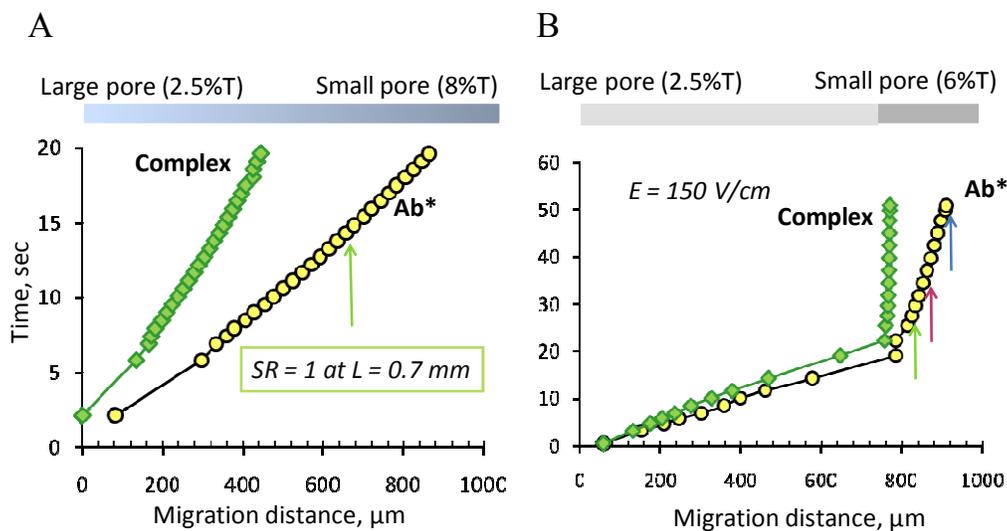


Figure 5-4. Antibody and complex migration were traced on a decreasing pore-size gradient gel and a discontinuous pore-size gel. As indicated by the colored arrows in B, discontinuous gel achieved SR = 1 at an antibody migration distance of 75 μm after the discontinuous interface,

45

SR=1.55 at an antibody migration distance of 100 μm after the interface, and SR = 1.85 at an antibody migration distance of 155 μm after the interface.

Besides improving separation resolution, discontinuous pore-size gels stack antibodies and complexes into sharper and brighter bands as they migrate across the discontinuous interface. The stacking effect can be modeled by conservation of mass: $c_1 v_1 = c_2 v_2$ where $v_1$ and $v_2$ is the analyte migration velocity before and after the interface, $c_1$ and $c_2$ is the analyte concentration before and after the interface, respectively. Analyte mobility decreases with increased acrylamide concentration according to the Ferguson[1] relationship: $\mu = \mu_0 10^{-KT}$. Assuming a uniform electric field throughout the separation channel, increasing T leads to reduced migration velocity ($v$) and increased analyte concentration ($c$). The stacking factor ($c_2/c_1$) is experimentally measured for the 3 chips characterized in Figure 5-3 and correlates well with theoretical expectation based on $\frac{c_2}{c_1} = \frac{v_1}{v_2} = \frac{\mu_1}{\mu_2}$ (Figure 5-5). As shown in Figure 5-5B, Ab* experiences a 5-15 fold increase in fluorescence intensity across the discontinuous interface which improves detection sensitivity. The slight discrepancy in stacking factor between experimental measurement and theoretical calculation mainly arises from the assumption of constant electric field. In reality, E would be higher in the small pore-size separation region due to increased resistivity from increased gel density; therefore, the corresponding increase in analyte mobility in the separation gel results in a slight reduction in overall stacking factor.
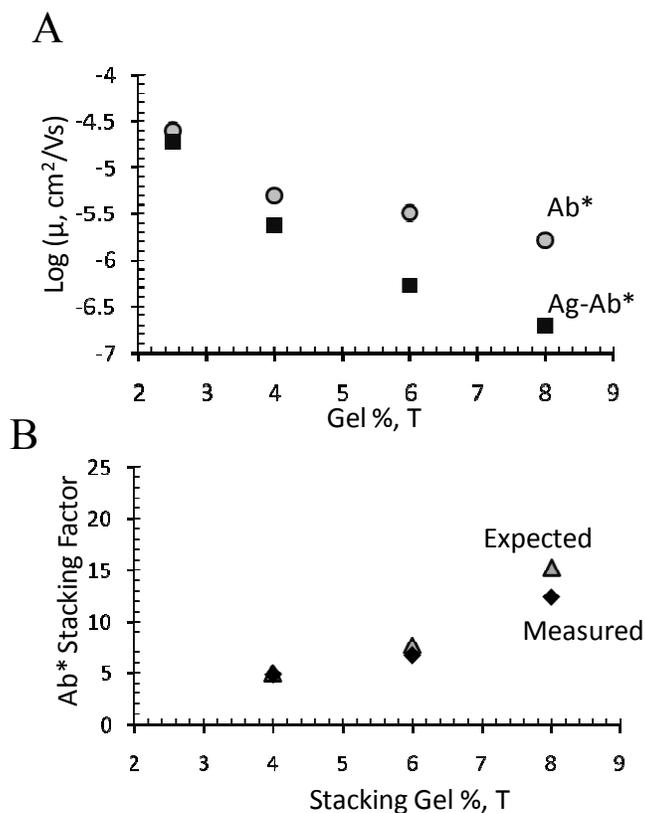


Figure 5-5. Discontinuous gels improve signal intensity by a stacking effect. (A) Ab* and complex mobility were plotted for the discontinuous gel structures characterized in Figure 5-3; mobility was measured in both 2.5%T loading gel region as well as in separation gel region with

46

different %Ts. (B) The theoretical stacking factor was calculated by dividing analyte mobility in the loading gel by analyte mobility in the separation gel. The experimental stacking factor was measured by calculating fluorescence change across the discontinuous interface.

As shown in Figure 5-3, the discontinuous interface starts ~ 1mm after the injection junction. Hence, nearly 20 seconds of separation time were "wasted" by protein migration in the large pore-size separation gel region. Therefore, in order to reduce overall separation length, a better light source than the uncollimated UV lamp is needed. As shown in the next section, an IX-50 microscope equipped with a mercury lamp and a 4x UV objective (UPLANS-APO, N.A. = 0.16) was applied to discontinuous gel fabrication. The collimated light source from the mercury arc lamp has better reproducibility in controlling discontinuous interface location. However, direct exposure to the mercury arc lamp results in exclusion of immune complexes from entering the small pore-size separation gel.

## 5.4    Mobility measurements estimate apparent gel pore sizes

To examine the effectiveness of different fabrication protocols, a better measurement of gel pore-size distribution is needed. Characterization of gel pore-size along the separation axis followed previously described approaches[2] to extrapolate equivalent %T based on mobility tracking. Briefly, anti-CRP Ab* mobility was measured in a gradient gel or a discontinuous gel as a function of migration distance and the measured mobility was compared with analyte mobility in known gel pore-sizes to extrapolate gel composition within a region of interest.

To calibrate the relationship between unknown gel pore sizes and measured protein mobility, anti-CRP Ab* mobility was measured in five uniform pore-size PA gels (2.5%T, 3.5%T, 4%T, 5%T, and 6%T). Calibration yielded a linear relationship between gel pore size and apparent electrophoretic mobility: $\log$ (mobility, $cm^2V^{-1}s^{-1}$) = - 0.111·(T) – 3.71 ($R^2$= 0.974).

To characterize the pore-sizes of gradient and discontinuous gels, anti-CRP Ab* was injected in the separation channel. Electrophoretic mobility ($\mu$) as a function of migration distance ($L$) was extracted from CCD separation images. Specifically, the fluorescence intensity across the separation channel within the entire field of view (~ 1.25 mm) was extracted using the built-in "Plot Profile" function in ImageJ. A built-in least square fitting algorithm in MATLAB (MathWorks, Natick, MA) and an in-house single-peak Gaussian fitting script were used to identify peak location or antibody migration distance at each time point (every 0.33 sec). The time-derivative of migration distance was calculated using a 5-point quadratic first-derivative Savitzky-Golay smoothing filter[3]. The time-derivative of the migration distance divided by the applied electric field yielded mobility: $\mu = \frac{1}{E}\frac{\partial L}{\partial t}$. Substituting the calculated mobility value into the pore-size calibration relationship that was established in uniform gels generates effective gel pore-sizes.

Using the approach outlined above, we characterize discontinuous gels fabricated using the mercury arc lamp. As shown in a separation montage taken across the first mm of the separation channel (Figure 5-6A), significant dispersion ("de-stacking") of the Ab* peak was observed during the first 300 μm aft of the gel discontinuity. Tracking of Ab* migration distance as a function of time (Figure 5-6B) revealed variation in antibody mobility after the discontinuous

interface, an indication of pore-size variation. Assessment of anti-CRP Ab* migration velocity along the separation axis revealed a smaller than expected pore-size at the PA 2.5/5%T gel interface (Figure 5-6C, D). Based on mobility calibration data, an apparent pore-size of 9%T was observed instead of the desired 5%T PA gel. The 2.5/5%T gel discontinuity acted to exclude CRP immune complex despite observations that uniform 5%T PA gels fabricated with flood illumination allowed free migration of immune complex (data not shown). Mobility calibration revealed that the apparent pore-size near the discontinuous interface increased from that of a 9%T gel to that of a 6%T PA gel (circled by a dashed red line) thus resulting in band "de-stacking" observed in the separation montage. Similar de-stacking effects were observed in microfluidic proteomic assays using discontinuous gels[4] and were addressed with a discontinuous buffer system for band sharpening.
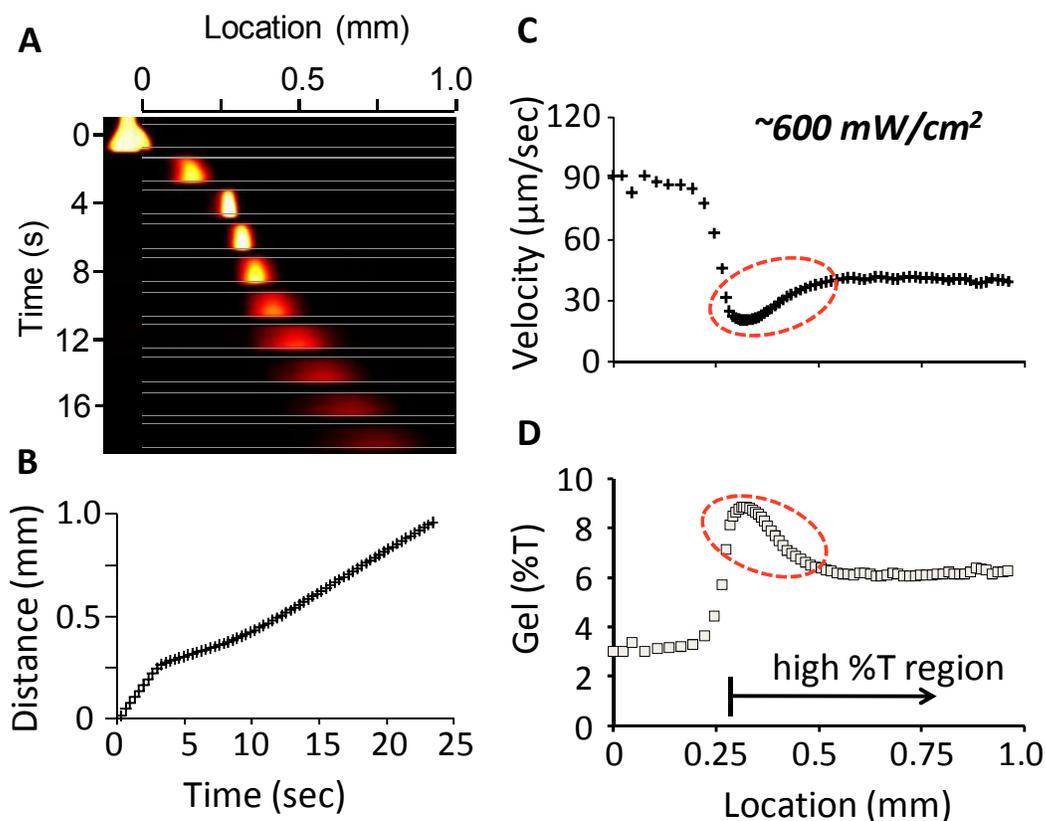


Figure 5-6. Fabrication of PA gel pore-size discontinuity using high intensity illumination from mercury arc lamp results in non-ideal pore-size distribution. 5% separation gel was exposed for 3 minutes under ~ 600 mW/cm$^2$ illumination power. (A) Separation montage of anti-CRP Ab* as a function of time reveals band dispersion and non-uniform migration velocity after the discontinuous interface. (B) Migration distance was obtained from separation montage by using a single peak Gaussian fitting script in MATLAB to identify peak location in each time frame. (C) Migration velocity was calculated by taking the time-derivative of migration distance using a 5-point Savitzky-Golay smoothing filter. (D) Equivalent gel pore-size was determined by comparing measured mobility to anti-CRP Ab* mobility in uniform gels with known pore sizes.

## 5.5 Reducing illumination intensity improves pore-size uniformity

Table 5-1 summarizes desired properties for discontinuous gels and compares mercury arc lamp and UV lamp based fabrication approaches in achieving the desired properties. Mercury arc lamp achieves reproducible control of discontinuous interface location, but results in exclusion of immune complexes from entering the discontinuous interface. On the other hand, the 100 W UV lamp was able to achieve a more uniform pore-size distribution after the discontinuous interface; however, due to the uncollimated light source, the interface location varied significantly across fabrication runs. Therefore, an improved fabrication approach would combine the advantages of mercury arc lamp and UV lamp based fabrication approaches.

Table 5-1. Requirements for discontinuous gel fabrication setup.

| Desired Discontinuous Gel Properties | Mercury arc lamp based fabrication | UV lamp based fabrication |
|---|---|---|
| Reproducible control of discontinuous interface location | +++ | |
| Uniform pore-size distribution after discontinuous interface | | + |
| Apparent pore-size close to precursor concentration | | Sometimes |

Modification of fabrication setup requires better understanding of observed non-idealities. Theoretical modeling suggests that UV photopolymerization under partial illumination can result in non-ideal pore-size variation near the polymer/precursor interface[5]. The mechanism stems from a monomer concentration gradient established across the masked region to the exposed region during the photopolymerization process. As monomers are consumed in the irradiated zone, a concentration gradient is established across the illumination interface. Due to the concentration gradient, acrylamide monomers from the masked region diffuse into the UV exposed region, subsequently become cross-linked near the illumination interface, and lead to a smaller than desired pore-size near the edge of the exposed region.

Theoretical explanation of non-ideal pore-size distribution under partial illumination coincides with our experimental observations on how illumination power influences discontinuous gel pore-sizes. Illumination power affects the rate monomers are consumed in the illuminated region. At high illumination power as in the mercury arc lamp fabrication setup, there is rapid generation of radicals and consumptions of monomers in the irradiated zone; as a result, large amount of monomers diffuses into the illuminated region from the masked region and gets polymerized immediately near the discontinuous interface. Polymerization with additional monomers leads to smaller than desired pore-sizes as observed in Figure 5-6C, D. On the other hand, discontinuous gels that were fabricated using the UV lamp at lower illumination power exhibit much less pore-size variation near the discontinuous interface. Therefore, we hypothesize reducing the illumination power should mitigate non-ideal pore-size variation at the interface by (1) reducing the amount of monomers diffusing into the exposed region and (2) allowing incoming monomers to diffuse for longer distance before being cross-linked into the growing polymer chain.

To reduce the illumination power, various combinations of metallic-coated neutral density filters (1%, 10%, 25% 30%, or 50% from Omega Optical) were used. Filters were inserted in the IX-50 light path between the mercury arc lamp and the 4x UV objective. Following fabrication, anti-

CRP Ab* was injected and separated on-chip to characterize the separation gel pore-size distribution using previously described approach (5.4). Empirical optimization of the discontinuous gel fabrication protocol followed by pore-size characterization identified an attenuated power of 1.25% total transmission using the 10%, 25%, and 50% filters and an adjusted exposure time of 3.3 min as optimal. In this case, power exiting the UV objective was approximately ~7.5 mW/cm$^2$ (measured by UV340, Mannix Ultra Violet Light Meter).

Figure 5-7 presents the spatial pore-size variation along the separation axis for discontinuous gels fabricated using the modified partial illumination approach. The modified partial illumination approach yielded an interface with an effective 6%T pore-size (Figure 5-7D) which results in no exclusion of immune complex. As can be observed aft of the interface, the modified partial illumination approach also yielded a more uniform pore-size separation gel (circled by green dashed lines) and results in significantly less 'de-stacking' for analytes migrating along the separation axis (Figure 5-7A) as compared to previous demonstration (Figure 5-6). Thus, all discontinuous gels described in the next chapter utilized the attenuated partial illumination instrument.

Using the anti-CRP Ab* mobility calibration curve (section 5.4), effective acrylamide concentration was obtained for discontinuous gels fabricated with various precursor concentrations (2.5%, 3.5%, 4%, and 5%). A linear relationship between effective acrylamide concentration and precursor concentration was obtained: $T_{eff}\% = 1.28 (T_{precurso} \%) - 0.466$, $R^2 = 0.996$. The effective acrylamide concentration is still higher than that in the precursor solution as the monomer diffusion process during partial illumination is inevictable. Nevertheless, by reducing the illumination power and selecting an optimal exposure time, we prevented exclusion of immune complexes and, most importantly, improved pore-size uniformity after the interface.
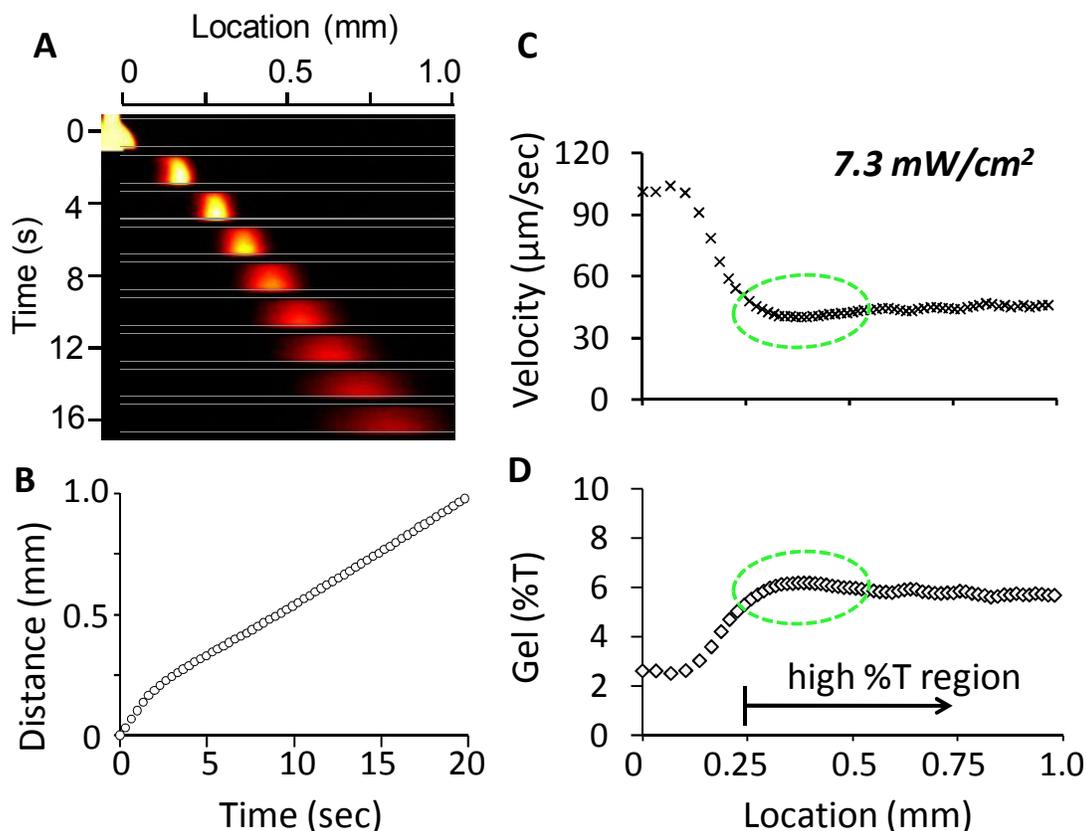
Figure 5-7. Neutral density filter used to decrease illumination power results in well-controlled pore-size distribution near the discontinuity. The 5% separation gel was exposed for 3.3 minutes with 7.5 mW/cm$^2$ illumination power. (A) Separation montage of anti-CRP Ab* as a function of time reveals reduced band dispersion and uniform migration velocity after the discontinuous interface. (B) Anti-CRP Ab* migration distance was tracked as a function of time using a single peak Gaussian fitting script in Matlab to identify peak location in each time frame. (C) Migration velocity was calculated by taking the time-derivative of migration distance using a 5-point Savitzky-Golay smoothing filter. (D) Equivalent gel pore-size was determined by comparing measured mobility to anti-CRP Ab* mobility in uniform gels with known pore sizes.

## 5.6    Summary

While gradient gel may be more appropriate for fractionation of proteins spanning a large range of molecular weights, discontinuous gels are optimal for separation of antibodies and immune complexes by enhancing the relative mobility difference ($\Delta\mu/\mu$) between the pair of interests. Our preliminary data demonstrates separation completion within 100 μm after the pore-size discontinuity but also reveals non-idealities in pore-size distribution. The smaller than desired pore-size near the interface led to undesirable exclusion of immune complexes while the small to large pore-size gradient after the interface led to dispersion of analyte peaks. By optimizing exposure conditions, we are able to achieve discontinuous gels with uniform pore-size distribution after the interface and therefore for the first time experimentally address non-idealities that have been observed by our group and others[4, 6].

51

## 5.7 References

(1) Ferguson, K. A. *Metabolism-Clinical and Experimental* **1964**, *13*, 985-1002.
(2) Lo, C. T.; Throckmorton, D. J.; Singh, A. K.; Herr, A. E. *Lab on a Chip* **2008**, *8*, 1273-1279.
(3) Savitzky, A.; Golay, M. J. E. *Analytical Chemistry* **1964**, *36*, 1627-1639.
(4) Yang, S.; Liu, J. K.; Lee, C. S.; Devoe, D. L. *Lab on a Chip* **2009**, *9*, 592-599.
(5) Fuxman, A. M.; McAuley, K. B.; Schreiner, L. J. *Chemical Engineering Science* **2005**, *60*, 1277-1293.
(6) Herr, A. E.; Throckmorton, D. J.; Davenport, A. A.; Singh, A. K. *Analytical Chemistry* **2005**, *77*, 585-590.

# Chapter 6 On-chip Discontinuous Gel Architecture with Ultra-short Separation Length

In chapter 5, we developed an optimized fabrication protocol for on-chip discontinuous gels. In this chapter, we present the theoretical basis (section 6.1) and experimental approach (section 6.2) to optimize discontinuous gel architectures for two assay detection methods: full-field imaging (section 6.3) and single point detection (section 6.4). The sieving matrix optimized for full-field imaging detection completes immunoassay in a separation length of < 200 μm and is appropriate for integration with CMOS image sensors that can be placed underneath the separation channel[1]. On the other hand, the sieving matrix optimized for single point detection is suitable for detection using PMTs or photodetectors placed at a mere 270 μm downstream from the injection junction. Besides the capability to quantify multiple biomarkers in a rapid and low power fashion, the discontinuous gel architecture is also suitable for continuous monitoring through sequential loading and injections (section 6.5). Lastly, we present future design ideas to adapt discontinuous gel architecture for POC testing.

## 6.1    Theoretical derivation

At a given antibody migration distance ($L_{Ab}$), separation resolution is the peak-to-peak distance between the immune complex and free antibody ($\Delta$L) divided by sum of analyte peak widths ($2\,\sigma_{Ab*}+2\,\sigma_{complex}$). We first revised the derivation of SR presented in chapter 1 with appropriate parameters representing the migration of immune complexes and antibodies:

$$SR = \frac{\Delta\mu Et}{2\sqrt{\sigma_0^2 + 2D_{Ab}t} + 2\sqrt{\sigma_0^2 + 2D_{Complex}t}}$$

Next, we will express the numerator and denominator of SR as a function of antibody migration distance ($L_{Ab}$) to illustrate how adjusting sieving matrix composition affects SR at a given $L_{Ab}$.

First, peak-to-peak distance between the immune complex and free antibody ($\Delta L$) is directly proportional to the mobility difference between the two species: $\Delta L = \frac{\Delta\mu}{\mu_{Ab}} L_{Ab}$. Mobility ($\mu$) and differential mobility ($\Delta\mu/\mu$) are a function of PA gel composition according to the Ferguson relationship[2]: $\mu_{Ab} = \mu_0 10^{-K_{Ab}T}$ and $\mu_{complex} = \mu_0 10^{-K_{complex}T}$. Here $K_{Ab}$ and $K_{complex}$ are the antibody and complex retardation coefficients, respectively, and T is the total acrylamide concentration in the PA gel precursor solution. The larger immune complex will have a larger retardation coefficient compared to the antibody: $K_{Ab} < K_{complex}$. As shown in Figure 6-1, increasing T or decreasing gel pore size will increase log mobility differences (*log $\mu_{Ab}$* - *log $\mu_{complex}$*) or equivalently the differential mobility ($\Delta\mu/\mu$) which is expressed as $\frac{\Delta\mu}{\mu_{Ab}} = 1 - 10^{-(K_{complex}-K_{Ab})T}$. Therefore, increasing T or decreasing PA gel pore-size increases $\Delta L$ or SR at a given $L_{Ab}$.
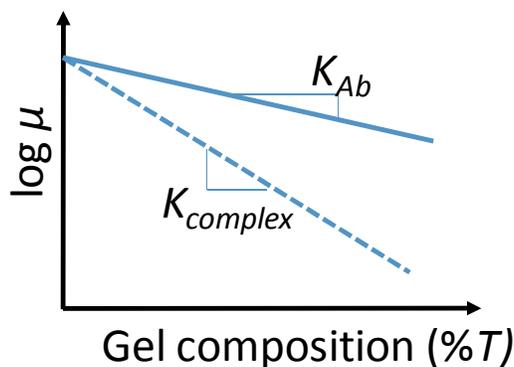
Figure 6-1. Antibody and complex mobility follow an empirically derived Ferguson relationship with respect to gel composition.

Another factor in the expression of SR is analyte peak width, which increases due to diffusion: $\sigma = \sqrt{\sigma_0^2 + 2Dt}$ where $\sigma_0$ is the injected peak width, D is the diffusion coefficient, and t is the elapsed separation time. Assuming constant electric field and Ab* mobility, $t = L_{Ab}/(\mu_{ab} E)$. Peak width is expressed as a function of separation length: $\sigma = \sqrt{\sigma_0^2 + 2\frac{D}{\mu_{Ab}}\frac{L_{Ab}}{E}}$. When altering gel pore-sizes, $D$ changes with $\mu$ since migration by electrophoresis and diffusion encounter the same drag force[3]. Therefore, for a given migration distance, the analyte peak width is constant regardless of sieving matrix composition.

In summary, increasing T or decreasing the PA gel pore-size yields an increased *SR* at a given migration distance ($L_{Ab}$). A trade-off exists, however, as decreasing the PA gel pore-size results in slower migration velocities and thus longer assay duration when using single-point detection. Nevertheless, tuning of the gel pore-size allows assay developers to maximize the SR while minimizing the separation length ($L_{Ab}+2\sigma_{Ab}$) and assay duration. Practical considerations require large pore-size gels in the loading channel to allow unbiased introduction of immune complexes (i.e., CRP complex ~175 kDa, TNF-α complex ~200 kDa) as discussed in chapter 3. This chapter focuses on the optimization of discontinuous gel architecture in which large pore-size loading gel allows unbiased introduction of immune complexes with the affinity probes (Ab*) and small pore-size separation gel enables rapid separation of immune complexes from the affinity probes.

## 6.2    Experimental Optimization

While SR ≥ 1.5 indicates two completely resolved peaks (baseline resolution), SR = 1 is more than adequate to indicate separation completion and employed here as a performance metric. To obtain SR during each electrophoretic immunoassay, a built-in least square fitting algorithm in MATLAB (MathWorks, Natick, MA) and an in-house multi-peak Gaussian fitting script were used to identify peak location and peak variance at each time point.

To minimize the separation length and time required to achieve baseline resolution between antibody and immune complex, a series of discontinuous separation gels having progressively more pronounced pore-size transitions were analyzed (Figure 6-2). Table 6-1 compares the separation performance for the series of discontinuous gels studied, all with a pore-size

discontinuity located ~200 μm downstream in the separation channel. The data in Table 6-1 is plotted graphically in Figure 6-3. Small pore-size gels in the separation channel enhanced $\Delta\mu/\mu_{Ab}$ and, in turn, reduced the separation length needed to achieve SR $\geq$ 1 (plotted in Figure 6-3B, C). For example, comparison of a 2.5/3.5%T discontinuous gel and a 2.5%/6%T gel show a 3x reduction in the separation length, resulting in a total separation length of 335 μm for the discontinuous 6%T separation gel. A commensurate reduction in the elapsed separation time needed was also observed.
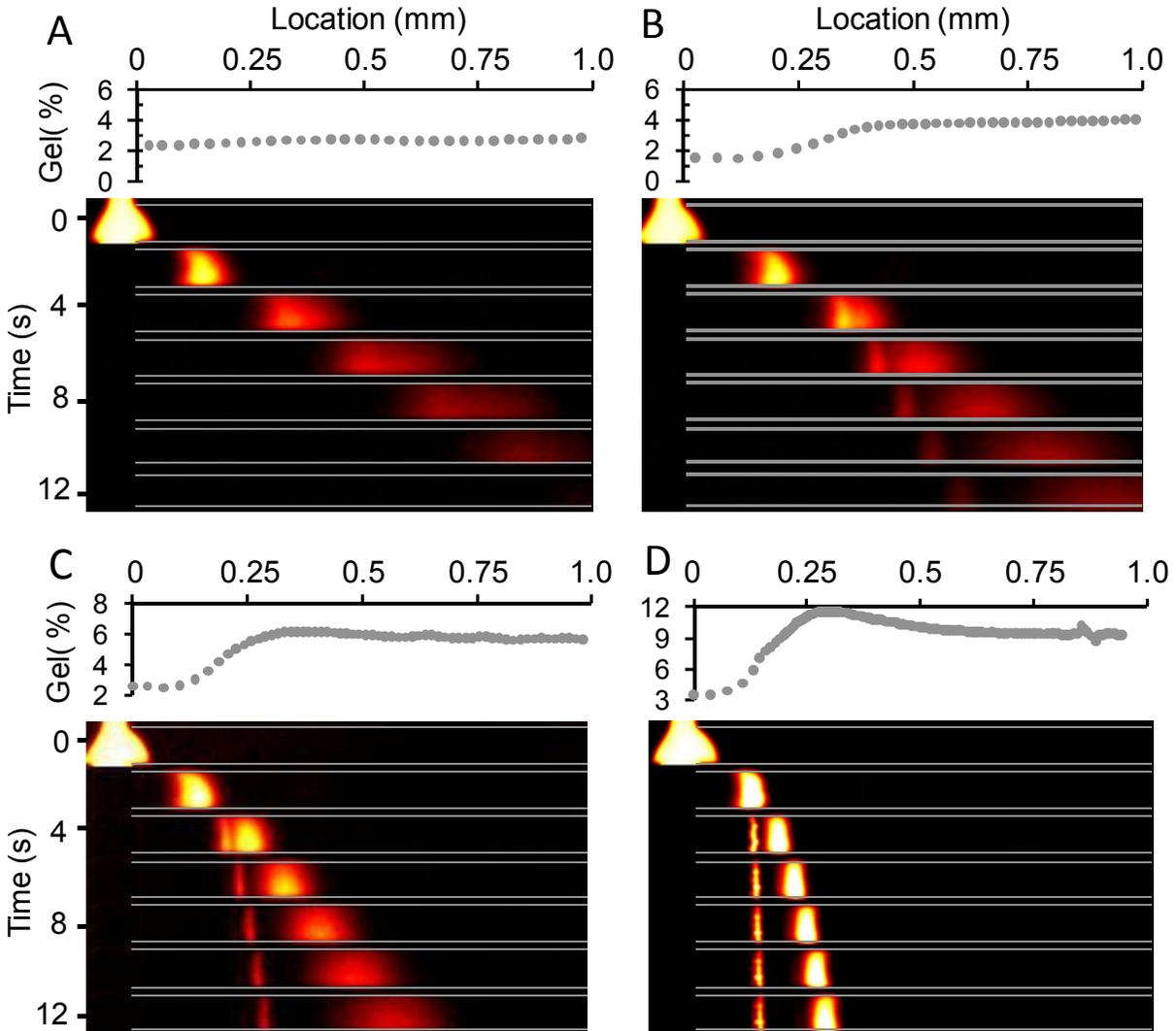


Figure 6-2. Discontinuous gel optimization yields decrease in separation length required for CRP immunoassay. Gel pore sizes are measured using method described in section 5.4. CRP assay on (A) 2.5/2.5%T, (B) 2.5/3.5%T, (C) 2.5/5%T, (D) 2.5/8%T discontinuous gel. E = 102 V/cm. [anti-CRP Ab*] = 66 nM, [CRP] = 16 nM.

Table 6-1 Optimization of polyacrylamide gel format for CRP immunoassay.

| Gel architecture | Uniform | Gradient | Discontinuous | | | | |
|---|---|---|---|---|---|---|---|
| | 2.5%T | 2.5%T-to-8%T | 2.5/2.5 | 2.5/3.5 | 2.5/4.0 | 2.5/5.0 | 2.5/6.0 |
| $\Delta\mu/\mu_{Ab*}$ in separation gel | < 5% | varies | 7.3% | 52% | 68% | 79% | 85% |
| $Ab*$ migration distance ($L_{anti\text{-}CRP\ Ab*}$) for SR $\geq 1$ [μm] | > 4000 | 750 | > 3000 | 850 | 515 | 320 | 285 |
| Separation length ($L_{anti\text{-}CRP\ Ab*} + 2\sigma_{anti\text{-}CRP\ Ab*}$) for SR $\geq 1$ [μm] | > 4000 | 925 | > 3000 | 1080 | 650 | 390 | 335 |
| Elapsed separation time for SR > 1 [s] | | 12.2 | | 10.9 | 6.3 | 5.6 | 5.2 |
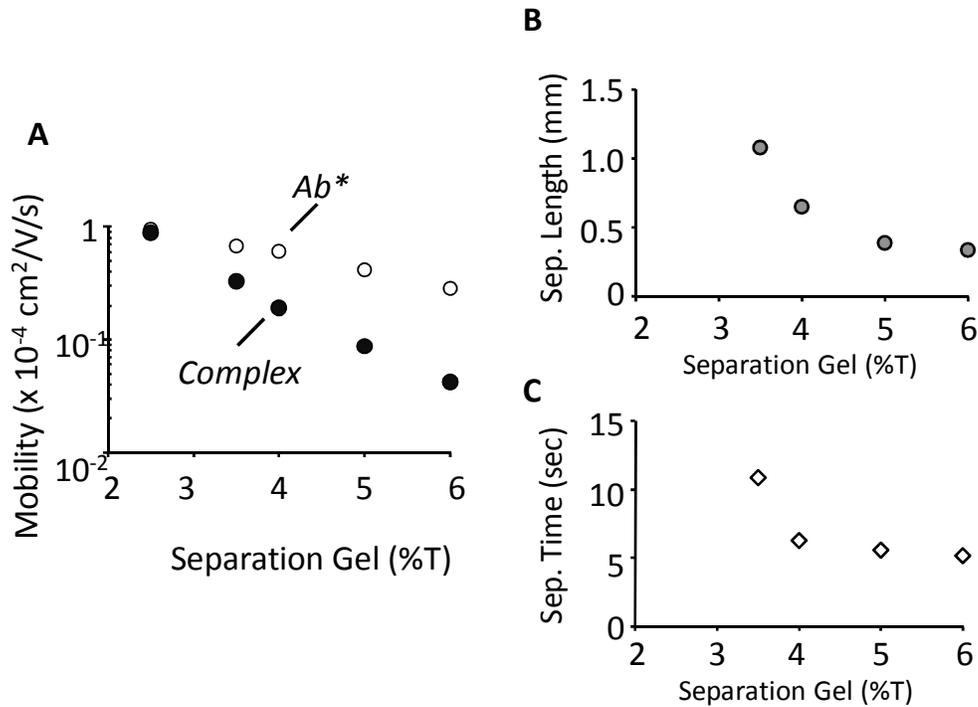


Figure 6-3. Increased mobility difference between the antibody and complexes (A) leads to reduced assay separation length (B) and separation time (C).

## 6.3    Adapting Discontinuous Gels for Full-field Imaging Based Detection

When full-field imaging is used as an assay detection method, all species within the field of view are imaged at every time point. Therefore, to achieve maximum separation resolution, the

separation gel should be designed to exclude immune complexes while allowing antibody to migrate through the discontinuity. Such design maximizes the mobility difference ($\Delta\mu/\mu$), and achieves maximum separation resolution within a given separation length. Figure 6-2D illustrates a CRP immunoassay performed on a 2.5/8%T discontinuous gel where SR > 1 was achieved in just 3 s in a separation length of 188 μm. SR > 1.5 is achieved within 4 s and a separation length of 200 μm. CRP immune complex was excluded at gel discontinuities with T > 8%. Exclusion of immune complex has previously aided homogeneous immunoassay completion, most often in conjunction with full-field CCD imaging[4, 5].

As discussed in Chapter 5, a secondary performance benefit offered by the discontinuous gels is the ability to "stack" proteins, hence improving signal-to-noise ratio and detection sensitivity. The "stacking" effect stems from the slowed migration of the protein analytes across the large-to-small pore-size discontinuity. Figure 6-4 compares the time and length scale for CRP immunoassay to achieve SR > 1 on 3 gel architectures. Compared to the 2.5%T-to-8%T gradient gel, the 2.5/5%T and 2.5/8%T discontinuous gels exhibit significant improvement in separation resolution as well as detection sensitivity. The 2.5/5%T discontinuous gel allows completion of a CRP immunoassay with a nearly 3x reduction in separation length and assay duration compared to a 2.5%T-to-8%T gradient gel. A 2.5/8%T discontinuous gel further reduces separation lengths to < 200 μm (Figure 6-4, bottom panel). Compared to the 2.5%T-to-8%T gradient gel, the 2.5/5%T discontinuous gel achieved nearly 4 times improvement in signal-to-noise ratio whereas an 8 times improvement was observed on the 2.5/8%T discontinuous gel (Figure 6-4, left panels).
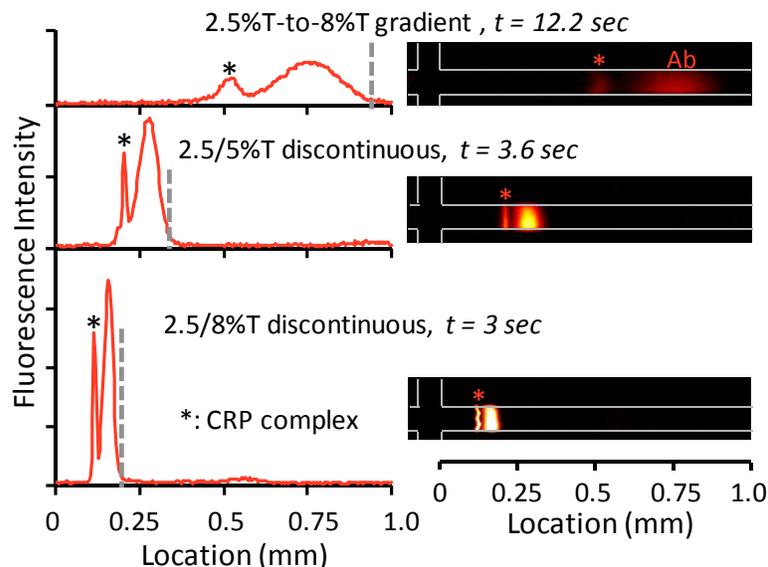


Figure 6-4. Tuning pore-size of discontinuity achieves baseline resolution in a shorter separation length (indicated by grey dashed lines). Channel fluorescence intensity profiles for separation resolution ≥ 1 are shown on the left for three separation gel formats whereas corresponding CCD separation images are shown on the right. Sample contains 16 nM CRP. Grey dashed line indicates effective separation length ($L_{Ab}+2\sigma_{Ab}$)

## 6.4    Adapting Discontinuous Gels for Simultaneous 2-Color Single-point Detection.

Although the 2.5/8%T discontinuous gel resulted in the shortest separation length using full-field imaging for detection, the expense and size of scientific-grade CCD cameras makes PMT or photodetector based single-point detection a preferred method for point-of-care instruments. Under single point detection, assay duration is largely determined by the slowly migrating proteins. If using a 2.5/8%T discontinuous gel, the immune complexes could take an infinitely long time to reach the single point detector due to physical exclusion by the small pore-size gels. Therefore, the 2.5/5%T discontinuous gel was chosen for single-point detection studies as both TNF-α and CRP immune complexes could enter the separation gel as shown in Figure 6-5. TNF-α and CRP are detected with corresponding antibodies labeled with distinct fluorophores (anti-TNF- α Ab* labeled with AF 488, anti-CRP Ab* labeled with AF 568). Using dual-color imaging, only one channel network is required to analyze both biomarkers. An SR $\geq$ 1 was achieved for CRP in a separation length of 330 μm and an elapsed separation time of 3.6 s; while for TNF-a the separation was completed in 310 μm and 4 s. Using the discontinuous gel format, both immune complexes were resolved from their respective free antibodies by 150 μm aft of the 2.5/5%T gel interface. A 2.5/5%T discontinuous gel yields immunoassays that complete with a nearly 3x reduction in separation length and assay duration compared to a 2.5%T-to-8%T gradient gel (Figure 6-6). Spectral multiplexing is also key to achieving a short separation length for multi-analyte assays by resolving spatially overlapped analyte peaks in a single channel (Figure 6-6).



58
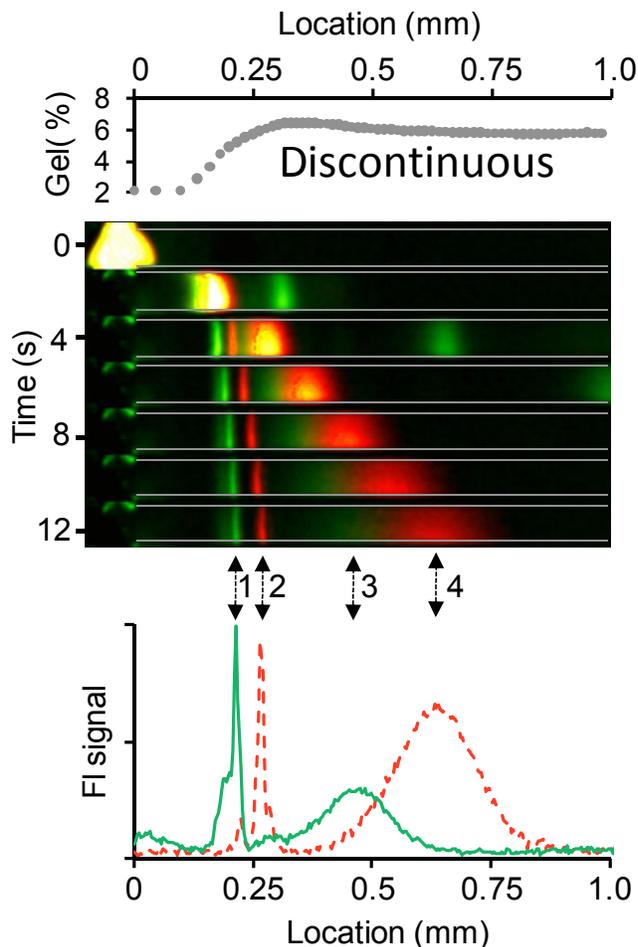
Figure 6-5. Two-color detection enables concurrent immunoassays for TNF-α and CRP in a discontinuous 2.5/5%T PA gel. Effective gel pore-size along the separation axis (top panel). Fluorescence images from the concurrent assays are shown for the first 12 s of the separation (false color, middle panel). Fluorescence intensity profiles are shown at 12 s for both immunoassays (bottom panel). E = 102 V/cm. Labels indicate: 1 – TNF-α complex; 2 – CRP complex; 3 – anti-TNF-α Ab*; 4 – anti-CRP Ab*. [TI*] = 50 nM, [anti-CRP Ab*] = 66 nM, [CRP] = 16 nM, [anti-TNF-α Ab*] = 68 nM, [TNF-α] = 22 nM.

To increase the separation electric field for the single-point detection assays, a modified voltage program was used. An upper limit on the electric field was set by gel breakdown observed when E > 500 V/cm for extended duration. The maximum field constraint most directly impacted the short channel segment connecting the injection junction to BW during the separation phase, thus a two-step pull-back voltage scheme was utilized. To inject a tight plug into the separation channel and limit injection leakage, for the first 5.5 s of the separation 800 V was applied to BW, B was grounded, S was set to 400 V and SW was set to 600 V. Thereafter, 1100 V was applied to BW while the S and SW voltages were reduced to 195 V and 220 V, respectively. The resulting separation electric field was increased to 200 V/cm with the channel segment B to the injection junction set at 250 V/cm, well under the gel breakdown limit. Due to high viscosity of the polyacrylamide gel and application of high pull-back electric field in the first step, there was no leakage from the loading channels even after reducing pull-back electric field to 25 V/cm.
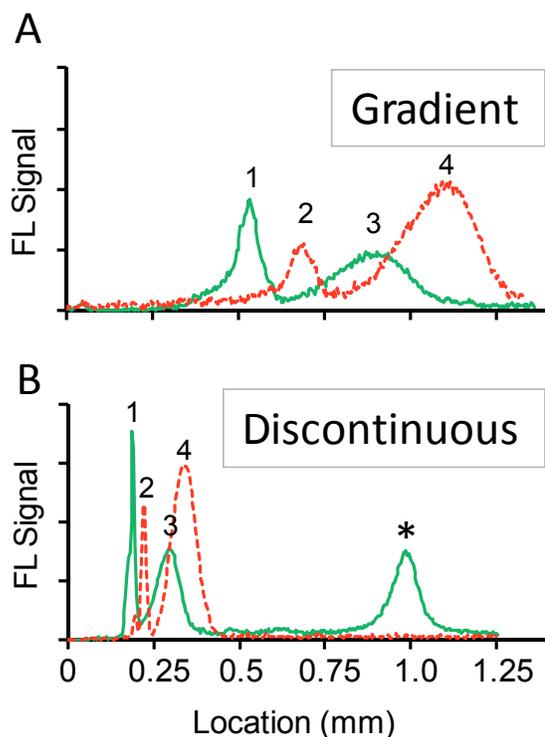


Figure 6-6. Discontinuous gel significantly decreased separation length required to achieve similar SR for two-color assays. (A) Gradient gel axial fluorescence intensity profile taken 12.5 s after injection: SR for TNF assay: 1.24; SR for CRP assay: 1.39. (B) Discontinuous gel axial

fluorescence intensity profile taken at 5.3 s after injection: SR for TNF assay: 1.27; SR for CRP assay: 1.43. E = 102 V/cm (first 5.5 s of separation) and E = 200 V/cm (thereafter). Fluorescence intensity normalized by loading channel intensity. Labels indicate: 1 – TNF complex; 2 – CRP complex; 3 – anti-TNF Ab*; 4 – anti-CRP Ab*. The "*" symbol indicates TI*, an internal standard.

To develop discontinuous gels for homogeneous electrophoretic immunoassays compatible with PMT based single-point detection, the detector location for simultaneous two-color immunoassays was optimized through consideration of SR and assay duration. The required separation length for single-point detection is defined as the detector location resulting in well-resolved species peaks (SR > 1). Using CCD separation images, peak center and peak width ($4\sigma$ spread indicated by error bars) were tracked as a function of time for both the CRP free antibody and immune complex peaks (Figure 6-7). As described, at the 5.5 s elapsed separation time point, a two-step pull back voltage program was implemented to increase the separation electric field from 102 V/cm to 200 V/cm.

The change in electric field can be observed as a shift in the slope of migration distance vs. time for the discontinuous gel (middle panel, Figure 6-7). SR ~ 1.5 was achieved at an elapsed separation time of 5.6 s for discontinuous gels and at 13.2 s for gradient gels (right panel, Figure 6-7). At an SR ~ 1.5, the minimum between the two peaks informs selection of the optimal detector location which yields well-resolved electropherograms. Using this approach, the single-point detector was placed at ~250 μm for the discontinuous gel (2.5/5%T) and ~800 μm for the decreasing pore-size gradient gel (2.5%T-to-8%T). As compared to the gradient gel architecture, the discontinuous gel format achieved a 3x reduction in separation distance when using single-point detection.
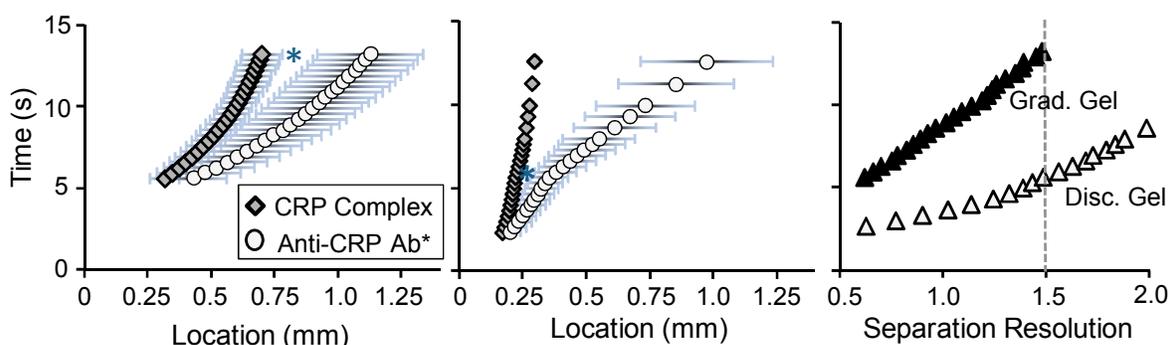


Figure 6-7. Single point detection location optimization through determination of baseline separation condition. Analysis of anti-CRP Ab* and CRP complex peak migration and peak widths for gradient gel (left panel) and 2.5/5% discontinuous gel (middle panel). Right panel: separation resolution for gradient and discontinuous gel formats vs. time. Optimal single point detector location is indicated as "*". E = 102 V/cm (first 5.5 s) and E = 200 V/cm.

Simultaneous detection of TNF-α and CRP was implemented on the 2.5/5%T discontinuous gel using two-color single-point PMT detection (Figure 6-8A). A injector-to-detector length of 270 μm was estimated by first extracting the times required for antibody and complex migration to the detector (from electropherograms) and then obtaining analyte migration distance from CCD image sequences at the same migration times (Figure 6-7, middle panel for CRP assay). Dose

response curves for CRP and TNF-α (Figure 6-8B,C) showed a quantitative capability with a lower limit of detection for the CRP assay of 11.5 ng/mL and a lower limit of detection for TNF-α assay of 40 ng/mL. No notable cross-reactivity between the TNF-α protein and the CRP antibody, or for the CRP protein and TNF-α antibody, was observed in the concurrent assay (Figure 6-8B,C insets).
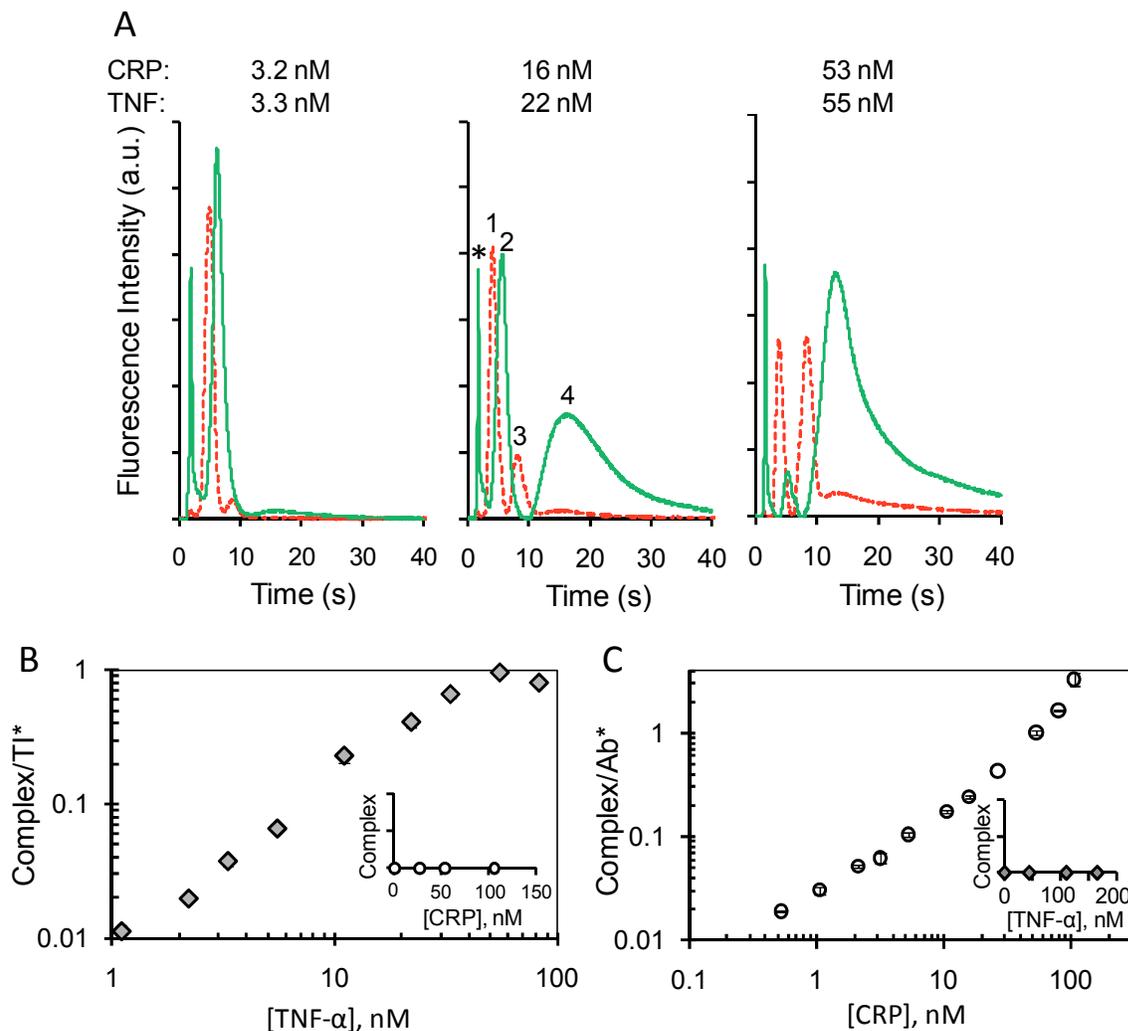


Figure 6-8. Two-color immunoassay is quantitative. (A) Electropherogram generated on discontinuous gel chip with incubates containing CRP=3.2nM/TNF=3.3nM, CRP=16nM/TNF=22nM, CRP=53nM/TNF=55nM. Labels indicate: 1 – anti-CRP Ab*; 2 – anti-TNF Ab*; 3 –CRP complex; 4 – TNF complex. The "*" symbol indicates TI*, an internal standard. (B) TNF-α assay dose response curve with LLOD of 2.2 nM (40 ng/mL) (C) CRP assay dose response curve with LLOD of 500 pM (11.5 ng/mL). Error bars denote standard deviation based on 3-5 runs; detection at 270 μm; E = 102 V/cm (first 5.5 s) and E = 200 V/cm.

## 6.5    Sequential injection and quantitation

As species were not immobilized in the separation gel, the 5%T pore-size allowed sequential injections and separations which make the separation format compatible with both continuous monitoring assays and chip re-use in clinical settings. Assay reproducibility was evaluated by conducting ten sequential CRP immunoassays over a 20 min period (Figure 6-9A). As shown in Figure 6-9C, antibody peak migration exhibited a %RSD of 2.5% and the complex peak migration %RSD was 2.2%. The %RSD for the SR was 1.0% and the antibody-to-complex peak height ratio exhibited a 2.7% RSD. The reproducibility performance is expected as polyacrylamide gels exhibit low non-specific adsorption and separation gel pore-size was properly selected to allow unrestricted migration of analyte species.
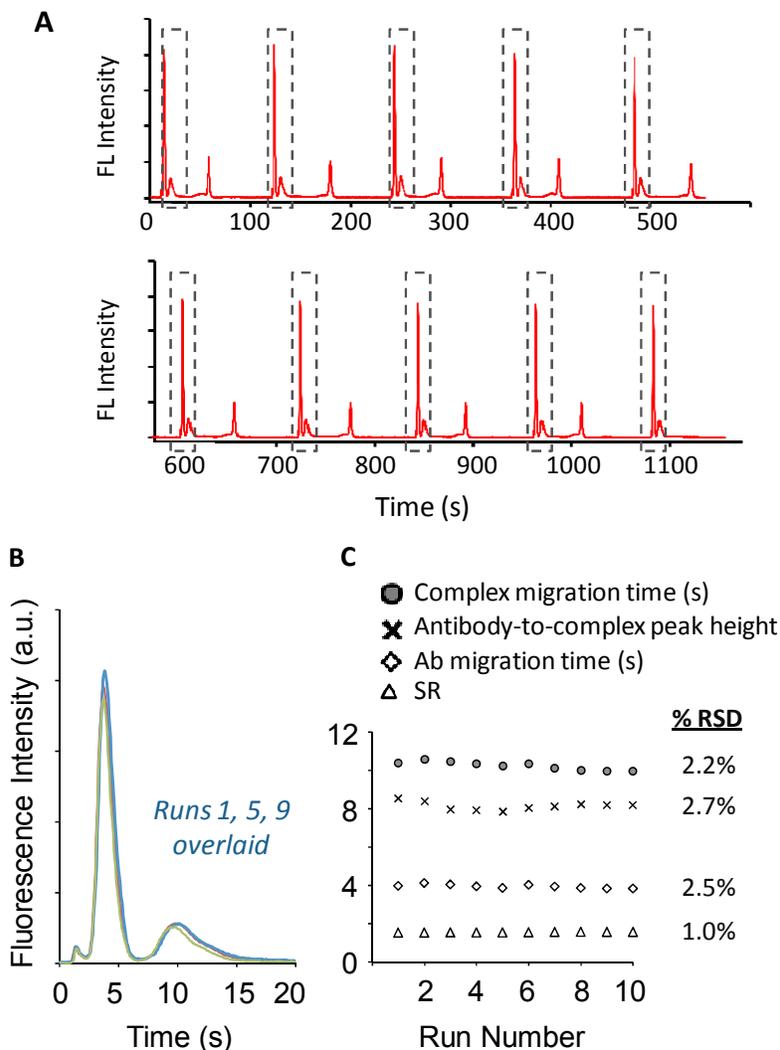


Figure 6-9. Reproducibility of ten CRP assays conducted on 2.5/5%T discontinuous gel. [CRP] = 10.6 nM. Detector Location: 280 μm. (A) 10 CRP separation using the same sample is performed over 20 minutes. Each separation is indicated by the dashed box. (B) Overlay of Ab* and complex peaks from runs 1, 5, and 9. (C) Ab* migration time, complex migration time, peak height ratio, and separation resolution for each of the injections with mean values of 3.93 s, 10.2 s, 8.12, and 1.54 for each, respectively.

## 6.6    Summary

62

A systematic approach to assay development allows us to optimize the homogeneous electrophoretic immunoassay performance. In particular, on-chip discontinuous gels were introduced to enhance antibody and complex mobility differences, hence, achieving assay completion in an ultra-short separation distance. Further, spectral multiplexing and concurrent two-color detection is key to maintain short separation length for quantifying multiple biomarkers. Using CRP and TNF-α as model biomarkers, we demonstrate assay completion within 350 μm. Importantly, short separation lengths enable sufficient applied electric field strengths for rapid electrophoresis, with low applied electrical potential requirements; for the discontinuous gels demonstrated here, an applied electric field strength of 100 V/cm would require 3.5 V across the required separation length. In optimizing discontinuous pore-size gels for both full field imaging and single-point detection, we introduce an improved partial illumination approach that results in well-controlled gel pore-size fabrication via mask-based in-situ photopolymerization. While developed for the discontinuous separation gels, the approach is widely applicable to fabrication of various functional polymer units (e.g., membranes, filters) in microfluidic channels. Using spectral multiplexing, we demonstrate simultaneous immunoassays for CRP and TNF-α as quantitative with no appreciable cross-reactivity for the targets considered.

Using the design approach described, homogeneous electrophoretic immunoassays for other protein biomarkers can be optimized through tuning sieving matrix pore-size to generate sufficient mobility differences between the antibody and immune complex. Further separation length reductions (< 200 μm) can be achieved by excluding immune complex from the separation gel, which is applicable for implementation with full-field imaging. However, single-point detection is often desired for low-cost point-of-care diagnostic instruments, thus separation gels allowing entry of immune complexes were the focus of this study.

## 6.7    Future directions

### 6.7.1    On-chip preconcentration to improve assay sensitivity
While the CRP immunoassay developed meets the specification to assess cardiovascular risk, the TNF-α assay requires further sensitivity improvement to detect TNF-α at clinically relevant range. CRP immunoassay developed has a lower limit of detection (LLOD) of 11.5 ng/mL and a linear dose response over 2-log concentration range. The LLOD and dynamic range is appropriate for measuring CRP in diluted serum for cardiovascular risk assessment[6]. Shown in Figure 6-10 is detection of CRP spiked in 20x diluted serum. On the other hand, normal TNF-α serum level is at 75 pg/ml and can rise up to 5 ng/ml during severe sepsis[7], suggesting further sensitivity improvement is required.
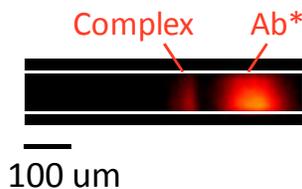


Figure 6-10. Measurement of CRP in spiked serum. Separation was performed in 2.5/5% discontinuous gels after incubation with anti-CRP Ab*.

The sensitivity of microchip homogeneous immunoassay is ultimately limited by the injected sample volume as defined by the channel geometry. Although several μLs of sample was placed in the sample well, less than 0.1 nL of sample is actually introduced into the separation channel for chip dimensions used in this work. Therefore, less than 300,000 fluorescence molecules are introduced into the separation channel assuming an immune complex concentration of 1 nM and a degree labeling of 5 fluorescence dyes per antibody. Additionally, the mid-high pM sensitivity we have achieved is on par with theoretical detection limit that was previously predicted for competitive homogeneous immunoassay using on-chip capillary electrophoresis[8].

Immunoassay sensitivity can be improved by integrating discontinuous gel design with an upstream preconcentration step using photopolymerized membranes. Photopolymerized membrane was previously applied in concentration and sizing of proteins which achieved a concentration factor of 1000 times within 5 min[9]. With the membrane design, all materials reaching the membrane from the loading channel (with a length of 0.5 cm) will be compressed into a confined plug (with width of < 50 μm) near the membrane. Therefore, the concentration factor achieved by the membrane is equal to

$$\frac{Loading\ channel\ length}{Plug\ width\ near\ membrane} \times \frac{Total\ concentration\ time}{Analyte\ migration\ time\ in\ loading\ channel}.$$

Theoretically, 1000 fold increase in analyte concentration can be achieved with 5 min of preconcentration time assuming the immune complex requires 0.5 min to reach the membrane from the sample well.

Besides improving sensitivity, incorporation of a photopolymerized membrane upstream of separation can also improve assay dynamic range[10] and perform on-chip incubation of affinity reagent and target analyte[11].

### 6.7.2 Single channel immunoassay architecture to further reduce device footprint

As shown in Figure 6-5 and quantified in section 6.4, we are able to complete immunoassays within a separation length of 330 μm and a separation time of 4 sec. Further reduction in separation length to less than 100 μm can be achieved by fabricating the discontinuous interface closer to the injection junction with high resolution photopatterning on a mask aligner. In addition, we propose a single channel immunoassay architecture to reduce total assay time and device footprint. The single channel design monitors step changes in fluorescence intensity as new analytes enter the region of interests and eliminates the loading time required to introduce analytes to the injection junction prior to separation.

The single channel immunoassay architecture is inspired by previous demonstration of gradient elution moving boundary electrophoresis (GEMBE) assay in a single channel network[12]. In GEMBE, analyte detection is accomplished by monitoring a step change in fluorescence intensity as analyte enters the channel network one by one due to different electrophoretic mobility. In the published GEMBE work, a pressure and electroosmotic-driven buffer counter flow was applied to reduce effective separation length required. In our proposed design, we optimize gel composition to maximize electrophoretic mobility differences as in demonstrated discontinuous gel work. On-chip gel electrophoresis can resolve immune complexes more effectively than free solution electrophoresis without requiring application of any counter flow and increased hardware complexity.

Theoretical analysis of separation resolution reveals the proposed single channel immunoassay architecture can achieve SR > 1 in an even shorter separation length than the demonstrated discontinuous gels architecture. Figure 6-11A displays a schematic view of the channel during electrokinetic injection of both the antibodies (Ab*) and the immune complexes. The concentration profile of each analyte across the separation channel is obtained by solving the following transport equation: $\frac{\partial c}{\partial t} = -U\frac{\partial c}{\partial x} + D\frac{\partial^2 c}{\partial x^2}$ with the boundary conditions of $c(x < 0) = c_0$ and $\frac{\partial c}{\partial x}(x < 0) = 0$ where $c_0$ is analyte concentration in the sample well. Hence, each analyte concentration profile can be described by $c(x,t) = c_0 \text{erfc}(\frac{x-Ut}{\sqrt{4Dt}})$ where erfc is the complementary error function with $\text{erfc}(x) = \frac{2}{\sqrt{\pi}}\int_x^\infty e^{-z^2} dz$. The total fluorescence intensity is the sum of antibody and complex fluorescence intensity. As the derivative of the resulted analyte concentration profile is a Gaussian function ($\frac{dc(x,t)}{dx} = \frac{c_0}{\sqrt{\pi Dt}}e^{-\left(\frac{x-Ut}{\sqrt{4Dt}}\right)^2}$), analysis of separation in the single channel assay design is similar to that of previously used cross channel designs (Figure 6-11 B). By selecting an appropriate sieving matrix composition (T), we can maximize the peak-to-peak distance (ΔL) among analytes without excluding the immune complex from entering the channel. The single channel design with continuous injection can achieve better SR in a given separation length as $\sigma_0 = 0$ (analyte concentration profile resembles a sharp step function near the well prior to electrophoretic injection).
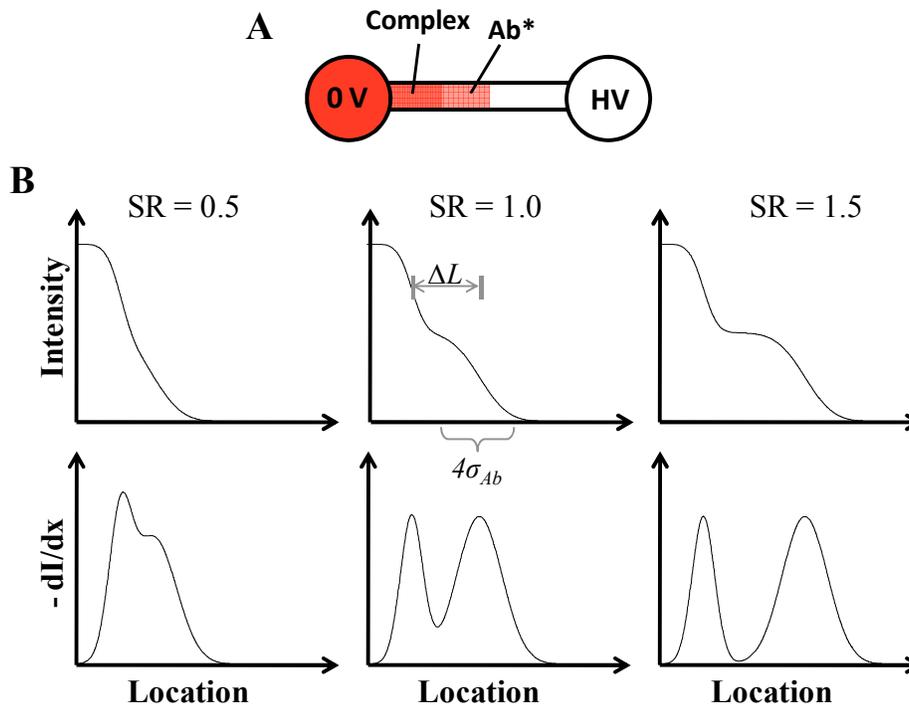


Figure 6-11. Proposed single channel immunoassay architecture. (A) Differences in antibody and complex mobility result in step changes of channel fluorescence intensity during sample injection. (B) The *x*-derivative of intensity profile is equivalent to the sum of two Gaussian peaks.

Displayed are intensity profile and corresponding derivatives for different separation resolution. The two peaks have the same peak height and the faster peak has 2x σ than the slower peak.

The benefits of single channel immunoassay architecture include: (1) reduced device footprint and electrode requirement (from 4 to 2) which increases the number of networks that can be integrated on a single chip for high throughput analysis and (2) reduced separation length and total assay time by elimination of the loading gel. The main drawback is that, as analytes aren't resolved into individual bands, separation using the single channel design is difficult to interpret visually without image processing.

## 6.8    References

(1)     Cui, X. Q.; Lee, L. M.; Heng, X.; Zhong, W. W.; Sternberg, P. W.; Psaltis, D.; Yang, C. H. *Proceedings of the National Academy of Sciences of the United States of America* **2008**, *105*, 10670-10675.
(2)     Ferguson, K. A. *Metabolism-Clinical and Experimental* **1964**, *13*, 985-1002.
(3)     Ornstein, L. *Annals of the New York Academy of Sciences* **1964**, *121*, 321-349.
(4)     Yamada, M.; Mao, P.; Fu, J. P.; Han, J. Y. *Analytical Chemistry* **2009**, *81*, 7067-7074.
(5)     Reichmuth, D. S.; Wang, S. K.; Barrett, L. M.; Throckmorton, D. J.; Einfeld, W.; Singh, A. K. *Lab on a Chip* **2008**, *8*, 1319-1324.
(6)     Pepys, M. B.; Hirschfield, G. M. *Journal of Clinical Investigation* **2003**, *111*, 1805-1812.
(7)     Damas, P.; Reuter, A.; Gysen, P.; Demonty, J.; Lamy, M.; Franchimont, P. *Critical Care Medicine* **1989**, *17*, 975-978.
(8)     Taylor, J.; Picelli, G.; Harrison, D. J. *Electrophoresis* **2001**, *22*, 3699-3708.
(9)     Hatch, A. V.; Herr, A. E.; Throckmorton, D. J.; Brennan, J. S.; Singh, A. K. *Analytical Chemistry* **2006**, *78*, 4976-4984.
(10)    Wang, Y. C.; Han, J. Y. *Lab on a Chip* **2008**, *8*, 392-394.
(11)    Herr, A. E.; Hatch, A. V.; Throckmorton, D. J.; Tran, H. M.; Brennan, J. S.; Giannobile, W. V.; Singh, A. K. *Proceedings of the National Academy of Sciences of the United States of America* **2007**, *104*, 5268-5273.
(12)    Ross, D.; Kralj, J. G. *Analytical Chemistry* **2008**, *80*, 9467-9474.

# Chapter 7 Introduction to Microfluidic Western Blotting Assay with SDS Removal in Transit

Our previous work focuses on development of ultra-short separation length homogeneous immunoassays that are enabled by photopatterned discontinuous gels. Besides providing superior separation resolution, photopatterning of polyacrylamide gels facilitates seamless integration of multiple functional units within a single device. In the second part of my thesis work, we developed a microfluidic western blotting assay with single-chip integration of SDS removal and protein renaturation strategies with upstream SDS-PAGE separation and downstream immunoaffinity recognition. This chapter first presents an overview and limitations of existing macroscale and microscale western blotting assays (7.1-7.2). Then we propose a microscale western blotting assay design with SDS removal in transit (7.3). The "SDS removal" terminology used in our work refers to removal of SDS from denatured proteins as is necessary for protein renaturation. SDS is not physically removed from our devices but rather isolated from proteins to prevent further denaturation. By developing a simple model describing protein renaturation process, two strategies to remove SDS and renature proteins are conceived (7.4).

## 7.1 Introduction to western blotting assay

### 7.1.1 Comparison of western blotting assays with immunoassays

Immunoassays[1] and western blotting assays[2] differ in their assay implementation, assay output, and target application areas as summarized in Table 7-1. Immunoassays report the presence and concentration of target analytes by quantifying immune complex formation between target analytes and affinity probes. For homogeneous immunoassays (as presented in our previous work), electrophoretic separation is performed after complex formation to resolve immune complexes from excess affinity probes. In comparison, the western blotting assay, a powerful and ubiquitous technique for protein analysis, first performs electrophoretic separation of a complex sample and then simultaneously assays binding characteristics of resolved proteins to an antibody probe. While homogeneous immunoassays measure electrophoretic mobility of the complex formed, western blotting assays report on electrophoretic mobility prior to complex formation. Electrophoretic mobility, which is related to protein charge to size ratio in native states or molecular weight in denaturing conditions, can distinguish target analytes from nonspecifically bound analytes. Thus, the western blotting assay is suitable for analysis of complex samples such as tissue or cell cultures to elucidate signaling pathways[3]. In clinical settings the western blotting assay also serves as a confirmatory test to immunoassays to reduce the incidence of false positives. For example, the western blotting assay is currently employed as a confirmatory HIV diagnostic test [4].

Table 7-1. Comparison of immunoassays and western blotting assays

|  | Immunoassay | Western blotting assay |
|---|---|---|
| Assay output | Target analyte concentration | Target and non-target analyte molecular weight and binding information |
| Implementation | Quantification of immune complex formation | Electrophoretic separation followed by transfer and immunoaffinity blotting |
| Application | Clinical diagnostics | Analysis of complex samples in laboratory settings and confirmatory diagnostics in clinical settings |

### 7.1.2 Conventional western blotting assay is labor intensive and inefficient

Despite its capabilities, western blotting assay suffers from a labor-intensive nature. Surprisingly, the assay format has changed little since its introduction. Figure 7-1 illustrates an operation flow for western blotting assays with assay time indicated for each step. In the first step, polyacrylamide gel electrophoresis (PAGE) of proteins can take hours on slab gels. In the second step, proteins on the gel are transferred to a nitrocellulose or polyvinylidene fluoride (PVDF) membrane for subsequent affinity detection. The transfer step is prone to material loss and variable reproducibility[5]. After transfer, the membrane is subsequently blocked with BSA or nonfat dry milk which reduces nonspecific binding for subsequent antibody probing. Then the membrane is incubated with primary antibodies and washed to remove unbound antibody probes. If using secondary antibodies with enzymatic labels to increase detection sensitivity, additional incubation and washing steps are required. The assay can take up to 2 days to complete. Futhermore, the blotting step requires a substantial amount of antibody mass (~ 10 μg) which translates to tens of dollars spent on purchasing high quality antibodies for one assay.

| PAGE | Transfer | Blocking & Washing | Immuno-blotting |
|---|---|---|---|
| ~ 2 hrs | ~ 2-4 hrs | ~ 2-12hrs | ~ 2-10 hrs |

Figure 7-1. Western blotting is a time consuming and labor intensive process that requires multiple pieces of lab equipments and frequent human intervention.

## 7.2 Microfluidic implementation of western blotting assay

Microfluidic implementation of western blotting assays results in significant throughput and performance improvement. Miniaturization reduces sample and reagent consumption. Reduced sample consumption expands application of western blotting assays from analysis of tissue and cell cultures to study of a single cell or several cells. Microfluidic based single cell analysis opens up new frontiers in biology by revealing actions of individual cells instead of measuring collective behaviors of thousands and millions of cells[6]. Reduced reagent consumption reduces assay cost by minimizing the amount of antibody consumed in the blotting step. Furthermore, seamless integration of multiple functionalities in a single device reduces the material loss and improves assay reproducibility.

Recently, several western blotting assay designs with improved throughput have emerged. Efforts by other groups have been limited to replacing one or two components of the

conventional assay with microscale analysis. In a recent report of high throughput microwestern arrays, Ciacco et al printed cell lysates via noncontact microarrayer on slab gels in 96 identical blocks[7]. After a semidry electrophoresis, proteins were transferred to a nitrocellulose membrane; a 96-well plate was assembled on top of the nitrocellulose membrane; the cell lysates were then probed with 96 different antibodies as compared to single antibody probing in conventional western blotting assay. In a separate effort to increase the number of antibody probes, a nitrocellulose membrane containing transferred proteins was assembled with a PDMS microfluidic device in which a different detection antibody was flown through each microfluidic channel[8]. Anderson et al replaced slab gel electrophoresis with capillary gel electrophoresis for improved mass sensitivity and faster separation time and was able to complete western blotting within 1 hour[9].

Our laboratory reported a microfluidic-based native western blotting assay. Separation, transfer, and blotting are seamlessly integrated on a single chip and automated by programmable voltage control[10]. As depicted in Figure 7-2, photopatterning of polyacrylamide gels created discrete functional unit within a rectangular 2D chamber. Within the 2D chamber, a loading and separation gel ensured high resolution separation of proteins by charge-to-mass ratios. Optimized voltage programming and chip design allowed for low-dispersion transfer of resolved proteins from the separation gel into a protein-binding gel that contained immobilized detection antibody. As polyacrylamide gels exhibit low nonspecific adsorption, only target proteins are retained by the detection antibodies; no blocking and washing steps are necessary. A native immunoblot for free human prostate specific antigen (PSA) completes in less than 5 minute and exhibits superior transfer efficiency and reproducibility than conventional western blotting assays. To enable multiplexing capability, my colleagues extended the original design to accommodate multiple detection antibodies by fabricating blotting gels decorated with different antibodies adjacent to each other[11]. In addition, operation parameters (i.e., electric field) and design parameters (i.e., blotting gel length and antibody density) of microfluidic western blotting assay can be optimized to maximize detection sensitivity.
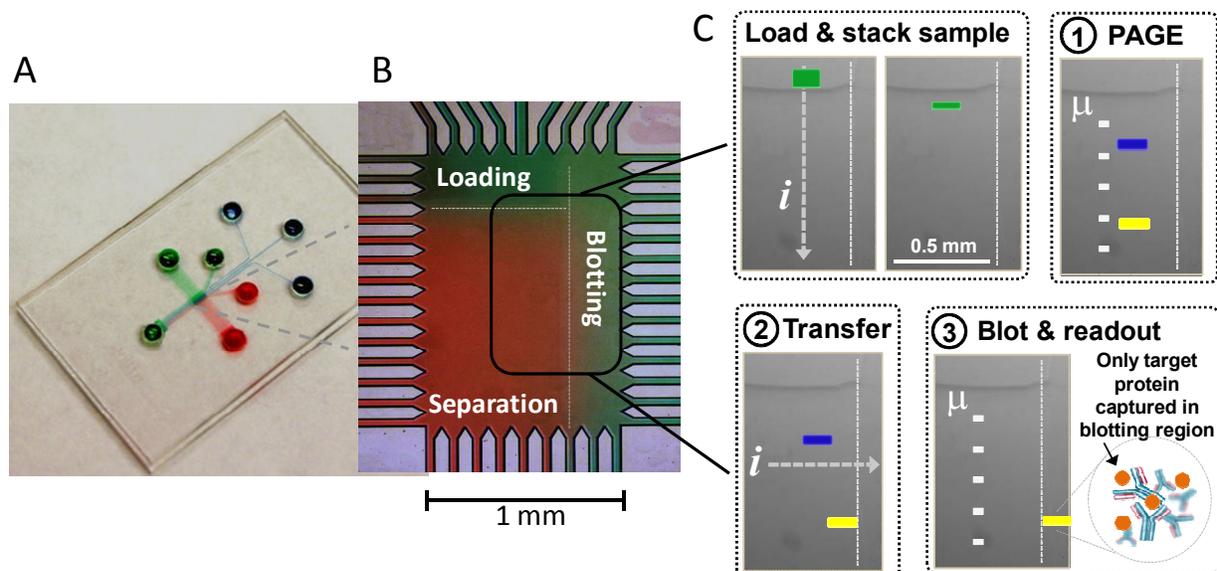


Figure 7-2. Photopatterning of polyacrylamide gels within a 2D microfluidic geometry enables fully integrated protein immunoblotting. (A) Bright field image of microfluidic device with

photopatterned PA gels. (B) Magnified view of 2D chamber where immunoblotting is performed. (C) Individual immunoblotting steps are overlaid on top of chamber images. (Picture Courtesy: Dr. Mei He).

## 7.3 Universal adoption of microfluidic western blotting requires sizing capability

While native western blotting assay can report charge-to-size ratio and conformation information of target and nontarget proteins[12], it lacks the capability to resolve proteins based on molecular weight which is a functionality required in laboratory settings. Therefore, prevalent adoption of microfluidic western blotting assays requires integration of molecular weight measurement with downstream immunoaffinity detection.

### 7.3.1 SDS PAGE identifies protein molecular weight

Denaturing proteins with sodium dodecyl sulfate (SDS) and performing separation in SDS gels are the laboratory standards to resolve proteins based on size for molecular weight determination[13]. As shown in chapter 1, Ferguson relationship[14] describes protein mobility ($\mu$) as a function of polyacrylamide gel concentration ($T$): $\mu = \mu_0 10^{-KT}$ where $\mu_0$ is the free solution electrophoretic mobility and $K$ is the retardation coefficient proportional to protein size. Under native conformation, $\mu_0$ of a protein is proportional to its charge-to-size ratio. Due to differences in amino acid sequences, different proteins exhibit different $\mu_0$. With a reducing agent (DTT or 2-mercaptoethanol), SDS denatures proteins to polypeptides and binds to proteins at a constant 1.4 g SDS/1 g protein ratio[15]. As each dodecyl sulfate molecule carries one negative charge, SDS treatment results in each protein carrying a total charge proportional to its molecular weight, or equivalently, a constant $\mu_0$ for all proteins. As a result, protein mobility in polyacrylamide gel becomes a function of $K$ which is proportional to protein molecular weight. SDS PAGE can determine protein molecular weight with great confidence and was able to generate a linear relationship between protein mobility and log molecular weight[13].

### 7.3.2 Existing methods for SDS removal and protein renaturation within western blotting assays

While treatment of proteins with SDS is necessary for molecular weight determination, treatment with SDS destructs enzymatic or biological properties of treated proteins[16]. Fortunately, enzymatic activities can be restored following SDS removal and renaturation[17]. Thus, SDS removal is indispensable to western blotting assays. In conventional western blotting, SDS removal occurs during the transfer step where proteins are transferred from slab gels to membranes in absence of any denaturants (such as SDS)[18]. Prior to detection with antibody probes, the membrane is also washed for 30 minutes to hours to remove excess SDS and SDS bound to proteins. My colleagues have developed 2 approaches to integrate detergent-based separation with immunoaffinity recognition in microfluidic formats. In the first approach[19], SDS-treated proteins were transferred to discrete membranes after sizing. The membranes act like a size-cutoff filter: small SDS molecules (molecular weight: 288 g/mol) are able to pass through while larger proteins (10 – 150 kg/mol) are retained. Using an optimized membrane design with low nonspecific retention, proteins can be retained near the membrane for a desired renaturation time of several minutes before being transferred to a blotting gel for antibody probing. In another approach[20], proteins coated with cationic detergent (CTAB) were first

immobilized after separation by electrophoretic transfer into a negatively charged gel region; a buffer exchange step was performed to remove SDS and renature proteins.

Both microfluidic implementations of SDS removal with western blotting assay developed by my colleagues enabled immunoaffinity recognition of proteins that were previously denatured for sizing purposes. However, both approaches have performance and implementation limitations. In the first membrane-based approach, protein position may be shifted and separation resolution may be lost following transfer to membranes. In the second approach that utilizes electrostatic immobilization, separation resolution achieved in the first step was conserved. However, subsequent blocking and multiple washing steps were required to reduce nonspecific binding to the negatively charge gels.

### 7.3.3 Proposed strategy: SDS removal in transit

Given the limitations of previously reported approaches, we seek to remove SDS and renature proteins in transit. Figure 7-3 depicts the proposed assay architecture. As on-chip SDS-PAGE and immunoblotting in the 2-D separation chamber have previously been reported, my work focuses on removing SDS and renaturing protein during the lateral transfer stage (step 2 in the proposed assay architecture). Compared to the membrane based approach to remove SDS[19], SDS removal in transit can preserve separation resolution achieved in the separation stage. Compared to the immobilization-based approach followed by buffer exchange to remove SDS[20], the proposed method is streamlined without introducing additional reagents.



**1. SDS-PAGE Separation**  **2. Transfer and SDS Removal**  **3. Blot and Detection**
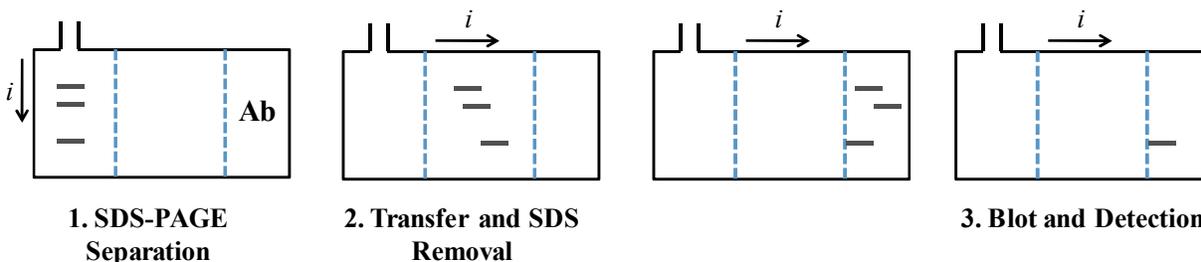
Figure 7-3. Western blotting assay with SDS removal in transit. Step 1: SDS-PAGE resolves protein based on molecular weight; "$i$" indicates the direction of current flow. Step 2: lateral electrophoresis transfers resolved protein across the chamber to remove SDS. Step 3: proteins bound to Ab are retained whereas unbound proteins migrate out of the chamber.

## 7.4 Theoretical basis of proposed SDS removal strategies

By developing a simple model to describe SDS-protein complex dissociation process, we propose two SDS removal strategies that can act either independent of each other or in parallel.

### 7.4.1 A simple model to describe SDS dissociation

To have an intuitive understanding of the SDS removal process, we model SDS dissociation from SDS-protein complex using a chemical reaction: $CRP^* \cdot SDS \xrightarrow{k_{on}, k_{off}} CRP^* + SDS$. $CRP^* \cdot SDS$ represents C reactive protein (CRP) coated with SDS molecules. CRP is fluorescently labeled for visualization purposes. $CRP^*$ represents the portion of CRP that can bind to the blotting gel as a result of SDS removal and renaturation, and SDS represents free SDS in the system as well as free SDS that has dissociated from the protein-SDS complex. CRP

is applied as a model protein to characterize the performance of our microfluidic western blotting assay for its diagnostic significance and for exhibiting distinct conformations at native state (as a pentamer of 115 kDa) and reduced state (as a monomer of 23 kDa)[21]. $k_{on}$ represents the binding rate of CRP with free SDS; $k_{off}$ encompasses both the dissociation rate of SDS-CRP complex and the renaturation rate of CRP to a conformation recognizable by antibodies.

### 7.4.2 Two strategies conceived from analyzing the simple model

Using the simple model, we formulate our design goal as to increase the dissociation of SDS from CRP*-SDS to CRP* that can be blotted by antibodies. Based on the simple model, we obtain the rate of CRP concentration change as a function of time:

$$\frac{\partial [CRP*]}{\partial t} = -k_{on}[SDS][CRP^*] + k_{off}[SDS \cdot CRP^*].$$

Therefore, by removing free SDS from the system or by isolating SDS from CRP*, we can minimize the formation of new SDS-CRP* while maximizing the formation of CRP*.

We have developed two strategies to maximize the recovery of CRP*. Both strategies aim to decrease the association of free SDS with CRP ($k_{on}[SDS][CRP^*]$). In the first strategy, we immobilize cyclodextrin, an inclusion complex, in the lateral transfer region to sequester free SDS so free [SDS] is reduced. While cyclodextrin is used extensively for drug delivery applications[22], several studies demonstrated the application of cyclodextrin to assist detergent removal and renaturation of previously denatured proteins. Incubation of creatine kinase with 2-hydroxylpropyl β-cyclodextrin increased enzymatic activity from 0% following SDS denaturation to 80% compared to the activity of its native conformation[23]. In a separate study, treatment with β-cylodextrin recovered enzymatic activity of carbonic anhydrase from 3% following SDS treatment to 92% compared to the activity of its native state[24]. Previous applications of cyclodextrin have been limited to recovering enzymatic activities partly due to readily available enzyme activity assays. With our ability to rapidly quantify antibody-antigen binding interactions via on-chip homogeneous immunoassays or immunoblotting assays, we expand the application of β-cylodextrin to recovering antigen-antibody binding following SDS denaturation.

In the second approach, we optimize the separation of free SDS from CRP* during the transfer stage to prevent formation of SDS-CRP*, or equivalent reducing [SDS]·[CRP*]. As demonstrated in our previous development of ultra-short separation length homogeneous immunoassays, optimization of sieving matrix properties such as pore sizes and spatial distribution has resulted in substantial improvement of separation resolution between the immune complex and antibodies within a given separation distance. Here, we apply a similar optimization procedure to enhance the separation of SDS from CRP* to prevent formation of new SDS-CRP*.

### 7.4.3 Available dissociation time can be a limiting factor

While both strategies can significantly improve the rate of CRP* formation by either reducing free SDS concentration or by isolating SDS and CRP*, there is an upper limit to the maximum rate of CRP* formation set by

$$\frac{\partial [CRP*]_{free}}{\partial t}|_{max} = k_{off}[SDS \cdot CRP^*].$$

72

In the absence of any association reactions, the rate of dissociation for SDS-CRP* is described as

$$\frac{\partial [SDS \cdot CRP*]}{\partial t} = -k_{off}[SDS \cdot CRP^*].$$

The two differential equations are solved with initial conditions representing CRP* and SDS-CRP* concentration prior to the transfer stage. Prior to the transfer stage, all C reactive proteins are coated with SDS, hence there is no free CRP* ($[CRP^*]_{t=0} = 0$). In addition, we make a simplified assumption that all CRP exist in either one of the two forms: either coated with SDS or free of SDS ($[CRP^*]_{total} = [CRP^*] + [SDS\text{-}CRP^*]$). Applying the initial conditions, we obtain the maximum recovery of CRP* as a function of transfer time and dissociation rate:

$$\frac{[CRP*]_{free}}{[CRP*]_{total}}\Big|_{max} = 1 - e^{-k_{off}\cdot t}.$$

As shown in Figure 7-4, when the transfer time is the inverse of dissociation rate ($k_{off}t = 1$), 63% of total CRP is renatured and be able to bind to the blotting gel.
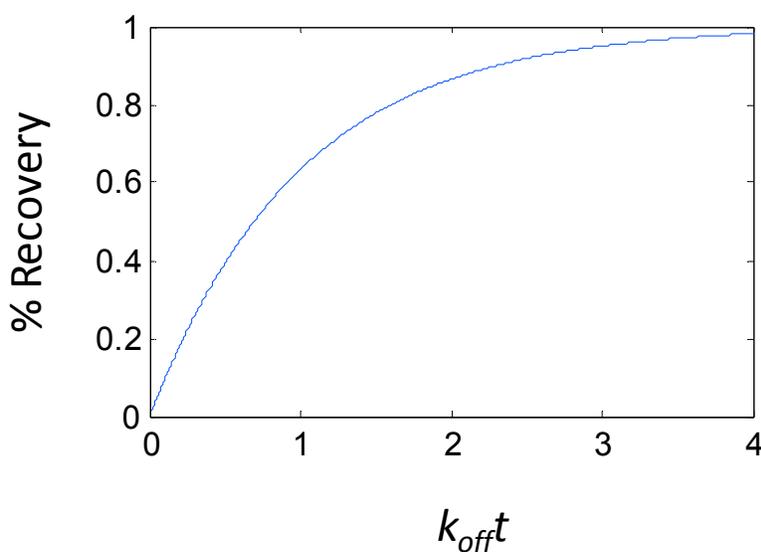


Figure 7-4. Maximum protein recovery is a function of dissociation rate and transfer time.

Previous measurements of protein refolding rates confirm that the timescale associated with our on-chip implementation can achieve substantial protein renaturation over the available lateral transfer time. Circular dichroism measurements of protein secondary structures indicate various proteins (lysozyme[25], chymotrypsin inhibitor 2[25], cytochrome c[26]) refold at a rate constant above 1 s$^{-1}$ from SDS denatured states. Assume perfect isolation of SDS from proteins achieved by either electrophoresis or using immobilized cyclodextrin, the protein refolding rate constant multiplied by the available SDS dissociation time in our system (i.e., seconds to minutes) should, in theory, result in sufficient protein recovery. Therefore, the goal of next three chapters is to discuss how to enhance isolation of SDS from proteins for maximum SDS removal efficiency.

## 7.5 Overview of thesis contribution: microfluidic western blotting assay with on-chip protein renaturation

The western blotting assay, which combines electrophoretic separations and immunoaffinity recognition, is a powerful technique to identify proteins in complex samples and to perform

confirmatory diagnostics. While a microfluidic implementation of native western blotting assay by our group has led to significant reduction in assay time and exhibits superior transfer efficiency than conventional western blotting assays, prevalent adoption of microfluidic western blotting assays requires integration of molecular weight measurement with downstream immunoaffinity detection. Therefore, a key design challenge is how to remove denaturing detergents, which are required for molecular weight measurement, from proteins prior to downstream immunoaffinity detection as those detergents disrupt antibody-antigen interactions.

Based on a simple model describing SDS removal and protein renaturation process, we proposed two strategies to remove SDS and renature protein in transit. The first strategy focuses on removing free SDS from the system while the second strategy aims to isolate SDS from proteins. Both strategies assist protein renaturation by minimizing the formation of new SDS-protein complexes while maximizing SDS dissociation from proteins.

Implementation of microfluidic western blotting assays requires optimization of experimental conditions for each assay stage. In chapter 8, we demonstrate the application of discontinuous gels to monitor either the extent of protein denaturation under SDS conditions or to examine the effectiveness of SDS removal conditions. With the ability to perform sequential injection and separation, homogeneous immunoassay is an efficient method to elucidate the required experimental conditions. Information obtained in this chapter is translated to implementing microfluidic western blotting assay with electrophoretic isolation of SDS in chapter 9 and immobilized cyclodextrins in chapter 10.

In chapter 9, we demonstrate a novel strategy for on-chip protein renaturation. Electrophoretic separation of SDS from proteins assists dissociation of SDS-protein complexes and aids protein renaturation. Photopatterning enables precise control over sieving matrix composition for efficient SDS removal and allows seamless integration of protein renaturation with upstream sizing and downstream immunoaffinity recognition. As a result, the entire assay is completed within 3 minutes and we observe a 55% antibody-binding efficiency for previously denatured proteins. Chapter 9 concludes with a discussion on how the demonstrated binding efficiency can be further improved, which leads to on-chip immobilization of cyclodextrins.

Chapter 10 details the development of an on-chip cyclodextrin immobilization strategy for seamless integration with microfluidic western blotting assays. Understanding polymer chemistry enables us to select an optimal approach which results in effective crosslinking of cyclodextrin with polyacrylamide gels. Finally, we conclude with a discussion on how immobilized cyclodextrin can further improve the binding efficiency that was already achieved using electrophoretic isolation of SDS as detailed in the last chapter.

## 7.6 References

(1)     Herr, A. E.; Throckmorton, D. J.; Davenport, A. A.; Singh, A. K. *Analytical Chemistry* **2005**, *77*, 585-590.
(2)     Towbin, H.; Staehelin, T.; Gordon, J. *Proceedings of the National Academy of Sciences* **1979**, *76*, 4350-4354.

(3)     Hoebe, K.; Du, X.; Georgel, P.; Janssen, E.; Tabeta, K.; Kim, S. O.; Goode, J.; Lin, P.; Mann, N.; Mudd, S.; Crozat, K.; Sovath, S.; Han, J.; Beutler, B. *Nature* **2003**, *424*, 743-748.

(4)     Branson, B. M. *Jaids-Journal of Acquired Immune Deficiency Syndromes*, *55*, S102-S105.

(5)     Gershoni, J. M.; Palade, G. E. *Analytical Biochemistry* **1983**, *131*, 1-15.

(6)     Zare, R. N.; Kim, S. In *Annual Review of Biomedical Engineering, Vol 12*; Annual Reviews: Palo Alto; Vol. 12, pp 187-201.

(7)     Ciaccio, M. F.; Wagner, J. P.; Chuu, C.-P.; Lauffenburger, D. A.; Jones, R. B. *Nat Meth*, *7*, 148-155.

(8)     Pan, W.; Chen, W.; Jiang, X. *Analytical Chemistry*, *82*, 3974-3976.

(9)     Anderson, G. J.; Cipolla, C. M.; Kennedy, R. T. *Analytical Chemistry*, *83*, 1350-1355.

(10)    He, M.; Herr, A. E. *Journal of the American Chemical Society*, *132*, 2512-2513.

(11)    Tia, S. Q.; He, M.; Kim, D.; Herr, A. E. *Analytical Chemistry* **2011**, 3581-3588.

(12)    Betts, S.; Speed, M.; King, J. In *Amyloid, Prions, and Other Protein Aggregates*; Academic Press Inc: San Diego, 1999; Vol. 309, pp 333-350.

(13)    Weber, K.; Osborn, M. *Journal of Biological Chemistry* **1969**, *244*, 4406-4412.

(14)    Ferguson, K. A. *Metabolism-Clinical and Experimental* **1964**, *13*, 985-1002.

(15)    Pittrive.R; Impiomba.Fs *Biochemical Journal* **1968**, *109*, 825-830.

(16)    Choi, N. S.; Hahm, J. H.; Maeng, P. J.; Kim, S. H. *Journal of Biochemistry and Molecular Biology* **2005**, *38*, 177-181.

(17)    Hager, D. A.; Burgess, R. R. *Analytical Biochemistry* **1980**, *109*, 76-86.

(18)    Dunn, S. D. *Analytical Biochemistry* **1986**, *157*, 144-153.

(19)    He, M.; Novak, J.; Julian, B.; Herr, A. E., Atlanta, GA 2011.

(20)    Kim, D.; He, M.; Tia, S. Q.; Herr, A. E., Cancun, Mexico 2011.

(21)    Taylor, K. E.; van den Berg, C. W. *Immunology* **2007**, *120*, 404-411.

(22)    Zhou, J. W.; Ritter, H. *Polymer Chemistry*, *1*, 1552-1559.

(23)    Couthon, F.; Clottes, E.; Vial, C. *Biochemical and Biophysical Research Communications* **1996**, *227*, 854-860.

(24)    Hanson, P. E.; Gellman, S. H. *Folding & Design* **1998**, *3*, 457-468.

(25)    Chen, E.; Van Vranken, V.; Kliger, D. S. *Biochemistry* **2008**, *47*, 5450-5459.

(26)    Otzen, D. E.; Oliveberg, M. *Journal of Molecular Biology* **2001**, *313*, 479-483.

# Chapter 8 Ultra-short Separation Length Homogeneous Assay to Guide Microfluidic Western Blotting Design

As shown in Figure 8-1, implementation of microfluidic western blotting assays requires optimization of experimental conditions for each assay stage. With the ability to perform sequential injection and separation, homogeneous immunoassay is an efficient method to elucidate the required experimental conditions. For SDS-PAGE separation, treatment of proteins with negatively charged SDS changes protein mobility and conformation. Capillary electrophoresis has been applied toward understanding protein denaturation[1] and refolding[2] kinetics. Furthermore, proteins have characteristic electrophoretic patterns under association and denaturation in SDS[3]. Here, we perform on-chip separation on discontinuous gels (detailed in chapter 5 and 6) to monitor either the extent of protein denaturation under SDS conditions or to examine the effectiveness of SDS removal conditions. The goal of the SDS removal process in microfluidic western blotting assay is to recover antibody-binding capabilities of previously denatured proteins prior to downstream recognition within blotting gels. Therefore, antibodies can function as immunological probes for studying the renaturation process[4]. By performing rapid immunoassays on discontinuous gels (demonstrated in chapter 6), immune complex formation between antibodies and previously denatured proteins is quantified to evaluate the effectiveness of cyclodextrin in removing SDS. Information obtained in this chapter is translated to implementing microfluidic western blotting assay with electrophoretic isolation of SDS in chapter 9 and immobilized cyclodextrin in chapter 10.
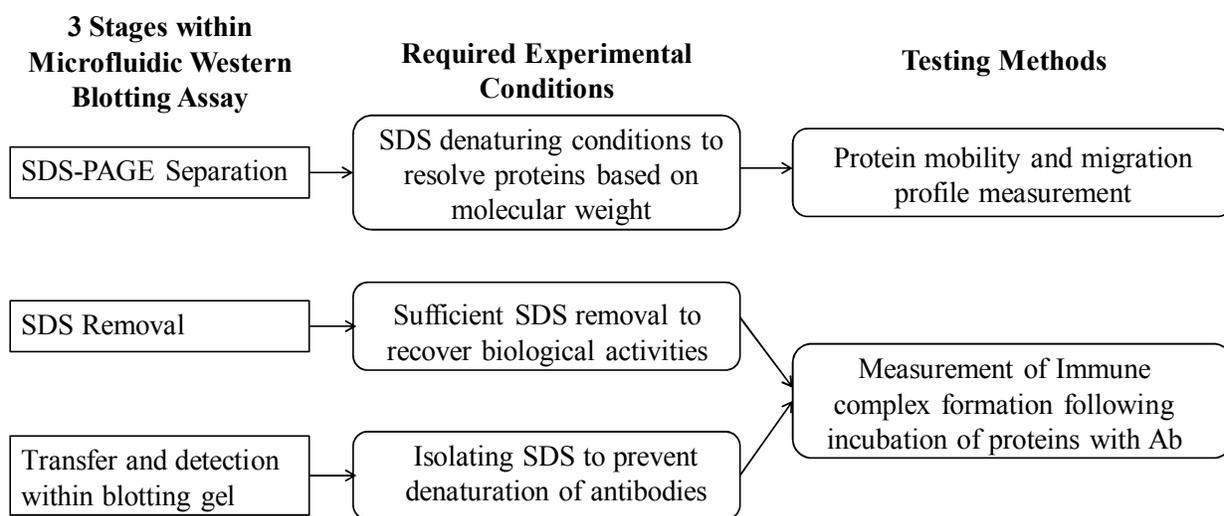
Figure 8-1. Microfluidic implementation of western blotting assay requires optimization of experimental conditions for each stage. Measurements are performed using homogeneous immunoassays to quantify protein mobility and immune complex formation and to observe migration profile change.

## 8.1 Rapid separation on discontinuous gel enables identification of proper denaturing conditions

As shown in Figure 8-2, we performed separation on discontinuous gels to optimize denaturing conditions for SDS-PAGE separation. Due to limitations of an initial denaturing condition (detailed in section 8.1.1-8.1.4), we developed a new denaturing condition (8.1.5-8.1.7) satisfying the design requirements listed in Figure 8-1. Fabrication of discontinuous gels follows that described in Chapter 5 and operation of discontinuous gels to conduct separation and homogeneous immunoassays follows that described in Chapter 2.

| Initial denaturing condition | Experimental observations | Modified denaturing condition | New observations |
|---|---|---|---|
| RT incubation with 1% (w/v) SDS | 1. CRP* is quite resistant to denaturation<br><br>2. Antibodies are denatured<br><br>3. Mixing denatured proteins dissolved in 1% SDS with 5% (w/v) cyclodextrin does not result in SDS removal | 85C incubation with 0.1% (w/v) SDS followed by 0.1% (w/v) 2-mercaptoethanol | 1. CRP* is reduced to monomers for sizing<br><br>2. Antibodies maintain most activity<br><br>3. Mixing denatured proteins dissolved in 0.1% SDS with 4% (w/v) cyclodextrin result in SDS removal |

Figure 8-2. Experimental derivation of an appropriate denaturing condition for on-chip SDS-PAGE separation.

### 8.1.1 Initial denaturing condition does not satisfy separation requirements

The initial denaturing condition of using 1% (w/v) SDS with room temperature incubation is able to generate linear log MW vs. mobility plots for four test proteins (Figure 8-3). For albumin proteins (BSA*, Ova*, and Parv*), treatment under 1% (w/v) SDS results in similar mobility compared to treatment with 10% (w/v) SDS. Reducing agent (2-mercaptoehtnaol) and heating (at 85C), which are commonly used in preparing proteins for SDS-PAGE, were eliminated for reduced degree of denaturation. Compared to separation performed in native conditions, SDS treatment improves mobility differences among various proteins.
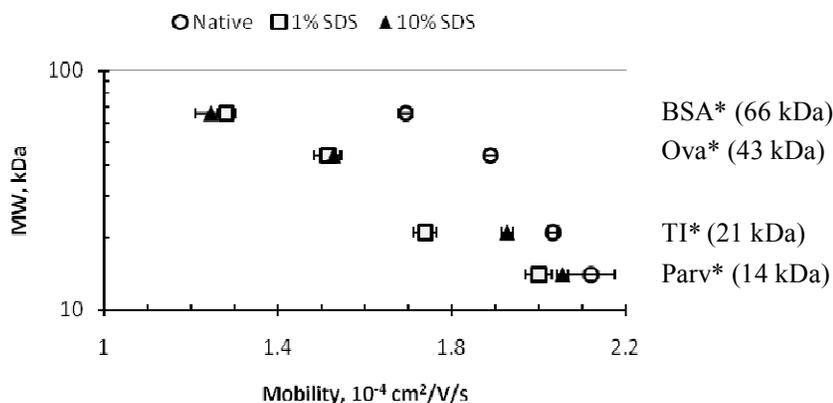


Figure 8-3. Treatment of proteins with SDS results in mobility proportional to log MW. Fluorescently labeled bovine serum albumin (BSA), ovalbumin (Ova), trypsin inhibitor (TI), and parvalbumin (Parv) are purchased from Invitrogen and reconstituted in Tris-glycine buffer. Separation was performed on a 5% uniform gel. Electrophoretic mobility is measured using method described in section 5.4.

However, room temperature incubation with 1% (w/v) SDS cannot efficiently denature CRP*. As shown in Figure 8-4, upon SDS treatment (b-d), CRP* was resolved into two peaks. The presence of a slower peak with mobility similar to native CRP* suggested that a significant portion of CRP* was still in native pentamer form after room temperature incubation of 3 and 30 minutes. In fact, 70 minutes of incubation time was necessary to convert a majority of CRP* to denatured monomer state. Our observations of multiple peaks agree with previous reports on coexistence of multiple protein conformations subsequent to transient contact with SDS[5].
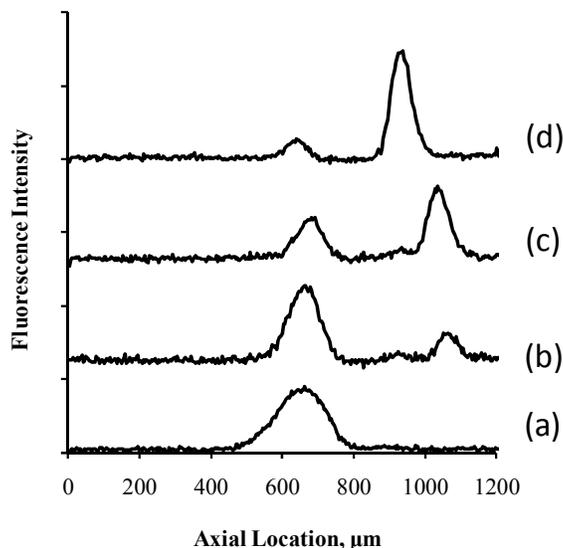


Figure 8-4. CRP* appears in two conformations with relative distribution of each conformation as a function of incubation time with 1% SDS. Separation was performed on 2.5/5% discontinuous gels and the axial fluorescence intensity was plotted after an elapsed separation time of 8 sec. E = 102 V/cm for the first 5.5 sec and increased to 200 V/cm afterwards. In (a), no SDS was added to CRP*. CRP* was incubated with SDS for 3 min (b), 30 min (c), and 70 min (d) prior to the initiation of separation.

### 8.1.2    Antibodies lose significant biological activity under 1% (w/v) SDS

Under incubation with 1% (w/v) SDS, antibodies lost most of their biological activities toward antigens. As shown in Figure 8-6A, anti-CRP antibody formed complex within minutes of incubation with native CRP*. On the other hand, no complex was formed between anti-CRP antibody and SDS treated CRP* (Figure 8-6B). Figure 8-5 depicts the thought process to conclude the lack of complex formation was due to antibody being denatured instead of CRP* being denatured. As CRP* was incubated with SDS for a relatively short period of time prior to separation (< 8 minutes), more than half of CRP* remained in native form as reflected by the separation montage in Figure 8-6B. The lack of complex formation with CRP*$_N$ suggests that incubation in 1% (w/v) SDS severely deteriorates biological activity of antibodies.

Figure 8-5. By combining immunoassay results and previous understanding of CRP denaturation, we conclude the lack of immune complex formation is due to antibody denaturation.
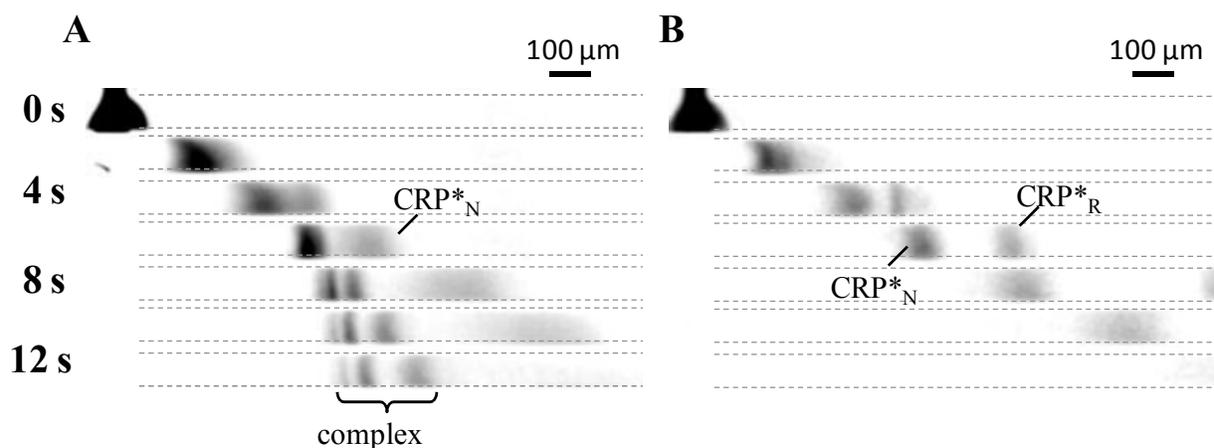


Figure 8-6. Incubating antibody with native CRP* results in complex formation (A) whereas incubation with SDS treated CRP* results in no complex formation (B). Anti-CRP Ab (13.3 nM) was incubated with 210 nM native CRP* (in A) and 210 nM SDS treated CRP* in (B). Separation was performed on a 2.5/5% discontinuous gel within 5 minutes of incubation. E = 102 V/cm (first 5.5 sec) and E = 200 V/cm (thereafter). Separation channel images are displayed as a function of elapsed separation time. In B, CRP* was incubated with 1% SDS for 3 minutes at room temperature prior to addition of Ab. $CRP^*_N$ represents CRP* in native form whereas $CRP^*_R$ represents CRP in denatured state.

### 8.1.3 A cyclodextrin:SDS molar ratio of 1:1 can protect antibodies from denaturation

Although 1% (w/v) SDS destructs biological activities of antibodies (Figure 8-6), addition of cyclodextrin along with antibodies to SDS solution protects antibody from denaturation. As shown in Figure 8-7, antibody can now form immune complexes with the portion of CRP* that was in or close to native conformation under room temperature incubation in SDS. The decreased signal to noise ratio in Figure 8-7 compared to Figure 8-6 was due to a destacking phenomenon that occured when the sample containing SDS and cyclodextrin was electrophoretically introduced into the loading channel. At SDS concentration above the critical

79

micellar concentration, addition of cyclodextrin breaks up SDS micelles and increases solution conductivity as cyclodextrin binds to individual SDS monomers[6]. The increased conductivity led to a conductivity mismatch between the sample well and the loading channel. Hence, analytes migrated at higher velocities in the loading channel which resulted in decreased concentration due to conservation of mass.
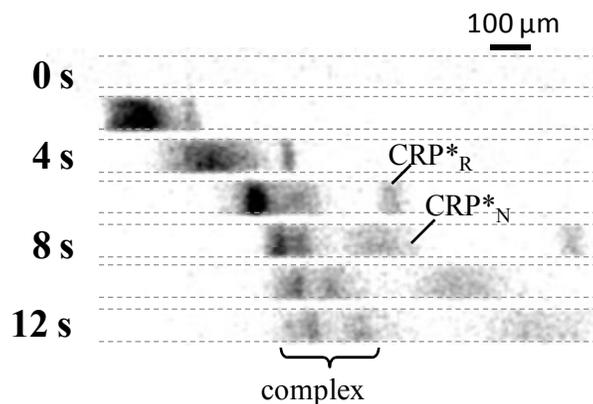


Figure 8-7. Cyclodextrin protects antibody from denaturation by SDS and results in complex formation with CRP*. CRP* was incubated with 1% SDS at room temperature for 3 minutes; 5% cyclodextrin and 13.3 nM anti-CRP Ab were then mixed with CRP* and SDS. Separation was performed on a 2.5/5% discontinuous gel within 5 minutes of incubation with Ab. E = 102 V/cm (first 5.5 sec) and E = 200 V/cm (thereafter). Separation channel images are displayed as a function of elapsed separation time.

### 8.1.4   A cyclodextrin:SDS molar ratio of 1:1 cannot remove SDS from denatured proteins

However, at 1:1 molar ratio, cyclodextrin cannot enhance SDS dissociation from CRP* as confirmed by homogeneous immunoassay of SDS denatured CRP* and antibody (Figure 8-8). After 70 minutes incubation with 1% SDS at room temperature, most CRP* were in a reduced form (Figure 8-4d). Previous measurement indicates the binding ratio of cyclodextrin to SDS is approximately 1:1[6]. Therefore, the amount of cyclodextrin available in solution is only sufficient in preventing excess SDS from denaturing antibodies but insufficient to enhance SDS dissociation from CRP*.
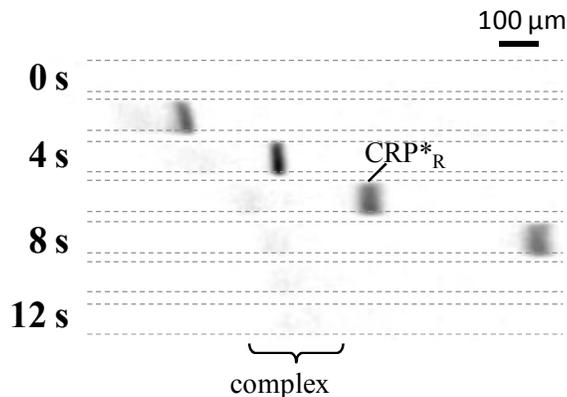


Figure 8-8. Cyclodextrin failed to increase complex formation for denatured CRP*. CRP* was incubated with 1% SDS at room temperature for 70 minutes; 5% cyclodextrin and 13.3 nM anti-

80

CRP Ab were then mixed with CRP*. Separation was performed on a 2.5/5% discontinuous gel within 5 minutes of incubation with Ab. E = 102 V/cm (first 5.5 sec) and E = 200 V/cm (thereafter). Separation channel images are displayed as a function of elapsed separation time.

In summary, by performing on-chip separation and homogeneous immunoassays under various conditions, we conclude room temperature incubation with 1% SDS is insufficient to denature CRP* to monomeric form for molecular weight measurement whereas 1% SDS can significantly deteriorate binding activity of antibodies. While the SDS binding capability of cyclodextrin protected antibodies from SDS denaturation, an increased cyclodextrin to SDS ratio is needed to enhance SDS removal from CRP*.

### 8.1.5   A new denaturing condition satisfies separation requirements

We made modifications to SDS denaturing conditions based on previous literature reports. Characterization of SDS binding to proteins using dialysis revealed that only the monomeric form of SDS was bound to proteins[7]. Furthermore, a 1.4 g SDS per 1 g protein binding ratio is achieved with monomer equilibrium concentration above 0.5 mM. As room temperature incubation of proteins with SDS can require 4-10 days to reach equilibrium[8], heating at 85C is often used to speed up the denaturation process. Therefore, by incorporating heating and a reducing agent (i.e., 2-mercaptoethanol), we are able to reduce the amount of SDS needed while still accomplishing denaturation. As will be described in later sections, reducing SDS concentration used in denaturation not only preserves biological activities of antibodies (8.1.6) but also facilitates subsequent SDS removal from CRP (8.2).

As shown in Figure 8-9A, treatment of CRP* with 0.1% (w/v) SDS at 85C for 3 minutes, which was followed by addition of 0.1% (w/v) 2-mercaptoethanol, results in fully reduced CRP* with monomeric conformation. Furthermore, a linear calibration curve was obtained by plotting mobility vs. log molecular weight for various proteins (Figure 8-9B).
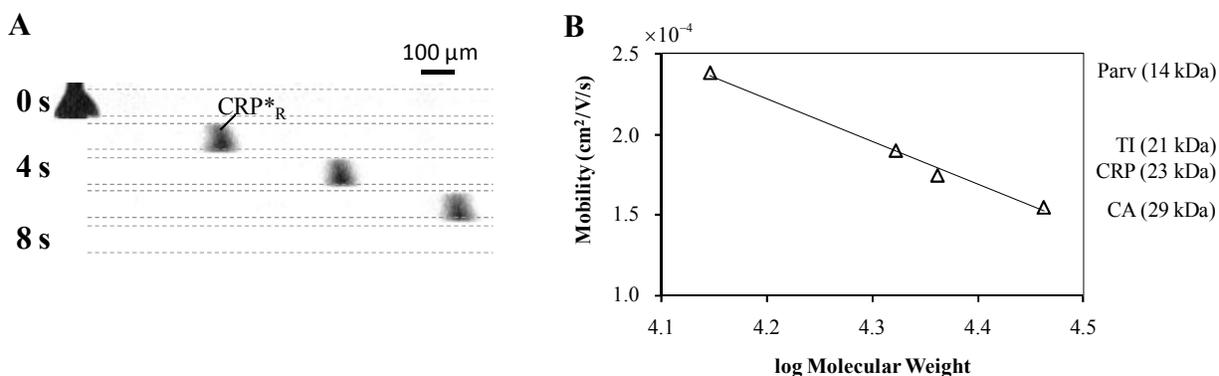


Figure 8-9. Treatment of proteins with 0.1% SDS and 0.1% 2-mercaptoethanol under heating conditions results in reduced CRP* (A) and a linear mobility vs. log Molecular Weight calibration curve (B). Separation was performed on a 2.5/5% discontinuous gel. E = 102 V/cm.

### 8.1.6   Antibody maintains most of its functionality under the new denaturing condition

Antibody retains most of its binding affinity after room temperature incubation with 0.1% SDS as indicated by its ability to form immune complexes with CRP* that are in native conformation

81

(Figure 8-10). In comparison, room temperature incubation of antibody with 1% SDS can significantly deteriorate antibody binding capability (Figure 8-6B).
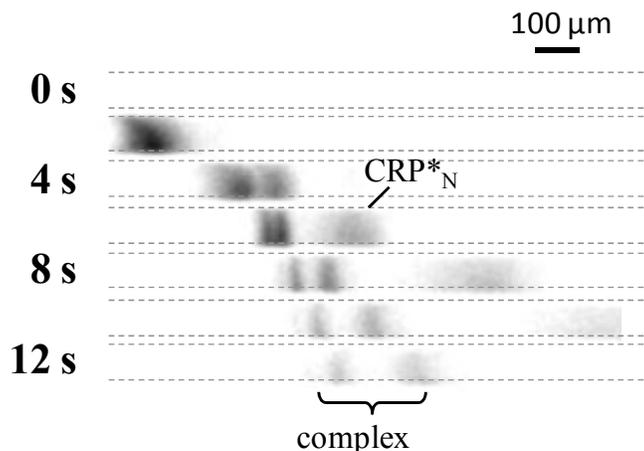


Figure 8-10. Antibody retains most of its binding affinity under room temperature incubation with 0.1% SDS. CRP* was incubated with 0.1% SDS at room temperature for 7 minutes (a condition not sufficient to denature CRP*); 13.3 nM anti-CRP Ab was then mixed with CRP*. Separation was performed on a 2.5/5% discontinuous gel within 6 minutes of incubation with Ab. E = 102 V/cm (first 5.5 sec) and E = 200 V/cm (thereafter). Separation channel images are displayed as a function of elapsed separation time.

### 8.1.7 SDS removal is necessary for downstream immunoaffinity recognition

Under the new denaturing condition, CRP* loses biological activity as revealed by a lack of complex formation upon incubation with anti-CRP antibody. As shown in Figure 8-11, upon treatment with 0.1% SDS at 85C, CRP* was in its reduced form. As antibody retains most of its binding affinity under room temperature incubation with 0.1% SDS (Figure 8-10), the lack of complex formation in Figure 8-11 is attributed to CRP* losing binding affinity. The result is not surprising as hydrophobic interaction between SDS and proteins at high binding ratios (112 SDS molecules bound to 1 CRP monomer) can obscure binding epitodes on CRP that are necessary for subsequent recognition by the antibody.
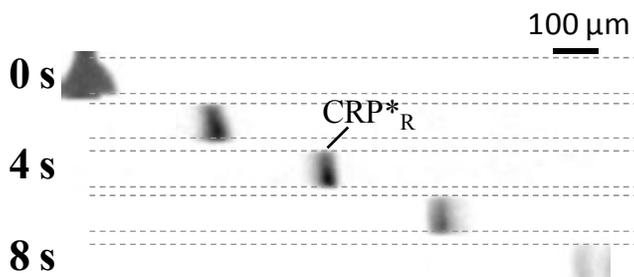


Figure 8-11. Reduced CRP* fails to form immune complexes. CRP* was incubated with 0.1% (w/v) SDS at 85 C for 3 minutes, and 0.1% (w/v) 2-mercaptoethanol was added. After cooling for 3 minutes, 67 nM anti-CRP Ab was introduced into the SDS-CRP* mixture. Separation was performed on a 2.5/5% discontinuous gel within 17 minutes of incubation with Ab. E = 102 V/cm (first 5.5 sec) and E = 200 V/cm (thereafter). Separation channel images are displayed as a function of elapsed separation time.

By performing on-chip separation on discontinuous gels, we validated a new denaturing condition that resulted in reduced CRP* with monomeric conformation; furthermore, a linear log molecular weight vs. mobility curve was constructed for sizing purposes. Unfortunately, reduced CRP* cannot form immune complexes with antibody which indicates SDS must be removed from CRP* for downstream immunoaffinity recognition. Therefore, in the next section, we apply cyclodextrin, an inclusion complex with binding capability toward SDS, to assist SDS removal process.

## 8.2 Homogeneous immunoassays on discontinuous gels illustrate how cyclodextrin assists in SDS removal

In this section, we confirmed that, at an appropriate cyclodextrin to SDS molar ratio, cyclodextrin can assist SDS dissociation from denatured CRP* based on three observations. Firstly, incubation of SDS denatured CRP* with cyclodextrin results in change in protein mobility and migration profile (8.2.1). Secondly, incubation of SDS denatured CRP* with cyclodextrin recovers complex formation with antibodies (8.2.2). Lastly, following cyclodextrin treatment, SDS denatured CRP* shows structural resemblance to CRP* polypeptides (8.2.3). This section details experiments performed which led to the above conclusions.

### 8.2.1 Cyclodextrin incubation results in change in mobility and migration profile of denatured CRP*

By reducing SDS concentration necessary to denature CRP*, we are able to increase cyclodextrin to SDS molar ratio for more effective SDS removal. Figure 8-12 compares CRP* migration on discontinuous gels in 3 forms: native (A), 0.1% SDS reduced (B), and 0.1% SDS reduced followed by incubation with 4% cyclodextrin (C). Incubating reduced CRP* with cyclodextrin at 8:1 cyclodextrin:SDS molar ratio changes CRP* migration profile (C) to a form that is distinct from both native CRP* (A) and reduced CRP* (B). As reduced CRP exists as polypeptides coated with SDS, cyclodextrin assists SDS removal from CRP by sequestering any SDS dissociating from CRP. The resolved bands in Figure 8-12C represent CRP with different degrees of SDS removal and renaturation.
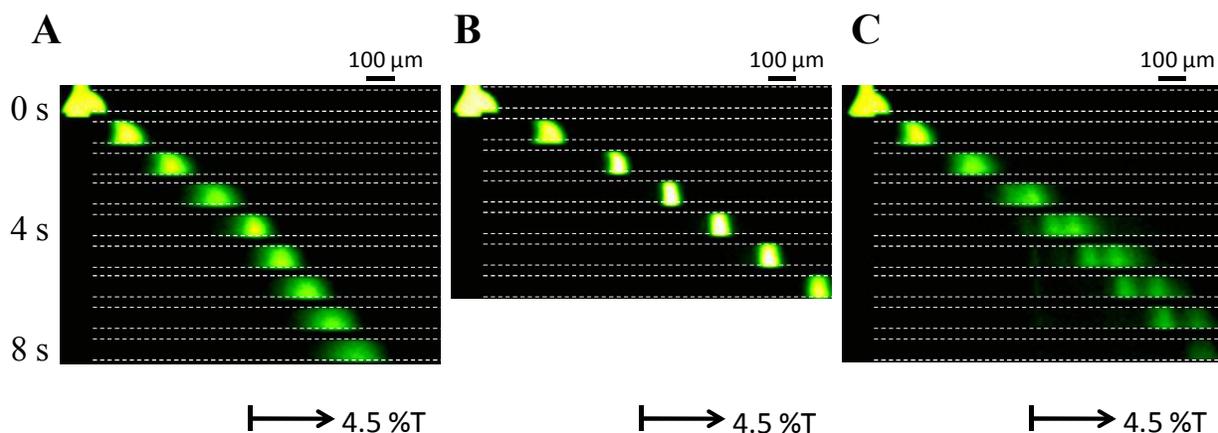


Figure 8-12. Incubation of reduced CRP* (B) with cyclodextrin changes analyte band profile (C). (A) Native CRP* was loaded and injected into the separation channel at t = 0. (B) CRP* was incubated with 0.1% SDS at 85C for 3 minutes and followed by addition of 2-mercaptoethanol;

after cooling, reduced CRP* was injected for on-chip analysis. (C) CRP* was incubated with 0.1% SDS at 85C for 3 minutes and 2-mercaptoethanol was added; after cooling, reduced CRP* was incubated with 4% cyclodextrin and immediately loaded on chip. Separation was performed on a 2.5/4.5% discontinuous gel. E = 102 V/cm. Separation channel images are displayed as a function of elapsed separation time.

### 8.2.2   Cyclodextrin incubation recovers biological activities of denatured CRP

Utilizing spectral multiplexing and implementing homogeneous immunoassays on discontinuous gels, we confirmed cyclodextrin treatment can recover binding affinity of previously reduced CRP* with antibodies. In chapter 4 and 6, spectral multiplexing resolved immune complexes for different target analytes. Here spectral multiplexing confirmed that the immune complex was formed between binding of Alexa Fluor 488 labeled CRP* and Alexa Fluor 568 labeled antibody (Ab*). The immune complex peak is displayed in both spectral channels whereas unbound CRP* and unbound Ab* are displayed in one of the two spectral channels. As shown in Figure 8-13, following cyclodextrin treatment, previously reduced CRP* can form immune complexes with antibodies.   Increasing antibody concentration from B to C resulted in increased complex formation.   CRP may not refold back to native conformation after cyclodextrin treatment as indicated by the differences between CRP* migration patterns under different conditions (Figure 8-12). Nevertheless, as cyclodextrin treatment results in sufficient binding activity between previously denatured CRP and antibodies, we confirm its application for SDS removal in microfuidic western blotting assays.
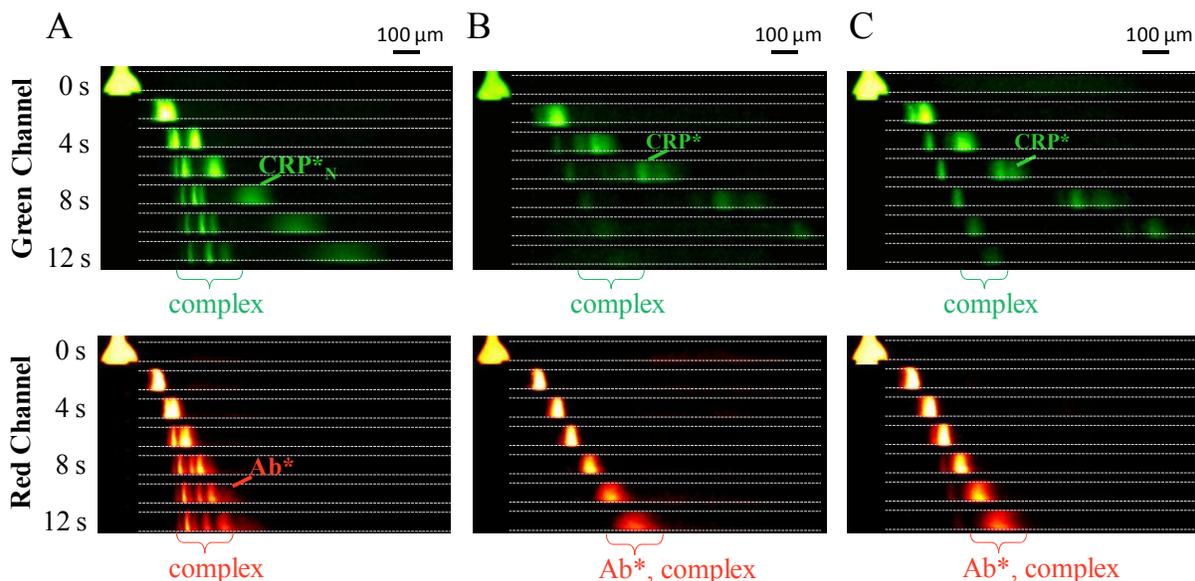


Figure 8-13. Cyclodextrin treatment of previously denatured CRP* results in complex formation in proportion to antibody concentration. Separation was performed on a 2.5/6% discontinuous gel.  (A) native CRP* (217 nM) was incubated with Ab* (33 nM). (B) CRP* (217 nM) was incubated with 0.1% SDS at 85C for 3 minutes which was followed by addition of 2-mercaptoethanol; after cooling, CRP* was incubated with 4% CD and Ab* (33 nM). (C) CRP* denaturing condition is the same as (B); after denaturation, CRP* was incubated with 4% CD and Ab* (100 nM). All separations were performed within 10 minutes of incubation. The green channel was imaged with the GFP filter cube and the red channel was imaged with the dsRed2

filter cube. E = 102 V/cm (the first 5.5 sec) and E = 200 V/cm (thereafter). Separation channel images are displayed as a function of elapsed separation time.

### 8.2.3 **Heat denatured CRP\* shows structural resemblance to cyclodextrin treated denatured CRP\***

Heating CRP\* alone without SDS unfolds protein to polypeptides form (Figure 8-14A) that retains binding activity toward Ab\* (Figure 8-14B). Figure 8-14A shows electrophoretic separation of CRP\* heated at 85C for 3 minutes. Complex formed between antibody and heat treated CRP\* (Figure 8-14B) has similar concentration and migration mobility as the complex formed between antibody and SDS denatured CRP\* treated with cyclodextrin (Figure 8-13C). Thus, cyclodextrin is effective in assisting SDS dissociation from SDS-CRP\* complex which results in structural resemblance to polypeptides without SDS coating.
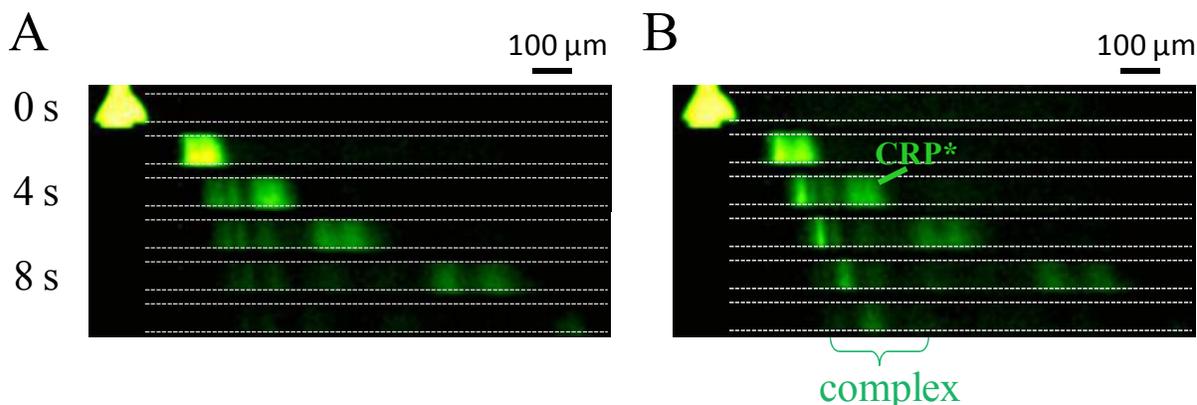


Figure 8-14. In absence of SDS, heat treated CRP\* (A) can form immune complex with antibody (B). Separation was performed on a 2.5/6% discontinuous gel. (A) CRP\* (217 nM) was heated at 85C for 3 minutes. (B) CRP\* (217 nM) was heated at 85C for 3 minutes; after cooling, CRP\* was incubated with Ab\* (100 nM). The green channel was imaged with the GFP filter cube. E = 102 V/cm (the first 5.5 sec) and E = 200 V/cm (thereafter). Separation channel images are displayed as a function of elapsed separation time.

## 8.3    **Summary**

By performing rapid separation and homogeneous immunoassays on discontinuous gels, we arrive at the following formulation to denature proteins for on-chip sizing in the separation stage: incubation with 0.1% (w/v) SDS at 85 C for 3 minutes followed by addition of 0.1% (w/v) 2-mercaptoethanol. The formulation is able to reduce CRP\* to its monomeric form efficiently. Incubation of SDS reduced CRP with cyclodextrin at a cyclodextrin to SDS molar ratio of 8:1 results in SDS removal and affinity recognition by the antibody.

While homogeneous immunoassays can quantify immune complex formation under different conditions, homogeneous immunoassay conditions are inherently different from the proposed western blotting assay architecture.  As homogeneous immunoassay quantifies immune complex formation from off-chip incubation of antibodies with antigens, it cannot be used to directly model the efficiency of SDS removal in transit. In the next two chapters, we incorporate

information obtained from this chapter to design western blotting assays with SDS removal in transit.

## 8.4   **References**

(1)    Schneider, G. F.; Shaw, B. F.; Lee, A.; Carillho, E.; Whitesides, G. M. *Journal of the American Chemical Society* **2008**, *130*, 17384-17393.
(2)    Fan, Z. H.; Jensen, P. K.; Lee, C. S.; King, J. *Journal of Chromatography A* **1997**, *769*, 315-323.
(3)    Gudiksen, K. L.; Gitlin, I.; Whitesides, G. M. *Proceedings of the National Academy of Sciences of the United States of America* **2006**, *103*, 7968-7972.
(4)    Chavez, L. G.; Benjamin, D. C. *Journal of Biological Chemistry* **1978**, *253*, 8081-8086.
(5)    Stutz, H.; Wallner, M.; Malissa, H.; Bordin, G.; Rodriguez, A. R. *Electrophoresis* **2005**, *26*, 1089-1105.
(6)    Palepu, R.; Reinsborough, V. C. *Canadian Journal of Chemistry-Revue Canadienne De Chimie* **1988**, *66*, 325-328.
(7)    Reynolds, J. A.; Tanford, C. *Proceedings of the National Academy of Sciences of the United States of America* **1970**, *66*, 1002-1007.
(8)    Pittrive.R; Impiomba.Fs *Biochemical Journal* **1968**, *109*, 825-830.

# Chapter 9 Microfluidic Western Blotting Assay with SDS Removal in Transit

This chapter focuses on development and demonstration of microfluidic western blotting assays with on-chip protein renaturation. Electrophoretic separation of SDS from proteins assists dissociation of SDS-protein complexes and aids protein renaturation. Photopatterning enables precise control over sieving matrix composition for efficient SDS removal. Guided by simulation results, we optimized the separation of SDS from proteins and improved downstream blotting gel binding efficiency from < 5% to 55%. The improved binding efficiency represents recovery of protein biological activity as a result of SDS removal and renaturation. Moreover, the entire assay was completed within 3 minutes. Lastly, we conclude with a discussion on how the reported binding efficiency can be further improved.

## 9.1 Microfluidic western blotting chip fabrication and testing

### 9.1.1 Fabrication

Glass microfluidic chips for western blotting assay were designed in-house. Initial wet etch of glass plates was conducted by Caliper Life Sciences (Hopkinton, MA). Fluid access wells were drilled on a separate glass plate and thermally bonded to etched glass plate in house at the Berkeley Biomolecular Nanotechnology Center (BNC).

Gel fabrication in blotting chips is similar to that described for discontinuous gels (Chapter 5) with additional UV exposure steps to pattern the blotting gel, separation gel, and loading gel sequentially. Figure 9-1 illustrates a general fabrication protocol used in this work. The protocol builds upon a fabrication procedure developed for native western blotting chips[1]. Two modifications are made for optimized assay performance: (1) a linear acrylamide coating step was introduced to minimize non-specific adsorption of anti-CRP blotting antibody to regions outside of the blotting gel; (2) illumination power for blotting gel and separation was empirically optimized to reduce pore size non-uniformity near the interface (as inspired by development detailed in Chapter 5).

| | NaOH Clean & Silane Coating | Linear Acrylamide | Blotting Gel | Separation Gel | Loading Gel |
|---|---|---|---|---|---|
| **Purpose** | Clean channels and enable covalent attachment of PA gel to glass walls | Minimize non-specific adsorption of blotting antibodies to silanized glass surfaces | Enable immunoaffinity recognition of target analyte | Improve SR in the separation stage | Enable unbias loading of all proteins. Eliminate bulk flow. |
| **Reagent** | NaOH, water, acetic acid, silane, methanol | 40% acrylamide, V-50 photoinitiator, 1x Tris/glycine buffer, water | Streptavidin-acrylamide, biotinylated antibody, 30% acrylamide/bisacrylamide, VA-86 photoinitiator, 1x Tris/glycine buffer, water | 30% acrylamide/bisacrylamide, VA-86 photoinitiator, 1x Tris/glycine buffer, water | |
| **Exposure equipment** | n.a. | 100 W UV lamp | Nikon Diaphot 200 microscope equipped with 200 W mercury arc lamp | | 100 W UV lamp |
| **Exposure conditions** | n.a. | 10 mW/cm$^2$, 10 min Flood exposure | 2.9 mW/cm$^2$, 4 min Partial illumination | 2.9 mW/cm$^2$, 4 min Partial illumination | 10 mW/cm$^2$, 9 min Flood exposure |

Figure 9-1. Overview of fabrication steps and exposure conditions for western blotting chip. Depicted here is a general protocol with 4 photopaternning steps: two using partial illumination and two using flood exposure of the entire chip. Illumination power was measured with a General Tool UV 513AB UV meter.

Appendix B details the motivation and benefits of applying linear acrylamide coating. As blotting gel is a critical component in western blotting assay, several optimizations were made to increase binding affinity. Antibodies are crosslinked with polyacrylamide gel via a biotin-streptavidin linkage. An optimized antibody biotinylation protocol, which is provided in Appendix C, results in on average two biotins per antibody molecule post labeling. A 2:1 streptavidin acrylamide to biotinylated Ab molar ratio is optimal for crosslinking all antibodies. Streptavidin acrylamide and biotinylated antibody are first incubated at 4C for more than 1 hour and then mixed with sonicated acrylamide/biscarylamide solution to a final volume containing 4.5%T acrylamide. Instead of using monoclonal antibodies that recognize a single epitope, we incorporate polyclonal antibodies that recognize multiple epitopes in the blotting gel for improved binding efficiency. Figure 9-2 shows binding of CRP* within a NS12 chip that contains 2.5%T in the loading channel and a 4.5%T blotting gel (with 0.8 μM biotinylated polyclonal anti-CRP antibody and 1.8 μM streptavidin acrylamide) in the separation channel. Native CRP* was immediately immobilized once injected into the blotting gel region which contains crosslinked polyclonal antibodies specific toward CRP*. As the binding rate of CRP* onto the blotting gel is a product of associate rate ($k_{on}$) and available binding sites (anti-CRP antibody concentration within the blotting gel), we further increased concentration of anti-CRP antibody contained in blotting gel to 2 μM to increase binding efficency. Unless specified, future experiments using the 2D geometry are performed on blotting gels crosslinked with 2 μM biotinylated antibody.
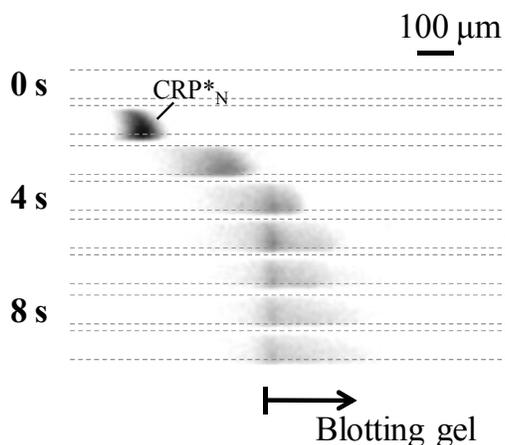
Figure 9-2. Native CRP* is immediately immobilized by blotting gel upon contact. CRP* (217 nM) was injected into a NS12 chip containing a 2.5%T loading gel and a 4.5%T blotting gel (with 0.8 μM anti-CRP antibody crosslinked via streptavidin-biotin linkage). E = 102 V/cm. Images of the separation channel are displayed as a function of elapsed separation time.

### 9.1.2 Voltage control

To conduct a western blotting assay, the western blotting chip is seated on a microscope stage with platinum electrodes inserted into each reservoir. ~4 μL analyte sample is pipetted into the sample well (well 1 in Figure 9-3) and all other reservoirs are filled with appropriate buffer solution (optimal buffer composition is described in 9.2). Table 9-1 provides a voltage programming for conducting western blotting assay. Voltage and feedback current control is enabled by a programmable high voltage power supply. Sample is first electrophoretically loaded from well 1 to well 3 using the loading program; pinched voltage is applied from wells 2 and 8 to generate a confined plug. After 2 minutes of loading, the plug is injected into the 2D chamber by applying an electric field between wells 8 and 2. Pullback currents are applied at wells 1 and 3 to minimize leakage. Currents applied at wells 4 and 5 result in vertical field lines within the 2D chamber and minimize possible bowing of injected sample due to fringing electric fields[2]. After a necessary time of 10-30 s for separating injected analytes, the electric field is switched to be across wells 6 and 7 to transfer the analyte band into the blotting gel. The side channels connecting wells 6 and 7 to the 2D chamber help to maintain horizontal field lines during the transfer stage.

Table 9-1 Voltage control enables automated assay operation

| Wells | 1 | 2 | 3 | 4 | 5 | 6 | 7 | 8 |
|---|---|---|---|---|---|---|---|---|
| **Loading** | -400 V | -0.2 μA | 0 V | 0 μA | 0 μA | 0 μA | 0 μA | -0.3 μA |
| **Separation** | 0.2 μA | -400V | 0.2 μA | -300 V | -300 V | 0 μA | 0 V | -200 V |
| **Transfer** | 0.05 μA | 0 μA | 0.05 μA | 0 μA | 0 μA | -125 V | -50 V | 0 μA |

### 9.1.3 Imaging

Imaging of western blotting assay was conducted by a CCD camera (CoolSnap HQ2, Roper Scientic, Trenton, NJ) and a 10x objective equipped on an IX-70 inverted epifluorescence microscope. Camera exposure time was set to 150 ms and a 4x4 pixel binning was employed to

increase signal intensity. Unless specified, proteins were labeled with Alexa Fluor 488 dyes and imaged with a GFP filter cube.

## 9.2 Optimization of separation conditions that are compatible with on-chip SDS removal

For microfluidic western blotting assay, our design goal is to efficiently resolve SDS-treated proteins in the separation stage and remove SDS during the transfer stage so transferred proteins can bind to the blotting gel. As introduced in chapter 7, the recovery rate of CRP* with binding capability toward the blotting gel can be modeled by

$$\frac{\partial [CRP*]}{\partial t} = -k_{on}[SDS][CRP^*] + k_{off}[SDS \cdot CRP^*].$$

Isolating SDS from CRP* drives the reaction toward SDS dissociation by preventing association of free CRP* with SDS. Therefore, to facilitate SDS and CRP* isolation, the lateral transfer and blotting gel region must be free of SDS. In this section, we compare the separation resolution and binding efficiency achieved when separation is performed in SDS-free buffer versus when separation is performed in SDS buffer.

### 9.2.1 Injecting denatured proteins into SDS-free chamber results in blotting but lacks separation resolution for the separation stage

We first performed separation of SDS treated proteins in native buffer. When the entire 2D chamber contained native buffer, SDS-CRP* was able to bind to the blotting gel after a lateral transfer distance of 800 μm and lateral transfer time of 38 s prior to entering the blotting gel (Figure 9-3). The capture efficiency is 80% which is calculated from dividing CRP* peak area bound to the blotting gel (at t = 85 s) by the peak area of CRP* injected (at t = 14 s). As a control experiment, we found SDS-BSA* does not bind to the blotting gel after being injected, separated, and transferred (data not shown). However, when SDS-CRP* was simultaneous injected with SDS-BSA*, separation in native buffer cannot sufficiently resolve the two proteins (Figure 9-4). SR is less than 1 after an elapsed separation time of 19 s. The "smearing" of CRP* and BSA* bands during separation stage indicates SDS is dissociating from proteins. Monitoring of protein migration patterns in capillary electrophoresis revealed that protein mobility was related to the number of SDS molecules bound[3]. Hence, proteins with less SDS molecules bound will migrate at a different mobility than the original conformation. As a result, the migrating peaks appear smeared.
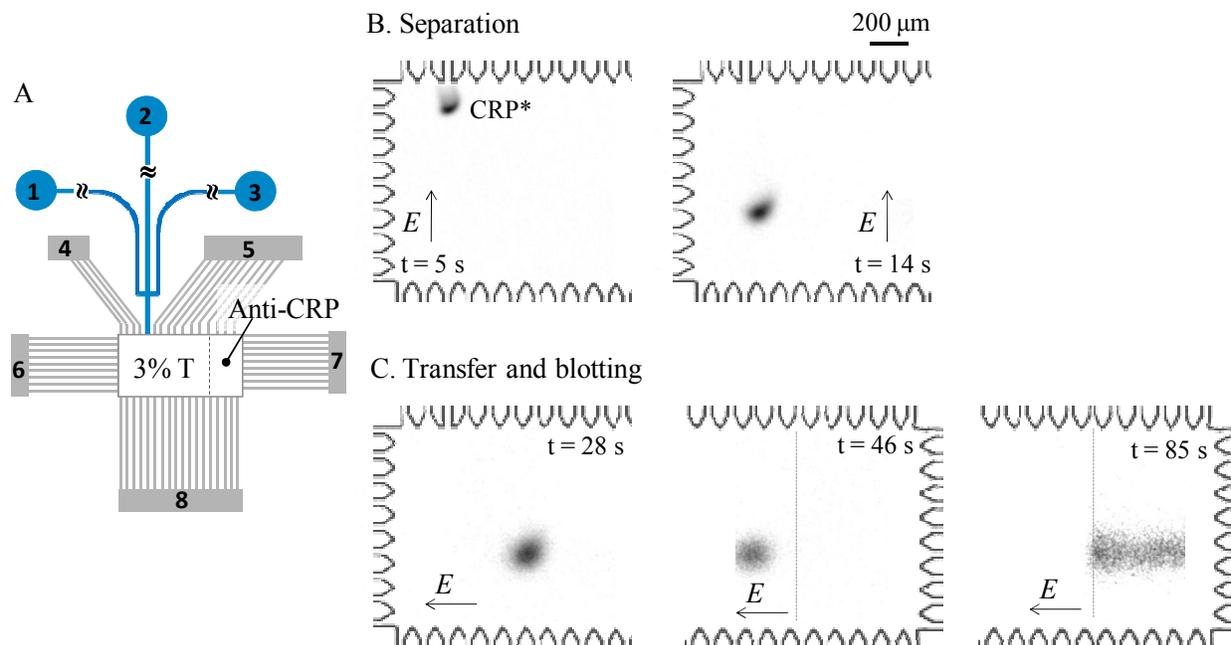
Figure 9-3. Previously reduced CRP* was able to bind to the blotting gel after separation performed in native buffer (B) and lateral transfer across the 2D chamber (C). The 1 mm x 2 mm 2D chamber contains 3%T gel in adjacent to an anti-CRP blotting gel (4.5%T with 2.1 µM biotinylated anti-CRP Ab and 5.7 µM streptavidin-acrylamide). Sample containing CRP* (440 nM), which was reduced in 0.1% SDS, was introduced in sample well 1; all other wells contain 1x Tris/glycine buffer. Voltage programming follows that described in section 9.1.2. Bright field images of the 2D chamber boundary are overlaid on top of separation and transfer images to give perspective to chamber location.
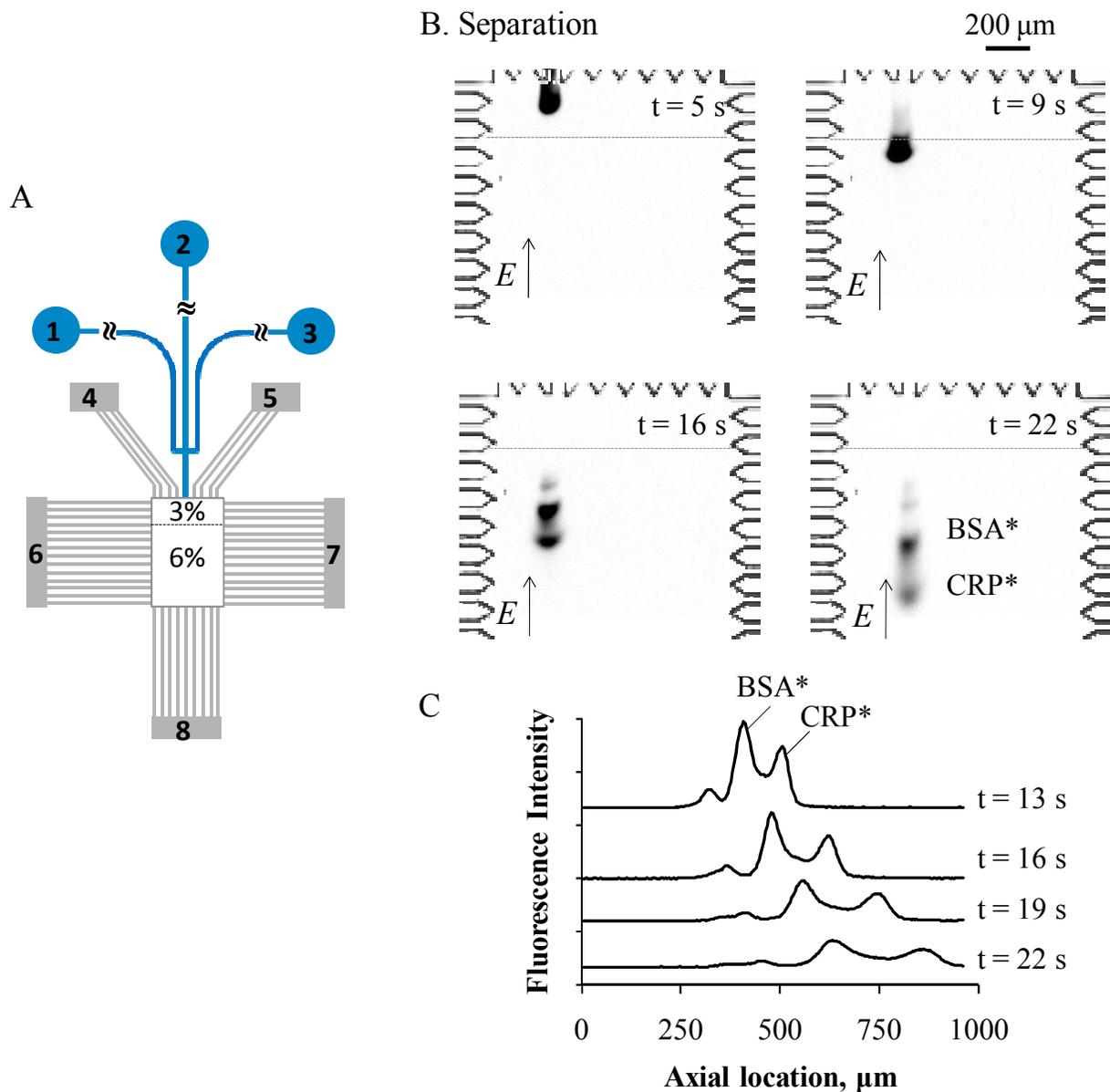
Figure 9-4. Reduced CRP* and BSA* are not sufficiently resolved during separation performed in native buffers. (A) The 1.5 mm x 1 mm 2D chamber contains a 3%T loading gel and a 6%T separation gel. Sample containing CRP* (440 nM) and BSA* (120 nM), which were reduced in 0.1% SDS, was introduced in sample well 1; all other wells contained 1x Tris/glycine buffer. Voltage programming follows that described in section 9.1.2. (B) Images of the 2D chamber are displayed as a function of separation time. (C) Fluorescence intensity across the separation axis is plotted with respective to elapsed separation time.

### 9.2.2 Co-injecting denatured proteins along with a stream of SDS results in sufficient separation resolution but lacks downstream immunoblotting capability

As separation performed in native buffer cannot result in sufficient separation resolution, we then conducted separation in 1x SDS buffer. Wells 2 and 8 contained SDS buffer (1x Tris/glycine with 0.1% (w/v) SDS) while wells 4, 5, 6 and 7 contained native buffer. During separation, a

stream of SDS was injected from well 2 to well 8 along with the denatured proteins. Currents applied in wells 4 and 5 helped to confine SDS within the separation region by co-injecting native buffer toward sample well 8. With SDS buffer in the separation stage, we observe improved separation between SDS-CRP* and SDS-BSA* (as shown in Figure 9-5).  SR = 1.65 after an elapsed separation time of 20 s. However, SDS-CRP* was unable to bind to the blotting gel after being transferred in a 3%T gel for 30 s over a transfer distance of 800 μm (as shown in Figure 9-6). The binding efficiency is less than 5%.
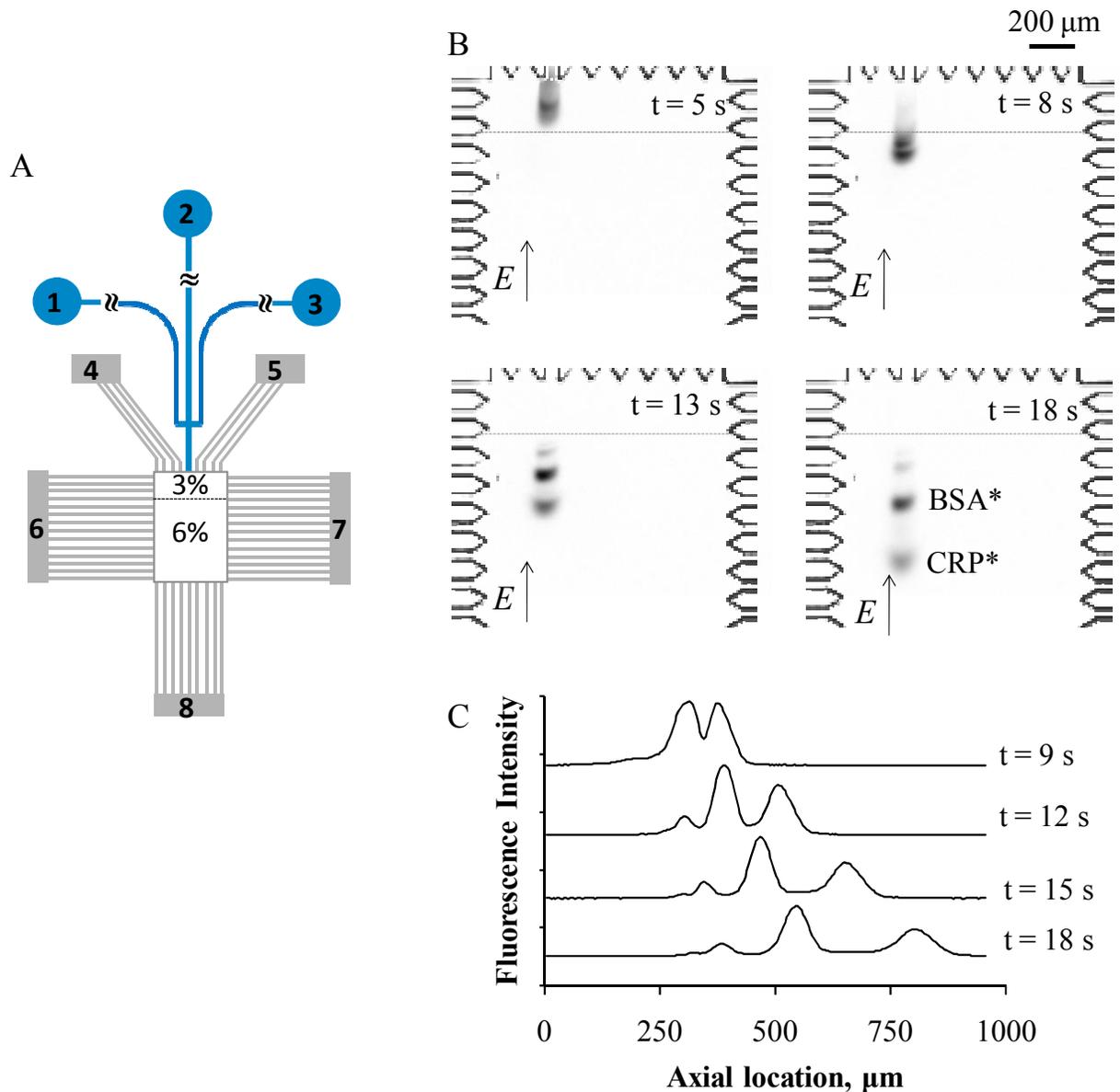


Figure 9-5. Reduced CRP* and BSA* are resolved during separation performed in a stream of SDS buffer co-migrating from well 2 toward well 8. (A) The 1.5 mm x 1 mm 2D chamber contains a 3%T loading gel and a 6%T separation gel. Sample containing CRP* (440 nM) and BSA* (120 nM) reduced in 0.1% SDS was introduced in sample well 1; wells 2 and 8 contain 1x Tris/glycine buffer with 0.1%SDS and all other wells contain 1x Tris/glycine buffer. Voltage

programming follows that described in section 9.1.2. (B) Images of the 2D chamber are displayed as a function of elapsed assay time. (C) Fluorescence intensity across the separation axis is plotted with respective of elapsed separation time.
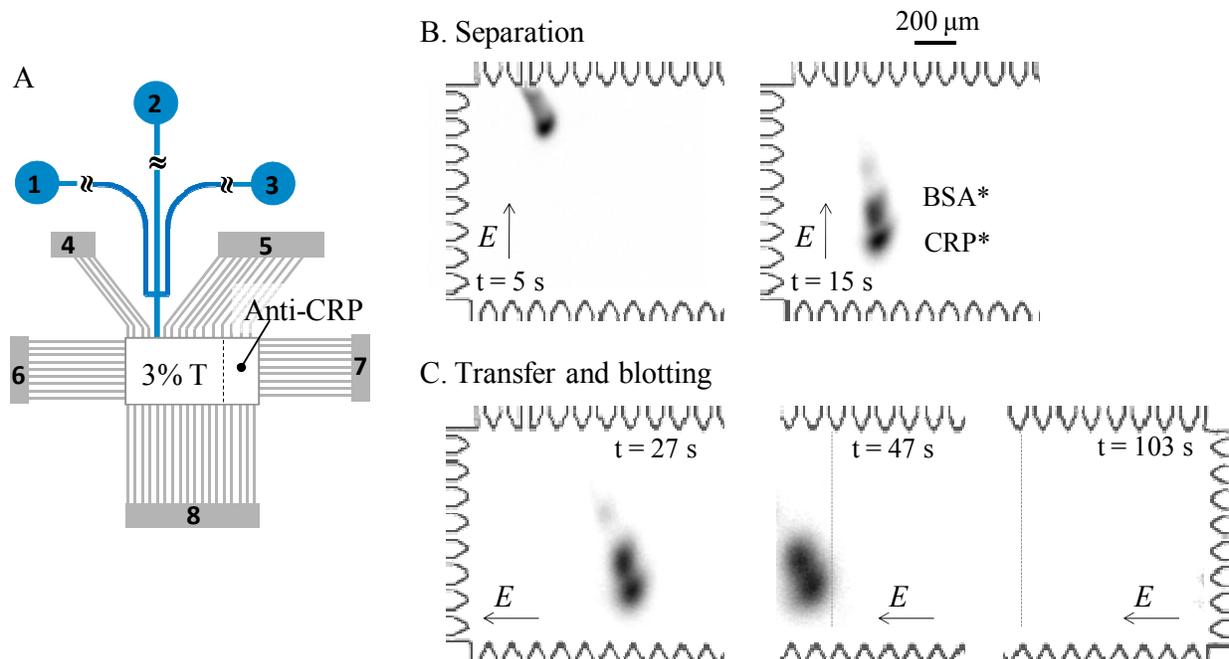


Figure 9-6. Previously reduced CRP* was not able to bind to blotting gel following separation performed in SDS buffer (B) and lateral transfer across the 2D chamber (C). The 1 mm x 2 mm 2D chamber contains a 3%T gel in adjacent to an anti-CRP blotting gel (4.5%T with 2.1 µM biotinylated anti-CRP Ab and 5.7 µM streptavidin-acrylamide). Sample containing CRP* (440 nM) and BSA* (120 nM) reduced in 0.1% SDS was introduced in sample well 1; wells 2 and 8 contained 1x Tris/glycine buffer with 0.1%SDS and all other wells contained 1x Tris/glycine buffer. Voltage programming followed that described in section 9.1.2.

SDS dissociates from reduced proteins when reduced proteins are injected into a region with background SDS concentration lower than that in the injected plug (0.1% or 3.47 mM). When SDS-reduced proteins are injected into a 2D chamber free of any SDS (as depicted in Figure 9-3 and Figure 9-4), the SDS dissociation process starts from the cross injector along the separation axis. SDS dissociation during the separation stage is unfavorable for separation, resulting in smearing of individual protein bands (Figure 9-4B, t = 16 s and t = 22 s). Yet, it is favorable for downstream immunoaffinity recognition by offering additional time and migration distance to isolate SDS from CRP* prior to the lateral transfer stage (for the case depicted in Figure 9-3, the extra time is 15 seconds over 1 mm long separation length). On the other hand, when SDS reduced proteins are injected into the 2D chamber along with a stream of SDS (as depicted in Figure 9-5 and Figure 9-6), no SDS dissociation occurs in the separation stage as the SDS concentration present in the separation axis is equal to SDS concentration present in the sample plug. The SDS dissociation process is initiated when reduced proteins are laterally transferred into regions free of SDS. Therefore, separating the stream of SDS from protein bands is critical to increase binding efficiency during the blotting stage. Figure 9-7 presents a schematic illustrating the necessary separation condition and the desired lateral transfer condition for

maximum SDS removal and protein renaturation prior to downstream immunoaffinity recognition. The rest of this chapter focuses on optimizing lateral transfer conditions both by simulation and experimental design.

**Separation**                             **Transfer**
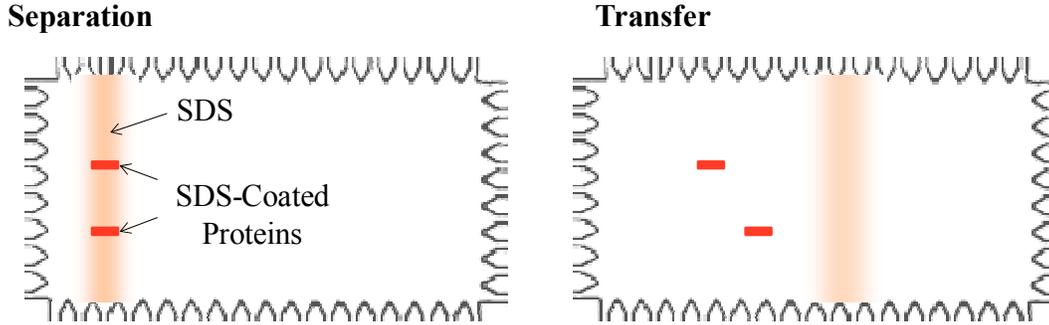


Figure 9-7. Performing separation in SDS is necessary for resolving proteins in the separation stage whereas resolving proteins from SDS is critical for protein renaturation in the transfer stage.

## 9.3 Simulation of SDS removal by electrophoresis

### 9.3.1 Overview of simulation model

We developed a simulation model to understand: (1) why co-injecting SDS reduced proteins with a stream SDS, as necessary for the separation stage, has significantly reduced SDS removal efficiency in the transfer stage and (2) how to improve SDS removal efficiency under the required separation condition. The simulation model is built by incorporating SDS dissociation model described in Chapter 7 with mass transport equations. The following rate equations describe migration behavior and concentration change of SDS-CRP* complex ($c_1$) without any binding affinity toward the blotting gel, free CRP* ($c_2$) with binding affinity toward the blotting gel, and free SDS ($c_3$).

$$\text{CRP*-SDS: } \frac{d\,c_1}{dt} = -\mu_1 E \frac{\partial c_1}{\partial x} + D_1 \frac{\partial^2 c_1}{\partial x^2} + k_{on} c_2 c_3 - k_{off} c_1$$

$$\text{CRP*: } \quad \frac{d\,c_2}{dt} = -\mu_2 E \frac{\partial c_2}{\partial x} + D_2 \frac{\partial^2 c_2}{\partial x^2} - k_{on} c_2 c_3 + k_{off} c_1$$

$$\text{SDS: } \quad \frac{d\,c_3}{dt} = -\mu_3 E \frac{\partial c_3}{\partial x} + D_3 \frac{\partial^2 c_3}{\partial x^2} - k_{on} c_2 c_3 + k_{off} c_1$$

In our model, CRP* and SDS are the products of SDS-CRP* dissociation with a dissociation rate constant of $k_{off}$ (unit: s$^{-1}$). The dissociation of SDS-CRP* is counterbalanced by formation of new SDS-CRP* due to the association of SDS and CRP* with an associate rate constant of $k_{on}$ (M$^{-1}$s$^{-1}$). Under the application of a lateral electric field (E), all three species migrate with electrophoretic mobility of $\mu$ and diffusion constant of $D$. As there is negligible shift in peak center along the separaton axis during lateral transfer[2], we can convert the 2D problem into a 1D problem by considering only the concentration profile along the axis intersecting the SDS-CRP* analyte (as indicated by the dashed line in Figure 9-8).
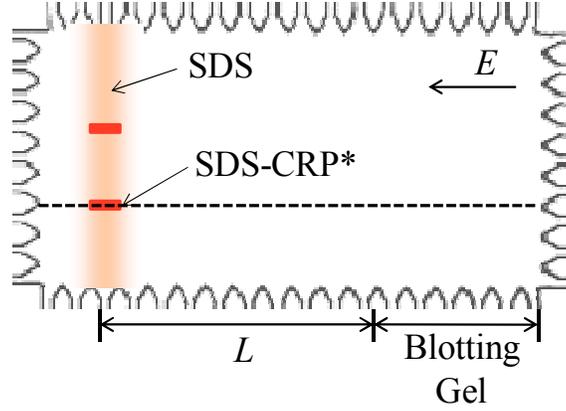
Figure 9-8. The 2D problem is converted into a 1D problem by considering only SDS-CRP*, CRP*, and SDS concentration profile along the dashed line that intersects the center of the SDS-CRP* peak.

### 9.3.2 Non-dimensionalization to identify key governing parameters

To identify key parameters governing the SDS removal process, we non-dimensionalize mass transport equations by performing normalizations on migration time and migration distance. Migration distance ($x$) is normalized with respect to available lateral transfer distance ($L$): $\bar{x} = \dfrac{x}{L}$ . Migration time ($t$) is normalized with respect to the time for CRP* to reach the blotting gel ($L/\mu_2 E$): $\bar{t} = \dfrac{t}{L/E\mu_2}$ . Our design goal is to maximize CRP* concentration at the end of lateral transfer ($x = L$ or $\bar{x} = 1$; $t = L/(E\mu_2)$ or $\bar{t} = 1$). Substituting $\dfrac{\partial c_i}{\partial t} = \dfrac{\partial c_i}{\partial \bar{t}} \cdot \dfrac{E\mu_2}{L}$, $\dfrac{\partial c_i}{\partial x} = \dfrac{\partial c_i}{\partial \bar{x}} \cdot \dfrac{1}{L}$, and $\dfrac{\partial^2 c_i}{\partial x^2} = \dfrac{\partial^2 c_i}{\partial \bar{x}^2} \cdot \dfrac{1}{L^2}$ into the mass transport equations, we obtain

$$\frac{\partial c_1}{\partial \bar{t}} = \frac{D_1}{E\mu_2 L} \frac{\partial^2 c_1}{\partial \bar{x}^2} - \frac{\mu_1}{\mu_2} \frac{\partial c_1}{\partial \bar{x}} + \frac{k_{on}L}{E\mu_2} c_2 c_3 - \frac{k_{off}L}{E\mu_2} c_1$$

$$\frac{\partial c_2}{\partial \bar{t}} = \frac{D_2}{E\mu_2 L} \frac{\partial^2 c_2}{\partial \bar{x}^2} - \frac{\partial c_2}{\partial \bar{x}} - \frac{k_{on}L}{E\mu_2} c_2 c_3 + \frac{k_{off}L}{E\mu_2} c_1$$

$$\frac{\partial c_3}{\partial \bar{t}} = \frac{D_3}{E\mu_2 L} \frac{\partial^2 c_3}{\partial \bar{x}^2} - \frac{\mu_3}{\mu_2} \frac{\partial c_3}{\partial \bar{x}} - \frac{k_{on}L}{E\mu_2} c_2 c_3 + \frac{k_{off}L}{E\mu_2} c_1$$

With the differential equations expressed in non-dimensional spatial and temporal scales, we can see that the formation of CRP* ($c_2$) is not only favored by isolation of CRP* from SDS (to minimize $c_2 c_3$) but also enhanced by increasing migration time during the transfer stage (to increase $L/(E\mu_2)$).

### 9.3.3 Selection of initial conditions and physical parameters

The non-dimensionalized partial differential equations are solved using MATLAB's pdepe solver with physical parameters listed in Table 9-2 and the following initial conditions approximating our assay conditions (Matlab codes are provided in Appendix D). At time = 0 (onset of lateral transfer process), the SDS-CRP* is modeled as a Gaussian peak

( $C_{SDS-CRP*}(x, t = 0) = c_{sds-crp*,0}e^{-\frac{x^2}{2\sigma_0^2}}$ ) with peak width (4$\sigma_0$) of 200 μm and peak concentration of 200 nM. Free SDS present during the separation is modeled as a Gaussian peak ($C_{SDS}(x, t = 0) = c_{sds,0}e^{-\frac{x^2}{2\sigma_0^2}}$) with the same peak width (4$\sigma_0$) of 200 μm and peak concentration of $c_{sds,\ 0}$.

The goal of our simulation is not to have an absolute prediction of CRP* recovery at the end of lateral transfer but to understand how parameters such as background SDS concentration ($c_{sds,\ 0}$), mobility ratios ($\mu_3/\mu_2$ & $\mu_1/\mu_2$), and CRP* mobility ($\mu_2$) can influence CRP* recovery rate. Therefore, we made approximations and assumptions of physical parameters either based on previous experimental results or based on theoretical understanding of our system. Electric field and transfer distance are set based on chip geometry. We made the following assumptions of CRP* mobility ($\mu_2$) and diffusitivity ($D_2$) as relevant to migration conditions in polyacrylamide gels: $\mu_2 = 4 \times 10^{-5} \frac{cm^2}{V \cdot s}$ and $D_2 = 5 \times 10^{-6} \frac{cm^2}{s}$. As there have been limited reports on renaturation and denaturation rate constants for the CRP*-SDS interaction system we are studying, we made assumptions of SDS dissociation rate and association rate based on previous experimental results displayed in Figure 9-3. As an 80% recovery rate of CRP* was obtained after a lateral transfer time of 38 s, we approximated $k_{off}$ as $4 \times 10^{-2}$ s$^{-1}$. Assuming a dissociation constant ($K_d$) of 1 μM, $k_{on}$ is calculated as $4 \times 10^{-4}$ M$^{-1}$s$^{-1}$. The assumption of dissociation constant ($K_d$) is reasonable as SDS binding to proteins is a much weaker interaction compared to specific antigen-antibody interaction with dissociation constant in the nM range.

Table 9-2. Simulation parameters

| Variable | Values in simulation |
|---|---|
| E [V/cm] | 25 - 200 |
| $D_2$ [cm$^2$/s] | $1 \times 10^{-6}$ |
| $\mu_2$ [cm$^2$/s/V] | $4 \times 10^{-5}$ |
| L [mm] | 1 |
| $k_{off}$ [s$^{-1}$] | $4 \times 10^{-2}$ |
| $k_{on}$ [M$^{-1}$s$^{-1}$] | $4 \times 10^{4}$ |
| $c_{sds,\ 0}$ | $0 - 3.47$ mM |
| $\mu_1/\mu_2$ | $1 - 2.5$ |
| $\mu_3/\mu_2$ | 1 |

### 9.3.4 Simulation results

In this section, we illustrate how experimental conditions such as analyte mobilities and SDS background concentration can influence CRP* recovery rate. We formally define CRP* recovery rate as the peak area of CRP* (i.e., peak concentration integrated over x-axis) at the end of lateral transfer ($\bar{x} = 1$ & $\bar{t} = 1$) divided by SDS-CRP* peak area at the beginning of lateral transfer ($\bar{x} = 0$ & $\bar{t} = 0$). In chapter 7, we defined the theoretical upper limit for recovery rate by assuming only dissociation and no association: $\frac{[CRP*]_{free}}{[CRP*]_{total}}|_{max} = 1 - e^{-k_{off} \cdot t}$. The maximum possible recovery rate is set by dissociation rate ($k_{off}$) and dissociation time ($t = L/\mu_2/E$). For the parameters listed in Table 9-2, the maximum recovery rate is 63.2% under an applied electric

field of 100 V/cm. We will refer back to this value during this section as a reference for SDS removal effectiveness.

Figure 9-9 illustrates how % CRP recovery rate decreases with increased SDS background concentration ($c_{sds,\ 0}$) with all three species (CRP*, SDS-CRP*, and SDS) migrating at the same mobility ($\mu_1/\mu_2 = \mu_3/\mu_2 = 1$). The result is not surprising as the emergence of CRP* ($c_2$) is a balance of dissociation ($k_{off}c_1$) and association ($k_{on}c_2c_3$). At $c_{sds,\ 0} = 0$, SDS molecules that are dissociated from SDS-CRP* at nM concentration level are the only SDS present in the system. Hence, the association rate ($k_{on}\ c_3$) is significantly less than the dissociation rate ($k_{off}$). As a result, we obtain a recovery rate of 62.5% which approaches the theoretical upper limit of recovery rate for the given lateral transfer time of 25 s. On the other hand, SDS concentration in the injected plug significantly increases overall SDS concentration ($c_3$) in the system. For the chosen $k_{on}$ and $k_{off}$ values, the association rate ($k_{on}c_3$) is larger than the dissocation rate ($k_{off}$) for SDS concentration above 1 µM. Hence, any free CRP* will re-bind with SDS due to their overlapping peak profile. As a result, recovery rate decreases significantly.
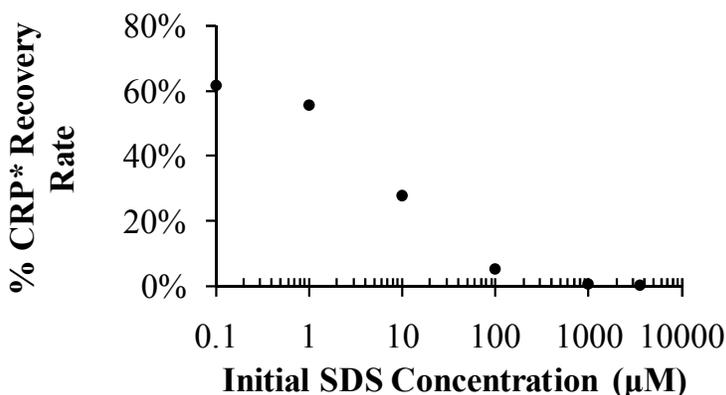


Figure 9-9. %CRP recovery rate decreases due to presence of SDS co-injected with SDS-CRP*. Simulation performed under E = 100 V/cm, L = 1 mm, $D_2 = 1 \times 10^{-6}$ cm²/s, $\mu_2 = 4 \times 10^{-5}$ cm²/s/V, $k_{off} = 4 \times 10^{-2}$ s⁻¹, $k_{on} = 4 \times 10^4$ M⁻¹s⁻¹, and $\mu_1/\mu_2 = \mu_3/\mu_2 = D_1/D_2 = D_3/D_2 = 1$.

Figure 9-10 illustrates that, despite a high SDS concentration in the injected sample plug ($c_{sds,\ 0} = 3.5$ mM), we can increase the recovery rate by enhancing the mobility difference among free SDS and free CRP* ($\mu_3/\mu_2$). For simplicity, SDS-CRP* mobility is set to be the same as CRP* mobility. In addition, to simulate conditions in polyacrylamide gels, the change in diffusitivity is proportional to change in mobility ($\mu_3/\mu_2 = D_3/D_2$) as diffusion and electrophoresis encounter the same drag force. Increasing mobility difference between SDS and free CRP* resolves SDS peak from CRP* peak at an earlier migration distance and migration time and reduces the association of CRP* with SDS. At a SDS to CRP* mobility ratio of 2.5 ($\mu_3/\mu_2 = 2.5$), we are able to achieve a 60.2% recovery rate which is close to the recovery rate achieved for a system without any SDS present in the injected sample plug.
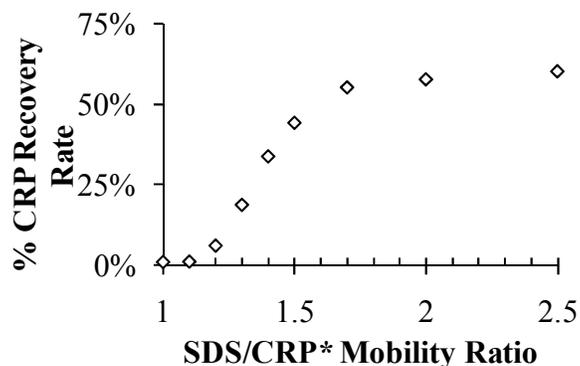
Figure 9-10. Enhancing SDS/CRP* mobility ratio increases CRP recovery rate. Simulation performed under $E = 100$ V/cm, $L = 1$ mm, $c_{SDS, 0} = 3.5$ mM, $D_2 = 1 \times 10^{-6}$ cm$^2$/s, $\mu_2 = 4 \times 10^{-5}$ cm$^2$/s/V, $k_{off} = 4 \times 10^{-2}$ s$^{-1}$, $k_{on} = 4 \times 10^4$ M$^{-1}$s$^{-1}$, and $\mu_1/\mu_2 = D_1/D_2 = 1$, $\mu_3/\mu_2 = D_3/D_2$.

As the maximum recovery rate is also determined by migration time allowed for SDS dissociation, we further examined the impact of electric field on recovery rate as migration time is inversely proportional to applied electric field. Figure 9-11 depicts two scenarios where decreasing electric field either improves recovery rate (A) or decreases recovery rate (B). In the scenario depicted in Figure 9-11A, there is sufficient mobility difference between SDS and CRP* ($\mu_3/\mu_2 = 2$). Decreasing electric field increases migration time allowed for SDS dissociation and correspondingly increases recovery rate. The downside of reducing electric field to improve recovery rate is reduced peak concentration as a result of band broadening due to increased diffusion. Reduced peak concentration may limit detection sensitivity. In the scenario depicted in Figure 9-11B, there is not sufficient mobility difference between SDS and CRP* ($\mu_3/\mu_2 = 1.4$). Decreasing electric field further reduces the separation resolution between SDS and CRP* and drives the reaction toward association of SDS with CRP* instead of dissociation of SDS-CRP*.
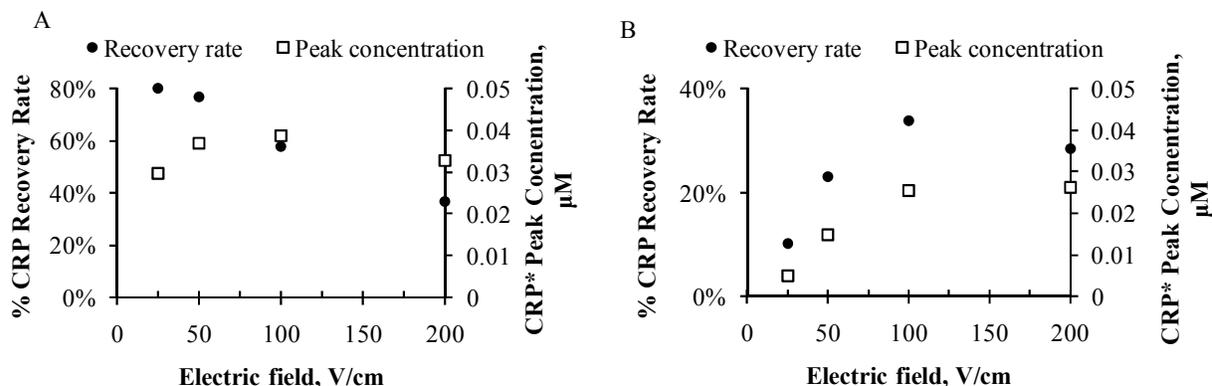


Figure 9-11. Decreasing electric field enhances CRP recovery rate at sufficient mobility differences ($\mu_3/\mu_2 = D_3/D_2 = 2$ in A) and decreases CRP recovery rate for insufficient mobility differences ($\mu_3/\mu_2 = D_3/D_2 = 1.4$ in B). Simulation performed under $L = 1$ mm, $c_{SDS, 0} = 3.5$ mM, $D_2 = 1 \times 10^{-6}$ cm$^2$/s, $\mu_2 = 4 \times 10^{-5}$ cm$^2$/s/V, $k_{off} = 4 \times 10^{-2}$ s$^{-1}$, $k_{on} = 4 \times 10^4$ M$^{-1}$s$^{-1}$.

### 9.3.5 Translating simulation results to experimental optimization

The simulation results presented in Figure 9-11 inform us that there are two operating regimes for on-chip SDS removal by electrophoretic transport. The first operating regime occurs when

there is sufficient separation resolution between SDS and CRP (as in the case of E = 100 V/cm and $\mu_3/\mu_2 = 2$), CRP* recovery rate is approaching the theoretical upper limit set by the migration time within the lateral transfer stage. Therefore, migration time or available SDS dissociation time is the limiting factor in the first operating regime. Increasing migration time by either one or a combination of decreasing electric field (E), increasing transfer distance (L), and decreasing electrophoretic mobility ($\mu_2$) can further improve recovery rate. The second operating regime occurs when CRP* recovery rate is limited by insufficient separation resolution between SDS and CRP (as in the case of E = 25 V/cm and $\mu_3/\mu_2 = 1.4$). Therefore, increasing separation resolution by increasing mobility ratios ($\mu_3/\mu_2$) is most effective in improving recovery rate (Figure 9-10).

Decreasing gel pore size can improve recovery rate for both operating regimes. As demonstrated in my previous work on ultra-short separation length homogeneous immunoassays (chapter 6), decreasing gel pore size increases relative mobility difference among analytes ($\Delta\mu/\mu$). Increasing $\Delta\mu/\mu$ improves the separation resolution achieved within a limited separation length. Therefore, reducing gel pore size can improve recovery rate for the second operating regime which is limited by separation resolution. Decreasing pore size also reduces analyte mobility and increases migration time. Thus, decrease gel pore size improves recovery rate for the first operating regime which is limited by available dissociation time. In the regime where available dissociation time is the limiting factor, decreasing gel pore size is a better method to improving recovery rate than decreasing electric field. Reducing electric field increases analyte peak width by diffusion: $\sigma = \sqrt{\sigma_0^2 + 2D\frac{L}{\mu E}}$. The increased peak width results in decreased peak concentration and decreased separation resolution and could adversely affect both detection sensitivity and recovery rate. On the other hand, decreasing gel pore size decreases both D and $\mu$ to the same extent. Hence, peak width at a given migration distance is maintained while separation resolution is improved by increasing mobility differences ($\Delta\mu/\mu$).

## 9.4 Experimental demonstration of SDS removal in transit

As informed by simulation results, we perform transfer in an 8%T region for improved SDS removal efficiency. As shown in Figure 9-12, separation of SDS reduced BSA* and CRP* was performed in 3% loading gel and 8% separation gel with a stream of SDS co-migrating along the separation axis. An SR of 2.55 was achieved at an elapsed separation time of 22 s. At t = 21 s, the electric field was switched to be across the lateral transfer region and SDS dissociation was initiated. After a lateral transfer distance of 1 mm and time of 60 s, SDS-CRP* reached the blotting gel. As evident in Figure 9-12, CRP* was able to bind to the blotting gel with a binding efficiency of 55%. On the other hand, the larger BSA* protein (66 kDa), which has no cross reactivity toward anti-CRP antibody, freely migrated through the blotting region (t = 188 s). The 55% binding efficiency is a significant improvement compared to transfer performed in a 3%T which results in less than 5% binding efficiency. Despite the high SDS background concentration present at the onset of transfer (3.5 mM), improving mobility differences among SDS and CRP* by reducing gel pore size increases recovery rate of CRP* that has binding affinity toward the blotting gel.
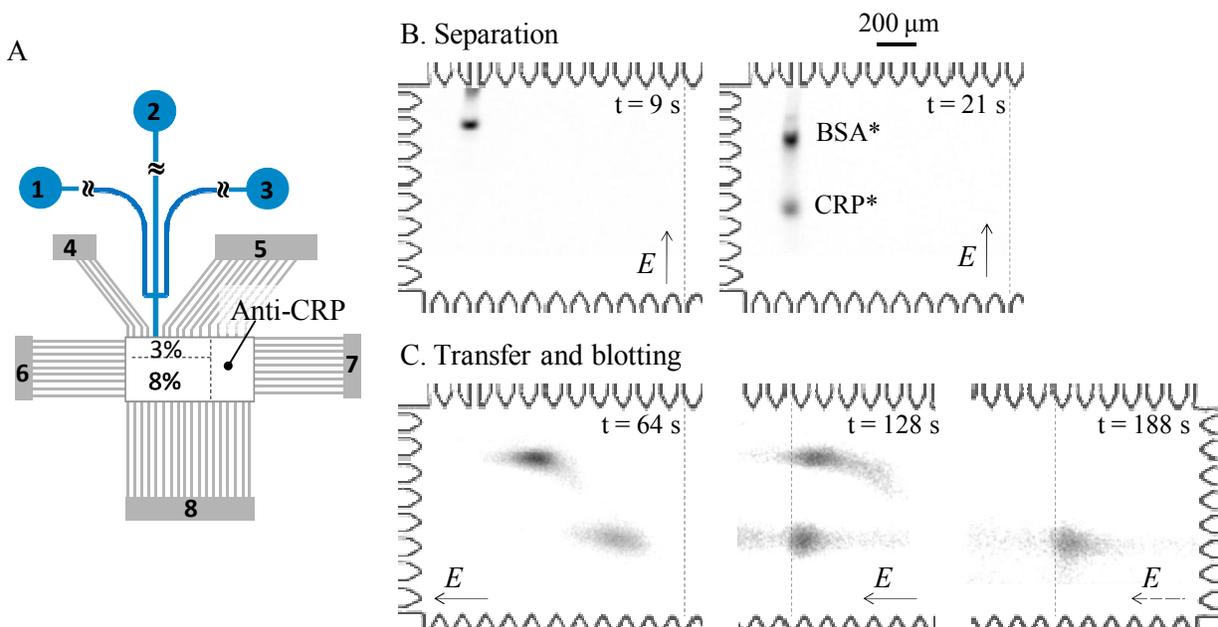
Figure 9-12. Reduced CRP* binds to blotting gel following separation performed in SDS buffer (B) and lateral transfer across the 2D chamber (C). The 1 mm x 2 mm 2D chamber contains a 3%T loading gel and an 8% separation gel in adjacent to an anti-CRP blotting gel (4.5%T with 2.1 µM biotinylated anti-CRP Ab and 5.7 µM streptavidin-acrylamide). Sample containing CRP* (595 nM) and BSA* (120 nM), which were reduced in 0.1% SDS, was introduced in sample well 1; wells 2 and 8 contain 1x Tris/glycine buffer with 0.1%SDS and all other wells contain 1x Tris/glycine buffer. Voltage programming follows that described in section 9.1.2.

Furthermore, we confirmed the binding observed in Figure 9-12 is due to specific interaction between renatured CRP* and anti-CRP Ab by injecting sample with the same composition into a chip without any blotting gel. As shown in Figure 9-13, in absence of a blotting gel, both CRP* and BSA* free migrate outside of the 2D chamber into well 7.
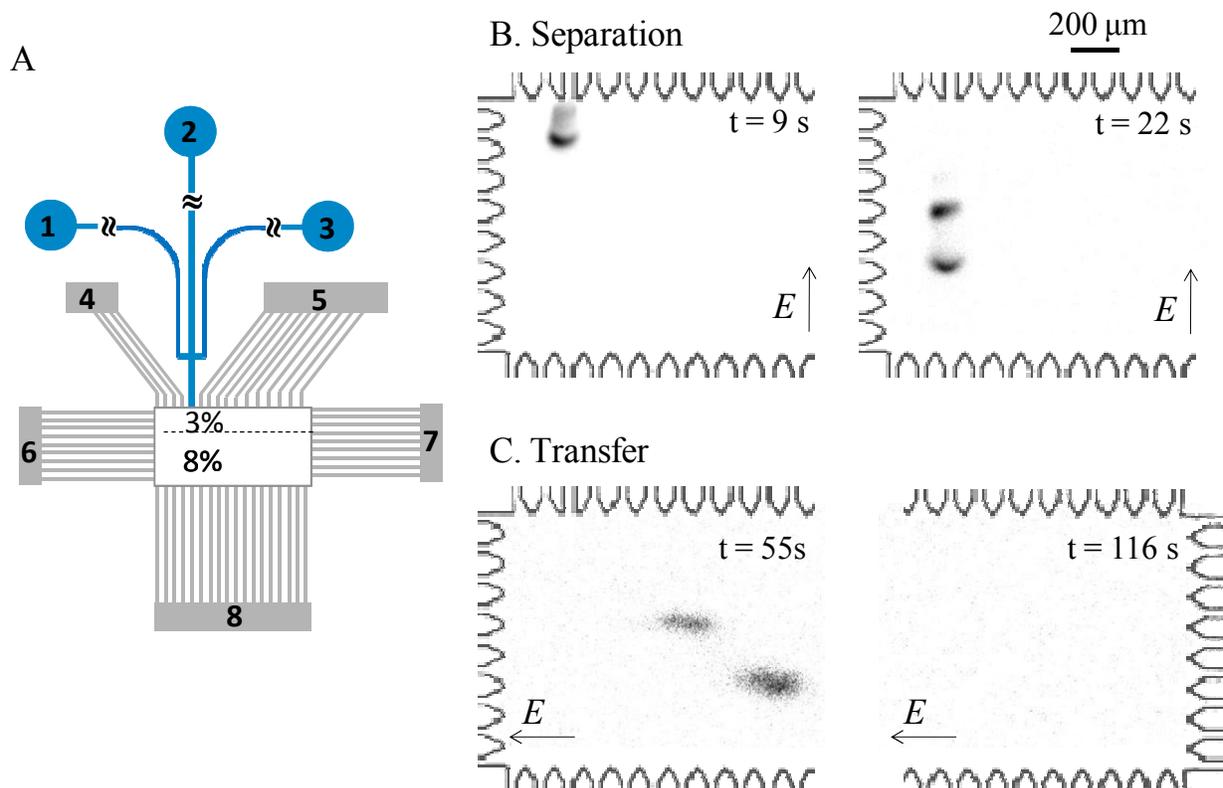
Figure 9-13. Reduced CRP* and BSA* freely migrate through the 2D chamber in absence of a blotting gel. The 1 mm x 2 mm 2D chamber contains a 3%T loading gel and an 8%T separation gel. Sample containing CRP* (595 nM) and BSA* (120 nM), which were reduced in 0.1% SDS, was introduced in sample well 1; wells 2 and 8 contained 1x Tris/glycine buffer with 0.1%SDS and all other wells contained 1x Tris/glycine buffer. Voltage programming follows that described in section 9.1.2.

## 9.5 Discussion: how to further improve binding efficiency

Performing lateral transfer in small pore size gel (8%T) improves CRP* recovery rate by increasing separation resolution of free SDS and CRP* and increasing available SDS dissociation time. While this chapter mainly focuses on increasing SDS removal and protein renaturation efficiency during the lateral transfer stage, we recognize the overall binding efficiency to blotting gel is dependent on renaturation efficiency in the lateral transfer stage as well as binding efficiency within the blotting gel region. As both devices have the same composition and use the same operating parameters for the blotting gel, the binding efficiency improvement from < 5% observed in Figure 9-6 to 55% demonstrated Figure 9-12 is mainly due to improved renaturation efficiency that was achieved by decreasing lateral transfer gel pore size from that of a 3%T to that of an 8%T.

We can further increase the overall binding efficiency observed in the later device by increasing binding efficiency of renatured CRP* within the blotting gel. Previous simulation and experimental results revealed native protein binding efficiency within the blotting gel region is a function of Damkohler number (Da)[4]: $Da = Lk_{on}b_m/\mu E$ where L is the blotting region length,

$k_{on}$ is the antigen-antibody association rate constant, $b_m$ is the available binding sites within the blotting gel, $\mu$ is the analyte mobility, and E is the applied electric field during blotting. A large *Da* leads to increased binding to the blotting gel. For our system, there are three most effective ways to increase binding efficiency of renatured CRP* to the blotting gel. The first is to improve antigen-antibody affinity ($k_{on}$) by using an antibody recognizing linear epitopes on the CRP polypeptide. The currently employed polyclonal antibody recognizes both linear epitopes present on the CRP polypeptide as well as possibly folded epitopes absent on the CRP polypeptide. The second way is to further increase antibody concentration within the blotting gel region. The currently used concentration is 2 μM which is the maximum concentration attainable following biotinylation. We can further increase the antibody concentration by running biotinylated antibodies through a commercially available spin filter that can concentrate the antibody by 2-10 folds. The third way is to reduce applied electric field once renatured CRP* has entered the blotting gel region to increase antibody-antigen interaction time.

We also ask if we can further increase SDS removal and protein renaturation efficiency during the lateral transfer stage. Our current strategy has been decreasing gel pore size to increase both separation resolution and available SDS dissociation time. However, gel pore size can only be decreased to a certain extent without physically excluding larger proteins. Separation resolution and available SDS dissociation time can also be improved by increasing lateral transfer distance. However, lateral transfer distance is ultimately limited by device geometry (a chamber width of 2 mm). Similarly, as shown in Figure 9-11, electric field can only be decreased to a certain range without adversely impacting separation resolution and peak concentration. Therefore, we propose another strategy that is to use immobilized cyclodextrin to remove SDS. The new strategy can be performed in parallel with electrophoretic removal of SDS. Removing SDS with immobilized cyclodextrin, which will be detailed in chapter 10, is especially appropriate for renaturation of small proteins (< 10 kDa) when reducing gel pore size may not be able to generate sufficient mobility difference between SDS and the small proteins without physically excluding the large proteins.

## 9.6  References

(1)     Ng, A. H. C.; Uddayasankar, U.; Wheeler, A. R. *Analytical and Bioanalytical Chemistry*, *397*, 991-1007.
(2)     He, M.; Herr, A. E. *Journal of the American Chemical Society*, *132*, 2512-2513.
(3)     Schneider, G. F.; Shaw, B. F.; Lee, A.; Carillho, E.; Whitesides, G. M. *Journal of the American Chemical Society* **2008**, *130*, 17384-17393.
(4)     Tia, S. Q.; He, M.; Kim, D.; Herr, A. E. *Analytical Chemistry*, *83*, 3813-3588.

# Chapter 10 On-chip Immobilization of Cyclodextrins for SDS Removal

In the previous chapter, we demonstrated microfluidic western blotting with electrophoretic isolation of SDS from proteins to facilitate protein renaturation process. As proposed in Chapter 8, immobilizing cyclodextrin, a SDS binding agent, within the transfer region can also assist SDS removal and protein renaturation. Cyclodextrin recovers antigen-antibody immune complex formation as assessed by on-chip homogeneous immunoassays (Chapter 8). In this chapter, we motivate and detail the development of an on-chip cyclodextrin immobilization strategy for seamless integration with microfluidic western blotting assays.

As illustrated in chapter 9, SDS removal capability must be isolated to the transfer region to avoid interference with upstream SDS-PAGE separation. Due to a lack of functional groups suitable for free radical polymerization, immbolization of β-cyclodextrin requires chemical modification of its original structure. Figure 10-1 depicts our strategy that was used to evaluate immobilization effectiveness of three approaches. In our previous work, we used homogeneous immunoassay to monitor denaturation and renaturation process (chapter 8) and found previously denatured CRP* was resolved into multiple bands during on-chip separation after off-chip incubation with β-CD. The electrophoretic separation pattern, which was unique from that of fully denatured CRP*, indicates occurrence of SDS removal and protein renaturation. Here we use electrophoretic separation pattern in the 2D chamber to monitor the effectiveness of β-CD immobilization strategies with the following caveat:  the separation pattern is used to recognize β-CD present in the separation stage due to inefficient confinement of β-CD within the transfer region.  This chapter will provide details on implementation and testing of each strategy as well as explaining why only the third strategy is effective whereas the first two are not. Finally, we conclude with a discussion on how immobilized cyclodextrin can further improve the binding efficiency that was already achieved using electrophoretic isolation of SDS as detailed in the last chapter.

| Previous Observation | Immobilization Strategies | Observations |
|---|---|---|
| Cyclodextrin removes SDS from denatured proteins and results in unique electrophoretic migration pattern | 1. Include unmodified cyclodextrin in PA gel precursor solution | Denatured CRP* was resolved into multiple bands prior to entering CD-PA gel |
| **Testing of immobilization effectivness** Electrophoretic separation of denatured proteins | 2. Co-polymerize PA gel with allyl-β-cyclodextrin | Denatured CRP* was resolved into multiple bands prior to entering CD-PA gel |
| | 3. Co-polymerize PA gel with acrylate- β-cyclodextrin | Denatured CRP* remained as 1 band |

Figure 10-1. Strategy to evaluate effectiveness of three immobilization approaches.

## 10.1 Unmodified β-cyclodextrin: inefficient cross linking with polyacrylamide gels

Due to its small molecular weight (1135 g/mol), β-CD (1135 g/mol) cannot be confined within polyacrylamide gel by physical entrapment. As shown in Figure 10-2, reduced SDS-CRP* was injected into a chip containing a 3%T loading gel and a 4%T in the transfer region. The 4%T in the transfer region is polymerized with 4% (w/v) 2-hydroxylpropyl β-cyclodextrin dissolved in the precursor solution. 2-hydroxylpropyl β-cyclodextrin was used instead of β-cyclodextrin due to its higher solubility in water. The multiple bands present in the separation stage indicate that cyclodextrin was diffusing out of the 4%T region and contributing to SDS removal during the separation stage. As discussed earlier, cyclodextrin aids SDS removal by sequestering free SDS molecules that were dissociated from SDS-CRP* complexes and drives the reaction toward more SDS-CRP* dissociation. While we confirmed SDS removing capability of cyclodextrin, the presence of cyclodextrin throughout the chip due to diffusion interferes with separation in the first stage. Therefore, we examined two chemical modification strategies to covalently crosslink cyclodextrin with polyacrylamide gels so SDS removal can be confined within the lateral transfer region.
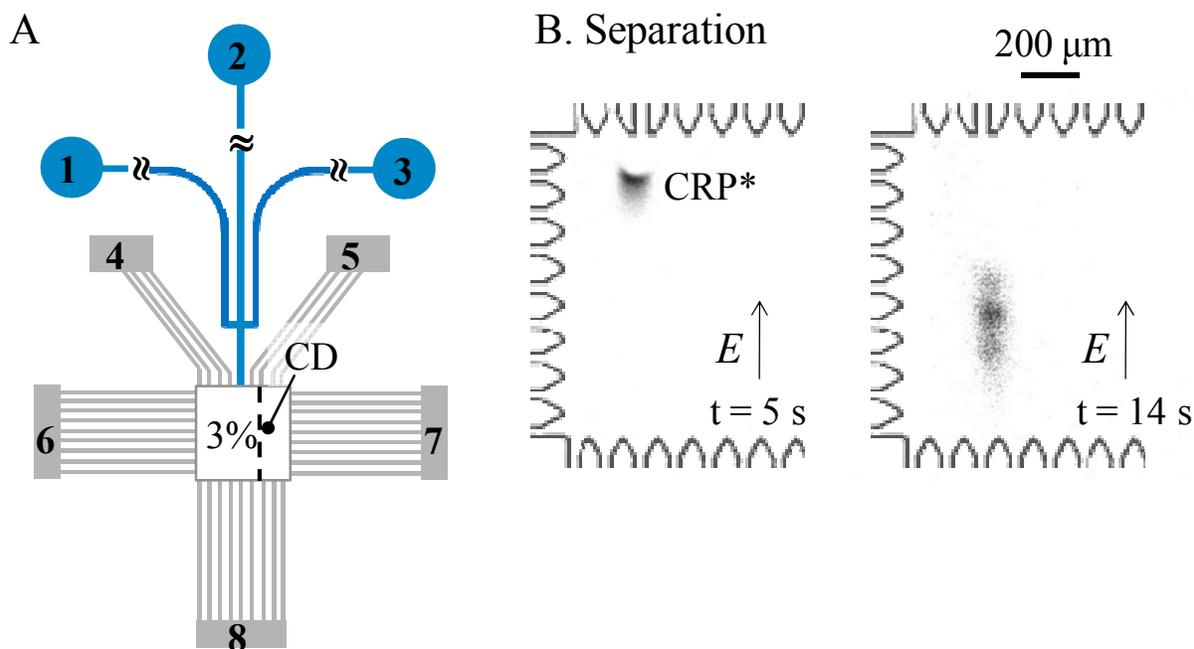


Figure 10-2. Reduced CRP* was resolved into multiple bands due to presence of cyclodextrin in the separation region as a result of diffusion. The 1 mm x 1 mm 2D chamber contains a 3%T gel in adjacent to a 4%T gel polymerized with 4% (w/v) 2-hydroxylpropyl β-cyclodextrin dissolved in the precursor solution. Sample containing CRP* (440 nM) reduced in 0.1% SDS was introduced in sample well 1; all other wells contain 1x Tris/glycine buffer. Voltage programming follows that described in section 9.1.2. Bright field image of the 2D chamber boundary is overlaid on top of separation and transfer images to give perspective to chamber location.

## 10.2  Synthesis of allyl-β-cyclodextrin: inefficient cross linking with polyacrylamide gels

Our second strategy to crosslink cyclodextrin involves the synthesis of 2-hydroxy-3-allylloxy-propyl-β-cyclodextrin (allyl-β-cyclodextrin) from β-cyclodextrin. 2-hydroxy-3-allylloxy-propyl-β-cyclodextrin contains the basic sugar ring structure of β-cyclodextrin for SDS binding and includes an allyl side group that can be polymerized with acrylamide and bisacrylamide during polyacrylamide gel fabrication. Our choice of allyl-β-cyclodextrin is inspired by previous demonstrations of crosslinking allyl-β-cyclodextrin with polyacrylamide gels in capillaries for chiral separation[1] and DNA sequencing[2]. Allyl-β-cyclodextrin has also been crosslinked with polyacrylamide gels within PDMS channels using photopatterning[3]. Further, the copolymerization of allyl-β-cyclodextrin with polyacrylamide gels has been marketed as "a new easy-to-prepare"[1] strategy for incorporating cyclodextrin into polyacrylamide gel sieving matrices as there is only 1 reaction step without requiring any purification steps.

### 10.2.1 Synthesis of allyl- β-cyclodextrin

As depicted in Figure 10-3, allyl-β-cyclodextrin is obtained by reacting β-cyclodextrin with allyl glycidyl ether (AGE) under alkaline conditions (at pH = 11). At pH = 11, the primary hydroxyl group on β-cyclodextrin gets deprotonated and becomes a reactive alkoxide. The alkoxide then opens up the oxacyclopropane ring on the AGE and creates 2-hydroxy-3-allylloxy-propyl-β-cyclodextrin. We synthesized allyl-cyclodextrin via the following steps:

(1) Dissolve 1.27 g β-cyclodextrin in 7.4 mL water
(2) Add 3 mL 1.5 M NaOH to increase solution pH to 11 – 12
(3) Add 0.5 mL allyl glycidyl ether gradually
(4) Stir the reactants for 48 hours.

**Overview of Reaction**



β-cyclodextrin      Allyl Glycidyl            Allyl- β-cyclodextrin
                    Ether
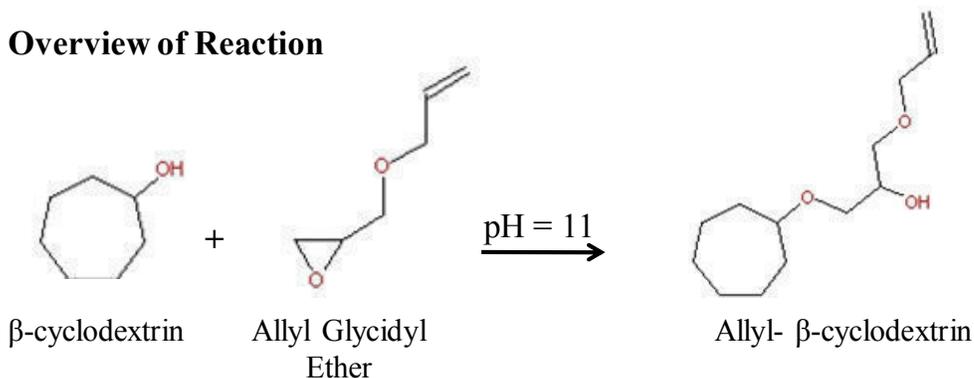
**Mechansim**
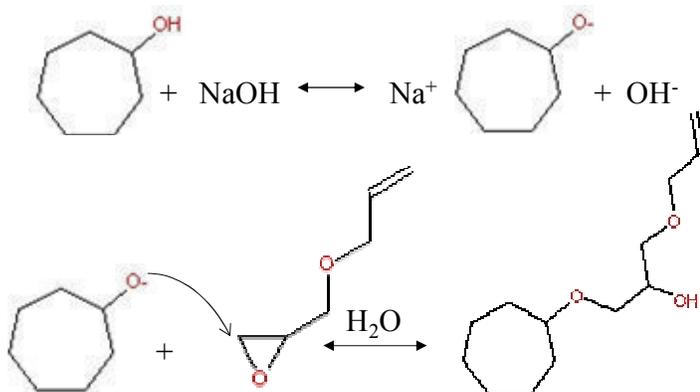


Figure 10-3. Overview and mechanism of allyl-β-cyclodextrin synthesis from β-cyclodextrin and allyl glycidyl ether.

The effective β-cyclodextrin concentration is 100 mM and AGE concentration is 0.39 M. The synthesis protocol follows previously described[1] with elimination of sodium borohydride (NaBH$_4$) used in the original protocol. Sodium borohydride is a reducing agent that reacts with water and Tris buffer releasing hydrogen gas. Shown below is a reaction of sodium borohydride with primary alcohols (ROH): NaBH$_4$ + 4 ROH → NaB(OR)$_4$ + 4 H$_2$. Tris buffer (present in polyacrylamide gel precursor solution) contains 3 primary hydroxyl groups. As a result, presence of sodium borohydride in allyl-β-cyclodextrin led to extensive bubble formation when allyl-β-cyclodextrin was mixed and sonicated with polyacrylamide gel precursor solution.  As sodium borohydride is not required for formation allyl-β-cyclodextrin, we removed it from our synthesis protocol.

10.2.2 **Copolymerization of allyl-β-cyclodextrin with polyacrylamide gels**
Cyclodextrin polyacrylamide (CD-PA) gel precursor solution was prepared by mixing synthesis product containing 100 mM allyl-β-cyclodextrin with 30% (w/v) acrylamide/bisacrylamide solution and Tris/glycine native buffer to a total volume containing 4%T (acrylamide), 40 mM allyl-β-cyclodextrin, and 0.5% (w/v) VA-086 photoinitiator.  The choice of 40 mM allyl-β-cyclodextrin concentration is based on our previous demonstration of 4% (w/v or 29 mM) 2-hydroxypropyl β-cyclodextrin being able to recover antibody binding affinity of denatured

CRP*. Compared to PA gel polymerization in absence of allyl-β-cyclodextrin, an increased photoinitiator concentration is needed for complete gel crosslinking.

CD-PA gel polymerization employs the same exposure settings as regular PA gels and antibody decorated blotting gels. For western blotting assays implemented in the 2D chamber, CD-PA gel is usually fabricated after the fabrication of blotting gel and prior to the fabrication of loading and separation gels.

### 10.2.3 **On-chip characterization of CD-PA gel**
To determine whether CD was efficiently crosslinked with polyacrylamides, reduced SDS-CRP* was injected into a chip that contained a 3%T loading gel and a 4%T in the transfer region. The 4%T in the transfer region was co-polymerized with 40 mM allyl-β-CD as described in section 10.2.2. As shown in Figure 10-4B, SDS-CRP* was resolved into several bands (t = 14 s) along the separation axis. The formation of multiple bands indicates diffusion of allyl-β-CD outside of the transfer region.  On the other hand, when SDS-CRP* was injected into another chip without any allyl-β-CD in the transfer region (Figure 10-4D), SDS-CRP* remained as one band which was expected in absence of any SDS dissociation.
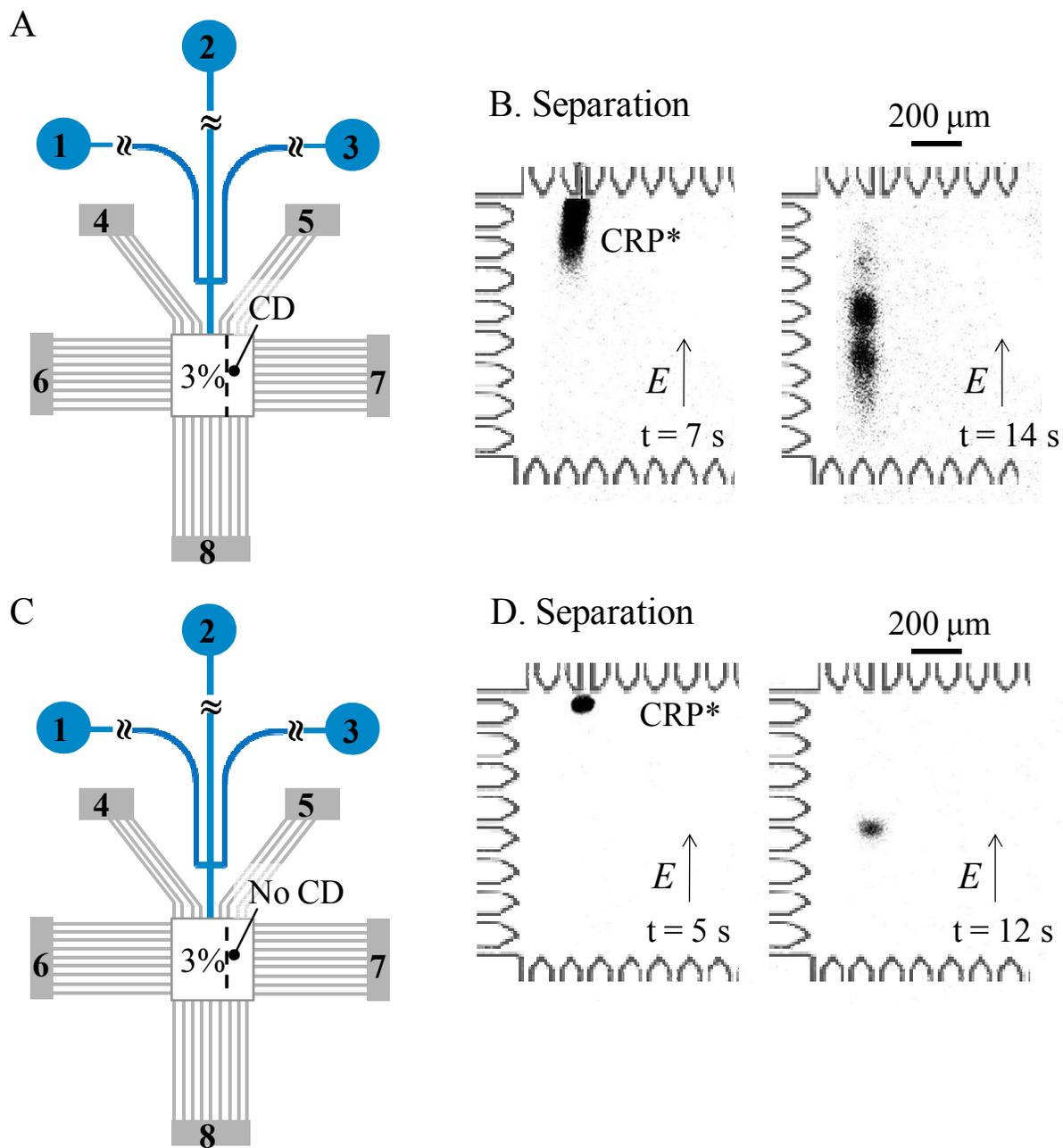
Figure 10-4. Inefficient crosslinking of cyclodextrin with polyacrylamide gels results in SDS removal during the separation stage (A, B). (A, B) SDS reduced CRP* was injected into a chip containing a 3%T gel in adjacent to a 4%T gel that was copolymerized with 40 mM allyl-β-cyclodextrin. Due to presence of cyclodextrin, CRP* was resolved into multiple bands. (C, D) Control experiment: SDS reduced CRP* was injected into a chip containing 3%T gel in adjacent to a 4%T gel that was polymerized in absence of allyl-β-cyclodextrin. CRP remains as 1 band during separation. Sample containing CRP* (440 nM), which was reduced in 0.1% SDS, was introduced in sample well 1; all other wells contain 1x Tris/glycine buffer. Voltage programming

109

follows that described in section 9.1.2. Bright field image of the 2D chamber boundary is overlaid on top of separation and transfer images to give perspective to chamber location.

### 10.2.4 Discussion: polymerization is favored by resonance stabilization

Puzzled by why allyl-β-cyclodextrin cannot be effectively crosslinked with acrylamide and bisacrylamide, we examined the chemistry behind acrylamide polymerization process and found the reaction of acrylamide radical with allyl-β-cyclodextrin can terminate polymer chain growth through a process known as hydrogen abstraction[4]. As shown in Figure 10-5, the reaction of acrylamide radical on a growing polymer chain with allyl-β-cyclodextrin can proceed by either abstracting a hydrogen from the secondary carbon neighboring the allyl group (labeled as a) or by recombining with another electron supplied by the allyl group (labeled as b). The hydrogen abstraction reaction (in a) proceeds at a faster rate than the propagation reaction (in b) as the products in *a* is resonance stabilized which lowers reaction activation energy. Resonance is a terminology in chemistry to describe molecules that can be represented by several Lewis structures (i.e., diagrams describing bonding and lone pair electron pair distribution within a molecule). For example, resonance occurs when a radical is located in proximity with an allyl group as in the products of path *a*. Resonance results in a lower energy for products that were formed in *a*. On the other hand, the reaction of acrylamide radical on a growing polymer chain with another acrylamide only proceeds by recombining with another electron supplied by the acrylamide monomer (labeled as path c). Hydrogen abstraction does not occur with acrylamide monomer due to the lack of any hydrogen containing secondary carbons in adjacent to the allyl bond.

110
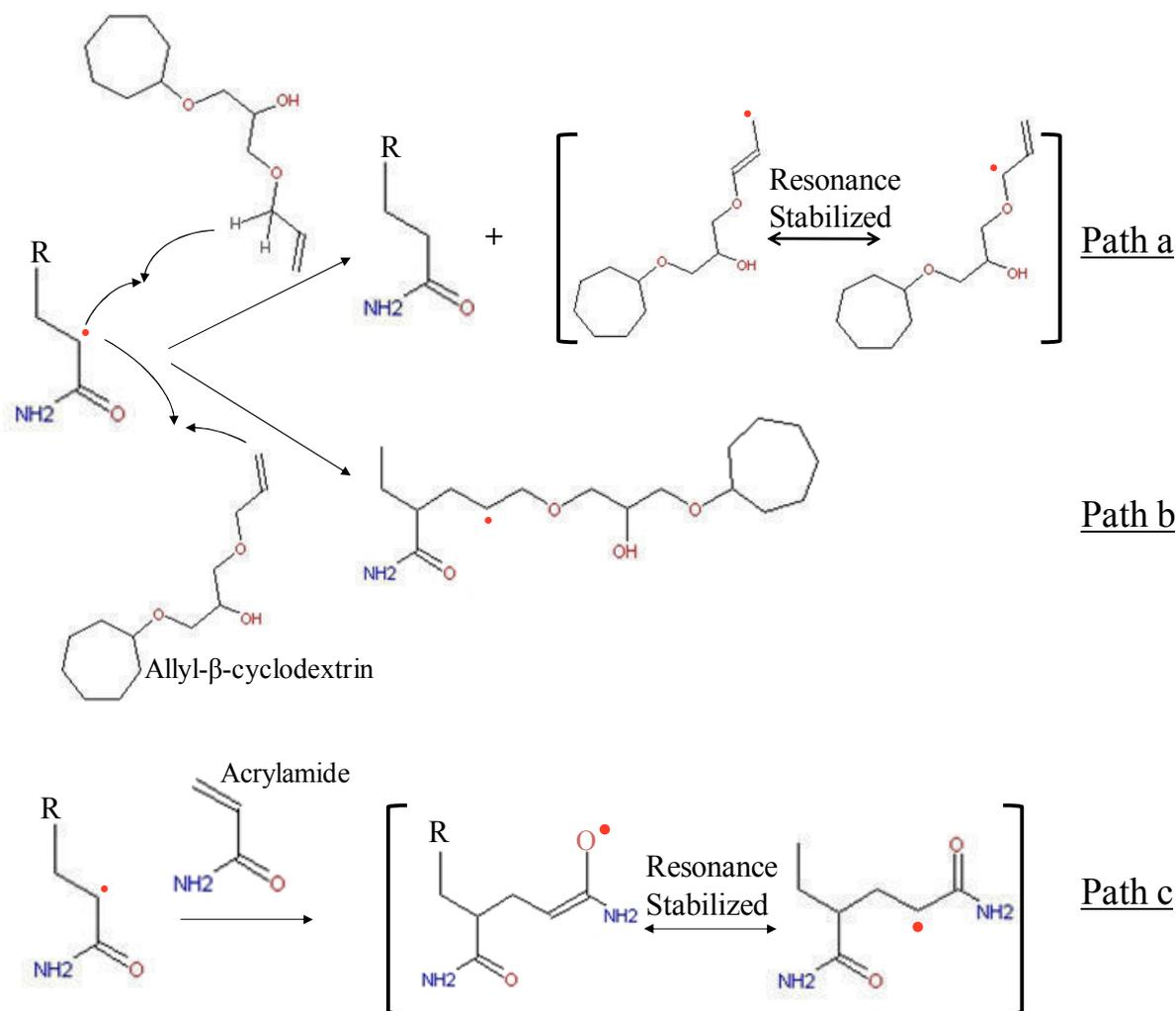
Figure 10-5. Possible reaction paths for copolymerization of allyl-β-cyclodextrin and acrylamide/biscarylamide. Path *a* is more favorable than path *b* due to formation of resonance stabilized products. However, path *a* terminates polymer chain growth. Therefore, chain growth proceeds via path *c*.

In previous reports[1, 3], allyl-β-cyclodextrin concentration is homogeneous throughout the separation capillary or the separation channel. Therefore, the effect of uncrosslinked allyl-β-cyclodextrin is less pronounced compared to in our system where we are trying to confine cyclodextrin within a certain region. Understanding polymer chemistry enables us to select an optimal approach which results in effective crosslinking of cyclodextrin with polyacrylamide gels.

## 10.3 Synthesis of acrylate-β-cyclodextrin: efficient cross linking with polyacrylamide gels

### 10.3.1 Synthesis of acrylate-β-cyclodextrin
We synthesized acrylate-β-cyclodextrin in a two-step reaction. The acrylate functional group, which is incorporated through chemical synthesis, resembles the acrylate group on acrylamide.

As a result, the growing polyacrylamide chain has equal likelihood to react with acrylamide or with acrylate-β-cyclodextrin. As shown in Figure 10-6, 1,1 carbonyldiimidazole containing two imidazole leaving groups is the key reagent. 1,1 carbonyldiimidazole first reacts with the hydroxyl group on 2-hydroxyethyl acrylate which produces imidazolyl carbamate. Imidazolyl carbamate then reacts with the hydroxyl group on β-cyclodextrin which generates β-cyclodextrin with an acrylate side group (acrylate-β-cyclodextrin). Both reactions are performed in dimethyl sulfoxide (DMSO) with constant stirring over 24 hours. The molar ratio of 2-hydroxylethyl acrylate to 1,1 carbonyldiimidazole is 1:1 and both compounds are at a 5 fold excess compared to β-cyclodextrin to ensure all β-cyclodextrin will contain at least one acrylate group at the end of the second reaction. 4-dimethylaminopyridine (DMAP) is added to the second reaction at 1 mg/ml as a catalyst.

Step 1
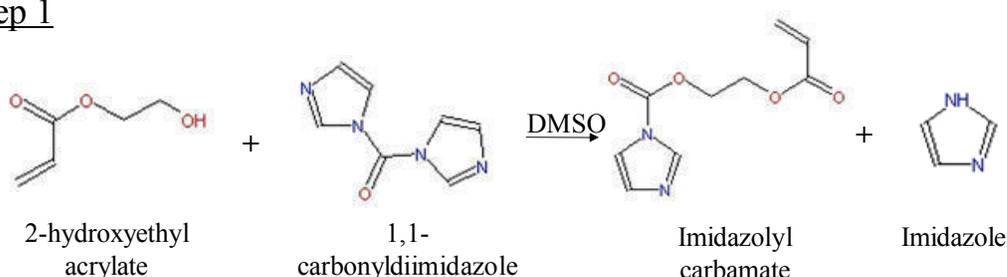


Step 2
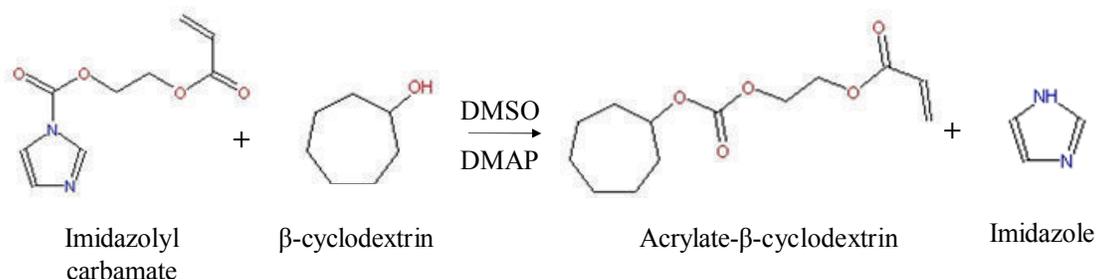


Figure 10-6. Synthesis of acrylate-β-cyclodextrin. 1,1-carbonyldiimidazole, which contains 2 imidazole leaving groups, reacts with primary hydroxyl groups on 2-hydroxyethyl acrylate and then reacts with hydroxyl groups on β-cyclodextrin.

## 10.3.2 **Purification of acrylate-β-cyclodextrin**

Acrylate-β-cyclodextrin is isolated from other molecules (2-hydroxylethyl acrylate, 1,1 carbonyldiimidazole, DMSO) in the final solution by precipitation in acetone[5]. Acrylate-β-cyclodextrin is poorly soluble in acetone whereas all other species are highly soluble in acetone. 100 μL of the final product is mixed with 900 μL acetone in an eppendorf tube. After mixing and spinning down the mixture in a centrifuge, the clear solution on the top was removed by pipetting whereas the white powder remained on the bottom was vacuum dried.

To confirm SDS-removal functionality of purified acrylate-β-cyclodextrin, we incubated 0.1% (w/v) SDS reduced CRP* with 4% (w/v) acrylate-β-cyclodextrin and injected the sample for on-chip separation in a double cross channel (NS12 chip). As shown in Figure 10-7, previously reduced SDS CRP* was resolved into multiple bands which indicate SDS dissociation.
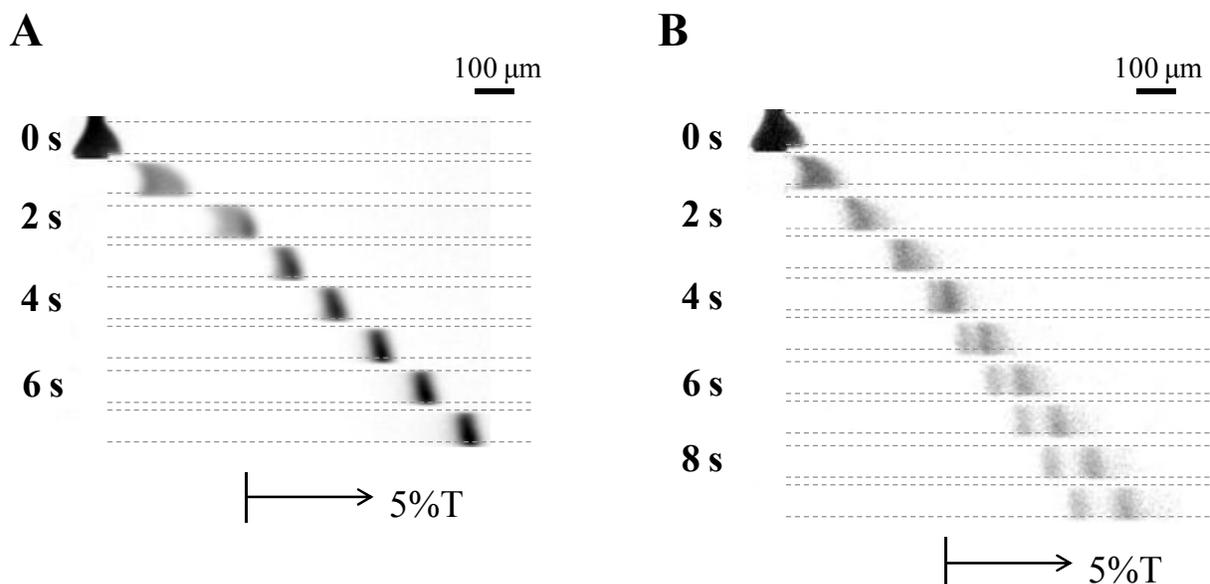
Figure 10-7. Purified acrylate-β-cyclodextrin retains SDS removal capability of β-cyclodextrin. Incubating SDS-reduced CRP* with 4% (w/v) acrylate-β-cyclodextrin results in SDS removal (B). (A) Control experiment: no incubation with acrylate-β-cyclodextrin was performed. Separation was performed on double T chips under E = 100 V/cm. The chip contains a 2.5%T loading gel and a 5%T separation gel.

### 10.3.3 Co-polymerization of acrylate-β-cyclodextrin with polyacrylamide gels

Acrylate-β-cyclodextrin was copolymerized with 4%T polyacrylamide gel in a 2D chamber. A 4.5%T blotting gel (containing 2μM polyclonal antibody) was first fabricated, a 4%T CD-PA gel containing 4% (w/v) acrylate-β-cyclodextrin was subsequently fabricated, and finally a 3%T loading gel was fabricated by flood exposure of the entire chip. As shown in Figure 10-8, reduced CRP* remained as one band in the separation channel. As summarized in Figure10-9, cyclodextrin immobilization via acrylate-β-cyclodextrin is a more suitable method.
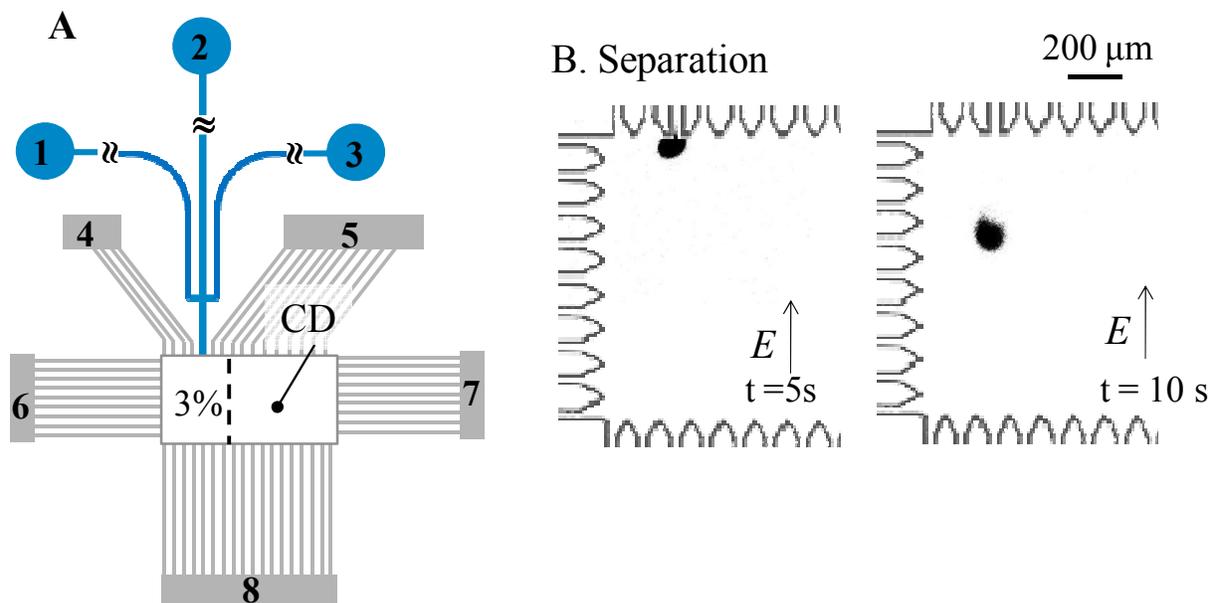
Figure 10-8. Reduced CRP* remains as one peak due to efficient immobilization of cyclodextrin within the transfer stage. The 1 mm x 2 mm 2D chamber contained a 3%T gel in adjacent to a 4%T gel which was co-polymerized with 4% (w/v) acrylate-β-cyclodextrin. Sample containing CRP* (440 nM) reduced in 0.1% SDS was introduced in sample well 1; all other wells contain 1x Tris/glycine buffer. Voltage programming follows that described in 9.1.2, Bright field images of the 2D chamber boundary are overlaid on top of separation and transfer images to give perspective to chamber location.
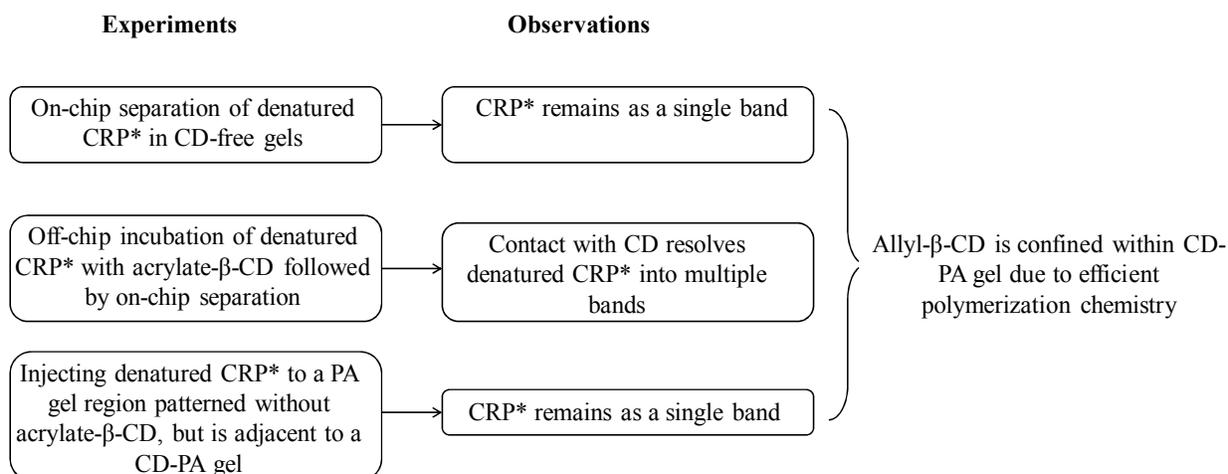


Figure10-9. Experimental observations confirm confinement of allyl-β-CD within the desired region.

## 10.4 **Discussion: how immobilized cyclodextrin can further improve SDS removal and protein renaturation**

Electrophoretic isolation of SDS and SDS removal by cyclodextrin can occur in parallel as denatured proteins are electrophoretically transferred across a region immobilized with

114

cyclodextrin. During the lateral transfer process, SDS will be isolated from proteins either by electrophoresis or by binding to cyclodextrin. Simulation results presented in chapter 9 revealed that there are two operating regimes during electrophoretic isolation of SDS for SDS-CRP* dissociation and protein renaturation in transit. Incorporation of cyclodextrin on-chip can further improve the renaturation efficiency for both regimes.

In one regime, the renaturation efficiency, as reflected experimentally by binding efficiency to blotting gels, is limited by insufficient resolution between SDS and CRP*. As we have pointed out at the end of Chapter 9, gel pore size can only be decreased to a certain extent without physically excluding larger proteins. Therefore, cyclodextrin, which removes excess SDS, can improve separation resolution between SDS and smaller proteins (< 10 kDa) when pore size decrease alone is insufficient in generating necessary separation resolution.

In the other regime, the renaturation efficiency is limited by available dissociation time. A convenient way to increase available dissociation time is to reduce electric field applied during the lateral transfer stage. However, reducing electric field decreases separation resolution between SDS and proteins. As we decrease electric field, cyclodextrin may be able to remove all SDS present in the system due to an increased SDS-cyclodextrin interaction time. Therefore, the downside of decreasing electric field, which is decreased SDS and protein separation resolution, may no longer be a limitation.

Going forward, we are interested in expanding the application of microfluidic western blotting assays to target proteins spanning a wide range of molecular weight (from < 10 kDa to > 150 kDa). Photopatterning of in-situ sieving matrices offers the capability to optimize assay conditions for improved efficiency. Developing experimental methods to determine operation regimes in a given assay condition will further improve renaturation efficiency.

## 10.5 **References**

(1)      Vegvari, A.; Foldesi, A.; Hetenyi, C.; Kocnegarova, O.; Schmid, M. G.; Kudirkaite, V.; Hjerten, S. *Electrophoresis* 2000, *21*, 3116-3125.
(2)      Vegvari, A.; Hjerten, S. *Journal of Chromatography A* 2002, *960*, 221-227.
(3)      Zeng, H. L.; Li, H. F.; Wang, X.; Lin, J. M. *Talanta* 2006, *69*, 226-231.
(4)      Brown, W. H.; Foote, C. S.; Iverson, B. L. *Organic Chemistry*; Cengage Learning, 2009.
(5)      Huang, Y.; Fan, X.-D. *Journal of Applied Polymer Science* 2009, *113*, 3068-3077.

# Chapter 11 Conclusions and Future Directions

## 11.1 Conclusions

Electrophoretic separation is a powerful technique in life sciences to identify and characterize proteins. In homogeneous immunoassays, electrophoretic separation of immune complexes from excess affinity probes is used to quantify protein biomarker concentrations. In western blotting assays, electrophoretic separation of proteins prior to immunoaffinity recognition can distinguish target analytes from nonspecifically bound analytes.

Separation resolution (SR), which is defined as the peak-to-peak distance between two neighboring analytes ($\Delta L$) divided by average analyte peak width ($4\sigma$), is the most useful criterion in evaluating separation efficiency. Microfluidic implementation of electrophoretic assays improves separation resolution by (1) reducing initial injected plug widths ($4\sigma_0$) and (2) allowing application of higher electric fields. In our work, we further improve separation resolution by optimizing the sieving matrices in which the separations are conducted in. Performing separations in photopatterned polyacrylamide gels improves separation resolution by enhancing mobility differences among analytes and completes separations in shorter separation lengths. Furthermore, photopatterning enables on-chip integration of electrophoretic separations with other functional units.

In the first part of my thesis work, we employ a discontinuous nanoporous polyacrylamide sieving matrix architecture to realize low-power electrophoretic immunoassays. Theoretical analysis revealed increasing T or decreasing the polyacrylamige gel pore size decreases the separation length required to achieve SR > 1. However, practical considerations require large pore-size gels in the loading channel to allow unbiased introduction of immune complexes. Thus, a discontinuous sieving matrix architecture is developed with large pore-size loading gels and small pore-size separation gels. An optimized mask-based fabrication protocol is introduced to eliminate protein exclusion and "destacking" dispersion near the pore-size discontinuity. Homogeneous electrophoretic immunoassays for protein biomarkers are optimized through tuning sieving matrix pore-size to generate sufficient mobility differences between the antibodies and immune complexes. With the optimized fabrication protocol, separations on a 2.5/5%T discontinuous gel completed simultaneous two-color immunoassays for inflammation biomarkers within a separation length of 350 μm in < 10 s. Further reduction in separation length to < 200 μm can be achieved by excluding immune complexes from entering the separation gel, which is applicable for implementation with full-field imaging. Further, the efficient homogeneous electrophoretic immunoassays detailed here are spectrally multiplexed and conducted in a compact microfluidic format, as is relevant to near-patient monitoring of protein biomarker panels including markers of infection and inflammation.

In the second part of my thesis work, we developed a novel strategy for on-chip protein renaturation based on electrophoretic separation. Protein renaturation is a critical component in western blotting assays. To address the performance and implementation limitations of previous microfluidic western blotting assays, we propose to remove SDS and renature proteins in transit. SDS removal in transit preserves separation resolution achieved during the separation stage and maintains a streamlined assay format. Based on a simple model describing SDS-protein complex

dissociation process, we developed two strategies to maximize the dissociation of SDS from proteins as SDS interferes with downstream immunoaffinity recognition. In the first strategy, electrophoretic separation during the transfer stage is applied to isolate SDS from proteins. By preventing the association of SDS and proteins, the dissociation of SDS-protein complexes dominates. Numerical simulations reveal two operation regimes for the SDS removal process: in the first regime, the separation resolution between SDS and proteins is the limiting factor; in the second regime, the available dissociation time is the limiting factor. Decreasing transfer gel pore sizes improves SDS removal and protein renaturation efficiency under both operating regimes by (1) enhancing relative mobility differences between SDS and the proteins and (2) increasing available dissociation time. After a lateral transfer distance of 1 mm and a lateral transfer time of 1 minute, 55% of previously denatured proteins are able to bind to the antibodies in the downstream immunoaffinity recognition stage. Our second strategy, which is to use immobilized cyclodextrins to remove SDS, can be performed in parallel with the first strategy. Removing SDS with immobilized cyclodextrin is especially appropriate for renaturation of small proteins (< 10 kDa) when reducing gel pore size alone may not generate sufficient mobility difference between SDS and the smaller proteins without physically excluding the larger proteins. Thus, we have developed a protocol for efficient crosslinking of cyclodextrins within polyacrylamide gels.

In conclusion, application and optimization of photopatterned polyacrylamide gels enable us to significantly improve the efficiency of existing homogeneous immunoassays and to impart new functionalities for microfluidic western blotting assays. Our future work centers on adapting both assay platforms as critical components to realize point of care diagnostics.

## 11.2 Future directions

As introduced in Chapter 2, point of care (POC) diagnostics, which rely on quantitation of one or several protein biomarkers specific to a clinical condition, can enable early diagnosis and improve treatment efficacy. Despite the tremendous impact POC diagnostics would make, we are seeing very limited use for two reasons. The first reason, which was introduced previously, is due to a lack of POC diagnostic instruments that can perform rapid and sensitive biomarker measurement in a low power and portable fashion. The second reason is due to a lack of disease-specific biomarkers that can be incorporated in diagnostic tools. Despite thousands of publications appearing each year on biomarkers, only 1 or 2 new protein biomarkers are approved by the U.S. Food and Drug Administration (FDA) per year[1].

Microfluidic protein assays, which offer rapid analyses and automated operation, can address the key challenges in realizing point of care diagnostics. While further system-level integration is underway by our group, low-power electrophoretic immunoassays enabled by discontinuous gel sieving matrices comprise the basis of a battery-operated diagnostic platform for quantitation of protein biomarkers in near-patient environments. With the capability to profile multiple biomarkers and to perform continuous monitoring, we envision the developed technology to diagnose infectious disease at resource poor communities, aid treatment of severe sepsis at emergency rooms, and achieve long term monitoring of chronic disorders such as autoimmune diseases.

Given the significantly reduced assay time and sample consumption, microfluidic implementation of western blotting assays will expand the application of western blotting assays to the analysis of a single cell or several cells. Single-cell based measurements performed on microfluidic western blotting assays will provide better understanding of pathogenesis and lead to the discovery, validation, and clinical translation of more biomarkers.  Our current work centers on improving the performance of the demonstrated microfluidic western blotting assay by (1) increasing the accuracy of protein size measurement in the separation stage through incorporation of a more comprehensive molecular weight ladder, (2) improving assay sensitivity through optimizing protein renaturation and blotting gel binding efficiency (as discussed in section 9.5 and 10.4), and (3) minimizing sample preparation (i.e., fluorescence labeling) through exploring alternative detection techniques.

(1)      Ludwig, J. A.; Weinstein, J. N. *Nat Rev Cancer* **2005**, *5*, 845-856.

# Appendix A. Fluorescence labelling of antibodies and proteins

## Overview of Labelling Procedure

4 steps if your protein/antibody was initially dissolved in a compatible buffer (primary amine-free buffer):

    Step 1: calculate the amount of dyes needed based on the amount of Ab/protein to be labelled

    Step 2: Incubate dye with Ab/protein

    Step 3: Run the incubated mixture through a purification column to eliminate free dyes

    Step 4: Calculate Ab/protein concentration post-labelling & dye: protein molar ratio.


**!!!:** If your protein/antibody is dissolved in buffer containing ammonium ions/Tris/glycine/ethanolamine/triethylamine/glutathione/ imidazole,  perform buffer exchange prior to step 2. Buffer exchange protocol described in Page 124.

If protein is dissolved in amine-containing buffer (Tris, etc.)

**Step 1:** Calculate the amount of dyes needed based on the amount of Ab/protein to be labeled. **(Details see Page 120 )**

Buffer exchange to PBS using P-6/P-30 gel in Bio-spin columns **(Details see Page 121)**

Protein is dissolved in amine-free buffer

**Step 2:** Pipette Ab/protein solution to low-bind tubes. Add 1/10 th volume of 1 M sodium bicarbonate buffer. Add appropriate volume of AF 488 dyes.

Wrap tube with aluminum foil. Incubate for 1 hour at Room Temperature.

**Step 3:** Purify incubate mixture with bioSpin columns with P-6/P-30 resins.  **(Details see Page 122)**

**Step 4:** Measure absorbance at 280 nm and 494 nm to deduce protein concentration and dye:protein ratio. **(Details see Page 123)**

Materials:
- Alexa Fluor® 488 carboxylic acid, **each vial contains 0.1 mg dye in 10 µL DMSO.**
- 1 M Sodium bicarbonate buffer
- 1.5 mL low-adhesion eppendorf tubes (VWR)

Materials:
- P-6/P-30 resin dissolved in preferred buffer (Tris/glycine, PBS)
- Bio-spin columns from Bio-Rad with ~1.2 mL Bed Volume

Equipment:
- Nanodrop spectrometer

## Calculating Amount of Dyes Required for Labeling

**Materials:** the blue box in the freezer contains vials of AF 488 dyes. Each vial contains 0.1 mg dye in 10 μL DMSO (11.2 mM).

Calculation:
    (1) Calculate the number of moles of proteins to be labelled.
    (2) Calculate the number of moles of dyes required by multiplying (1) by a molar ratio. The table below provides a reference.
    (3) Calculate the volume of dyes required based on molar concentration of 11.2 mM.

$$\frac{protein\ weight\ in\ g}{MW\ in\ g/mol} \times Molar\ Ratio\ (Table\ 1) \times \frac{1}{11.2\ mM} = Volume\ of\ Dyes\ to\ be\ Added\ in\ L$$

**!!!:** You likely won't use all 10 μL of dyes in the vial, save the left-over for next labelling reaction! DMSO is a stable solvent.

**Table 1.** Recommended Alexa Fluor® 488 dye: protein molar ratios (MR) and typical yields for labeling 12–150 kDa proteins.

| Protein (MW in kDa) | For Lower DOL | For Optimal DOL | For Higher DOL | % Yield |
|---|---|---|---|---|
| parvalbumin (12) | ≤2 | 5 | ≥8 | 60 |
| soybean trypsin inhibitor (20) | ≤15 | 19 | ≥25 | 60 |
| ovalbumin (40) | ≤40 | 60 | ≥70 | 60 |
| streptavidin (53) | ≤20 | 30 | ≥50 | 90 |
| transferrin (80) | ≤6 | 12 | ≥15 | 70 |
| F(ab)₂ (100) | ≤20 | 30 | ≥40 | 90 |
| IgG (150) | ≤25 | 55 | ≥65 | 90 |

**Protein Buffer Exchange Protocol (**not needed if your protein is dissolved in primary-amine-free buffer**)**

Goal:  if your protein is dissolved in buffer containing primary amines, with the use of Bio-spin columns and appropriate resins, the buffer will be exchanged to PBS.

Materials:
  o  P-6/P-30 resin dissolved in preferred buffer (Tris/glycine, PBS). **Resin preparation protocol, see Page 124.**
  o  Bio-spin columns from Bio-Rad with ~1.2 mL Bed Volume

Key idea: passing protein through a column containing resins dissolved in PBS will result in eluted protein in PBS buffer. Even if the resin wasn't prepared in PBS initially, the buffer can be replaced with PBS through multiple centrifugation runs.

Important note: the buffer exchange protocol is likely to dilute the protein. Therefore, don't dilute the protein prior to buffer exchange!!!



Load ~1.5 ml resins into the bio-spin column. The column height reaches the lower rim (indicated by the red arrow).
Place the column in a test tube; tape the two. Place the assemble into a 15 mL tube.

Centrifuge for 3 min at 1100 g to remove packing buffer.

The resin is prepared in PBS buffer

The resin isn't prepared in PBS

Take bio-spin column out of the test tube. Tape to a low-adsorption tube for collecting protein sample. Place the assemble in a 15 mL tube.

Load < 100 µL protein sample to the column. Centrifuge for 5 min at 1100 g to elute protein. Proteins should be in PBS.

Add ~ 0.5 mL PBS buffer to the bio-spin column so column height is at the red arrow.
Centrifuge for 3 min at 1100 g.
Repeat this step 4 times (add buffer & centrifuge). The resins are now in PBS buffer.

# Protein Purification After Labeling

Goal: by spinning incubated mixture through bio-spin column, the free dyes are retained in the column whereas the Ab/protein is eluted off.

Materials:
- P-6/P-30 resin dissolved in preferred buffer (Tris/glycine, PBS). Resin preparation protocol see Page 124.
- Bio-spin columns from Bio-Rad with ~1.2 mL Bed Volume

Notes:
- Use P-6 resin for proteins < 40 kDa and P-30 resin for antibodies and proteins > 40 kDa.
- Purified protein will be in the same buffer as the resins were dissolved in. You do have the option to change the buffer with the following protocol.



**Load resins to here**

End cap
Reservoir
5 cm
3.7 cm working bed height
1.2 ml bed volume
Porous 30 μm polyethylene bed support retains fine particles
Luer end fitting with snap-off tip

Load ~1.5 ml resins into the bio-spin column. The column height reaches the lower rim (indicated by the red arrow).
Place the column in a test tube; tape the two.
Place the assemble into a 15 mL tube.

Centrifuge for 3 min at 1100 g to remove packing buffer.

Have the protein dissolved in the current buffer in the column

Exchange to a different buffer

Take bio-spin column out of the test tube. Tape to a low-adsorption tube for collecting protein sample. Place the assemble in a 15 mL tube.

Load < 100 μL protein sample to the column. Centrifuge for 5 min at 1100 g to elute protein.

Add ~ 0.5 mL desired buffer to the bio-spin column so column height is at the red arrow.
Centrifuge for 3 min at 1100 g.
Repeat this step 4 times. The resins are now in the desired buffer.

**Measuring Protein Concentration & Labeling Ratio**

Materials:
- 100 µL buffer in one UV cuvette as a blank
- Dilute labeled Ab/protein solution 10 – 20x to 100 µL and place in a UV cuvette

Equipment:
Nanodrop spectrometer

(1) Measure absorbance at 280 nm (corresponding to protein concentration) and 494 nm (corresponding to dye concentration). Note: the spectrophotometer reading may be unstable in the first few runs. I often discard the first 6-10 readings I got. Clean the UV cuvette with alcohol using Kimwipes.

(2) Calculate protein concentration based on $A_{280}$ and $A_{494}$. This step requires knowing the molar extinction coefficient ($\varepsilon$, in $cm^{-1}M^{-1}$) of your protein at 280 nm or $A_{280}$ at 1 mg/mL (which is also $\varepsilon$ / MW in g/mol). For antibody, $\varepsilon = 210,000$ $cm^{-1}M^{-1}$; $A_{280}$ at 1 mg/mL = 1.4.

$$Protein\ Concentration\ (M) = \frac{(A_{280} - 0.11 \cdot A_{494}) \cdot dilution factor}{(A_{280}\ at\ 1mg/mL) \cdot (MW\ in\ g/mol)}$$

(3) Calculate dye concentration based on $A_{494}$.

$$Dye\ Concenration\ (M) = \frac{(A_{494}) \cdot dilution factor}{71,000}$$

$$Degree\ of\ Labeling = \frac{Dye\ Concentration}{Protein\ Concentration}$$

To reduce degree of labeling: reduce incubation time & dye:protein ratio.

**P-6/P-30 Resin Preparation Protocol**

| Gel Type | Hydrated Bed Volume, ml/g |
|---|---|
| P-6 gel, extra fine | 6.5 |
| P-30 gel | 9 |


Fig. 1.


Fig. 2.

Step 1: Weight ~4 g of P-6 resin or ~3g P-30 resin. (the weight is appropriate for performing incubation in 50 mL conical tubes)


Fig. 3.


Fig. 4.

Step 2: Add twice as much buffer as the expected bed volume to the conical tube. Buffer added: P-6 weight in g x 13ml/g or P-30 weight in g x 18 ml/g. Slowly pour the resins into the buffer. **DON'T STIR.** (the resins are very fragile)

Step 3: Allow gels to hydrate overnight to a uniform suspension. Afterwards, let the resins settle (Figure 2).

Step 4: Decant half of the supernatant (Figure 3). Attach to a vacuum source and degas for 5-10 minutes with occasional swirling of the tube. Again, don't use a stir bar.

Step 5: Add 2 bed volumes of degassed buffer & swirl gel. Allow gel to settle until 90-95% of the particles have settled to the bottom (Figure 4). Decant the supernatant. Repeat Step 5 up to 4 times.

**Appendix B Linear acrylamide coating to minimize non-specific adsorption during blotting gel fabrication**

**Motivation**

When blotting gel is fabricated directly on silanized glass surfaces, we observe significant fluorescence staining of the loading channel during sample loading. As a result, only a small portion of the injected CRP* was introduced into the blotting gel (Figure 1A). Nonspecific adsorption of anti-CRP antibodies, contained in the blotting gel precursor solution, with silanized glass channel walls results in fluorescence staining when CRP* was introduced

To test our hypothesis, we incubated silanized glass channels with 4.5%T acrylamide precursor containing either 1 µM biotinylated anti-CRP Ab or 1.33 µM anti-CRP Ab for 30 minutes. After incubation, the antibody and acrylamide solution were replaced with a 2.5%T acrylamide solution (without any antibodies) by pressure driven flow. The chip was flood exposed on a 100 W UV lamp for 9 minutes at 10 mW/cm$^2$. Native CRP* was loaded and separated on both chips. Majority of CRP* was retained on loading channels there were in previous contact with either biotinylated anti-CRP Ab (Figure 1B) or anti-CRP Ab (Figure 1C). On the other hand, BSA*, with no cross reactivity to anti-CRP Ab, can freely migrate in a channel network that was also in previous contact with biotinylated anti-CRP Ab (Figure 1D). Interestingly, antibodies exhibit much less non-specific adsorption when incubated in unsilanized glass channel walls (Figure 2). Therefore, the non-specific adsorption of antibodies is due to hydrophobic interaction with silane coating. While eliminating silane coating could be a solution to circumvent the protein retention problem, silane coating is necessary to prevent gel shift during prolonged electric field application[1].
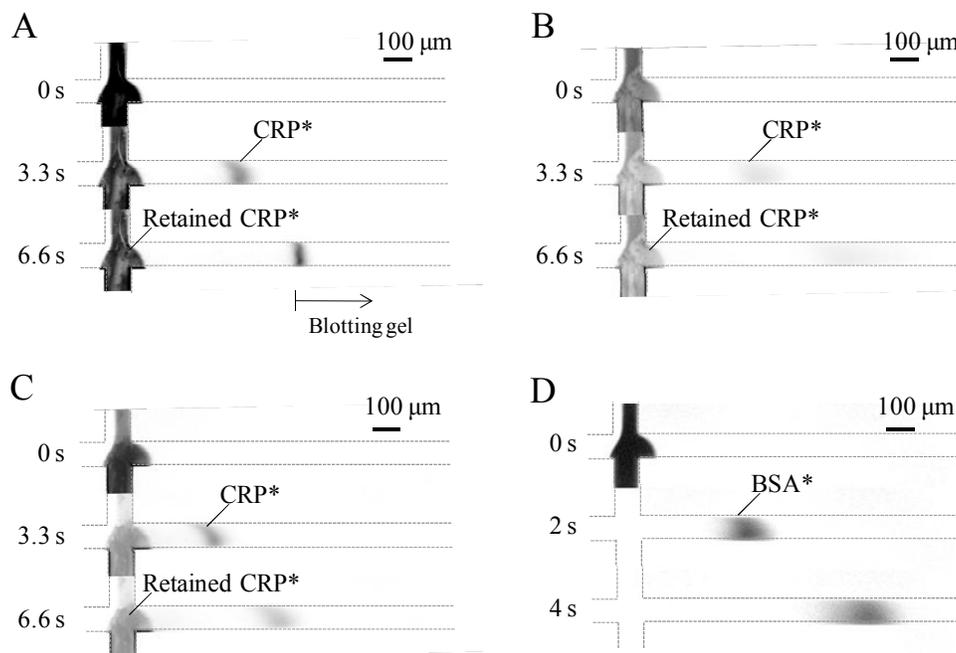


Figure 1. Antibodies in blotting gel precursor solution may non-specifically adsorb onto regions outside of blotting gels; nonspecifically adsorbed antibodies later retain injected CRP*. (A) A 4.5%T blotting gel containing 1µM biotinylated anti-CRP antibody was fabricated by partial

illumination followed by fabrication of a 2.5%T loading gel. (B) & (D) 2.5%T gels were fabricated on chips that were previously incubated with 4.5%T blotting gel precursors containing 1 μM biotinylated antibody. (C) 2.5%T gel was fabricated on a chip that was previously incubated with 4.5%T blotting gel precursor containing 1 μM antibody. E = 102 V/cm. Image of the separation channel was displayed as a function of elapsed separation time.
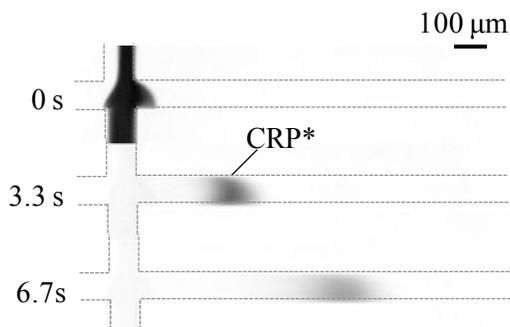


Figure 2. Antibodies adsorb less on unsilanized channels. A 2.5%T gel was fabricated on a chip that was previously incubated with a 4.5%T blotting gel precursor containing 1 μM antibody. No silane coating was performed prior to introduction of precursor solutions. E = 102 V/cm. Image of the separation channel was displayed as a function of elapsed separation time.

**Linear acrylamide coating is effective in reducing non-specific adsorption**
Inspired by previous work of using linear acrylamide to reduce adhesion of cells onto silanized surfaces[2], 5% linear (w/v) acrylamide was polymerized within microfluidic channels to reduce adsorption of proteins onto silanized surfaces. A 40% acrylamide solution was diluted to a final volume containing 5% acrylamide, 1x Tris/glycine buffer, and 0.5% (w/v) V-50 photoinitiator. The linear acrylamide precursor was wicked into silanized channels. The chip was subsequently flood exposed by a 100 W UV lamp for 10 minutes. Following exposure, channels were flushed with DI water via pressure driven flow to remove all linear acrylamide not chemically bond to silanized glass surfaces. Linear acrylamide coating is compatible with downstream blotting gel, separation gel and loading gel fabrication as polyacrylamide can be crosslinked with linear acrylamide on channel walls. As shown Figure 3, linear acrylamide is effective in reducing non-specific adsorption of anti-CRP antibodies onto silanized glass channel walls. As a result, CRP* can be efficiently loaded and injected for separation.
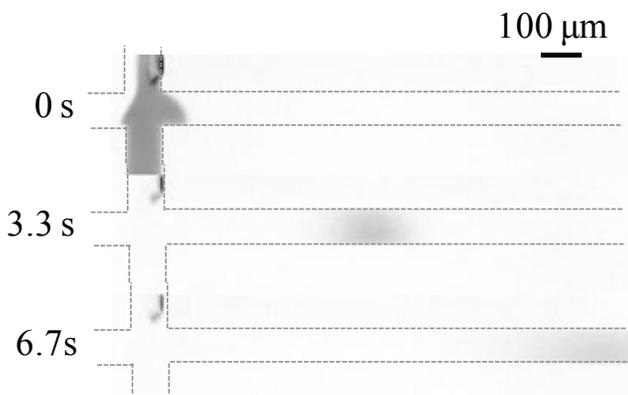


Figure 3. Linear acrylamide coating is effective in reducing non-specific adsorption of antibodies to silanized glass channel walls. As a result, analytes can be efficiently injected. The chip tested

was silanized, coated with linear acrylamide, and incubated with 4.5%T blotting gel precursor containing 1 μM biotinylated antibody for 30 minutes before fabricating a 2.5%T gel. E = 102 V/cm. Image of the separation channel was displayed as a function of elapsed separation time.

While linear acrylamide treatment is incorporated to fabrication of all chips containing blotting gels, linear acrylamide treatment isn't necessary for fabricating discontinuous and gradient gels for homogeneous immunoassays. We do not observe similar analyte retention effect on previously described discontinuous gels and gradient gels for two reasons: (1) silanized channel walls never come into contact with antibody solutions during fabrication; and (2) polyacrylamide gel which comes into contact with protein solutions exhibits low non-specific adsorption and the pore size of the loading gel is optimized to allow unrestricted migration of analytes.

(1)     Tia, S. Q.; He, M.; Kim, D.; Herr, A. E. *Analytical Chemistry*, *83,* 3581-3588.
(2)     Kirby, B. J.; Wheeler, A. R.; Zare, R. N.; Fruetel, J. A.; Shepodd, T. J. *Lab on a Chip* **2003**, *3*, 5-10.

# Appendix C. Biotinylation of antibodies

## Overview of Antibody Biotinylation Procedure

4 steps if your antibody was initially dissolved in a compatible buffer (primary amine-free buffer):

Step 1: calculate the amount of biotin needed based on the amount of Ab to be labelled

Step 2: Incubate biotin with Ab

Step 3: Run incubate mixture through purification column to eliminate free biotins

Step 4: Calculate Ab concentration post-labelling & biotin to Ab molar ratio.

**!!!:** If your antibody is dissolved in buffer containing ammonium ions/Tris/glycine/ethanolamine/triethylamine/glutathione/ imidazole, perform buffer exchange prior to step 2. Buffer exchange protocol described in Page 130.

If Ab dissolved in amine-containing buffer (Tris, etc.)

**Step 1:** Calculate the amount of biotin needed based on the amount of Ab to be labeled. **(Details see Page 129)**

Buffer exchange to PBS using P-30 gel in Bio-spin columns **(Details see Page 130)**

Protein dissolved in amine-free buffer

**Step 2:** Pipette Ab solution to low-bind tubes. Add 200 µL **DMSO** to the biotin tube. Pipette appropriate volume of biotin to Ab.

Incubate for 1 hour at Room Temperature.

Materials:
- 1 mg biotin in microtubes.
- 1.5 mL low-adhesion eppendorf tubes, from VWR

**Step 3:** Purify incubate mixture with bioSpin columns with P-30 resins. **(Details see Page 131)**

Materials:
- P-30 resin dissolved in preferred buffer (Tris/glycine, PBS)
- Bio-spin columns from Bio-Rad with ~1.5 mL Bed Volume

**Step 4:** Measure absorbance at 280 nm and 500 nm to deduce Ab concentration and biotin:Ab ratio. **(Details see Page 132)**

Equipment:
- Nanodrop spectrophotometer

**Calculating Amount of Biotins Required for Labeling**

**Materials:** No-weigh sulfo-NHS-biotin in the freezer contains 1 mg Biotin per microtube. 200 μL of DMSO is added to the biotin solution prior to labelling (molar concentration of 11 mM). To minimize biotin hydrolysis, I recommend using DMSO instead of water/PBS to dissolve the biotin. If your calculation reveals less than 1 μL Biotin solution is needed, dilute down further to avoid pipetting 1 μL.

Calculation:
    (1) Calculate the number of moles of Ab to be labelled.
    (2) Calculate the number of moles of biotin required by multiplying (1) by a molar ratio of 50.
    (3) Calculate the volume of biotin required based on molar concentration of 11 mM.

$$\frac{Ab\ weight\ in\ g}{MW\ in\ g/mol} \times 50 \times \frac{1}{11\ mM} = Volume\ of\ Biotin\ Solution\ to\ be\ Added\ in\ L$$

**Antibody Buffer Exchange Protocol (**not needed if your Ab is dissolved in primary-amine-free buffer**)**

Goal:  if your protein is dissolved in buffer containing primary amines, with the use of Bio-spin columns and appropriate resins, the buffer will be exchanged to PBS.

Materials:
- P-30 resin dissolved in preferred buffer (Tris/glycine, PBS). **Resin preparation protocol, see Page 133.**
- Bio-spin columns from Bio-Rad with ~1.2 mL Bed Volume

Key idea: passing Ab through a column containing resins dissolved in PBS will result in eluted protein in PBS buffer. Even if the resin wasn't prepared in PBS initially, the buffer can be replaced with PBS through multiple centrifugation runs.

Important note: the buffer exchange protocol is likely to dilute the Ab. Therefore, don't dilute the Ab prior to buffer exchange!!!

Load ~1.5 ml resins into the bio-spin column. The column height reaches the lower rim (indicated by the red arrow).
Place the column in a test tube; tape the two. Place the assemble into a 15 mL tube.

Centrifuge for 3 min at 1100 g to remove packing buffer.
**!!!:** use counter weight

The resin is prepared in PBS buffer

The resin isn't prepared in PBS

Add ~ 0.5 mL PBS buffer to the bio-spin column so column height is at the red arrow. Centrifuge for 3 min at 1100 g. Repeat this step 4 times (add buffer & centrifuge). The resins are now in PBS buffer.

Take bio-spin column out of the test tube. Tape to a low-adsorption tube for collecting protein sample. Place the assemble in a 15 mL tube.

Load < 100 µL Ab sample to the column.
Centrifuge for 5 min at 1100 g to elute protein.
Proteins should be in PBS.

End cap
Reservoir
**Load resins to here**
5 cm
3.7 cm working bed height
1.2 ml bed volume
Porous 30 µm polyethylene bed support retains fine particles
Luer end fitting with snap-off tip

## Antibody Purification

Goal: by spinning incubated mixture through bio-spin column, the free biotins are retained in the column whereas the Ab is eluted off.

Materials:
- o P-30 resin dissolved in preferred buffer (Tris/glycine, PBS). Resin preparation protocol see Page 133 .
- o Bio-spin columns from Bio-Rad with ~1.2 mL Bed Volume

Notes:
- o Purified antibody will be in the same buffer as the resins were dissolved in. You do have the option to change the buffer with the following protocol.



End cap
Reservoir
**Load resins to here**
5 cm
3.7 cm working bed height
1.2 ml bed volume
Porous 30 µm polyethylene bed support retains fine particles
Luer end fitting with snap-off tip

Load ~1.5 ml resins into the bio-spin column. The column height reaches the lower rim (indicated by the red arrow).
Place the column in a test tube; tape the two. Place the assemble into a 15 mL tube.

Centrifuge for 3 min at 1100 g to remove packing buffer.
**!!!:** use counter weight

Have protein dissolved in the current buffer in the column

Exchange to a different buffer

Take bio-spin column out of the test tube. Tape to a low-adsorption tube for collecting protein sample. Place the assemble in a 15 mL tube.

Load < 100 µL Ab sample to the column.
Centrifuge for 5 min at 1100 g to elute Ab.

Add ~ 0.5 mL desired buffer to the bio-spin column so column height is at the red arrow.
Centrifuge for 3 min at 1100 g.
Repeat this step 4 times. The resins are now in the desired buffer.

**Measuring Ab Concentration & Labeling Ratio**

Materials:
- Prepare HABA/Avidin solution: add 1 mg of avidin & 60 μL of 10 mM HABA to 1.94 ml of PBS (can be other buffer your Ab is dissolved in)
- 100 μL buffer in one UV cuvette as a blank
- Dilute labeled Ab solution 10 – 20x to 100 μL and place in a UV cuvette for A280 measurement
- 90 μL HABA/Avidin in one UV cuvette for A500 measurement

Equipment:
Nanodrop spectrophotometer.

(1) Measure absorbance of 10-20x diluted Ab at 280 nm to deduce Ab concentration post labeling. Note: the spectrophotometer reading may be unstable in the first few runs. I often discard the first 6-10 readings I got. Clean the UV cuvette with alcohol using Kimwipes.

For antibody, molar extinction coefficient, $\varepsilon = 210{,}000$ cm$^{-1}$M$^{-1}$; $A_{280}$ at 1 mg/mL = 1.4.

$$Ab\ Concentration\ (M) = \frac{A_{280} \cdot Dilution\ Factor}{210{,}000}$$

(2) Measure and record absorbance of HABA/Avidin at 500 nm. Add 10 μL of undiluted biotin-labeled Ab to the same cuvette, measure and record absorbance at 500 nm.

$$Biotin\ Concentration\ (M) = \frac{[0.9 \cdot (A_{500}\ of\ HABA/Avidin)] - A_{500}\ of\ HABA/Avidin/Biotin}{34{,}000}$$

$$Degree\ of\ Labeling = \frac{Biotin\ Concentration}{Ab\ Concentration}$$

To reduce degree of labeling: reduce incubation time & biotin:Ab ratio.

**P-6/P-30 Resin Preparation Protocol**

| Gel Type | Hydrated Bed Volume, ml/g |
|---|---|
| P-6 gel, extra fine | 6.5 |
| P-30 gel | 9 |


Fig. 1.


Fig. 2.

Step 1: Weight ~4 g of P-6 resin or ~3g P-30 resin. (the weight is appropriate for performing incubation in 50 mL conical tubes)


Fig. 3.


Fig. 4.

Step 2: Add twice as much buffer as the expected bed volume to the conical tube. Buffer added: P-6 weight in g x 13 ml/g or P-30 weight in g x 18 ml/g. Slowly pour the resins into the buffer. **DON'T STIR.** (the resins are very fragile)

Step 3: Allow gels to hydrate overnight to a uniform suspension. Afterwards, let the resins settle (Figure 2).

Step 4: Decant half of the supernatant (Figure 3). Attach to a vacuum source and degas for 5-10 minutes with occasional swirling of the tube. Again, don't use a stir bar.

Step 5: Add 2 bed volumes of degassed buffer & swirl gel. Allow gel to settle until 90-95% of the particles have settled to the bottom (Figure 4). Decant the supernatant. Repeat Step 5 up to 4 times.

**Appendix D. Matlab code for modeling of on-chip protein renaturation**

```
function pdex1

m = 0;
x = [linspace(0, 0.9, 100) linspace(0.91, 2.7, 1000) linspace(2.71, 4, 100)];
t = linspace(0,1,1001); % time to reach 2mm; starting position: 1 mm

%options = odeset('NonNegative',2);
sol = pdepe(m,@pdex1pde,@pdex1ic,@pdex1bc,x,t);

% Extract the first solution component as u.
u1 = sol(:,:,1); % crp complex
u2 = sol(:,:,2); % free crp
u3 = sol(:,:,3); % free sds

% A surface plot is often a good way to study a solution.
surf(x*1000,t,u1,'FaceColor','interp',...
    'EdgeColor','none',...
    'FaceLighting','phong')
colormap gray
colorbar
view(2)
set(gca,'Ydir','reverse');
xlabel('Distance x, um')
ylabel('Time t/t0')
title('SDS-CRP*')
axis([1000 2000 0 1])

% c2
figure
surf(x*1000,t,u2,'FaceColor','interp',...
    'EdgeColor','none',...
    'FaceLighting','phong')
colormap gray
colorbar
view(2)
set(gca,'Ydir','reverse');
xlabel('Distance x,um');
ylabel('Time t/t0');
title('CRP*')
axis([1000 2000 0 1])

figure
surf(x*1000,t,u3,'FaceColor','interp',...
```

```matlab
    'EdgeColor','none',...
    'FaceLighting','phong')
colormap gray
colorbar
view(2)
set(gca,'Ydir','reverse');
xlabel('Distance x,um');
ylabel('Time t/t0');
title('free SDS')
axis([1000 2000 0 1])


figure
for i=1:11
    hold on;
    plot(x*1000,u1((i-1)*100+1,:));
end
xlabel('distance, um')
ylabel('SDS complex CRP')

figure
for i=1:11
    hold on;
    plot(x*1000,u2((i-1)*100+1,:));
end
xlabel('distance, um')
ylabel('free CRP')

% to calculate recovery rate
freeCRP=sum(u2(1001,:))
peakCRP=max(u2(1001,:))
initCRP=sum(u1(1,:))


% --------------------------------------------------------------
function [c,f,s] = pdex1pde(x,t,u,DuDx)
% adjust the parameters to vary migration conditions
L = 0.1; %cm
% 1- sds-cpr; 2- crp; 3-sds
% mu1/mu2 Ratio
r1 = 1;
% mu3/mu2 Ratio
r3 = 1.4;
mu =[4e-5*r1; 4e-5; 4e-5*r3];% CRP cm^2/V/s
E = 200; %V/cm
```

```matlab
D = [1e-6*r1; 1e-6;1e-6*r3]; % CRP cm^2/s
Pe = 1./(D./mu(2)/L/E);
v = mu./mu(2);


Kon = 4e-2; %unit uM-1
Koff = 4e-2; % unit s-1



Don = Kon/E*L/mu(2);
Doff = Koff/E*L/mu(2);
y = Don*u(2).*u(3)-Doff*u(1);

c = [1; 1;1];
f = (1./Pe).*DuDx;
s = [(-v(1)*DuDx(1) + y); (-v(2)*DuDx(2) - y);(-v(3)*DuDx(3) - y)] ;
% --------------------------------------------------------------
function u0 = pdex1ic(x)
u0 = [0.2*exp(-(x-1).^2*800);0;3500*exp(-(x-1).^2*800)]; % unit uM
% --------------------------------------------------------------
function [pl,ql,pr,qr] = pdex1bc(xl,ul,xr,ur,t)
pl = [ul(1);ul(2);ul(3)];
ql = [0;0;0];
pr = [ur(1);ur(2);ur(3)];
qr = [0;0;0];
```